INAUGURAL-DISSERTATION

zur

Erlangung der Doktorwürde

der

Naturwissenschaftlich-Mathematischen

Gesamtfakultät

der

Ruprecht-Karls-Universität

Heidelberg

vorgelegt von
Diplom-Geologe Sebastian Kollenz
aus Walldorf (Baden)

2015

Tag der mündlichen Prüfung: 21.07.2015

Long-term landscape evolution, cooling and exhumation history of the South American passive continental margin in NE Argentina & SW Uruguay

Gutachter: apl. Prof. Ulrich A. Glasmacher
Prof. Peter Kukla

„Wenn sie nur kann, wird die Natur dich dreist belügen."
- Charles Darwin

"Ein Eiszeitalter da, eine Million Jahre Gebirgsbildung dort. Geologie ist ein Studium von Druck und Zeit. Mehr braucht es eigentlich nicht. Nur Druck und Zeit."
- Die Verurteilten

Acknowledgements

First of all I want to thank my supervisor apl. Prof. Ulrich A. Glasmacher, who brought me close to Thermochronology, gave me the chance for this dissertation and the input to get through this study.
I also want to thank Prof. Peter Kukla for the expertise he contributed and the discussions on the annual project meetings.
I appreciate very much the discussions with members of the SPP-1375 SAMPLE. Furthermore, I would also like to thank Danny Stockli´s team for the analytical assistance, Richard A. Ketcham and Raymond A. Donelick for providing the software HeFTy, Raymond A. Donelick allowing us to use Dpar© as a kinetic factor, and Istvan Dunkl for providing the software TrackKey.
In addition, I appreciate the support given by the Forschungs-Neutronenquelle FRM II at Garching, TU München, Germany, organized by Dr. Gerstenberg.
Special thanks go to my colleagues in South America, who helped me during field-work, introduced me in the regional geology and were always open for questions (Prof. E. A. Rossello, Prof. P. C. Hackspacher, Prof. C. Gaucher, Ricardo Pereyra, Sebastian Oriolo and Silvia Japas).
I want to thank also the members of ThermoArcheo research group, in particular our Lab-manager Margit for her work, my roommate Sabrina for everything she has done and helped (and this was much) and nonetheless Sebastian Dedera for the professional and non-professional discussions.

Mein ganz besonderer Dank gilt meiner Familie, vor allem meinen Eltern und meiner Schwester und nicht zuletzt Katja für die Launen, die sie ertragen mussten und dass sie mich durch alle Höhen und Tiefen begleitet haben.

Without the mentioned people, this work would not be like it is now.

- THANK YOU

Additional information

In the scope of this PhD-study, the former Master-student Sabrina Pfister, attended the second field-campaign to Argentina in 2012. After the fieldwork she worked on some samples from the Sierras Septentrionales, and applied the fission-track dating (apatite) on 11 samples in the frame of her Master-thesis. She was introduced in the technique and supervised during laboratory-work by myself. The samples she dated were also used for this PhD-thesis and are marked in the particular table.

Funding

Of course I owe thanks for the financial support, with grants to Ulrich A. Glasmacher, to the German Research Foundation (Deutsche Forschungsgemeinschaft, DFG, GL182/14-1, 14-2) within the Priority Program 1375 (SAMPLE) and to the DAAD.

Abstract

Passive continental margins are extraordinary geo-archives that result from processes related to continental rifting, breakup, sea-floor spreading, post-breakup, and climate changes. Whereas the South Atlantic passive continental margins (SAPCM's) in Brazil, Namibia, and South Africa are partly high-elevated margins (~2,000m a.s.l.), the SAPCM in Argentina and Uruguay is of low elevation. The northern part of the Argentinean passive margin is represented by the Sierras Septentrionales (Tandil Hills or Sierras Tandil) and the Sierras Australes (Ventana Hills or Sierra de la Ventana). They are key areas to unravel the thermal and exhumation history of the low-elevation SAPCM. In addition, this area has been part of the Gondwanides Orogeny. During the Permo-Triassic both areas were influenced by compressive deformation and diagenetic to low grade metamorphism. Thermochronological data from the Sierras Australes are characterized by apatite (U-Th-Sm)/He ages between 107.4 (3.5) Ma and 163.0 (9.8) Ma. Apatite fission-track ages range from 129.2 (9.3) Ma to 242.7 (17.1)Ma, zircon (U-Th-Sm)/He ages show values from 206.6 (16.5) Ma to 343.6 (27.5) Ma. AHe-ages from the Sierras Septentrionales range between 121.2 (7.3) Ma and 163.0 (9.8) Ma, AFT-ages between 104.0 (7.1) Ma and 228.9 (22.3) Ma, ZHe-ages between 167.8 (10.1) and 272.7 (16.4) Ma and ZFT-ages between 218.1 (79.4) Ma and 262.4 (36.1) Ma. The AFT-ages from SE-Uruguay range between 200.2 (19.3) Ma and 325.7 (24.8) Ma. This indicates that all dated samples are younger than the corresponding formation-, intrusion- or sedimentation-age. The Time-Temperature models from the Sierras Australes lead to a differentiated thermal evolution throughout the region, whereas the thermal history in the Sierras Septentrionales, seems to be very homogeneous. Thermal overprint related to Jurassic volcanism is very reasonable and supported by thermokinematic HeFTy-models. Thermal modelling for SE-Uruguay revealed, that also this area was covered by thick late Jurassic extrusive layers (depending on the assumed geothermal gradient 1000 to 2000 m).

Zusammenfassung

Passive Kontinentalränder sind hervorragende Archive die durch geologische Prozesse wie Grabenbildung, Aufbrechen von Kontinenten, extensionale Bewegungen von Ozeanböden und Klimawandel entstehen. Während der südatlantische Kontinentalrand im Bereich von Brasilien, Namibia und Südafrika eine deutliche Topographie (Steilküste mit Höhen im Bereich von 2000m ü. N. N.) aufweisen, ist der südatlantische Kontinentalrand im Bereich von Uruguay und Argentinien nur durch leichten Erhebungen gekennzeichnet. Am nördlichen Teil des argentinischen, passiven Kontinentalrandes befinden sich zwei Gebirgszüge (Sierras Septentrionales und Sierras Australes). Sie stellen in diesem Bereich des Kontinentalrandes ein Schlüsselgebiet dar, um etwas über die thermische Geschichte und der Exhumierungs-Geschichte der beiden Gebirgszüge zu erfahren. Zusätzlich war dieser Teil des Kontinentes an der Gonwanidischen Orogenese beteiligt. Im Übergang von Perm zu Trias wurden beide Gebirge von kompressiver Deformation und Tektonik im diagenetischen bis niedrig-metamorphosen Bereich überprägt. Die ermittelten thermochonologischen Alter der (U-Th-Sm)/He-Messungen an Apatiten liegen zwischen 107.4 (3.45) Ma und 163.0 (9.8) Ma. Apatit Spaltspurmessungen ergaben Alter zwischen 129.2 (9.3) Ma und 242.7 (17.1) Ma in the Sierras Australes, während (U-Th-Sm)/He-Datierungen an Zirkonen Alter von 206.6 (16.5) Ma bis 343.6 (27.5) Ma ergaben. Die gemessenen AHe-Alter aus den Sierras Septentrionales variieren zwischen 121.2 (7.3) Ma und 163.0 (9.8) Ma, AFT-Alter zwischen 104.0 (7.1) Ma und 228.9 (22.3) Ma, ZHe-Alter zwischen 167.8 (10.1) und 272.7 (16.4) Ma und ZFT-ages zwischen 218.1 (79.4) Ma und 262.4 (36.1) Ma. Die AFT-Alter von SO-Uruguay liegen zwischen 200.2 (19.3) Ma and 325.7 (24.8) Ma. Thermokinematische Modellierungen ergaben eine differenzierte Zeit-Temperatur-Geschichte für die Sierras Australes und eine recht homogene Exhumierungsgeschichte für die Sierras Septentrionales. Eine Aufheizungsphase durch überlagernde jurassische Basalte scheint sehr wahrscheinlich und wird auch durch die thermokinematischen Modellierungen unterstützt.

Auch der Südosten Uruguays wurde durch diese vulkanischen Abfolgen (abhängig vom angenommenen geothermischen Gradienten Mächtigkeiten zwischen 1000 und 2000 m) thermisch beeinflusst. Die HeFTy-Modellierungen für das Gebiet zeigen eine hervorragende Übereinstimmung mit diesem Szenario.

Keywords: low-temperature thermochronology; long-term landscape evolution; Sierras Australes; Sierras Septentrionales; Argentina; Uruguay; Passive Margin; South Atlantic Ocean; Gondwanides; apatite; zircon; fission-track analysis; (U-Th-Sm)/He analysis; HeFTy©

Table of Contents

List of Figures

1

Introduction

"Passive" continental margins (PCMs) are "first-order" topographic features of Earth's surface , that result from processes related to continental rifting, breakup, sea-floor spreading, post-breakup and climate changes. Along strike, the elevation of the continental margin vary from high elevations (> 1000 m a.s.l.) to very low elevations (< 50 m a.s.l.). Reasons for such strong variations in topography are still in debate (Bauer et al., 2010, submitted 2013). Bishop (2007) described the topography of high elevated margins from the coast to the inland as followed: "The classic morphology of high-elevation PCMs consists of a coastal plain of varying width, backed by a steep, often wall-like escarpment and a low-relief plateau surface inland of the escarpment lip". Traditionally, escarpments were suggested to be results of early stage rifting and followed by a steady retreat landward into the upland plateau surface (Ollier, 1985; Kooi and Beaumont, 1994, 1996; Gallagher et al., 1998; Summerfield, 2000; Braun and van der Beek, 2004; Braun et al., 2006; Cogné et al., 2012; Sacek et al., 2012). Initial tectonic and surface uplift of the rift shoulders was related to mantle and asthenospheric processes such as plume activity, asthenospheric up-welling, and melt intrusion during rifting processes (McKenzie, 1978; Wernicke, 1985; Kusznir et al., 1987; Kusznir and Ziegler, 1992; Ziegler and Cloetingh, 2004). Recently, the concept of dynamic topography evolution is supporting the mantle driven surface activities. Huismans and Beaumont (2011, 2015) tested two different rifted margin evolutions from rifting stage to PCM stage (the first 40 Myr). ("Type I", "Type II") by using thermo-mechanical numerical modeling. The Iberia-Newfoundland PCM, an example for the "type I", is characterized by large tracts of continental mantle lithosphere at the sea-floor. The central South Atlantic margin with its thin continental lower crust or mantle lithosphere and the fact that the continental lower crust and mantle lithosphere have been removed, is considered to be a representative for the "type II" margins. "Type I" rift evolution leads to a high elevated rift shoulder and "type II" to a low elevated rift shoulder.

The occurrence of PCMs with high elevations (> 1,000 m) close to the recent coastline long after the active rifting stage, is still subject of recent research (Bishop, 2007; Japsen, 2006; Hiruma et al., 2010; Cogné et al., 2012; Sacek et al., 2012; Karl et al., 2013; Green et al., 2013). Osmundsen and Redfield (2011) proposed that the gradient of crustal thinning and the evolution of onshore seaward-facing escarpments are related to each other. They showed that the highest escarpments and the most asymmetric margin morphology are situated where the crystalline crust is tapering sharply, while escarpments of lower altitudes are situated on more gentle tapers (Osmundsen and Redfield, 2011). Processes related to the formation, and denudation of onshore post-rift high elevations influence the sediment distribution (variation in sediment flux) in the related offshore basins through time and space (Franco-Magalhaes et al., 2010). The South Atlantic "passive" continental margin (SAPCM) process-response systems are proposed to be caused by the interaction of endogenous and exogenous forces. These forces are related to the Early Cretaceous to recent rift – drift – "passive" continental margin stage, and the climate change since the Early/ Late Cretaceous climate maximum. The SAPCM's in Brazil, Namibia, and South Africa are prevailing high-elevated margins (~2000 m a.s.l.), whereas the SAPCMs in Argentine and Uruguay are of low elevations (Fig. 1.1). The contrast between the South African and the Argentine margin is very distinctive. The onshore part of the SAPCM in Argentine is mostly characterized by a very flat topography with elevations up to 50 m a.s.l. The research area extends from SW-Uruguay to the Argentinean Atlantic Sierras Australes, located on the continental margin in the South of the state of Buenos Aires. The research area is located on the Atlantic continental margin of Argentina (Fig. 1.2).

In the middle of the so called Pampean flats, two lower mountain ranges, the Sierras Septen-

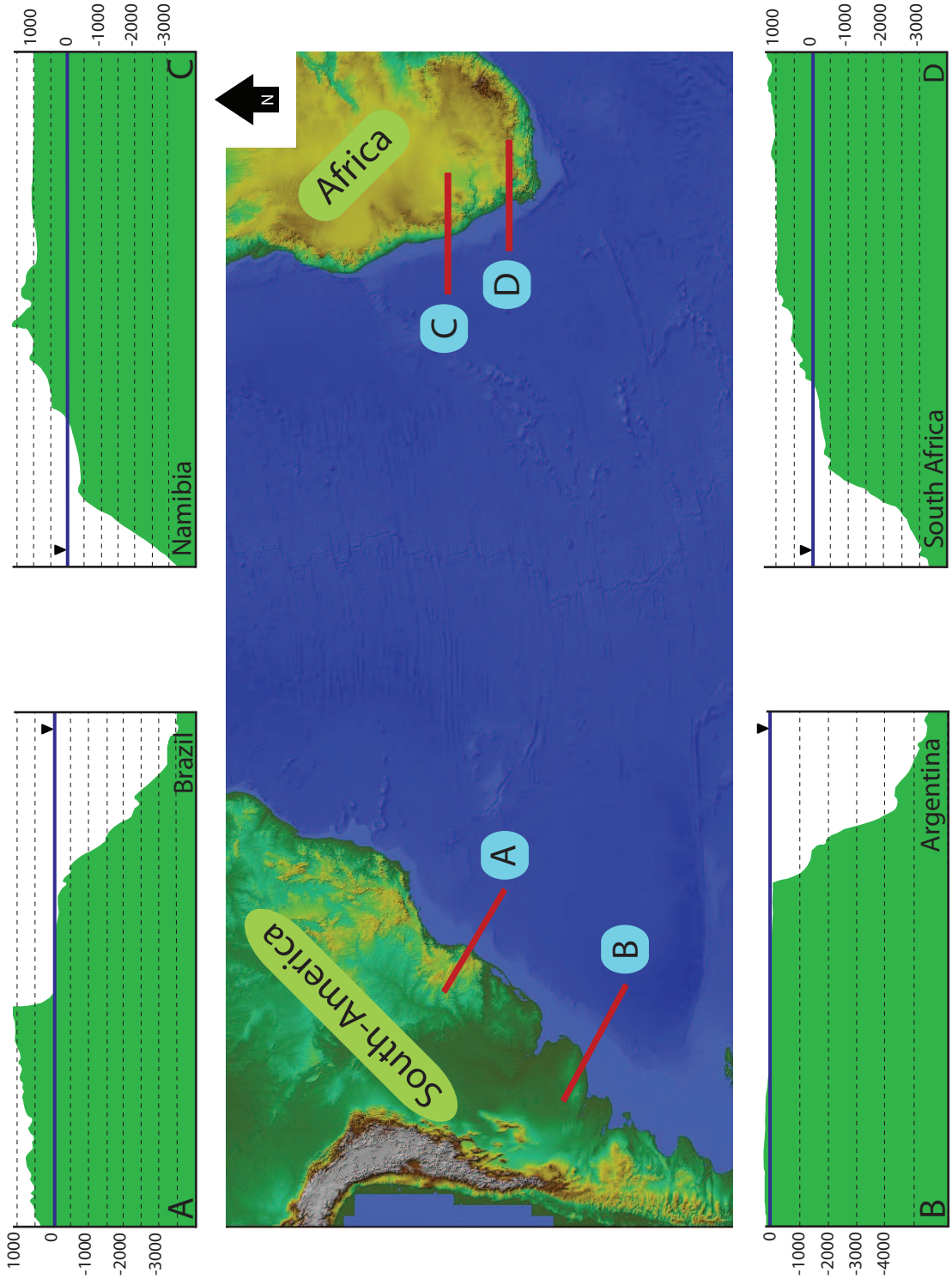

Fig. 1.1: Distribution of different styled continental margin in the South Atlantic (based on the DEM90).

trionales (elevations up to 300 m) and Sierras Australes (elevations up to more than 1000 m) are arising. Both lower mountain ranges trend nearly perpendicular to the continental margin. The general topographic features of the SAPCM in Argentina lead to important questions:

- Are the thermochronological ages reset or are there samples containing provenance information?

- Did the tectonics in the Sierras Australes influence the Sierras Septentrionales?

- Why is the recent Argentine margin so different to the SAPCM in Brazil and to the African SAPCM?

- Did the margin ever evolved to a high-elevated margin at all and was it fast retreated or did it subside, thereafter?

- Does differentiated exhumation occur and is it controlled by Pre- and Post rift structures?

For quantifying the rate at which landforms adapt to a changing tectonic, heat flow, and climate environment on a broad time scale, low-temperature thermochronology (LTT) is used. LTT dating techniques, such as fission-track (FT) and (U-Th-Sm)/He (He) dating of apatite and zircon provide information on the cooling and heating history of rocks during exhumation or subsidence, and allow deducing accordant subsidence and exhumation rates. The research of this work uses LTT data and tests various geological histo-

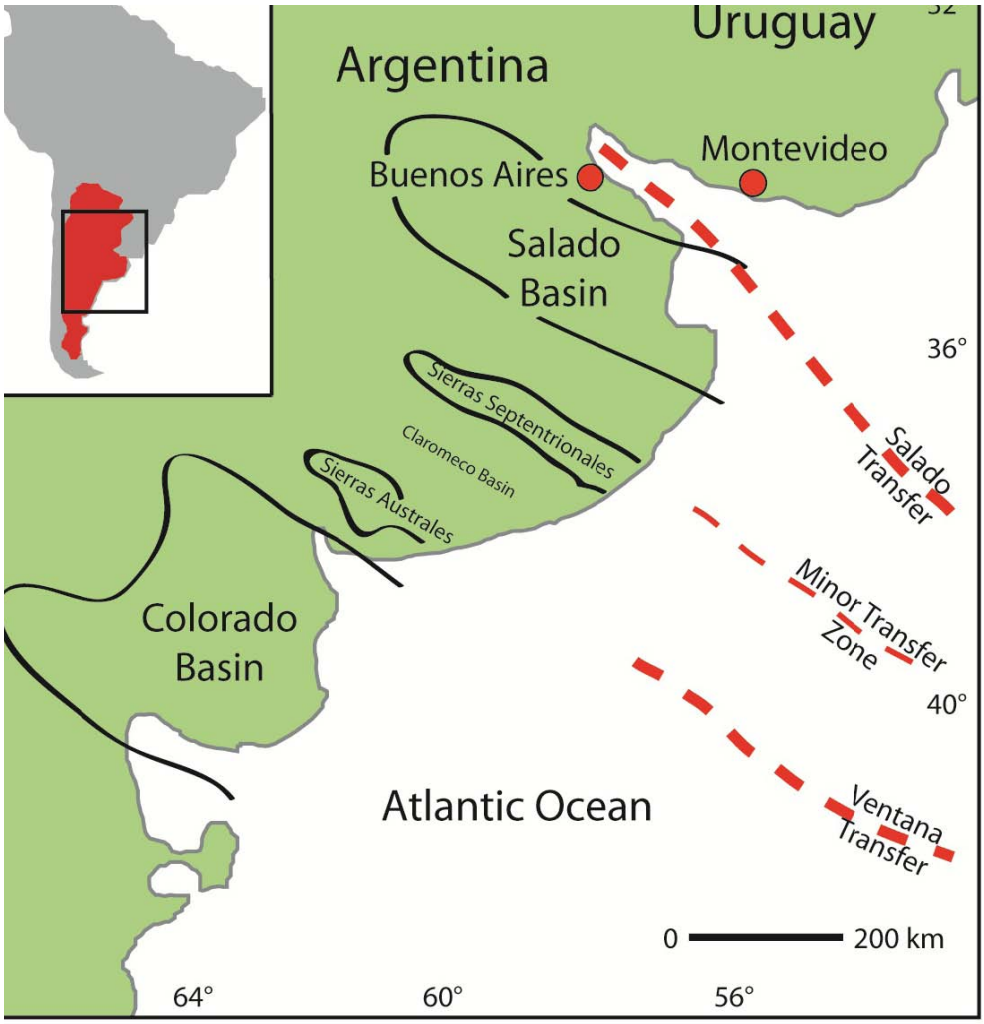

Fig. 1.2: Location map of the Sierras Septentrionales, the Sierras Australes and Location map of the Sierras Septentrionales, the Sierras Australes and the basin structures of the area (modified from Tomezzoli, 2001), combined with the margin segmentation by transfer zones (Franke et al., 2007).

ries against the LTT data set to quantify the t-T evolution by using the software HeFTy. Based on the t-T histories and a certain geothermal gradient multiple exhumation rates were calculated. The combined data lead to new conclusions, giving new insights and information to the above described questions of interest. Francisco Pangaro and Victor Ramos (2012) presented a new concept for the region, in which the Salado basin and Colorado basin experienced differing tectonic evolutions. They suggest the existence of two independet basins and support this model with gravimetric, magnetic and seismic data.

The authors concluded further, that the formation of the Salado basin was controlled by an old Precambrian (2.1-2.2 Ga) old suture. The Colorado basin is showing different depocenters, therefore reflects multiple displacements controls, with varying basin axis.

The controlling factor seemed to be the neighbouring Paleozoic orogen, with its dominating Paleozoic structures (Fig. 1.3). Most important Pangaro & Ramos (2012) do not show a onshore-portion of the Colorado basin as it was done in other studies (e. g. Tomezzoli, 2001; Ramos & Turic, 1996;)

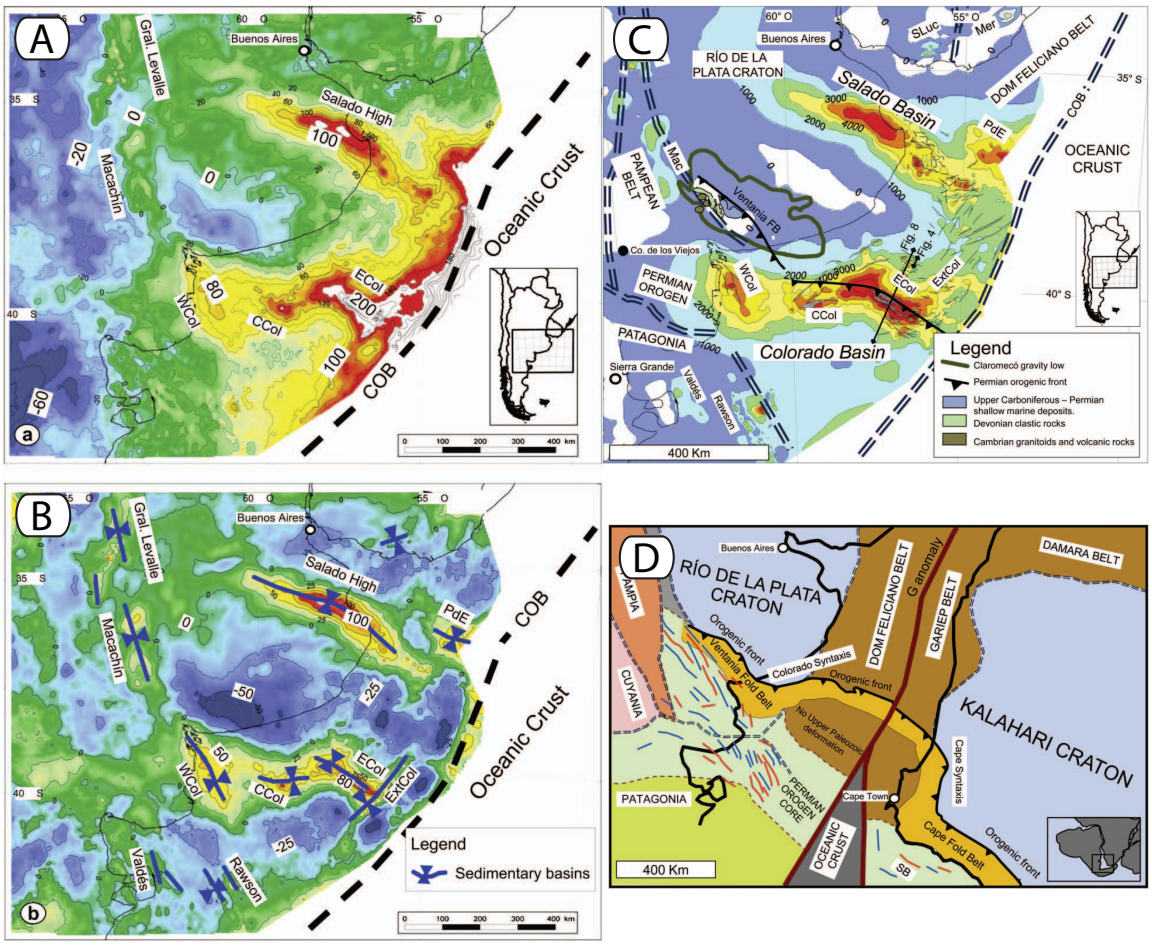

Fig. 1.3: A: Compensated Bouguer anomaly map; B: e Fifth-order polynomial residue of the compensated Bouguer map. Values in milligals. SLuc: Santa Lucía Basin. Mer: Merín Basin. GLev: General Levalle Basin. PdE: Punta del Este Basin. Mac: Macachín Basin. Wcol: western Colorado Basin. CCol: central Colorado Basin. ECol: eastern Colorado Basin. ExtCol: external Colorado Basin. CmLow: Claromecó gravity low. COB: continent-ocean boundary. C: Phanerozoic structural features and isopach map of the Mesozoic plus Cenozoic sedimentary rocks. SLuc: Santa Lucía Basin. Mer: Merín Basin. GLev: General Levalle Basin.PdE: Punta del Este Basin. Mac: Macachín Basin.WCol: western Colorado Basin. CCol: central Colorado Basin. ECol: eastern Colorado Basin. ExtCol: external Colorado Basin. Ventania FB: Ventania Fold Belt. COB: continent-ocean boundary. The onshore sedimentary thickness is based on Webster et al. (2004), Veroslavsky et al. (2004), Chebli et al. (1999) and Zambrano (1974). The thicknesses of the Rawson and Valdés basins are from Marinelli and Franzin (1996); D: Paleogeographic restoration at 134 Ma. (Pangaro & Ramos 2012).

2

Geological Background - Argentina

Contents

2.1 Study area

The area of investigation is situated on the Argentinean Atlantic continental margin. It consists of two NW-SE trending mountain ranges, the Sierras Australes and the Sierras Septentrionales. Both mountain ranges are surrounded and separated by three basins: The Salado basin is located northeast of the Sierras Septentrionales, the intracratonic Claromeco basin extends from the Sierras Septentrionales to the Sierras Australes, and the Colorado basin is situated southwest of the Sierras Australes. Both, the Salado basin and the Colorado basin extend from onshore to offshore and are trending perpendicular to the continental margin and the recent spreading axes.

The moderate topography (Fig. 2.1) of the Pampean Flat (altitudes between 0 to 50 meters) is interrupted by two mountain ranges, the Sierras Septentrionales and the Sierras Australes. The landscape of the Sierras Septentrionales is characterized by gentle hills (350-400 m a.s.l.) and surrounded by plains and grasslands. The Claromeco basin between both lower mountain ranges reaches altitudes of about 200 to 250 m a.s.l. The Cerro Ventana (1,184 m a.s.l.) and the Cerro Tres Picos (1,239 m a.s.l.) of the Sierras Australes represent the highest elevation within the study area and are characterized by steep, scarp slopes. The significant difference in elevation of the two mountain ranges is related to the differences in lithologies, whereas the timing of tectonic processes also played an important role for the present day topography (Fig. 2.2). The highest peaks of both mountain ranges are formed of weathering resistant quartzites.

2.2 The Salado Basin

The graben-like Salado basin is constrained by NW-SE and N-S trending faults (Zambrano and Urien, 1970; Introcaso and Ramos, 1984) and is filled with thick Mesozoic and Cenozoic volcanic, siliciclastic and saline sedimentary sequences (Crovetto, 2007) with a compiled thickness of up to 6500 m (Fig. 2.3). The transition of the Salado basin towards the Tandil mountains is not well defined and the geological nature is still in discussion (Franke, 2007; Zambrano and Urien, 1970; Perez-Diaz and Eagles, 2014). Due to post

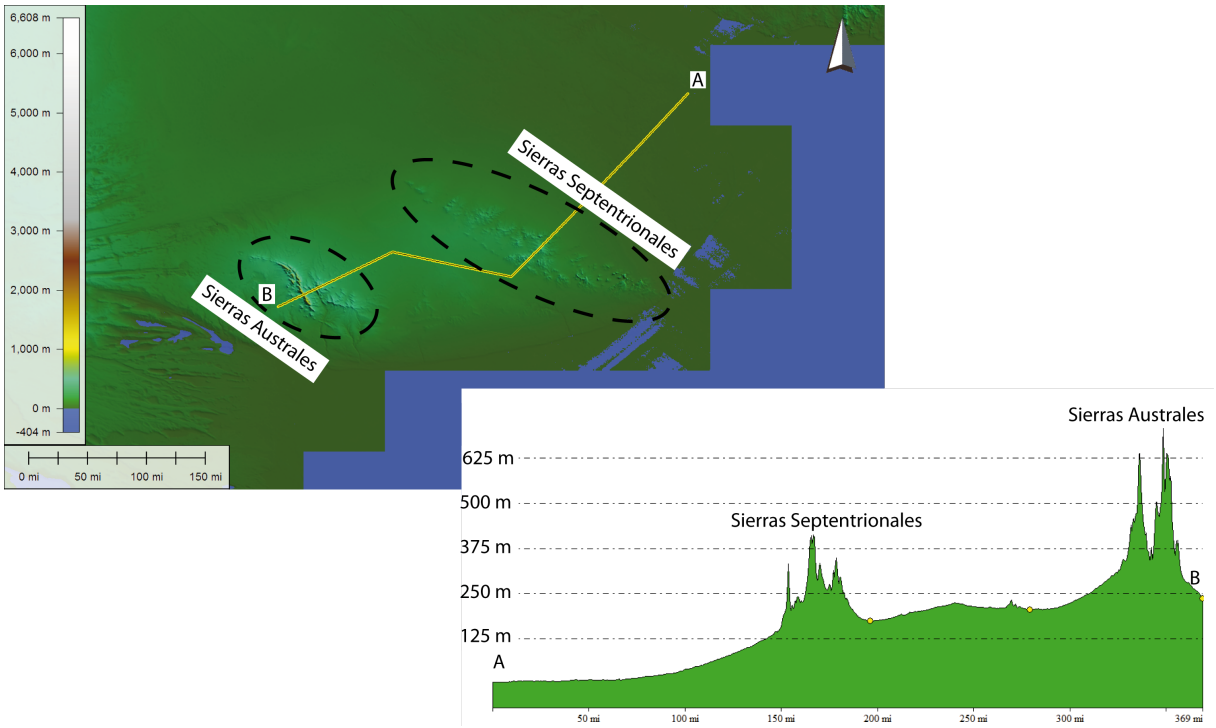

Fig. 2.1: DEM 90m with a cross-section through the research area.

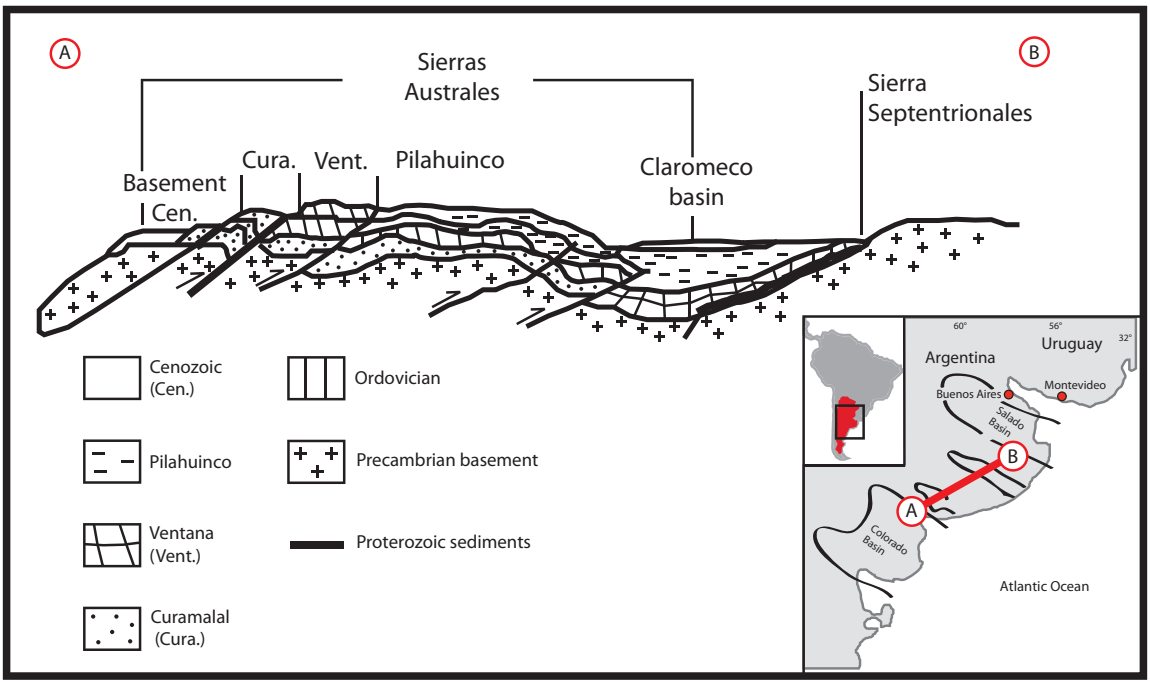

Fig. 2.2: Cross-section through the research area (redrawn and modified from Pucci, 1995)

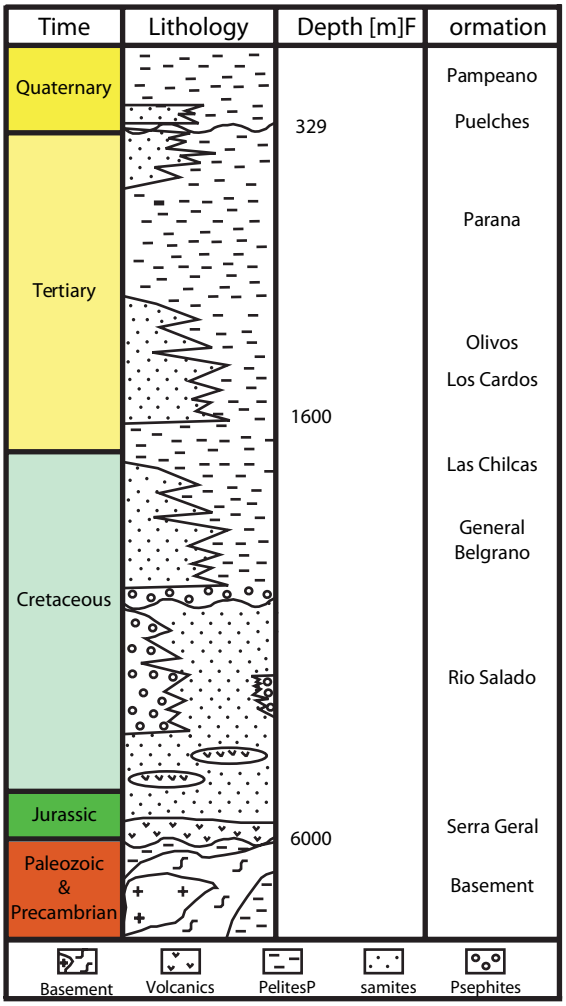

Fig. 2.3: Stratigraphy of the Salado basin (redrawn after Carol et al., 2010).

depositional faulting, the Precambrian metamorphic and intrusive basement locally emerges to the surface (e. g. Martin Garcia Island) (Crovetto et al., 2007). In contrast to the evolution of the Colorado basin, the Precambrian basement of the Salado Basin is similar to the Uruguayan basement rocks and is overlain by upper Jurassic to lower Cretaceous basaltic flows (Serra Geral Fm.; Zambrano and Urien, 1970). The Upper Cretaceous 3500 m thick siliciclastic "Rio Salado Formation" is dominated by an intercalation of cross-bedded sand- silt-, and claystones. It is overlain by the "General Belgrano Formation", a 890 m thick continental intercalation of claystones and sandstones with conglomerates. Zambrano (1974) proposes an Upper Cretaceous age, whereas Bracaccini (1980) suggested a lower Paleogene age for the sequence. Marine clay- and siltstones with anhydrite and gypsum of the Parana formation completes the sedimentary sequence (Introcaso and Ramos, 1984).

2.3 The Sierras Septentrionales

The stratigraphy in the Sierras Septentrionales (also called Tandil Hills) reaches from the Paleo-

proterozoic crystalline basement (Buenos Aires Complex) up to the Silurian siliciclastic sequence of the Balcarce Formation (Cingolani, 2010; Fig. 2.4, Fig. 2.5). The crystalline basement comprises calc-alkaline granitoids, orthogneisses of the granulite facies, schists of amphibolites, marbles, and migmatites (Dalla Salda, 1975; Zimmermann et al., 2010). Deformation and metamorphism of the rocks are related to the continental collision between 2.25 Ga- 2.08 Ga (Cingolani, 2010). The formation or reactivation of one of the mega-shear zones occurred between 2.0- 1.6 Ga (D'Angiola et al., 1992). The crystalline basement is discordantly overlain by the Neoproterozoic Sierras Bayas Group, consisting of diamictites, shales, quartz arenites, dolostones, and micritic limestones. The Sierras Bayas Group is discordantly overlain by the Neoproterozoic Cerro Negro Formation, which consists of shales, mudstones and sandstones. The unconformably overlying Balcarce Formation of Ordovician to Silurian age consist of siliciclastic sediments like quartz-arenites and kaolinitic shales (Poiré et al., 2003). Detrital zircon ages indicated Archean source rocks for the sedimentary sequence of Neoproterozoic to Lower Paleozoic age (Rapela et al., 2007).

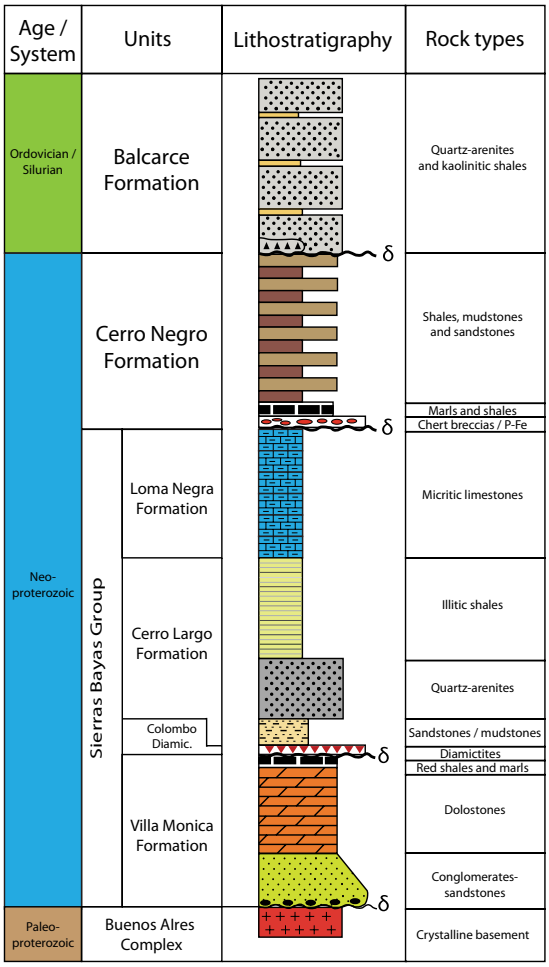

Fig. 2.4: Stratigraphy of the Sierras Septentrionales with corresponding depositional sequences (redrawn after Poiré, et al., 2003).

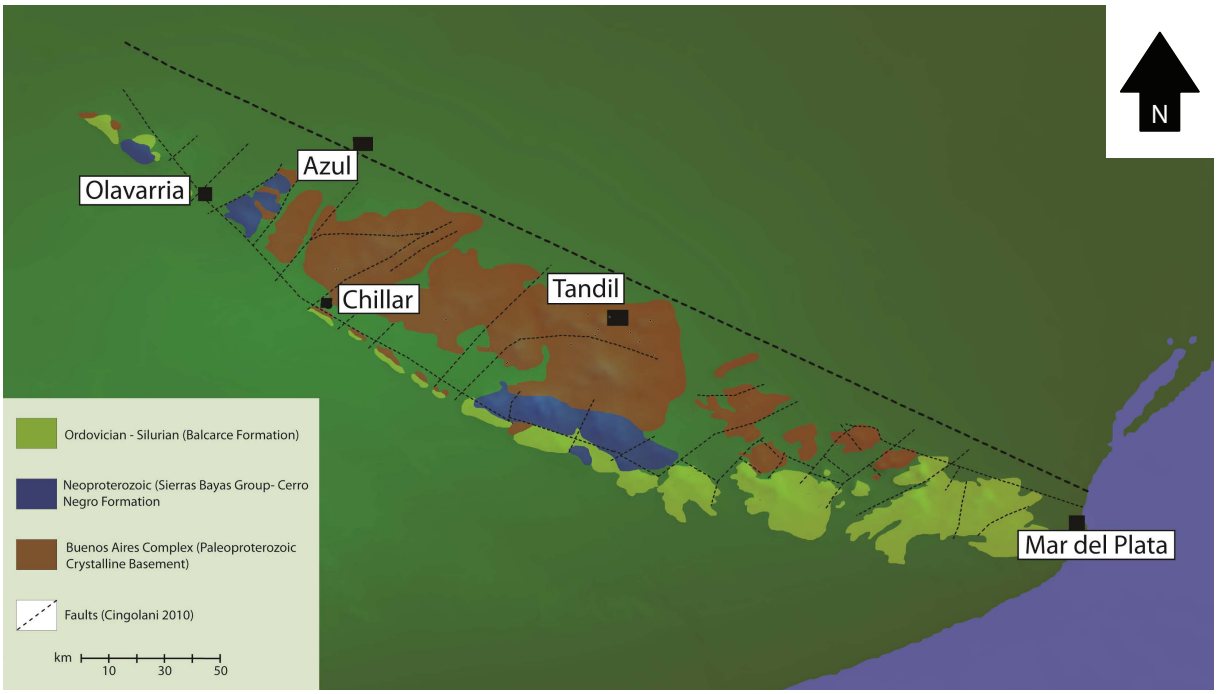

Fig. 2.5: Geological map of the Sierras Septentrionales combined with the DEM-90 (Jarvis, 2008; redrawn after Cingolani, 2010).

2.4 Lithologies - Sierras Septentrionales

2.4.1 Buenos Aires Complex

The Lithologies of the stratigraphic oldest unit of the Sierras Septentrionales show some variations in style and chemism. During the field work magmatic and metamorphic rocks (Fig. 2.6, Fig. 2.7, Fig. 2.8, Fig. 2.9, Fig. 2.10 and Fig. 2.11), e.g. migmatites, granitoids, mylonites and mica-schists were sampled. Some of the granitoids seemed to be metamorphically overprinted and showed some mylonitic features. The magmatites show the typical mineral-population (quartz, feldspar and micas), some showing isotropic features.

Selected migmatites still give strong hints to the metamorphic parental material and integrate garnets in the fabric (sample ARG 12-10, Fig. 2.9). In general, metamorphic rocks are distributed as gneissic rocks, schists, marbles with olivine or migmatites and related to the granulite facies (Cingolani, 2010). Several granite plutons (mostly gray granitoids), granodiorites and granites complete the magmatic portion of the basement-rocks. Additionally Precambrian mafic-tholeiitic dyke swarms are penetrating the crystalline basement.

The shear zones are characterized by mylonites (mainly derived from granitoids) and protomylonites. These rocks were developed in lower greenshist to amphibolite facies.

2.5 The Claromeco Basin

The NW-SE trending Claromeco Basin is located between the Sierras Australes and the Sierras Septentrionales (Fig. 2.5) , extending over an area of about 40000 km^2. It represents a foreland basin of variscan age with a long lasting sedimentary history and is orientated in NW-SE direction (Kostadinoff, 1982). Sedimentary rocks with a total thickness of 9 km thick are from Proterozoic, Paleozoic and Cenozoic age. The Pillahuinco Group consists of the Sauce Grande Formation,

Fig. 2.6: Foliated mylonite (ARG 12-01).

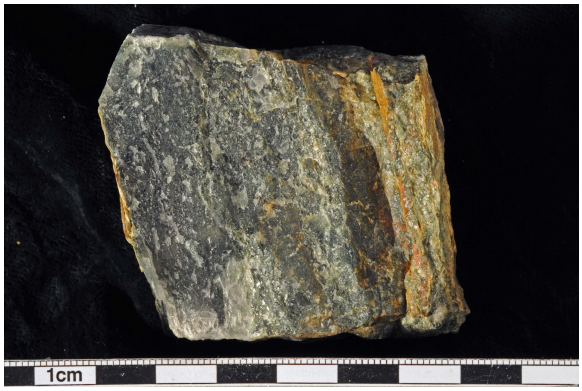

Fig. 2.7: Granitoid with metamorphic overprinting (ARG 12-06).

Fig. 2.8: Metamorphic rock with foliation (ARG 12-08)

Fig. 2.9: Migmatite with mafic minerals partly concentrated in some areas (ARG 12-10).

Fig. 2.10: Granitic mylonite (ARG 12-11).

Fig. 2.11: Granitoid (ARG 12-16).

the Piedra Azul Formation, the Bonete Formation and the Tunas Formation. The sedimentary sequences of this Group are composed of arkoses and subarkoses with volcanic clasts, also described as a synorogenic molasse foreland depositions (Alessandretti et al., 2013).

The subsurface strata is linked to the Sierras Australes and Sierras Septentrionales (Kostadinoff, 1982) and seen as a sink for these source areas.

The carbonatic and clastic sediments from the Sierras Septentrionales are assumed to occur also in the basin, but no reservoir analysis was carried out or published till now. Potential seals would be represented by Precambrian sediments from the Sierras Septentrionales, whereas shale intervals from the Piedra Azul and the Permian Tunas formation could represent the source rocks.

2.6 The Sierras Australes

The Sierras Australes (also called Ventana Hills) is a typical fold-and-thrust belt, which has been formed during the Carboniferous to lower Permian Gondwanide orogeny (Keidel, 1916, 1921; Ramos, 2013). The stratigraphy includes the lithologies from the Precambrian basement up to the Permian sandstones of the Tunas formation (Fig. 2.12). Similarly, the Cape Fold Belt was formed during the same orogeny (Keidel, 1916, 1921). Both fold-and-thrust belts are characterized by Precambrian basement rocks of similar age (Rapela et al., 2003), similar Palaeozoic biostratigraphy (Harrington, 1955; Benedetto, 2010), and similar glacial deposits of Carboniferous to Permian age (Keidel, 1913, Lopez Gamundi & Rossello, 1998). Upper Permian folding of the Paleozoic quarzites and sandstones (especially the Curamalal and Ventana Group) lead to the formation of chevron or concentric folds with flexural slip movement. The fold axes are trending NW-SE with local culminations (Cobbold et

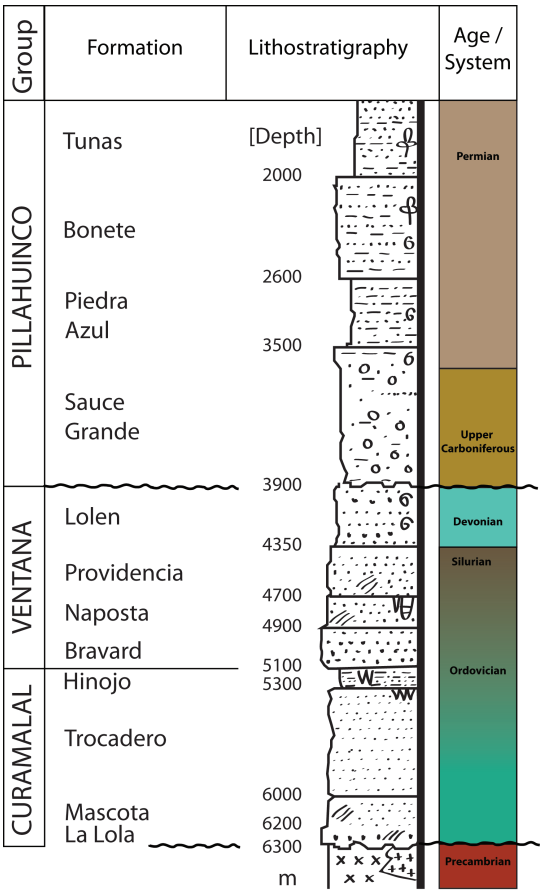

Fig. 2.12: Stratigraphy of the Sierras Australes fold belt (redawn after Buggisch, 1987).

al., 1986). Major wrench faults with a western thrust component separate the mountain range into lithological segments with variable degree of deformation and metamorphism (Fig. 2.13). Von Gosen and Buggisch (1990, 1991) reported a tectonic and thermal overprint of the basement rocks and the Paleozoic cover in the middle to upper Permian. They described the p-t environment as anchizonal to lower greenschist facies due to recrystallization and quartz deformation and most of all due to the crystallization of illite. At different locations within the Sierras Australes hills the K/Ar ages of the illite formation varies between 282 (3) Ma, and 260 (3) Ma.

The Western area consists of highly deformed, strongly cleaved (folding, reverse faulting) rocks from the lower greenschist facies (>300 °C). Siliciclastic rock sequences (>2300 m) are of Ordovician to Devonian age (Curamalal and Ventana Group; von Gosen et al., 1991). The Precambrian crystalline basement was intruded by S-type granites in Neoproterozoic time (607 (5) Ma, U-Pb zircon age) and during the Cambrian (531-524 Ma) by an A-type granite. Along the Sauce Grande wrench the Palaeozoic sedimentary rocks were overthrusted by the Eastern lower greenschist to anchizone siliciclastic rocks of the Upper Carboniferous to Permian Pillahuinco Group.

In the low grade Eastern area, the Upper Carboniferous to Permian siliciclastic rocks of the Pillahuinco Group are slightly deformed and reach upper diagenesis to low grade metamorphic conditions. Deformation and remagnetization occurred in early Permian time (Tomezzoli & Vilas, 1999; Tomezzoli, 2001).

Southwest of the Sierras Australes the Lopez Lecube granite occurs. K/Ar dating of hornblende revealed a Permian to Triassic cooling age of 245 (12) Ma (Rossello et al., 1997).

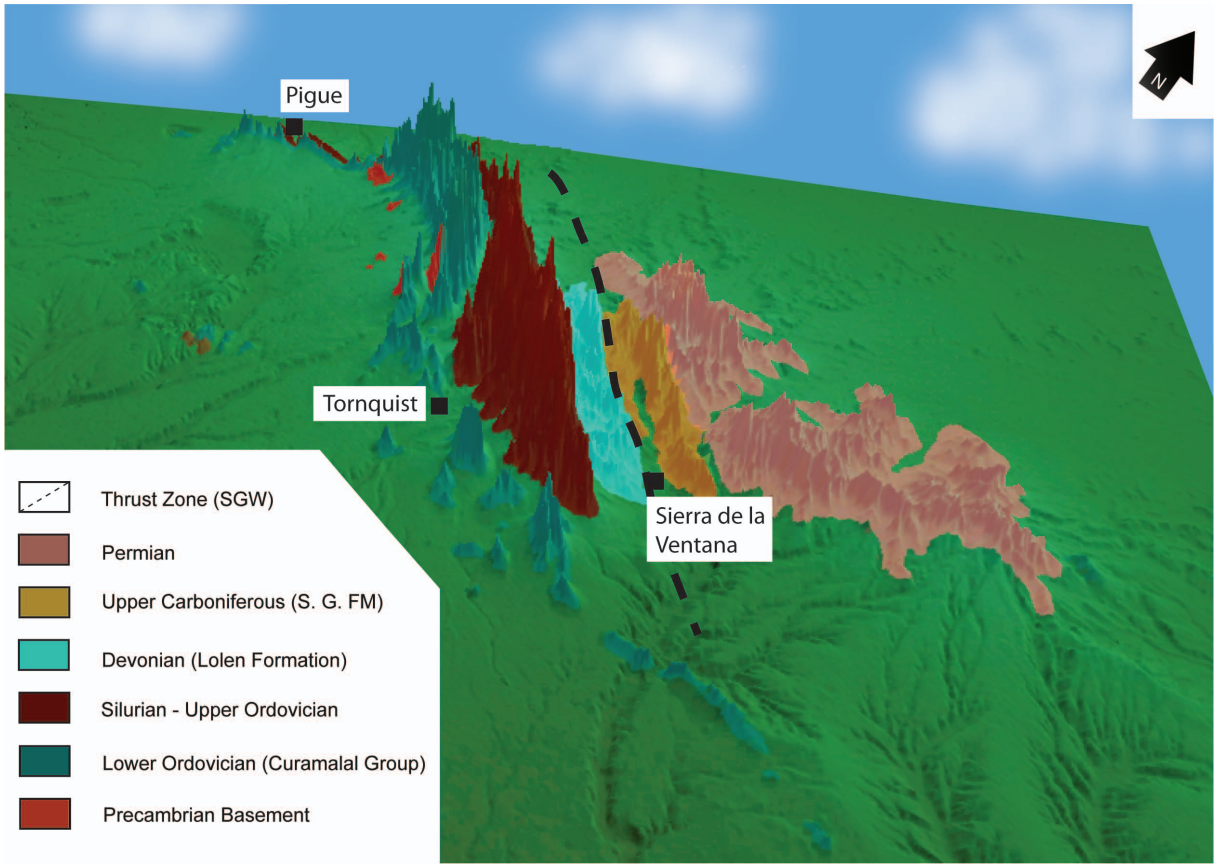

Fig. 2.13: Geological map of the Sierras Australes combined with the DEM-90m (redrawn after Buggisch, 1987 and Suero, 1972). The thrust zone is adapted from Cobbold et al. 1986; Rossello et al., 1997; Tomezzoli, 2001).

2.7 Lithologies - Sierras Australes

2.7.1 Basement

The crystalline Basement of the Sierras Australes is formed up of different crystalline rocks (Fig. 2.14; Fig. 2.15) like granites (ARG 12-24), ignimbrites or metamorphic rocks (e.g. schists). The granites consist of plagioclase and a well balanced ratio of feldspar besides quartz and mica crystals.

2.7.2 La Mascota Formation

The Cambrian Mascota Fm. consists of quarzites (Fig. 2.16; Fig. 2.17). Due to the composition and the physical strength they are not usable for the process of mineral separation and the following dating procedure. The thickness of this unit is about 100 m.

2.7.3 Naposta/Providencia Formation

The Naposta and Providencia formation are part of the Ventana Group. Both stratigraphic units are represented by massive quarzites (Fig. 2.20). On the picture you can see a specimen from the contact of both units. The Naposta Fm. comes up with a thickness of about 200 m whereas the Providencia Fm. is thicker (ca. 350 m).

2.7.4 Lolen Formation

The Devonian Lolen Fm. represents the youngest stratigraphic unit of the Ventana Group. It is built up of quartz-rich sandstones (Fig. 2.21), with a thickness of about 450 m.

2.7.5 Sauce Grande Formation

This formation is also built up of sedimentary rocks (Fig. 2.22) and is the oldest unit from the Pillahuinco Group. This Upper Carboniferous unit is also the oldest part of the low-metamorphic eastern part of the mountain range. The stratigraphic record shows a thickness of about 400 m.

2.7.6 Piedra Azul Formation

The Piedra Azul Fm. was deposited in lower Permian. It is also represented by sedimentary rocks (Fig. 2.23) with a slightly metamorphic overprint. The Piedra Azul Fm. is also part of the Pillahuinco Group, and therefore also part of the eastern section of the Sierras Australes with lower grades of deformation. The formation comes up with a sedimentary thickness of about 900 m.

2.7.7 Bonete Formation

The sandstones (Fig. 2.18) of the Bonete Fm. from the middle Permian are also part of the Pillahuinco Group. The thickness of this unit is about 600 m. The sandstones outcrops show fresh surfaces and no tectonic overprinting.

2.7.8 Tunas Formation

The slightly reddish sandstones (Fig. 2.19) from the Tunas Fm. are from the upper Permian and represent the youngest stratigraphic unit in the Sierras Australes.

Fig. 2.14: Granite of the basement (ARG 12-24)

Fig. 2.15: Precambrian ignimbrite (ARG 12-25).

Fig. 2.16: Quarzite from the La Mascota Fm. (ARG 12-34).

Fig. 2.17: Quarzite from the La Mascota Fm. (ARG 12-36).

Fig. 2.20: Quarzite from the Naposta-Provindencia contact (ARG 12-35)

Fig. 2.21: Sandstone from the Lolen FM. (ARG 12-29).

Fig. 2.22: Diamictite from the Sauce Grande FM. (ARG 10).

Fig. 2.23: Sandstone from the Piedra Azul FM. (ARG 12-38).

Fig. 2.18: Sandstone from the Bonete FM. (ARG 12-39).

Fig. 2.19: Sandstone from the Tunas FM. (ARG 12-19).

2.8 The Colorado Basin

Southwest of the Sierras Australes range, the NW-SE trending Colorado Basin is characterized by an on- and offshore part with the basin axis trending perpendicular to the NE-SW direction of the "passive" continental margin (Bushnell et al., 2000). The oldest known stratigraphic units deposited in the basin are Permian conglomerates, sandstones and black shales (Fig. 2.24) (Fryklund et al., 1996; Bushnell et al., 2000; Vayssaire et al., 2007). The Triassic and Jurassic geological evolution is not recorded within the sedimentary rock column. In addition, it is unknown if Triassic and/or Jurassic sedimentary units were deposited and eroded before the deposition of Lower Cretaceous sandstones and black shales. Continuous sedimentation of coarse continental to shallow marine conglomerates, sandstones, and black shales represent the Lower and Upper Cretaceous (Colorado Fm). Subsidence of the Colorado basin in the Cretaceous is thought to be caused by thermal and localized tectonic subsidence (Loegering et al., 2013). The Paleogene and Neogene are characterized by a shallow marine environment with the formation of shales, marls, marly shales, siltstones, and glauconitic sandstones. During the Pleistocene and Holocene parts of the Colorado basin were filled with fluvial to deltaic siliciclastic sediments. The accumulated thickness of the sedimentary record varies throughout the basin and reaches up to 16 km at its maximum. Since the Cretaceous the basin architecture was reworked by different tectonic activities, that caused the activation and reactivation of normal faults systems and transform fault systems (Loegering et al., 2013).

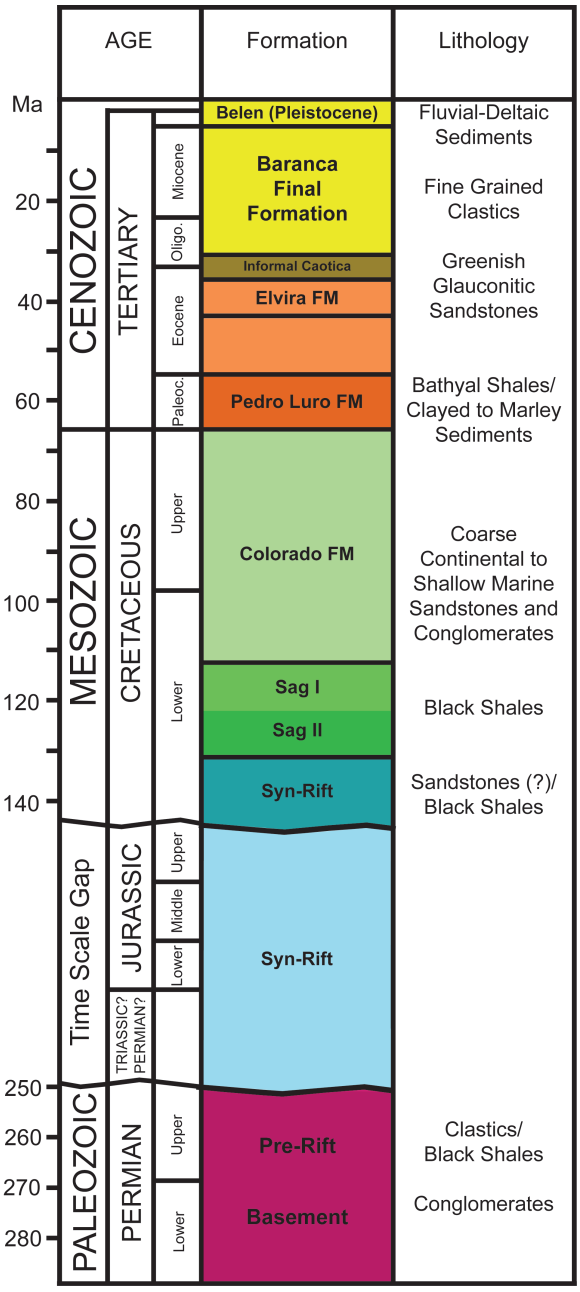

Fig. 2.24: Stratigraphy of the Colorado Basin (Bushnell et al., 2000).

3

Geological Background - Uruguay

Contents

3.1 General information

The Precambrian basement of Uruguay is divided into four tectonostratigraphic terranes (Fig. 3.1) separated by three megashears (Bossi et al., 1998; Bossi and Cingolani, 2009; Bossi and Gaucher, 2014a). Three of the terranes - the Piedra Alta, the Tandilia and the Nico Pérez Terrane- belong to the Río de la Plata Craton (Almeida et al., 1976), which was formed in the Mesoproterozoic (ca. 1.25 Ga, Gaucher et al., 2011). The fourth, the Cuchilla Dionisio Terrane, is regarded as a fragment of the Kalahari Craton rifted off 750 Ma (Bossi and Gaucher, 2004; Basei et al., 2005; Frimmel et al., 2011). Later the terrane evolved into a magmatic arc, known as Arachania (Gaucher et al., 2009). A topographic overview is given by figure (Fig. 3.2). A detailed geological map showing the stratigraphy and formations (Fig. 3.3) is given below.

3.2 Piedra Alta Terrane

The Piedra Alta Terrane is constrained by the dextral Sarandí del Yí Shear Zone to the W and by the sinistral Colonia Shear Zone to the S. Three granite-gneiss areas (Feliciano, Florida and Ecilda Paullier) alternate with E-W trending mobile belts (Andresito and San José belts: Bossi et al., 1993; Bossi and Cingolani, 2009; Bossi and Piñeyro, 2014). The contact between the granite-gneiss areas and the low-grade metamorphic belts is of tectonic origin (mostly subhorizontal thrusts). The age of both, the granite-gneiss bands and the mobile belts is constrained between 2.15 and 2.0 Ga, typical ages of the Transamazonian Cycle (Santos et al., 2003). The depositional age of the volcano-sedimentary pile is constrained by a U-Pb SHRIMP zircon age of 2146 (7) Ma for a metadacite (Santos et al., 2003) in the San José Belt. Volcanic rocks of the Andresito Belt showed a similar age of 2113 (8) Ma, determined by U-Pb zircon dating (Bossi and Piñeyro, 2014). U-Pb ages of intrusive granitoids of both mobile belts range between 2108 (23) Ma and 2065 (9) Ma (Bossi and Piñeyro, 2014; Hartmann et al., 2000). The youngest massif is the Gauycurú Complex, a layered gabbro and granite phacolith intruding the San José Belt, with a Rb-Sr age of 1998 (35) Ma (Umpierre and Halpern, 1971). On the other hand, the granite-gneiss areas yielded Rb-Sr ages ranging between 2100 and 2040 Ma (Umpierre and Halpern, 1971), and thus similar to the ages obtained in the belts. A major N70E-trending mafic dyke swarm crosscuting the region yielded an U-Pb baddeleyite age of 1790 (5) Ma (Halls et al., 2001). The last event recorded in the Piedra Alta Terrane is represented by sinistral shearing along the Colonia Shear Zone, dated between 1.79 and 1.59 Ga (Bossi and Cingolani, 2009).

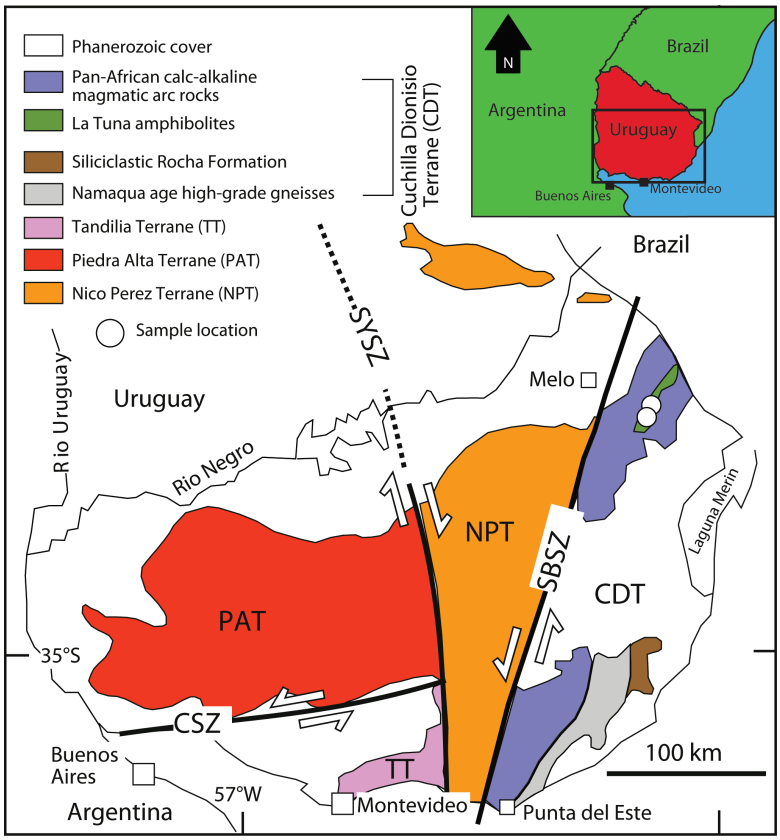

Fig. 3.1: Tectonostratigraphic map of SE-Uruguay (based on Bossi et al., 1998, 2005 and Bossi and Cingolani, 2009).

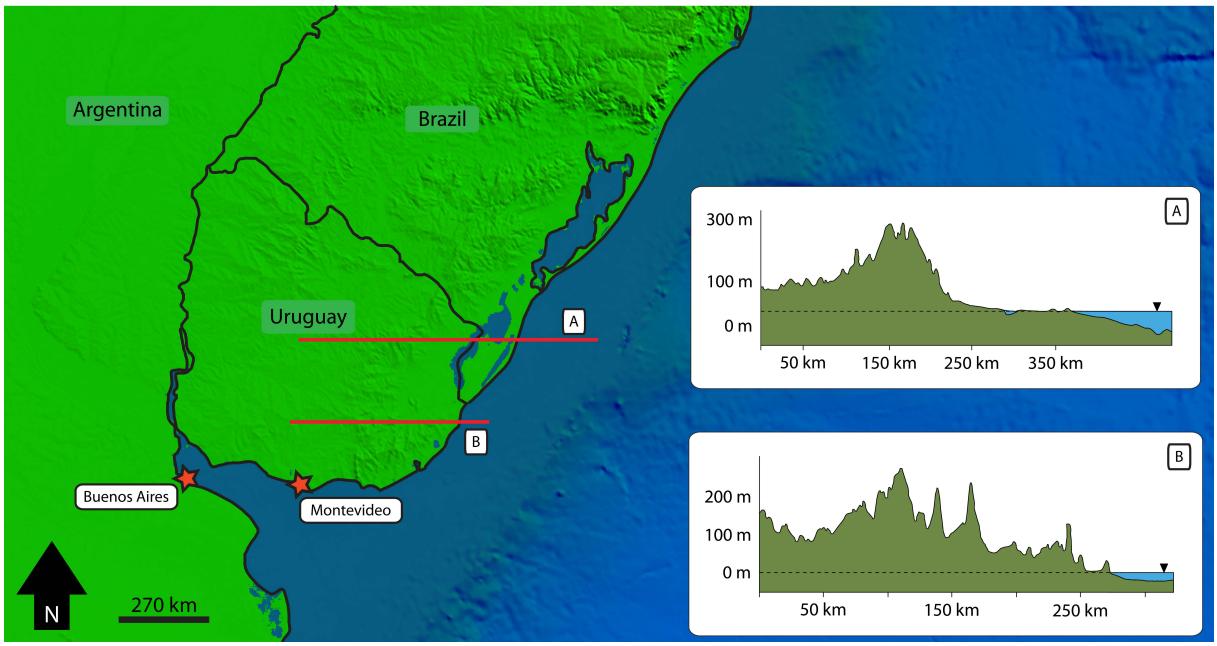

Fig. 3.2: DEM 90m (Jarvis et al., 2008) with a cross-section through the research area.

3.3 Tandilia Terrane

The Tandilia Terrane is best exposed in the homonymous range in the Buenos Aires Province (Argentina). Bossi et al. (2005) proposed that the block to the south of the Colonia Shear Zone in Uruguay is related to the outcrops in NE-Argentina. Together they form the Tandilia Terrane. Whereas in the Argentinian portion of the Tandilia Terrane U-Pb ages of basement rocks range between 2234 and 2065 Ma (Hartmann et al., 2002), in the Uruguayan outcrops ages between 2200 and 2000 Ma are reported (Santos et al., 2003; Pamoukaghlián, 2012; Abre et al., 2014). The Soca rapakivi granite intruded at 2056 (6) Ma (U-Pb on zircon, Santos et al., 2003) into a rigid, cratonized crust, while at the same time synorogenic plutons intruded in the Piedra Alta Terrane, showing different geotectonic settings for both blocks. Furthermore, Neoproterozoic rocks occur in the Tandilia Terrane in Uruguay and in Argentina, including the anorogenic La Paz Granite (585 (4) Ma, U-Pb on zircon: Abre et al., 2014) and marine sedimentary rocks of the Piedras de Afilar Formation (Uruguay) and its correlative Sierras Bayas Group in Argentina, both Ediacaran in age (Gaucher et al., 2008b; Poiré and Gaucher, 2009; Pamoukaghlián, 2012). It is worth noting that no Neoproterozoic rocks occur in the neighbouring Piedra Alta Terrane, but in turn anorogenic granitoids and sedimentary successions occur in the Nico Pérez Terrane to the E (e.g. Gaucher et al., 2008b).

3.4 Nico Pérez Terrane

The Nico Perez Terrane is the most complex tectonostratigraphic terrane of Uruguay, recording a protracted evolution between the Archean and Cambrian (e.g. Bossi and Gaucher, 2014a). It extends to the Sarandí del Yí Shear Zone in the west and to the Sierra Ballena Shear Zone in the east, both continental-scale megashears.

The oldest unit of the Nico Pérez Terrane is the La China Complex, a TTG (Tonalite-Trondhjemite-Granodiorite) complex with U-Pb zircon ages between 3.4 and 2.75 Ga and is in turn overlain by a Neoarchean sedimentary succession known as Cebollatí Group (Hartmann et al., 2001). Separated from these units by an intra-terrane transcurrent fault (Sierra de Sosa Shear Zone), the Valentines Formation is made up of a granulite-facies sedimentary succession with iron formations and interbedded volcanic rocks (Bossi et al.,

1998). This unit yielded Neoarchean U-Pb zircon ages overprinted by at least two Transamazonian metamorphic events between 2160 and 2060 Ma (Santos et al., 2003; Oyhantçabal et al., 2012). The Valentines Formation is intruded by the voluminous Illescas rapakivi granite of 1784 (5) Ma (U-Pb TIMS on zircon, Bossi et al., 1998). Mesoproterozoic volcanosedimentary rocks occuring in the Nico Pérez Terrane, are dated 1.49 to 1.43 Ga (Gaucher et al., 2011). The first deformational event of these successions is related to dextral shearing along the major Sarandí del Yí Shear Zone, dated 1.25 Ga (Teixeira et al., 1999; Gaucher et al., 2011). Neoproterozoic rocks of the Nico Pérez Terrane include anorogenic granites and dyke swarms (633-563 Ma, Gaucher et al., 2014), rift sediments (Gaucher et al., 2008a) and the Arroyo del Soldado Group, an Ediacaran to lowermost Cambrian marine platform succession (e.g. Gaucher et al., 2008b; Blanco et al., 2009; Poiré and Gaucher, 2009).

At ca. 530 Ma tangential collision with the Cuchilla Dionisio Terrane, part of the Arachania paleocontinent, took place along the sinistral Sierra Ballena Shear Zone (e.g. Bossi and Gaucher, 2004; Gaucher et al., 2008b, 2009; Blanco et al., 2009), deforming Neoproterozoic-lower Cambrian units and causing the intrusion of several granite plutons. This is assigned to the final stages of the Brasiliano-Pan African cycle.

3.5 Cuchilla Dionisio Terrane

The Cuchilla Dionisio Terrane (Bossi et al., 1998), also named Punta del Este Terrane (junior synonym), represents the central part of an exotic terrane rifted off the Kalahari Craton at ca. 750 Ma that later on evolved into a magmatic arc (Bossi and Gaucher, 2004; Basei et al., 2005). This paleocontinent, named Arachania by Gaucher et al. (2009), includes fragments at both sides of the Atlantic Ocean in South America and Africa. Apart from the Cuchilla Dionisio Terrane in Uruguay, the Pelotas Batholith in Brazil (Bossi and Gaucher, 2004), the Mar del Plata Terrane in Argentina (Rapela et al., 2011), the Tygerberg Terrane in South Africa (Frimmel et al., 2013) and the Marmora Terrane in Namibia (Basei et al., 2005) belong to Arachania. It is a key block for understanding the Atlantic Ocean opening, because

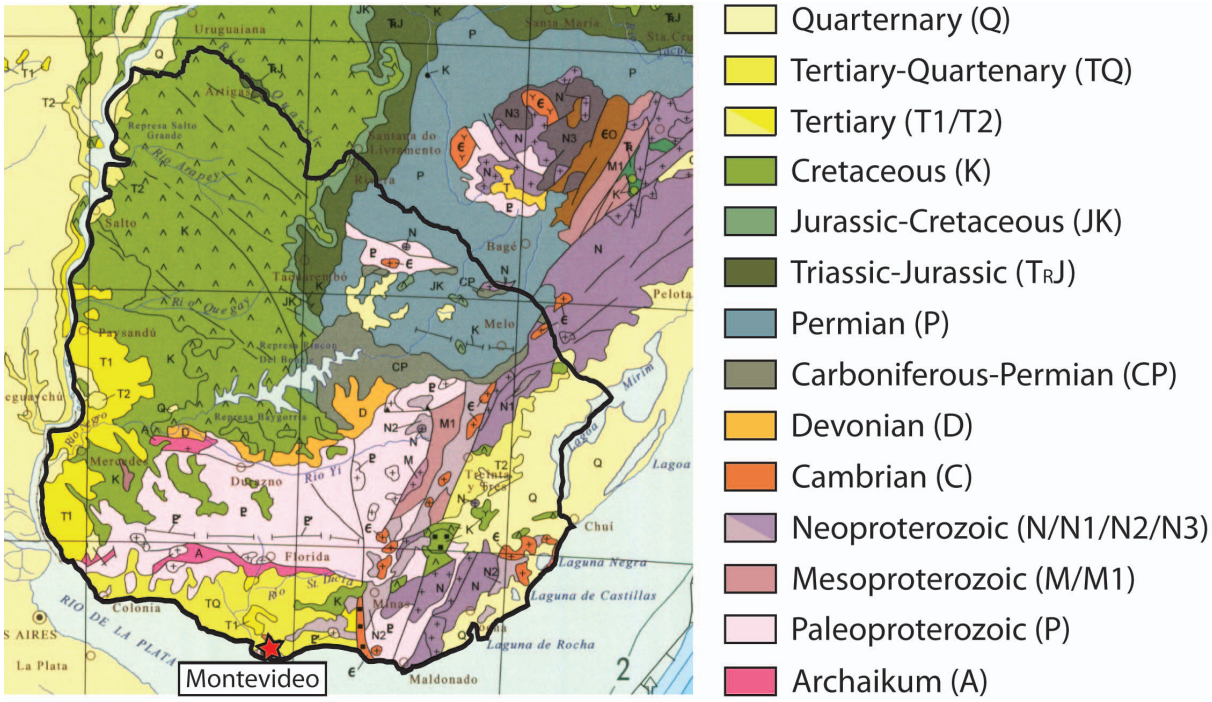

Fig. 3.3: Geological map of Uruguay (modified from the map published by the Geological survey of Brazil and the National Department of Mineral Production of Brazil, Schobbenhaus & Bellizzia, 2001)).

the latter exploited an intra-terrane weakness during the break up of Pangaea (Will et al., 2014).

The terrane is made up of a 1.0 Ga, Mesoproterozoic basement (Cerro Olivo Complex, e.g. Basei et al., 2011; Lenz et al., 2011) intruded by anorogenic plutons yielding U-Pb ages around 770 Ma (Oyhantçabal et al., 2009), which is correlated with the Richtersveld Complex in the Kalahari Craton (Bossi and Gaucher, 2014b). These rocks were metamorphosed in granulite-facies conditions around 640 - 660 Ma (Oyhantçabal et al., 2009; Lenz et al., 2011). Voluminous calc-alkaline granitoids intruded between 670 and 530 Ma (e.g. Oyhantçabal et al., 2009; Basei et al., 2011), attesting to the long-lived nature of the Arachania magmatic arc. At its eastern side, a back-arc basin, the Marmora Basin, opened at ca. 570 Ma and closed around 550 Ma (Gaucher et al., 2009; Frimmel et al., 2011, 2013). The Rocha Formation, the Oranjemund Group and the Tygerberg Formation were deposited in this basin in Uruguay and southern Africa (Basei et al., 2005; Frimmel et al., 2013). Incipient oceanic crust was formed and obducted later onto the Marmora Terrane and possibly also the Cuchilla Dionisio Terrane (Will et al., 2014). The axis of this back-arc basin served as the main weakness during the opening of the Atlantic Ocean.

3.6 Phanerozoic evolution and the opening of the South Atlantic

Post-Cambrian rocks are flat-lying and undeformed in Uruguay. The Paleozoic Parana basin shows a sedimentary record of Neo-Ordovician to Tertiary units. It is a huge foreland basin extending to Argentina, Bolivia, Brazil, Paraguay and Uruguay. The sedimentary record for the Uruguayan part shows lower Devonian to Lower Permian sequences (Panario et al., 2014; Veroslavsky et al., 2006). The sediments represent rocks from marine and continental environments and show an almost complete trangressive-regressive cycle. Former glaciation is recorded by Neopaleozoic glacial-influenced sediments (de Santa Ana et al., 2006b) and Late Carboniferous to Early Permian glacigenic units (de Santa Ana et al., 2006a; de Santa Ana and Veroslavsky, 2003). During Permian-Triassic time, a compressional event was identified by de Santa Ana and Veroslavsky (2003) in seismic sections and in outcrops. The Mesozoic tectonic evolution and processes were dominated by the initial rifting and the opening of the South Atlantic Ocean. However, the opening of the South Atlantic Ocean was also strongly influenced by the Precambrian megashears. The Santa Lucía graben is strongly influenced by both, the Colonia and Sarandí del Yí shear zone (Abre et al., 2014) and is filled with rift deposits (Panario et al., 2014; Sprechmann et al., 1981). The Laguna Merín graben, the onshore portion of the Pelotas Basin, follows at its western border the Sierra Ballena Shear Zone (Bossi and Gaucher, 2014b) and is predominantly filled with volcanic rocks, but also with a minor volume of clastic sediments, like conglomerates and red sandstones (Veroslavsky et al., 1999). Following Cernuschi et al. (2014) the Merin basin represents a Cretaceous aborted rift and is built up of lava flows and shallow intrusions. The aborted rift resulted in the formation of two basins, the Santa Lucia basin and the Merin Basin. The different igneous units and one sedimentary unit (conglomerates of the Quebracho Formation) from the Merin Basin are dated 133 to 127 Ma (Cernuschi et al, 2014). The extrusive rocks of the region are dated by U/Pb and Ar/Ar in several publications (Stewart et al., 1996; Lustrino et al., 2005; Muzio et al., 2000; Kirstein, 2000; and Cernuschi et al., 2014). The Treinta y Tres A and B types (sub-alkaline to mildly alkaline basaltic lavas) together with the Santa Lucia basalts represent the oldest extrusive rocks with ages between 133 and 131 Ma, followed by the Lavalleja rhyolitic ignimbrite eruptions (~130 – 128 Ma). The felsic rocks of the Valle Chico syenites are slightly younger and show ages between ~128 and 127 Ma. Some magmatic activity during and after this period is recorded by mafic to felsic intrusions into the extrusive centers also at ~128 to 127 Ma (Cernuschi, 2014). Besides

the magmatic and volcanic activity, hydrothermal alteration is identified in the Lascano-East intrusive complex. The Nico Pérez Terrane, being the oldest and possibly thickest lithospheric block, remained largely intact during early Cretaceous rifting, except for small grabens filled with vesicular basalts (Bossi and Schipilov, 2007).

The most important record of early Cretaceous rifting, apart from rift sediments in the abovementioned grabens, is represented in Uruguay by rift-related magmatism. The Arapey Formation is a ca. 1 km-thick pile of tholeiitic basalts extruded between 132.9 (1.3) Ma and 129.9 (1.1) Ma ($^{40}Ar/^{39}Ar$, Féraud et al., 1999), representing the southernmost outcrops of the Parana-Etendeka continental flood basalts. The Arapey Formation represents coeval rhyolitic volcanism (Bossi and Schipilov, 2007), as shown by $^{40}Ar/^{39}Ar$ ages of 131 (1) Ma (Féraud et al., 1999). The Valle Chico, Lascano and San Luis complexes are sub-alkaline to alkaline intrusive and volcanic rocks associated to the Laguna Merín graben (Bossi and Schipilov, 2007; Cernuschi et al., 2014). These rocks also yielded early Cretaceous ages between 134 and 127 Ma (Cernuschi et al., 2014).

Recent work on the topography and landscape evolution proposes that the lava flows from the Arapey Fm. coincided with a climate change from a very arid climate during Jurassic and Early Cretaceous to a less arid period during the Gondwana break-up (Panario et al., 2014). In Middle Cretaceous times semiarid and more humid periods alternated until with the Paleocene Thermal Maximum wet and warm conditions were constituted. This changed in the Oligocene to a semiarid climate, followed by more humid conditions in Miocene, semiarid conditions again in Pliocene and alternating semiarid and more wetter conditions in the Quaternary. This alternating climate changes strongly affected the topographic evolution and the generation of geomorphological surfaces (Panario et al, 2014).

During the Cenozoic, sea-level variations are recorded from drill-hole data (Ubilla et al., 2004) and marine sediments represent the Cretaceous-Tertiary boundary. The Cenozoic is represented by alluvial and fluvial deposits as well as landslide processes, which are linked to the Andean Orogeny (Ubilla et a., 2004).

4

Methods & Techniques

Contents

4.1 Basic principles

Thermochronologic methods, such as (U-Th-Sm)/He and fission-track (FT) dating, are based on the production of an isotope or radiation damage, resulting from nuclear decay, and the subsequent, thermally controlled retention of these decay products. As described e.g. by Reiners and Brandon (2006) the radioisotope production decreases exponentially with time but is predictable and otherwise steady, which gives the thermochronometer the ability to keep time. Due to the thermal sensitivity of thermochronometers, thereof revealed ages provide information about the cooling history of the rock, rather than the crystallization ages of its minerals (although in some cases they do record crystallization ages as well).

To resolve the thermal evolution of the Argentinean and Uruguayan passive continental margin, zircon and apatite fission-track (AFT, ZFT, respectively), zircon and apatite (U-Th-Sm)/He analyses (AHe, ZHe, respectively) were performed. Whenever possible all thermochronometers were applied to the same sample, allowing a more robust evaluation of the spatial and temporal cooling of the samples. Thermal modelling was used to determine the cooling histories of individual samples and trace their exhumation through the upper crust.

For this study 19 samples from the Sierras Septentrionales, 9 samples from the Sierras Australes, 1 sample from the Claromeco basin, 1 sample from the Lopez Lecube intrusion and 7 samples from Uruguay yielded enough apatite or zircon to proceed further thermochronological dating (Tab. 4-1, Tab. 4-2 & Tab. 4-3). The sampled lithologies reach from the Precambrian basement up to the Permian sandstones from the Tunas formation, while the Cambrian was not sampled as it is missing in the Sierras Australes and in the neighbouring Sierras Septentrionales. In the Sierras Septentrionales two Precambrian basement outcrops and a Ordovician rock were sampled.

To extract apatite crystals the collected samples were processed following the general heavy mineral separation routine (cp. Donelick et al. 2005 and literature cited therein). 7 samples could not be analysed, because they did not yield sufficient apatite grains for further analysis.

Tab. 4-1: Summary of the dated samples from the Sierras Septentrionales with corresponding sample numbers, lithologies, stratigraphic ages and coordinates (given in decimal degrees).

Sample No.	Lithology	Stratigraphy	Formation	Longitude	Latitude	altitude above sealevel [m]
ARG 01	Orthogneiss	Archean		-59.94886° E	-37.07085° N	153
ARG 02	Orthogneiss	Precambrian		-59.41496° E	-37.59413° N	273
ARG 03	Rhyolite	Ordovician		-59.42568° E	-37.64215° N	261
ARG 12-01	Mylonite	Paleoprot.	B.A.C.	-59.06554° E	-37.33711° N	218
ARG 12-02	Granite	Paleoprot.	B.A.C.	-58.99807° E	-37.38819° N	209
ARG 12-03	Mylonite	Paleoprot.	B.A.C.	-58.96817° E	-37.4178° N	224
ARG 12-04	Granitoide	Paleoprot.	B.A.C.	-58.95758° E	-37.34472° N	191
ARG 12-05	Granitoide	Paleoprot.	B.A.C.	-58.93459° E	-37.34899° N	191
ARG 12-06	Granitoide	Paleoprot.	B.A.C.	-59.10284° E	-37.37828° N	237
ARG 12-07	Granitoide	Paleoprot.	B.A.C.	-59.11284° E	-37.3977° N	235
ARG 12-08	metamorphic rock	Paleoprot.	B.A.C.	-59.97243° E	-37.29601° N	278
ARG 12-09	Granite	Paleoprot.	B.A.C.	-59.95081° E	-37.18212° N	280
ARG 12-10	Migmatite	Paleoprot.	B.A.C.	-60.05805° E	-37.08212° N	213
ARG 12-11	gran. Mylonite	Paleoprot.	B.A.C.	-59.75694° E	-37.06194° N	210
ARG 12-12	Granitoide	Paleoprot.	B.A.C.	-59.23391° E	-37.29571° N	201
ARG 12-13	Granitoide	Paleoprot.	B.A.C.	-59.19169° E	-37.42631° N	239
ARG 12-14	Gneiss	Paleoprot.	B.A.C.	-59.45934° E	-37.44442° N	239
ARG 12-16	Granitoide	Paleoprot.	B.A.C.	-58.92384° E	-37.46014° N	174
ARG 12-17	Mica-schist	Paleoprot.	B.A.C.	-58.62169° E	-37.62718° N	213
ARG 12-18	Gneiss	Paleoprot.	B.A.C.	-58.62169° E	-37.75377° N	136

Tab. 4-2: Summary of the dated samples the Sierras Australes with corresponding sample numbers, lithologies, stratigraphic ages and coordinates (given in degrees, decimal minutes).

Sample No.	Lithology	Stratigraphy	Formation	Longitude	Latitude	altitude above sealevel [m]
ARG 04	Clay-/Siltstone	Permian	Tunas	38° 3.307' S	60° 3.938' W	139
ARG 05	Syenite	Permian		38° 7.929' S	62° 42.613' W	96
ARG 06	Granite	Carboniferous-Jurassic		38° 4.238' S	62° 27.86' W	212
ARG 07	Ignimbrite	Paleozoic		37° 46.446' S	62° 17.345' W	375
ARG 08	Basement (Paragneiss)	Precambrian		37° 56.375' S	62° 10.305' W	426
ARG 09	Sandstone	Devonian/ Carboniferous	Lolen	38° 3.958' S	61° 52.247' W	353
ARG 09 A	granitic pebble from Diamictite	upper Carboniferous/Permian	Sauce Grande	38° 3.958' S	61° 52.247' W	353
ARG 10	granitic pebble from Diamictite	upper Carboniferous/ Permian	Sauce Grande	38° 7.816' S	61° 46.682' W	269
ARG 11	granitic pebble from Diamictite			38° 7.401' S	61° 48.066' W	258
ARG 12	Sandstone	Carboniferous/ Permian	Piedra Azul	38° 7.356' S	61° 43.775' W	319
ARG 13	Sandstone	Permian	Tunas	38° 3.516' S	61° 42.304' W	315
ARG 14	Sandstone	Permian	Tunas	38° 15.626' S	61° 21.537' W	367
ARG 15	Sandstone	Permian	Tunas	38° 12.629' S	61° 29.063' W	399
ARG 16	Diamictite	upper Carboniferous/ Permian	Sauce Grande	38° 0.287' S	61° 52.046' W	381
ARG 17	arkosic Sandstone	Permian	Tunas	37° 53.213' S	61° 51.585' W	416

Tab. 4-3: Summary of the dated samples from Uruguay with corresponding sample numbers, lithologies, stratigraphic ages and coordinates (given in degrees, decimal minutes).

Sample number	Lithology	Stratigraphy	Terrane	Longitude	Latitude	altitude above sealevel [m]
U 06	Gabbro	Precambrian	PAT	34°02'32''' S	056°59'17.2'' W	158
U 10	Granite	Precambrian	PAT	33°57'29.6'' S	056°14'16.2''W	126
U 11	Granitic gneiss	Precambrian	PAT	34°06'00.2''S	056°12'10.7''W	49
U 37	CDT granite	Precambrian	CDT	32°48'21.5''S	54°14'04.7''W	213
U 42	Orthogneiss	Precambrian	CDT	34°58'24.6''S	54°57'07.6''W	1
U 43	Gneiss	Precambrian	TT	34°55'14.1''S	56°10'08.1''W	14
U 47	Pegmatite	Precambrian	TT	34°55'53.1''S	56°09'31.1''W	0

4.2 Fission-Track dating and mineral separation

The fundamental concept of thermochonological methods is based on radiometric dating and the temperature-sensitivity of the particular system. Therefore the general decay equation describes the relationship between the decay of radiogenic mother isotopes and the production of measurable daughter isotopes:

$$N_d = N_{d0} + N_p(e^{\lambda t}-1)$$

As the sytem is thermodynamically at a certain temperature, the age is calculated with the general age equation:

$$t = \frac{1}{\lambda} ln\left(1+\frac{N_d}{N_p}\right)$$

The used thermochronomoeters are characterized by a thermally controlled retention or annealing of the decay products. This thermal dependency describes the cooling history of the particular sample and not the crystallization age (Reiners and Brandon, 2006). The data acquisition (Fig. 4.1) and the mineral separation (Fig. 4.2) for AFT and ZFT was completely executed in the Laboratories of the ThermoArcheo Research Group in Heidelberg. For counting and lengths measurement the Heidelberg Leitz FT station was used (Fig. 4.1). The basic concept of the fission-track dating technique is the spontaneous fission of ^{238}U, during which, the heavy fragments of this fission process leave chemically etchable latent tracks in minerals (e.g. apatite, zircon) and natural glasses (Wagner 1972). Information on the thermal history of apatite is stored in two archives: the etch pit areal density at an artificially polished internal surface, and the length distribution of horizontal confined tracks (e.g. Laslett et al. 1987, Green et al., 1986, Wagner and Van den Haute 1992; Lisker et al. 2009 and literature cited therein). Fission of ^{238}U generates spontaneous fission tracks (Fig. 4.3) that are metastable in relation to time and temperature. The temperature sensitive annealing of fission-tracks in apatite is constraint by two important effects

1.) the crystallographic orientation of the spontaneous tracks, and

2.) the chemical composition of the apatite.

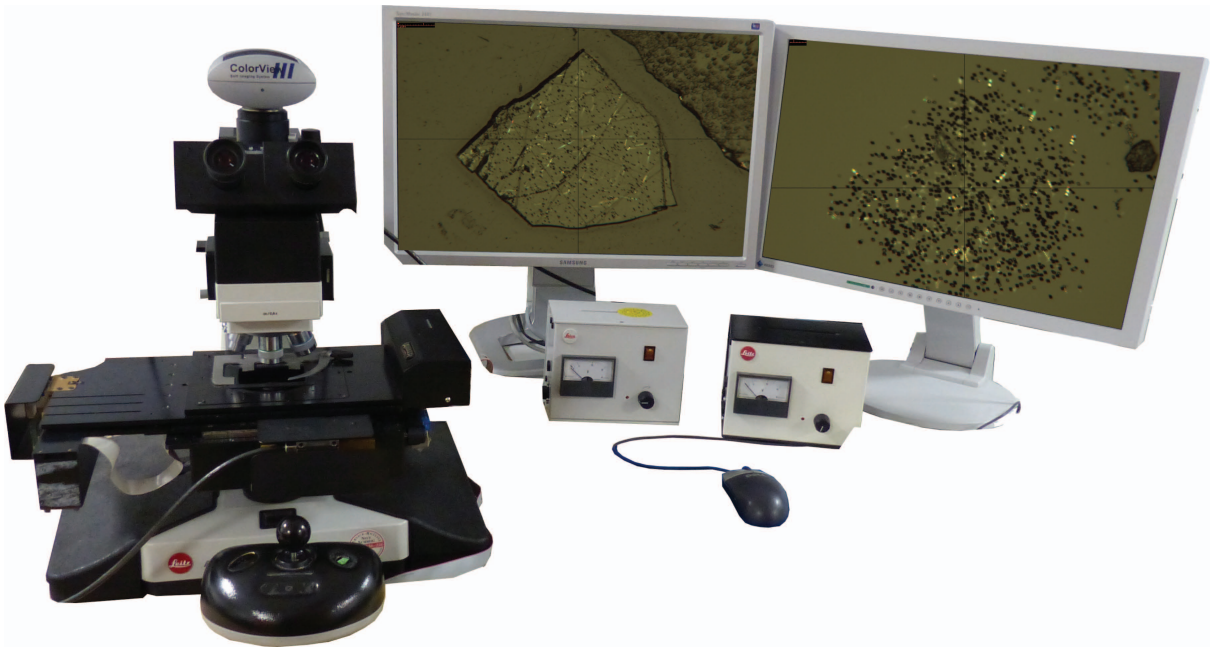

Fig. 4.1: Leitz FT station for data acquisition.

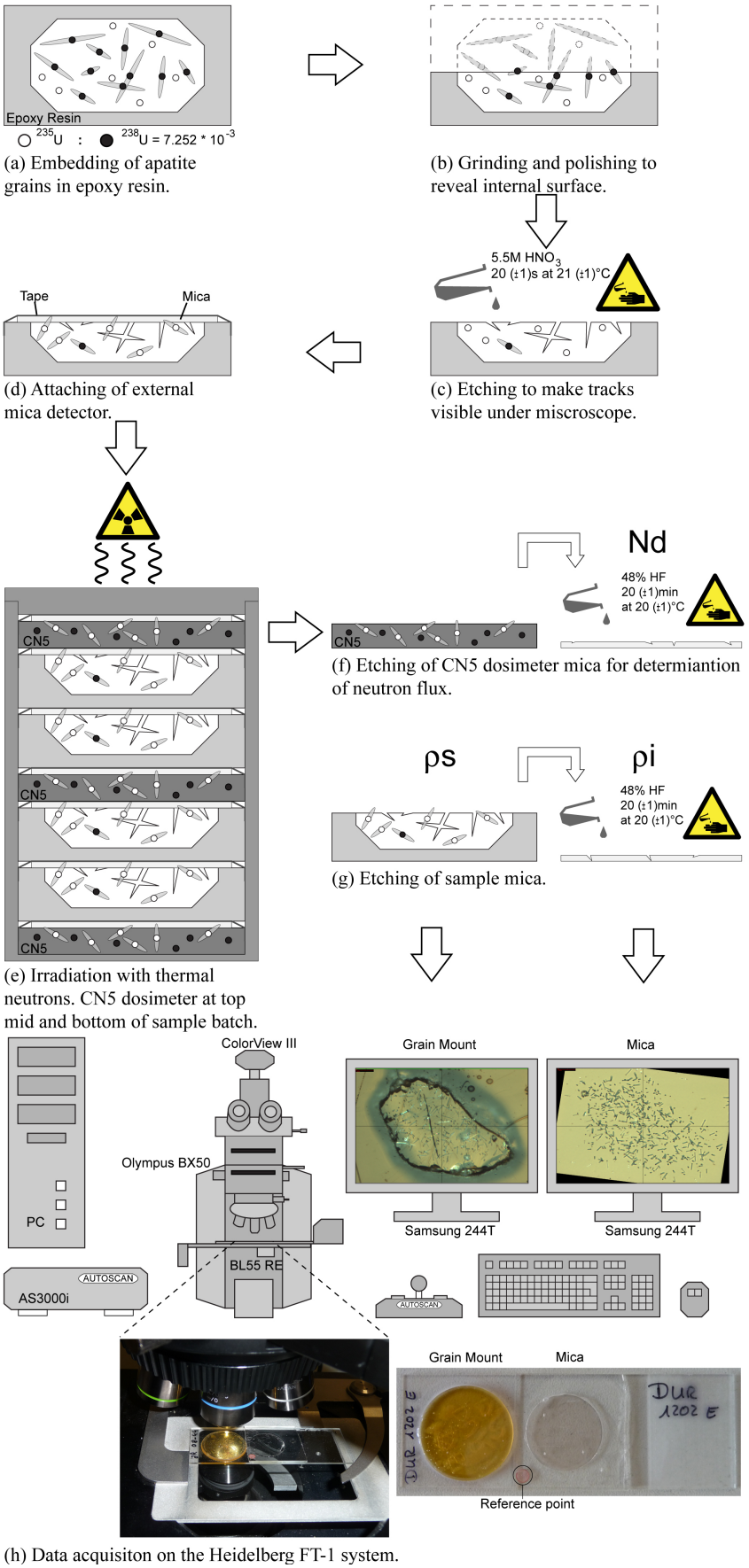

Fig. 4.2: Workflow for the apatite fission track analysis at the laboratory in Heidelberg (redrawn after Juez-Larre, 2003).

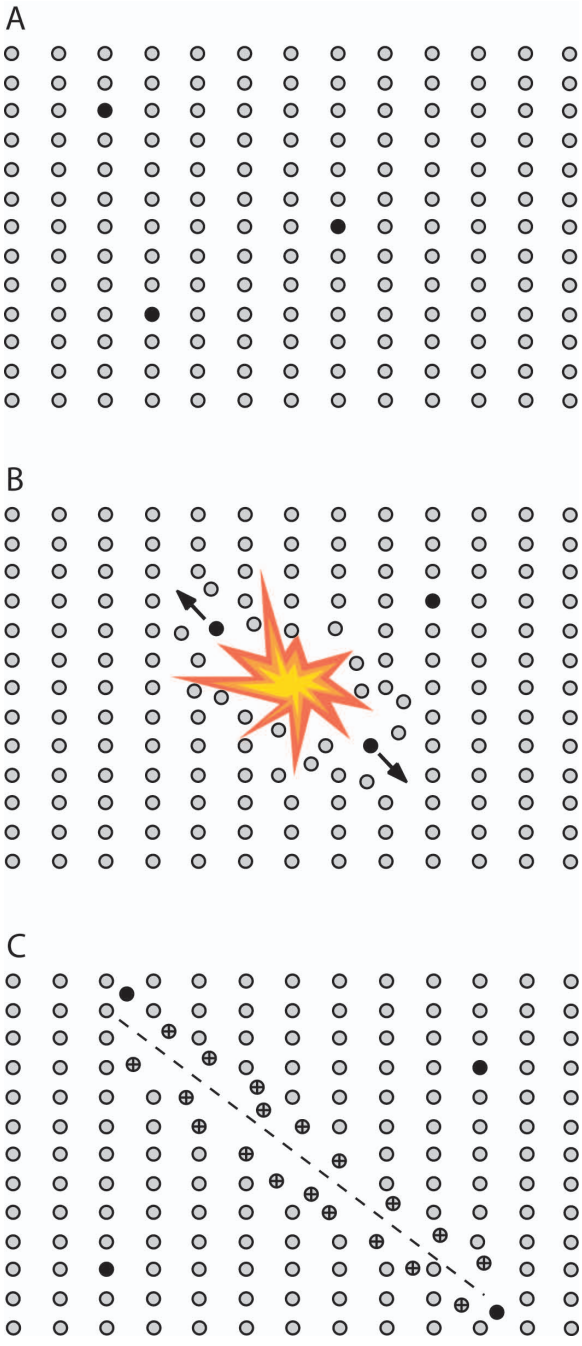

Fig. 4.3: Fission track formation (modified from Gallagher et al., 1998).(a) Trace amounts of radioactive ^{238}U are present in the crustal lattice (dark circles). (b) Spontaneous fission of ^{238}U produces two highly charged heavy particles. The masses of the two highly charged particles generally differ. The highly charged particles recoil as a result of Coulomb repulsion and interact with other atoms in the lattice initially by electron stripping or ionization. This leads to further deformation of the lattice as the ionized lattice atoms repel each other.(c) As the fission particles capture electrons, they slow down and begin to interact by atomic collisions, further reducing the particles' energy until they come to rest, leaving a damage trail or fission track. These cannot be observed optically unless chemically etched.

Tracks orthogonal to the c-axis anneal more rapid than tracks parallel to the c-axis (Green and Durrani 1977; Green 1981, 1988; Laslett et al. 1984; Donelick et al. 1999). Total annealing temperature of FT in apatite is governed by the fluorine- (90 - 110 °C/10 Myr) and chlorine content (110 - 150°C/10 Myr) (Fig. 4.5) . The partial annealing zone of FT's in apatite range down to 60°C/10 Myr. Annealing below 60 °C is still considered to be minor for 100 Myr time ranges. The change of arithmetic mean fission-track etch pit size parallel to the crystallographic c-axis (kinetic parameter D_{par}) is depended on the chemical composition and the etching conditions (5.5 N HNO^3, 20s, 21°C) (Sobel and Seward 2010, and literature therein). In zircon, the annealing process is also governed by the degree of metamictization. Metamictization is caused by the interaction of the alpha particle and the alpha-recoil nucleus with the crystal lattice of zircon (Zhang et al. 2008a,b; Nasdala 2009). The total annealing temperature of zircon decrease from 330 °C/10 Myr to 190 °C/10 Myr with increasing metamictization (Brix et al. 2002; Garver and Kamp 2002; Rahn et al. 2004).

With an average degree of metamictization a temperatures of about 240°C/10 Myr (Yamada et al, 1995, Hurford, 1986) is assumed.

Following the standard techniques for heavy mineral separation, as e.g. described by Grist and Ravenhurst (1992a, b), Donelick et al. (2005), apatite and zircon grains were prepared for the analysis of this study. The AFT grain mounts were etched in 5.5 N HNO_3 for 20 (±1) s at 21 (±1) °C and afterwards covered by U-free detection muscovite. The covered grain mounts, as well as two Durango apatite age standards and three glass neutron dosimeter (CN5, top, middle, and bottom of sample batch) were irradiated at the research reactor FRM II, Munich. After irradiation the detection mica were etched in 48 % HF for 20 (±1) min at 20 (±1) °C.

Zircons are embedded in Teflon sheets and etched in a NaOH – KOH eutectic melt at 228 (5)°C for 3-13 hours. The corresponding mica

external detectors were etched in 48% HF for 20 min at 20 (1) °C. The zircons were also irradiated in the research reactor FRM II in Munich, Germany in the presence of a glass neutron dosimeter (CN1) with known uranium content together a Fish River Canyon tuff zircon age standards. Area densities (tracks/cm²) of spontaneous and induced tracks, distribution of horizontal confined spontaneous fission-track lengths (length and c-axis related angle), and the c-axis oriented etch pit diameters (Dpar®, Donelick 1995, 1993) were measured with the Heidelberg FT-1 system (Fig. 4.1) . This system includes an optical microscope (Leitz) with a 3-axis microscope Autoscan®-stage, a high resolution Peltier-cooled CCD colour Olympus® CCD camera, and a high performing Windows® based computer system with two flat

screens. To advance the precision of the stage each axis is equipped with an external laser controlled Sony® sensor (BL 55 RE). These sensors guarantee a deviation of less than 500 nm along a movement of 4-5 cm. The whole setup is controlled by the Autoscan® Software trackscan® which also detects the track densities. Applying the largest possible resolution each pixel relates to less than 250 nm. Track densities were counted for apatites with a 80x objective (apatite) and 128 x objectives (zircon). Confined fission-track length and etch pit size of apatite fission-tracks were measured with a 100x objective using the Autoscan® computer code `EasyLength®`. The presented ages are central ages and were calculated by applying the ζ-method after Hurford and Green (1983, 1982). The ζ-value of 336.83 (19.51) for CN5 (apatite) and 123.0 (6.08) for CN1 (zircon) were gained using Durango apatite and Fish Canyon zircon age standards. All ages, 1ζ-errors and radial plots were calculated and drawn using the computer code `TRACKKEY`(Dunkl, 2002). Length measurements are presented in histograms. Certain lengths distributions represent different annealing histories and environments (Fig. 4.2).

4.3 (U-Th-Sm)/He-DATING

(U-Th-Sm)/He thermochronology is based on the accumulation of 4He during the α-disintegration of ^{238}U, ^{235}U, ^{232}Th, their daughter products and ^{147}Sm. The closure temperature (Tc) of mineral grains is dependent on: activation energy (E), a geometric factor for the crystal form (A), thermal diffusivity (D_0), the length of the average diffusion pathway from the interior to the surface of the grain (a) and the cooling rate at closure temperature (dT/dt) (Dodson, 1973). In general, the Tc of the apatite He system is ~70°C/1 Myr for cooling rates of 10°C/Myr, subgrain domain sizes > 60 µm and an activation energy of about 36 kcal/mol, and a log (D_0) of 7.7 (0.6) cm²/s (Farley, 2000). The crystal size itself represents the effective diffusion domain in apatites, with larger crystals having a higher closure temperature (Farley, 2000; Reiners and Farley, 2001). Alpha (α) particles are emitted with high kinetic energy during decay of U and Th, and travel significant distances before coming to rest, which in turn poses a complication for the He dating method, as α-particles may be ejected out of the crystal being dated or injected into the crystal from decay occurring in surrounding grains. Therefore, a correction has to be applied for the loss/gain of radiogenic He generated within an outer rim of the mineral grain by the α-stopping distances (for apatite: 25µm) (Wolf et al. 1996, Farley et al. 1996, Farley 2000). While the α-ejection correction is applied more routinely, the recently introduced correction for radiation damage is still in progress (Shuster et al. 2006; Shuster and Farley 2009; Flowers et al. 2007; Flowers et al. 2009). Shuster et al. (2006) noted that ^4He diffusion in apatite is impeded by radiation-induced damage to the crystal structure. Their ^4He production-diffusion model predicts that the effective ^4He closure temperature of apatite will vary with cooling rate and effective uranium concentration (eU), and may differ from the commonly assumed T_c of ~75 °C/1 Myr by up to ±15 °C (Shuster et al. 2006, Shuster and Farley 2009) (Fig. 4.5) . To account for the accumulation

of crystal defects due to the radioactive decay the eU factor (eU = [U] + 0.235 [Th], concentrations in weight %) was introduced (Shuster et al. 2006). This factor characterizes the dependency of ^{4}He-diffusion on the amount of accumulated crystal defects created by the movements of the fission products and the alpha-recoil nucleus' in the crystal lattice.

For the zircon He system the closure temperature is ~180°C/1 Myr, with the HePRZ in the range of ~170-200°C/Ma, given a cooling rate of 10°C/Myr, a crystal half width of 60 µm and an activation energy of ~170 kJ/mol (Reiners et al., 2002, 2004).

In the past for ZHe analysis the effects of radiation damage were seen as minor as long as U concentrations are less than ~1000 ppm; at higher U concentrations, however, zircon He ages decrease rapidly (cp. Reiners et al., 2004; Reiners, 2005). To accumulate corresponding radiation damage in zircons requires old ages, long-term residence at low temperatures, and relatively high U-Th concentrations (Reiners, 2005). While radiation damage in apatite leads to increased cooling ages (e.g. Shuster et al. 2006; Shuster and Farley 2009), He diffusivity in zircon is affected in a way, resulting either in younger or older cooling ages than it would be the case for a sample not influenced by radiation damage (Reiners et al. 2004, Farley 2007). Newer work done by Guenthner et al (2013) showed that two different effects of radiation damage affects the He diffusion in zircon. A step-heating experiment lead to decreasing diffusion, whereas diffusivity increases rapidly with increasing damage level of the crystal. This damage-diffusivity relationship combines both effects. Besides these factors and the cooling history of the host rock, the He diffusivity of a zircon can either be decreased, as He is trapped, resulting in a positive correlation with the eU content; or the He diffusivity can increase as numerous traps are connected, resulting in a negative correlation (cp. Guenthner et al. 2010). Such an inverse correlation can be seen by plotting the ZHe age as a function of eU (cp. Reiners 2005). If such a negative correlation trend is envisaged in the data the low-eU zircons are the most reliable ones to give a real ZHe cooling age. Compared with a compilation of data given by Reiners (2005) this trend falls right on top of the others, suggesting that above about 1 x 10^{18} α/g the ages start to get young as radiation damage has affected the He diffusivity.

The apatite and zircon single grain selection for (U-Th-Sm)/He dating was done in the Institute of Earth Sciences in Heidelberg by using a Olympus SZX 16 stereo microscope. It is equipped with two different lenses (Olympus SDF PLAPO 1XPF and the Olympus SDF PLAPO 2XPF). On top of the system a Olympus XC 50 with a Olympus TV1X-2 video adaptor tube is installed. As software for the selection and the measurements on the grains Olympus Stream Enterprise v. 1.5.1 was used. Each grain was photographed and measured for standard morphometric α-ejection age corrections. The aliquots were filled in Pt respectively Nb foil tubes and sent to the (U-Th-Sm)/He laboratory of Prof. Daniel F. Stockli at the Department of Geology of the University of Kansas (http://www.jsg.utexas.edu/he-lab). There the grains were loaded in the automated (U-Th-Sm)/He laser extraction line for extracting the radiogenic 4He in an ultrahigh vacuum chamber through heating with an Nd-YAG laser. The released gas was measured and quantified in terms of ^{4}He/^{3}He ratios with a quadrupole He mass spectrometry system. After complete degassing the aliquots were unwrapped and dissolved for U, Th, and Sm determination. For apatite, samples were spiked with ^{235}U, ^{230}Th, and ^{149}Sm and dissolved in 30% HNO_3 (90°C for 1 hour) whereas zircons were dissolved using standard U-Pb double pressure-vessel digestion procedures (HF-HNO_3 and HCl) for 4 days. After dissolution the single aliquots were analyzed in consideration of U, Th, and Sm using a VG PlasmaQuad IIXS Inductively Coupled Plasma Mass Spectrometer (ICP-MS). Further information of the analytical method is documented on the homepage of the Department of Geology of the University of Kansas (www.geo.

ku.edu/programs/tectonics). In order to minimize effects caused by undetected mineral inclusions, both mineral phases i.e. zircon and apatite were bombed to ensure complete digestions as described in Vermeesch et al. (2007). Reported errors are 6% for apatite and 8% for zircon based on the respective reproducibility of the Fish Canyon age standards. If the reproducibility of aliquots within one sample is poorer than 6% or 8% respectively the corresponding error is reported. All quantities were measured on a single crystal to eliminate uncertainties that arise from grain to grain heterogeneities; resulting He ages were corrected for α-ejection (Tab. 5, 6). For further details on the He analytical techniques see Farley (2002), Mitchell and Reiners (2003), and Reiners (2005).

4.4 2D THERMOKINEMATIC MODELING AND CALCULATION OF EXHUMATION RATES

One aim of thermochronological analysis is to determine the cooling and exhumation rates for crustal segments. Besides the direct quantification by using age-elevation plots, exhumation rates can be calculated by combining the cooling history determined by numerical modeling and assumed past geothermal gradients (Fig. 4.4). The software code HeFTy (Ketcham 2005; Ketcham et al. 2009; 2007a, b), allows to test geological time-temperature (t-T) evolutions (heating and cooling histories) against the thermochronological data set. Representative geological time-temperature histories are constructed from published geological data. The data used for the modeling are:

- AFT: single grain ages, confined spontaneous fission-track length distribution (> 50 individual length) corrected for c-axis related angle (Donelick et al. 1999; Ketcham 2009), etch pit size (Dpar®), annealing kinetics of Ketcham
- ZFT: only the central age based on laboratory work
- AHe: U-, Th-, and Sm concentration, radius of the single grains, uncorrected single grain ages, diffusion kinetics of Farley (2000)
- ZHe: U-, Th-, and Sm concentration, radius of the single grains, uncorrected single grain ages, diffusion kinetics of Reiners et al. (2004).

The software allows creating t-T forward models for the AFT models by calculating the apatite fission-track length distribution, and the apparent age and AHe and ZHe models by calculating a model age and a He-distribution within the grains. The initial inverse modeling is based on the best forward model revealed. The geologically framed

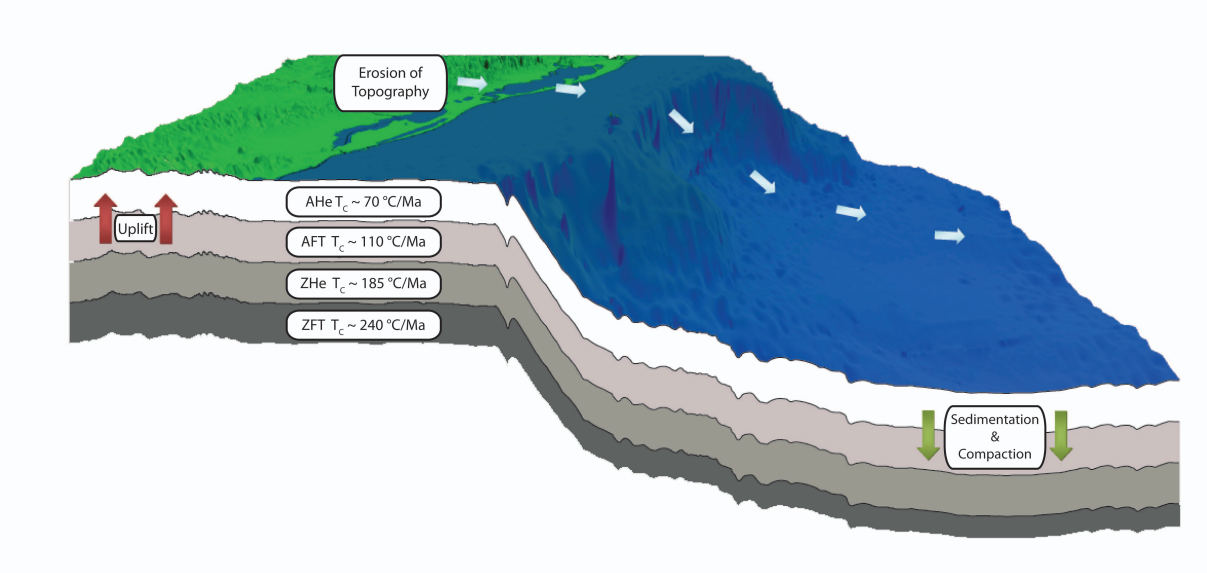

Fig. 4.4: Depth-Temperature relation for different thermochronometers (based on the DEM-90 m by Jarvis et al., 2008) on a low-elevated passive continental margin (e.g. SE-Uruguay).

t-T coordinates are included in the software as t-T boxes, that cover the possible error range of the t-T coordinates. For each sample we performed the numerical modeling as long as the program provides the same t-T evolution after the runs. In all cases presented in this publication, we tested 50.000 single t-T paths against the data set. Statistical tests are used to compare the calculated age and confined spontaneous fission-track length distribution against the determined thermochronological data set. The statistical test calculates a "goodness of fit" (GOF) value between 0 and 1. GOF values of ≥ 0.05 (≥ 5%) are an "acceptable" result (displayed as green paths), GOF values ≥ 0.5 (≥ 50%) are a "good" result (displayed as purple paths). The program also displays the t-T path with the "best GOF" fitting (Ketcham 2009; Ketcham et al. 2009). This path must neither be the right nor the only temperature history.

5

Thermochronological data and t-T modeling

Contents

5.1 Introduction

Most of the measured thermochronological ages are younger than the corresponding sedimentation, intrusion or metamorphic ages. Within error, AHe-ages generally range between 120.8 (7.3) Ma and 163.0 (9.8) Ma. AFT ages vary between 129.2 (9.3) Ma and 242.7 (17.1) Ma, whereas ZHe ages lie between 198.7 (15.9) Ma and 272.7 (16.4) Ma. ZFT ages range between 223.7 (32.1) Ma and 262.4 (36.1) Ma. The following dataset is sorted by the geographical distribution: 1. Sierras Septentrionales; 2. Sierras Australes (east of the Sauce Grande wrench) and the Claromeco basin; 3. Sierras Australes (west of the Sauce Grande wrench); 4. Permian intrusion of Lopez Lecube and 5. the thermochonological data from Uruguay.

The ages west of SGW vary slightly from the ages east of the SGW. In the high-metamorphic western part (ARG 05, ARG 07, ARG 08, ARG 09) of the mountain range (Curamalal group, Bravard group and the Ventana group) the ages are slightly older than the ages from the lower-metamorphic eastern part (ARG 10, ARG 12, ARG 14, ARG 15, ARG 16. ARG 17).

As already mentioned the Sierras Septentrionales are seen as a southern extension of the Rio de la Plata Craton. In contrary to this fact, the Sierras Australes experienced a completely different formation history. The Sierras Australes are correlated with the South African Cape fold-belt (Lopez-Gamundi & Rossello, 1998) and were influenced by a much higher tectonic overprint as the Sierras Septentrionales. Following the segmentation of the continental margin (Franke et al., 2007) the ages from the Sierras Septentrionales can be compared to those of the eastern part of the Sierras Australes in terms of different age clusters.

The measured spontaneous confined fission-track lengths are reported as corrected (LC) and uncorrected (CT) length data. In total, 691 fission-track lengths were measured in the apatite samples from the Sierras Septentrionales (Tab. 5-1). The mean corrected length values range from 9.8 (1) µm to 13.0 (1.5) µm. The fission-track lengths distribution for each sample shows the typical trend of a sample with a homogeneous, constant cooling. Of course, the overall trend of the models does not represent a constant cooling history, however since reaching the closure temperature and the partial annealing zone, the paths are following a constant trend until nowadays surface conditions.

The corresponding Dpar values (in total 1875 measurements) range between 1.1 (0.1) µm and 1.9 (0.1) µm, and are therefore by trend rather short. Carlson (1990) reported that fission tracks in grains are more stable against annealing with increasing CL/F ratio, suggesting that small Dpars are common in Fluorine-rich grains and bigger Dpars represent chlorine-rich grains.

The length data from the Sierras Australes (Tab. 5-2) are also presented as corrected (LC) and uncorrected (CT) fission-track lengths. The lengths data from the Sierras Australes revealed 388 lengths from 7 samples. The mean corrected length values range from 11.3 (1.8) µm to 13.1 (1.4) µm. The lengths distributions from the Sierras Australes show some variety due to the varying lithology and differing thermal histories the samples experienced. The corresponding Dpar values (in total 385 measurements) range between 1.7 (0.2) µm and 1.9 (0.2) µm and ,therefore, are by trend mid-ranged.

As mentioned above, small Dpar-values represent Fluorine-rich grains, whereas bigger Dpars represent chlorine-rich grains. In this case the mean Dpar-values indicate a relatively balanced Cl/F ratio.The lengths data from Uruguay (Tab. 5-3) are also presented as corrected (LC) and uncorrected (CT) fission-track lengths. The measured mean corrected lengths (280 measurements from 4 samples) from Uruguay range from 10.8 (1.4) µm to 12.2 (1.5) µm. The measured lengths distributions show some variety, but represent high values for confined tracks. This fact points towards a homogenous, constant cooling after passing the closure temperature and the

PAZ. The corresponding Dpar values (in total 420 measurements) range between 1.3 (0.2) µm and 1.6 (0.2) µm. The lower Dpar-values point to Fluorine-rich crystals.

Tab. 5-1: Apatite fission-track length and Dpar data of the Sierras Septentrionales. n CT: number of measured confined tracks, CT mean: mean confined track length, std: standard deviation, skew: skewness of distribution relative to the mean value (measure of asymmetry of the distribution), Lc mean: mean track length after c-axis correction, n Dpar: number of etch pit diameters measured, Dpar mean: mean etch pit diameter.

Sample number	n CT	CT mean (µm)	CT std (µm)	CT skew	Lc mean (µm)	Lc std (µm)	Lc skew	n Dpar	Dpar mean (µm)	Dpar std (µm)	Dpar skew
ARG 01	51	11.7	2.1	-0.304	13.2	1.4	-0.297	50	1.9	0.1	-0.899
ARG 02	51	12.5	1.6	-0.074	13.9	1.0	0.257	50	1.8	0.2	-0.184
ARG 12-01	8	12.1	1.9	-0.975	n.a.	n.a.	n.a.	70	1.2	0.2	0.561
ARG 12-02	102	12.6	1.6	-0.81	13.9	1.1	-0.831	155	1.4	0.2	0.444
ARG 12-04	5	9.8	1	0.199	n.a.	n.a.	n.a.	105	1.1	0.1	0.291
ARG 12-05	13	11.3	2.5	-0.246	n.a.	n.a.	n.a.	135	1.1	0.2	0.454
ARG 12-06	3	13	1.5	-1.732	n.a.	n.a.	n.a.	124	1.1	0.2	-0.139
ARG 12-07	20	12.9	1.5	-1	n.a.	n.a.	n.a.	27	1.3	0.2	0.047
ARG 12-08	2	12.7	0.6	-	n.a.	n.a.	n.a.	160	1.3	0.2	0.25
ARG 12-09	76	11.8	1.8	-0.297	13.5	1.3	-0.832	30	1.3	0.2	0.776
ARG 12-10	101	12.4	1.6	-0.643	13.9	1.2	-0.741	225	1.1	0.1	0.748
ARG 12-12	65	12.2	1.5	-0.727	13.7	1.1	-0.732	175	1.4	0.2	0.293
ARG 12-13	9	11.8	1.8	0.688	n.a.	n.a.	n.a.	175	1.1	0.2	-0.081
ARG 12-14	83	12.7	1.1	-0.557	14.2	0.7	-0.714	90	1.5	0.3	0.16
ARG 12-16	29	12.3	1.3	-0.154	n.a.	n.a.	n.a.	150	1.2	0.2	-0.228
ARG 12-18	73	11.8	1.2	-0.424	13.5	0.8	-0.524	154	1.1	0.1	-0.365

Tab. 5-2: Apatite fission-track length and Dpar data of the Sierras Australes. n CT: number of measured confined tracks, CT mean: mean confined track length, std: standard deviation, skew: skewness of distribution relative to the mean value (measure of asymmetry of the distribution), Lc mean: mean track length after c-axis correction, n Dpar: number of etch pit diameters measured, Dpar mean: mean etch pit diameter.

Sample number	n CT	CT mean (µm)	CT std (µm)	CT skew	Lc mean (µm)	Lc std (µm)	Lc skew	n Dpar	Dpar mean (µm)	Dpar std (µm)	Dpar skew
Sierras Septentrionales											
ARG 01	51	11.7	2.1	-0.304	13.2	1.4	-0.297	50	1.9	0.1	-0.899
ARG 02	51	12.5	1.6	-0.074	13.9	1.0	0.257	50	1.8	0.2	-0.184
Sierras Australes											
West of Sauce Grande wrench											
ARG 05	56	11.7	1.6	0.074	13.4	1.2	-0.029	55	1.9	0.2	0.239
ARG 08	51	13.0	1.6	-0.118	14.3	1.1	-0.171	50	1.8	0.2	-0.722
ARG 09	48	12.9	1.7	-0.110	14.2	1.2	-0.266	55	1.8	0.2	-1.221
East of Sauce Grande wrench											
ARG 12	52	11.3	1.8	0.224	13.0	1.4	-0.302	55	1.7	0.2	1.112
ARG 15	79	13.1	1.4	-0.639	14.3	1.1	-1.339	70	1.9	0.2	0.209

Tab. 5-3: Apatite fission-track length and Dpar data of Uruguay. n CT: number of measured confined tracks, CT mean: mean confined track length, std: standard deviation, skew: skewness of distribution relative to the mean value (measure of asymmetry of the distribution), Lc mean: mean track length after c-axis correction, n Dpar: number of etch pit diameters measured, Dpar mean: mean etch pit diameter.

Sample No.	n CT	CT mean (µm)	CT std (µm)	CT skew	Lc mean (µm)	Lc std (µm)	Lc skew	n Dpar	Dpar mean (µm)	Dpar std (µm)	Dpar skew
U 06	65	12.2	1.5	-0.072	13.7	1.2	-0.8	110	1.6	0.2	0.878
U 11	95	11.2	1.2	0.202	13.1	0.8	0.1	105	1.3	0.2	0.01
U 37	70	11.0	1.7	0.101	12.9	1.2	0.3	95	1.4	0.2	0.363
U 43	50	10.8	1.4	-0.055	12.8	0.9	0.0	110	1.3	0.2	-0.157

5.2 Sierras Septentrionales

5.2.1 Ages - Lengths - Dpar

As mentioned in the introduction, all thermochonological ages (Fig. 5.1) are reset and younger than their crystallisation or sedimentation age (Tab. 5-4; Tab. 5-5; Tab. 5-6; Tab. 5-7). Sample ARG 01 from the Buenos Aires Complex revealed an AHe age of 121.2 (7.3) Ma, an AFT-age of 129.2 (9.3) Ma and a ZHe-age of 343.6 (27.5) Ma. If considering the 1 σ-error of the thermochronological techniques this Archean orthogneiss (ARG 01, 153 m a.s.l.) of the Sierras Septentrionales is characterized by overlapping AHe- and AFT-ages , which might be interpreted as fast cooling and possibly fast exhumation at around 130 Ma.

Both age-elevation plots (Fig. 5.2, Fig. 5.3) of the Sierras Septentrionales (AFT and ZHe) reveal multiple tectonic (in this case vertical) movements along faults. Throughout the area at similar topographic altitudes, a wide range of AFT-, and ZHe-ages, were detected. This can be explained by vertical movements between both localities. As the area is cut by several faults, reactivation of these faults between 100 Ma and 150 Ma is visible.

The ages of the Sierras Septentrionales (detailed spread sheets of the fission-track data are listed in the appendix) can be divided into two clusters. A younger cluster and an older cluster (circles in Fig. 5.2). As all measured samples were taken from Precambrian rocks, this discrepancy is only explainable by a partial thermal overprint. Two causes for this overprint are reasonable. Cingolani et al. (2010) reported a thermal influence in the area due to hot fluids, that caused also mineral alterations. As no concrete temperature range and timing is known, a thermal influence by younger overlaying basalts is reasonable. This influence is only visible in the AFT-plot.

The relation between the Uranium content and the corresponding single grain age is presented in Fig. 5.4, Fig. 5.5, Fig. 5.6, Fig. 5.7, Fig. 5.8 and Fig. 5.9. These Diagrams illustrate the relation or

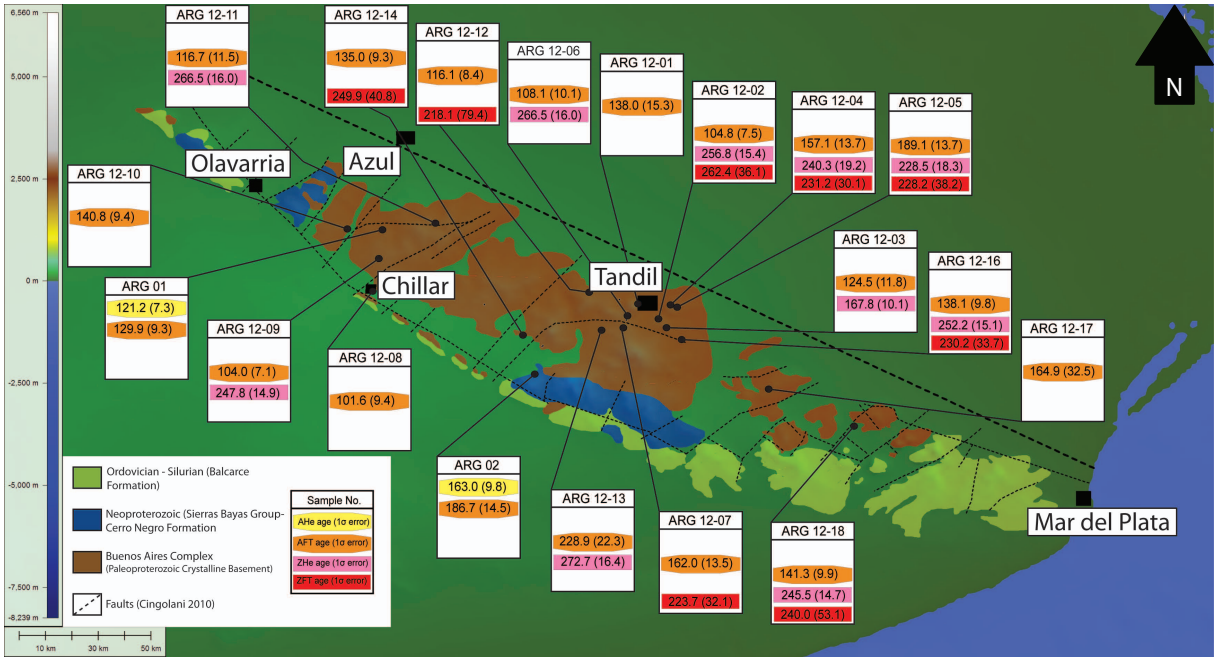

Fig. 5.1: Geological map (redrawn after Cingolani, 2010) and thermochronological data from the Sierras Septentrionales (combined with DEM-90 m by Jarvis et al., 2008).

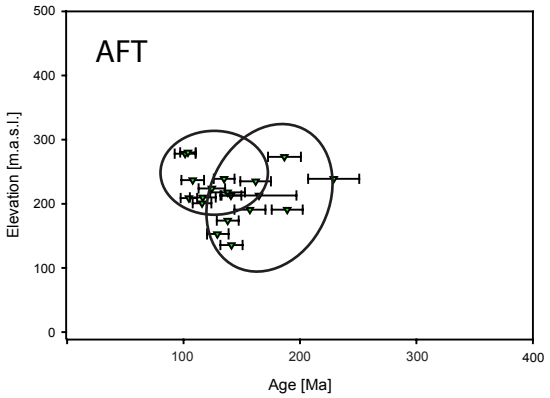

Fig. 5.2: AFT-age-elevation plot of the Sierras Septentrionales

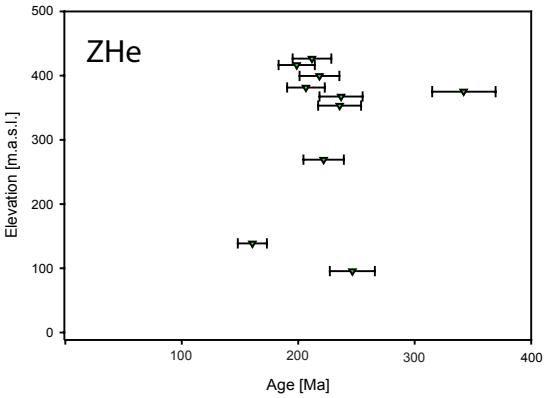

Fig. 5.3: ZHe-age-elevation plot of the Sierras Septentrionales

Tab. 5-4: Summary of apatite (U-Th-Sm)/He data of the Sierras Septentrionales. M: mass, contributing U, Th, Sm,and He concentration, eU = [U] + 0.235 [Th] (concentration in weight %), Ft: α ejection factor for apatite and zircon calculated after Farley et al. (1996), Raw (raw) ages and 1σ error for α-ejection with accordant 1σ error. The brown marked grains were the grains of our choice.

S.-No.	Lith.	U [µg/g]	Th [µg/g]	Sm [µg/g]	eU	Th/U	He [nmol/g]	M [ug]	Ft	raw Age	± 1σ raw age	Age [Ma]	± 1σ [Ma]
aARG01-1	Othogn.	96.7	121.8	125.0	125.3	1.26	55.9	2.28	0.67	81.5	4.9	121.2	7.3
aARG01-2	Othogn.	109.2	112.7	112.7	135.7	1.03	78.3	2.11	0.65	105.4	6.3	161.8	9.7
aARG01-3	Othogn.	123.0	174.4	166.1	163.9	1.42	68.5	2.24	0.67	76.3	4.6	114.1	6.8
aARG02-1	Othogn.	3.3	0.7	31.1	3.6	0.20	2.0	1.06	0.61	98.9	5.9	163.0	9.8
aARG02-2	Othogn.	18.3	1.6	32.6	18.8	0.09	8.7	0.98	0.59	84.7	5.1	143.0	8.5
aARG02-3	Othogn.	5.2	0.3	23.3	5.4	0.05	2.6	2.74	0.71	86.5	5.2	121.6	7.2

Tab. 5-5: Apatite fission-track data of the Sierras Septentrionales. U: uranium concentration in µg/g, n: number of counted grains, ρS: density of spontaneous tracks (x 105/cm²), Ns: number of spontaneous tracks, ρI: density of induced tracks (x 105/cm²), NI: number of induced tracks, P(χ^2) is the probability that single grain ages are consistent and belong to the same population. Test is passed if P(χ^2) > 5% (Galbraith, 1981). Ages calculated using a ζ- value of 336.83 (19.51) a/cm² for apatite, Nd =15148 tracks. (White lines measured by Sebastian Kollenz, brown lines measured by Sabrina Pfister).

S.-No.	Elevation [m.a.s.l.]	Lithology	Stratigraphy	n	U (std) [µg/g]	ρ_s	N_s	ρ_i	N_i	χ^2 [%]	Central age ± (1σ) [Ma]
ARG 01	153	Orthogneiss	Archean	20	38.5 (16.9)	23.349	867	43.519	1616	54.13	129.2 (9.3)
ARG 02	273	Orthogneiss	Precambrian	20	14.8 (5.6)	14.974	678	19.125	866	96.27	186.7 (14.5)
ARG 12-01	218	Mylonite	Paleoproterocoic	13	27.44 (14.2)	0.178	187	0.275	289	99.97	138.0 (15.3)
ARG 12-02	209	Granite	Paleoproterocoic	20	51.06 (18.9)	0.251	645	0.502	1288	99.15	104.8 (7.5)
ARG 12-03	224	Mylonite	Paleoproterocoic	20	7.68 (3.6)	0.051	255	0.086	431	100	124.5 (11.8)
ARG 12-04	191	Granitoid	Paleoproterocoic	27	9.23 (3.7)	0.073	354	0.099	476	99.1	157.1 (13.7)
ARG 12-05	191	Granitoid	Paleoproterocoic	23	16.22 (6.1)	0.173	744	0.194	834	90.64	189.1 (13.7)
ARG 12-06	237	Granitoid	Paleoproterocoic	6	32.84 (4.3)	0.182	284	0.371	580	98.62	108.1 (10.1)
ARG 12-07	235	Granitoid	Paleoproterocoic	24	15.68 (7.1)	0.127	417	0.168	554	99.89	162.0 (13.5)
ARG 12-08	278	Metamorphic rock	Paleoproterocoic	13	37.33 (22.7)	0.175	280	0.385	616	96.95	101.6 (9.4)
ARG 12-09	280	Granite	Paleoproterocoic	23	28.68 (8.0)	0.156	769	0.33	1629	81.53	104.0 (7.1)
ARG 12-10	213	Migmatite	Paleoproterocoic	24	31.69 (10.8)	0.225	960	0.352	1506	99.74	140.8 (9.4)
ARG 12-11	210	granitic Mylonite	Paleoproterocoic	20	9.32 (3.3)	0.056	239	0.11	469	100	116.7 (11.5)
ARG 12-12	201	Granitoid	Paleoproterocoic	25	22.73 (10.9)	0.137	613	0.265	1187	86.99	116.1 (8.4)
ARG 12-13	239	Granitoid	Paleoproterocoic	17	12.79 (4.7)	0.149	331	0.149	332	99.96	228.9 (22.3)
ARG 12-14	239	Gneiss	Paleoproterocoic	21	26.32 (9.7)	0.168	818	0.281	1368	61.21	135.0 (9.3)
ARG 12-16	174	Granitoid	Paleoproterocoic	22	17.49 (4.2)	0.128	703	0.211	1156	97.13	138.1 (9.8)
ARG 12-17	213	Mica shist	Paleoproterocoic	14	2.89 (1.6)	0.023	48	0.033	68	99.84	164.9 (32.5)
ARG 12-18	136	Gneiss	Paleoproterocoic	21	16.55 (7.9)	0.115	735	0.186	1188	98.58	141.3 (9.9)

Tab. 5-6: Summary of zircon (U-Th-Sm)/He data from the Sierras Septentrionales. M: mass, contributing U, Th, Sm,and He concentration, eU = [U] + 0.235 [Th] (concentration in weight %), Ft: α-ejection factor for apatite and zircon calculated after Farley et al. (1996), Raw (raw) ages and 1σ error for α-ejection with accordant 1σ error. Zircon-He data from the Sierras Septentrionales. The brown marked grains were chosen for continuative laboratory work.

S.-No.	Lithology	U [µg/g]	Th [µg/g]	Sm [µg/g]	eU	Th/U	He [nmol/g]	M	Ft	raw Age	± 1σ raw age	Age [Ma]	± 1σ [Ma]
ARG12-02-1	Granite	48.1	79.2	14.5	66.4	1.65	36.7	5.82	0.76	101.01	6.06	132.7	8.0
ARG12-02-2	Granite	20.0	39.5	4.5	29.2	1.97	32.8	8.93	0.79	203.48	12.21	256.8	15.4
ARG12-02-3	Granite	60.6	47.2	0.5	71.4	0.78	122.0	64.07	0.89	307.19	18.43	344.1	20.7
ARG12-03-1	Mylonite	323.1	42.6	8.4	332.9	0.13	246.6	10.32	0.81	135.67	8.14	167.8	10.1
ARG12-03-3	Mylonite	3.0	13.1	5.3	6.1	4.38	1.8	3.32	0.71	55.13	3.31	77.6	4.7
ARG12-04-1	Granitoid	183.6	42.9	11.1	193.5	0.23	231.2	18.61	0.84	216.99	17.36	258.1	20.7
ARG12-04-2	Granitoid	159.4	32.6	4.6	166.9	0.20	178.8	11.02	0.81	194.99	15.60	240.3	19.2
ARG12-04-3	Granitoid	159.4	53.0	3.1	171.6	0.33	199.2	17.49	0.84	210.85	16.87	250.9	20.1
ARG12-05-1	Granitoid	147.4	45.5	2.0	157.8	0.31	301.0	21.14	0.84	341.93	27.35	405.2	32.4
ARG12-05-2	Granitoid	337.7	91.5	4.4	358.8	0.27	370.6	13.57	0.82	188.12	15.05	228.5	18.3
ARG12-06-1	Granitoid	94.2	34.6	2.7	102.2	0.37	204.9	3.30	0.73	358.82	21.53	489.0	29.3
ARG12-06-2	Granitoid	191.5	94.0	4.7	213.1	0.49	206.9	3.45	0.74	176.87	10.61	240.6	14.4
ARG12-06-3	Granitoid	126.2	57.0	2.5	139.4	0.45	151.7	3.83	0.74	197.96	11.88	266.5	16.0
ARG12-09-2	Granite	190.4	31.6	3.4	197.7	0.17	193.1	3.55	0.72	178.19	10.69	247.8	14.9
ARG12-09-3	Granite	199.9	32.4	2.4	207.4	0.16	190.0	6.58	0.76	167.32	10.04	220.9	13.3
ARG12-10-1	Migmatite	775.4	117.1	5.1	802.3	0.15	228.5	20.94	0.85	52.58	3.16	62.1	3.7
ARG12-10-2	Migmatite	1023.2	202.0	55.9	1070.0	0.20	255.4	14.88	0.83	44.08	2.65	53.4	3.2
ARG12-11-1	gran. Mylo.	283.8	113.0	3.2	309.9	0.40	261.0	4.06	0.74	153.87	9.23	208.9	12.5
ARG12-11-2	gran. Mylo.	259.9	97.3	3.2	282.3	0.37	211.2	3.37	0.73	136.89	8.21	188.2	11.3
ARG12-11-3	gran. Mylo.	297.8	62.7	2.3	312.3	0.21	375.3	13.40	0.82	218.27	13.10	266.5	16.0
ARG12-12-1	Granitoid	802.6	258.6	15.3	862.2	0.32	388.9	8.76	0.79	82.95	4.98	104.9	6.3
ARG12-12-2	Granitoid	790.5	140.3	8.3	822.8	0.18	208.1	3.35	0.71	46.72	2.80	65.5	4.0
ARG12-12-3	Granitoid	1211.1	80.5	27.8	1229.8	0.07	338.1	2.57	0.69	50.79	3.05	73.8	4.4
ARG12-13-1	Granitoid	162.8	82.1	0.6	181.7	0.50	232.2	29.58	0.85	231.66	13.90	272.7	16.4
ARG12-13-2	Granitoid	247.4	119.2	2.4	274.8	0.48	382.3	29.04	0.85	251.67	15.10	297.5	17.9
ARG12-13-3	Granitoid	85.9	46.5	0.4	96.6	0.54	205.5	28.32	0.86	379.74	22.78	443.7	26.6
ARG12-16-1	Granitoid	34.4	9.9	1.0	36.7	0.29	191.8	2.73	0.71	873.68	52.42	1234.2	74.1
ARG12-16-2	Granitoid	367.0	66.2	12.8	382.3	0.18	372.1	2.67	0.70	177.52	10.65	252.2	15.1
ARG12-18-1	Gneiss	135.1	28.3	0.9	141.7	0.21	221.3	3.93	0.75	281.85	16.91	377.7	22.7
ARG12-18-2	Gneiss	268.9	56.1	5.9	281.8	0.21	300.1	8.41	0.79	193.88	11.63	245.5	14.7

Tab. 5-7: Zircon fission track data from the Sierras Septentrionales.

S.-No.	Elev. [m.a.s.l.]	Form. age	U [µg/g]	n	Sp. Tracks ρ_s	Sp. Tracks N_s	Ind. Tracks ρ_i	Ind. Tracks N_i	χ^2 [%]	Central age (1σ) [Ma]
ARG 12-02	209	Paläoprot.	215.09	11	280.148	478	41.026	70	100.0	262.0 (36.1)
ARG 12-04	191	Paläoprot.	267.41	9	315.585	482	53.034	81	100.0	231.2 (30.1)
ARG 12-05	191	Paläoprot.	309.31	8	282.442	273	47.591	46	99.99	228.2 (38.2)
ARG 12-07	235	Paläoprot.	162.75	10	126.83	377	21.867	65	99.14	223.7 (32.1)
ARG 12-12	201	Paläoprot.	191.66	2	217.347	53	36.908	9	87.96	218.1 (79.4)
ARG 12-14	239	Paläoprot.	252.45	9	284.357	310	44.029	48	99.24	249.9 (40.8)
ARG 12-16	174	Paläoprot.	209.54	11	199.682	370	33.46	62	100.00	230.2 (33.7)
ARG 12-18	136	Paläoprot.	178.01	3	229.183	156	36.728	25	96.27	240.0 (53.1)

trend between the two parameters, e.g. if grains with high (or low) Uranium content produce older (or younger) single grain ages. Three samples from the Sierras Septentrionales (ARG 12-02, ARG 12-04, ARG 12-05 show tendencies to a negative trend, meaning that grains with lower Uranium contents show older ages. A positive trend (high Uranium content leads to older ages) is not visible in the data set. Two more samples (ARG 12-07, ARG 12-16) point towards a balanced ration of Uranium and the corresponding age, suggesting that no trend is visible. The ages show no dependencies on the Uranium content. The dependency of Uranium content on the single grain ages leads to the assumption of a lower closure temperature for ZFT, as the closure temperature is rising with a higher grade of metamictization of the zircon grains.

The lengths distributions for the Precambrian samples from the Sierras Septentrionales (ARG 01, ARG 02) are similar to the typical distribution for basement and metamorphic influenced rocks

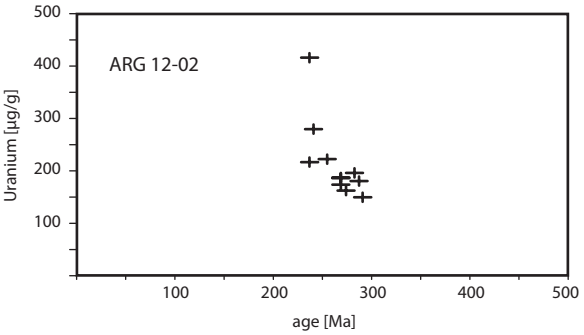

Fig. 5.4: Uranium-age ratio for the single grains of ARG 12-02.

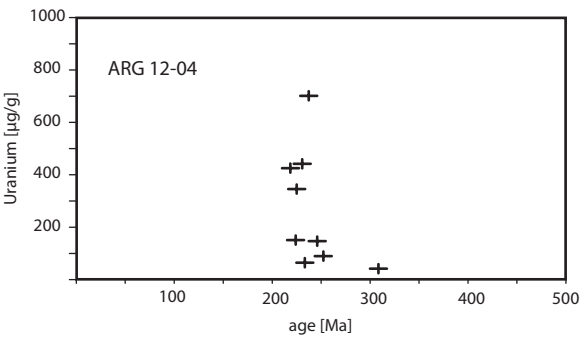

Fig. 5.5: Uranium-age ratio for the single grains of ARG 12-04.

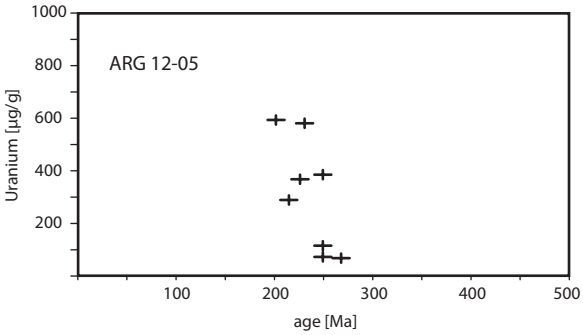

Fig. 5.6: Uranium-age ratio for the single grains of ARG 12-12.

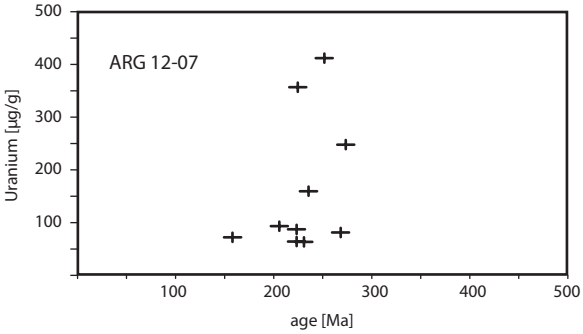

Fig. 5.7: Uranium-age ratio for the single grains of ARG 12-05.

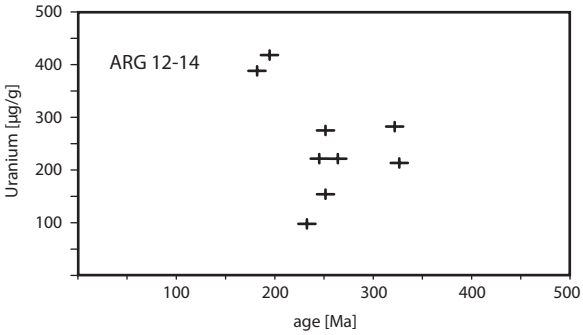

Fig. 5.8: Uranium-age ratio for the single grains of ARG 12-14.

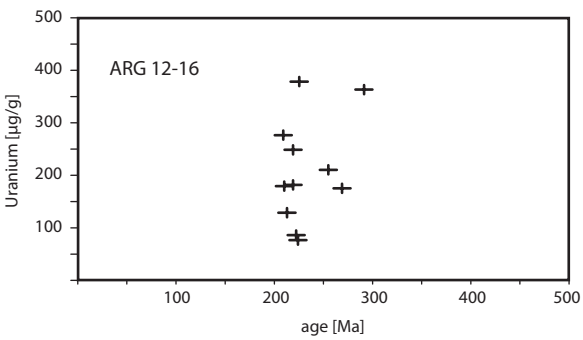

Fig. 5.9: Uranium-age ratio for the single grains of ARG 12-16.

described by Gleadow et al. (1986). Due to a slow cooling the lengths for ARG 01 and ARG 02 are shortened and come up with an average measured length of 13.4 (1.4) µm and 14.0 (1.2) µm.

The lengths measurements for the samples with a sufficient number of lengths for further HeFTy modelling are presented in the following bar charts. The measurements from the Sierras Septentrionales reveal for almost all samples a negative skewness, only ARG 12-04 shows a positive skewness. Fig. 5.10 shows the length distribution of ARG 01 and illustrates nicely the negative skewness. This negative skewness is also clearly visible in Fig. 5.11 and Fig. 5.12. The chart for ARG 12-04 (Fig. 5.12) reveals a more or less balanced, but slightly positive skewed length distribution. The charts for the samples ARG 12-09 (Fig. 5.13), ARG 12-12 (Fig. 5.14), ARG 12-14 (Fig. 5.15) and ARG 12-18 (Fig. 5.16) constitute lengths distributions with negative skewness.

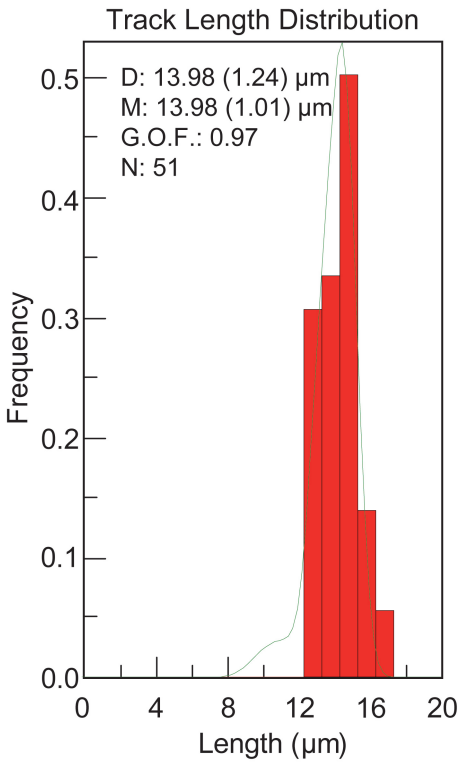

Fig. 5.11: Length distribution of ARG 02.

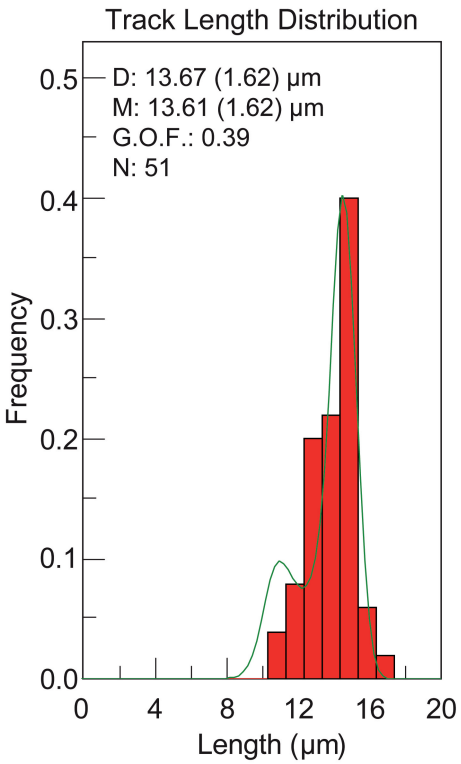

Fig. 5.10: Length distribution of ARG 01.

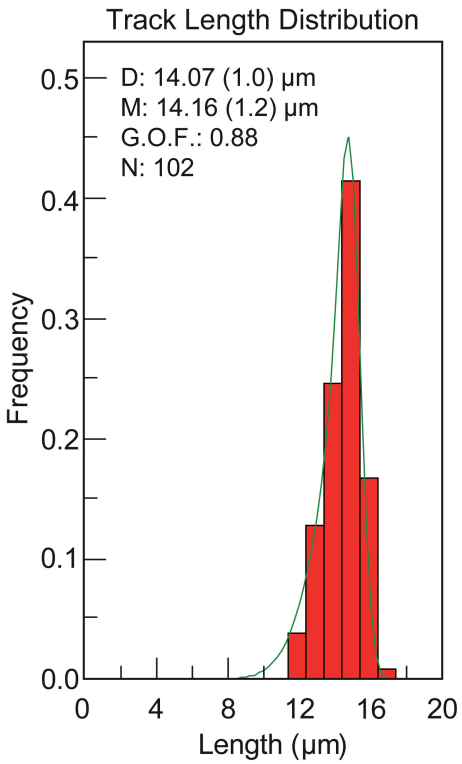

Fig. 5.12: Length distribution of ARG 12-04.

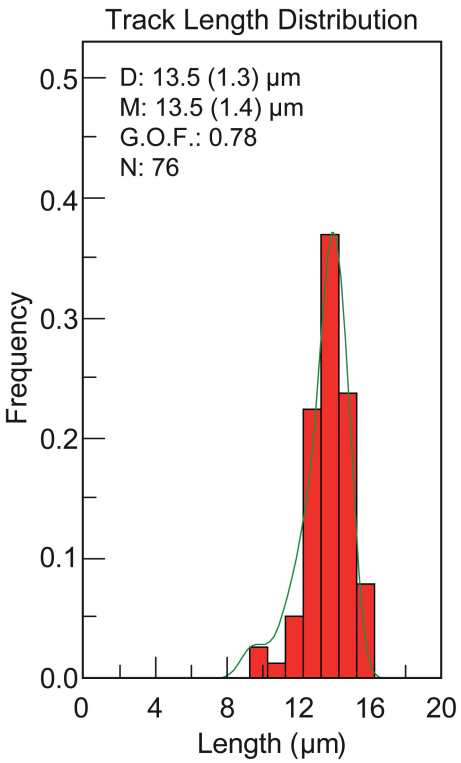

Fig. 5.13: Length distribution of ARG 12-09.

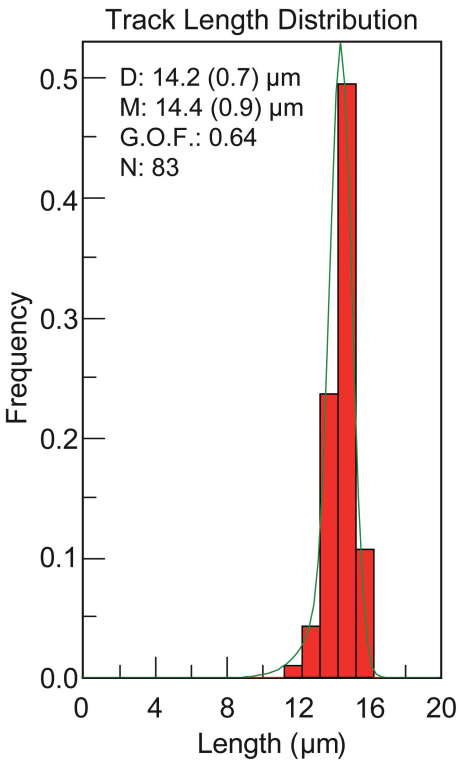

Fig. 5.15: Length distribution of ARG 12-14.

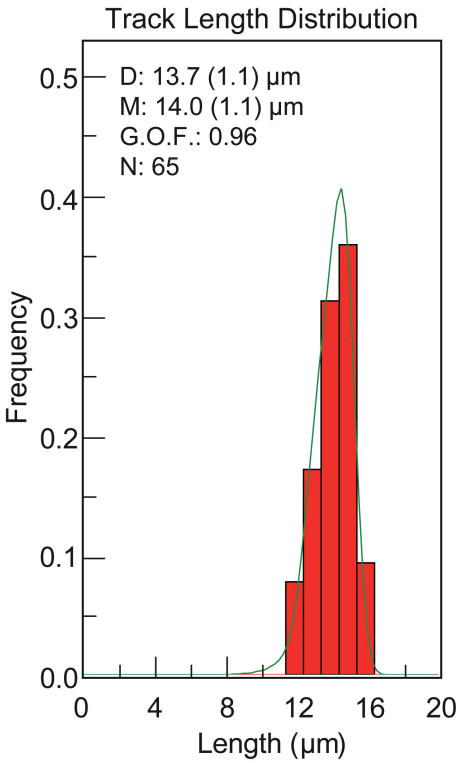

Fig. 5.14: Length distribution of ARG 12-12.

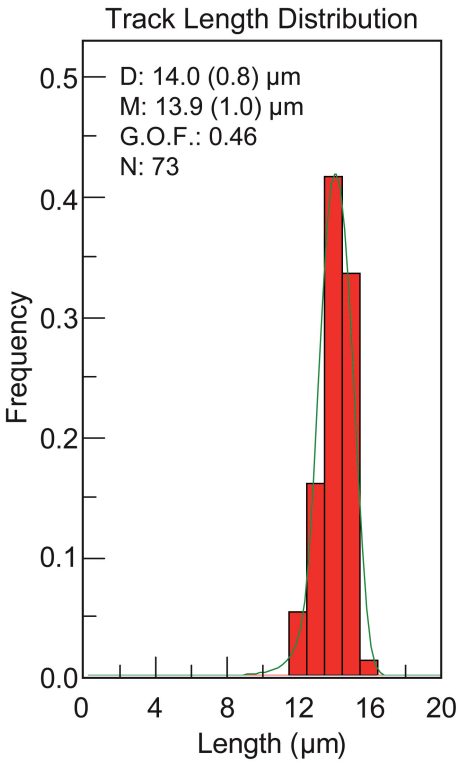

Fig. 5.16: Length distribution of ARG 12-18.

5.2.2 t-T models & exhumation rates

Fig. 5.17 and Fig. 5.18 show the modeled t-T history for the Achaean basement sample ARG 01. Fig. 5.19 and Fig. 5.20 show the modeled t-T evolution (detailed spread sheets of the t-T models are listed in the appendix) for the Precambrian Basement sample ARG 02. Due to the fact that Zambrano and Urien (1970) report some lower Cretaceous volcanic units in the neighbouring Salado basin, two different possible thermal histories were tested for the samples from the Sierras Septentrionales, one with a reheating event in lower Cretaceous (Fig. 5.18) and one without this 130 Ma event (Fig. 5.17).

The path for the model of ARG 01 (without the Cretaceous reheating) starts with fast cooling around 350 Ma (Fig. 5.17) . After reaching almost surface conditions at about 320 Ma this cooling is changing to a phase of burial and reaches temperatures up to 120-130°C. This burial lasts until 250 Ma. A second phase of constant cooling close to surface conditions changes into a second reheating event at about 200 Ma is followed by a phase of constant cooling at about 130 Ma. The alternative t-T-history without the second reheating impact (Fig. 5.17) in the Cretaceous shows a constant cooling since the Permian-Triassic border. Sample ARG 02, also from the Precambrian basement, presented slightly older ages (AHe: 121.6 (7.3); AFT: 186.7 (14.5)). The models for ARG 02 reveal a slightly different t-T history. After a phase of moderate heating from about 500 Ma until ca. 260 Ma the envelopes show a constant cooling since that time, with a slower exhumation rate at about 130 Ma. The alternative model with a second reheating event between 210 to 190 Ma and 150 to 130 Ma also fits the data-set and finds 148 acceptable paths. Both models for ARG 12-02 (Fig. 5.21) & (Fig. 5.22) show a permanent cooling since about 260 Ma. The initial cooling is slowing down at about 220 Ma. The model without the reheating (Fig. 5.21) is speeding up again at about 130 Ma.

The models of ARG 12-03 show similar pattern and start with an initial phase of cooling after a period of subsidence between 480 and 250 Ma (Fig. 5.23) & (Fig. 5.24). The initial cooling shows an average exhumation rate of 0.017 mm/a. The modelled time-temperature history for ARG 12-04 (Fig. 5.25) & (Fig. 5.26) reveals after the initial phase of subsidence between 480 to 250 Ma a slightly different cooling history. The initial cooling starts with rates of more than 2.5 °C/Ma and slows down to 1.0 °C/Ma at about 220 Ma. At about 150 Ma the cooling rate is decreasing until recent times.

The models of ARG 12-05 (Fig. 5.27) & (Fig. 5.28) show a similar trend and also similar values for the cooling- and exhumation rates. The initial exhumation points also towards the permo-triassic. The cooling is slowing down dramatically around 170 Ma.

The time-temperature paths for ARG 12-06 (Fig. 5.29) & (Fig. 5.30) show also a decreasing speed in cooling after the first phase of exhumation since the late Permian. From about 120 Ma, this cooling rate is doubled, compared to the slow cooling between late Permian and 130 Ma.

The HeFTy model for ARG 12-09 (Fig. 5.31) & (Fig. 5.32) reveals a concordant t-T history. The initial burial is changing into a fast exhumation at about 270 Ma and is consequently cooling until recent surface conditions.

The time-temperature paths for ARG 12-11 (Fig. 5.33) & (Fig. 5.34) show a period of cooling since the early Paleozoic-Mesozoic transition after a constant heating since 480 Ma.

Due to fewer t-T constraints, the modeled solutions for ARG 12-12 (Fig. 5.35) & (Fig. 5.36) are different in comparison to the other models. However, it also reveals a history of constant cooling since the permo-triassic border, after passing a phase of constant heating.

The model for ARG 12-13 (Fig. 5.37) & (Fig. 5.38) reveals a t-T history with an initial period of heating that switches into a phase of constant cooling at 260 to 250 Ma.

The modelled t-T history for ARG 12-14 (Fig. 5.39) & (Fig. 5.40) is similar to other t-T evolutions, also characterized by an initial phase of

heating. Roughly at the permo-triassic border, the conditions change into a phase of homogeneous cooling until present. ARG 12-16 (Fig. 5.41) & (Fig. 5.42) and ARG 12-18 (Fig. 5.43) & (Fig. 5.44) show an initial period of heating followed by a constant cooling since the Permian-Triassic transition. Both tested t-T evolutions are concordant with the data, but the model with the Jurassic reheating revealed the most t-T solutions. The calculated exhumation rates (Tab. 5-8) for the Sierras Septentrionales can be summarized in 4 different clusters. The oldest cluster with the rates for the first period of heating (rates between 0.024 mm/a and 0.032 mm/a), the following period of cooling (rates between ~ 0.02 mm/a and 0.067 mm/a), the second phase of heating

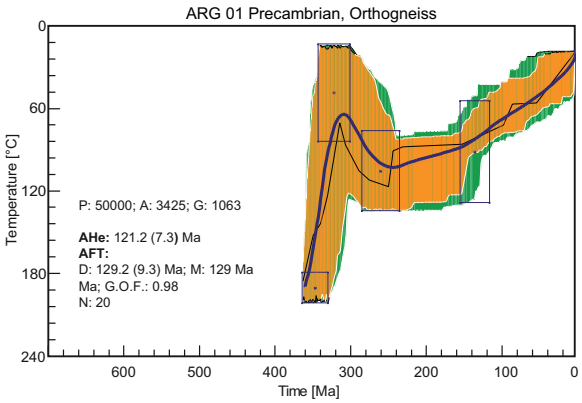

Fig. 5.17: modelled t-T history for ARG 01 (without reheating).

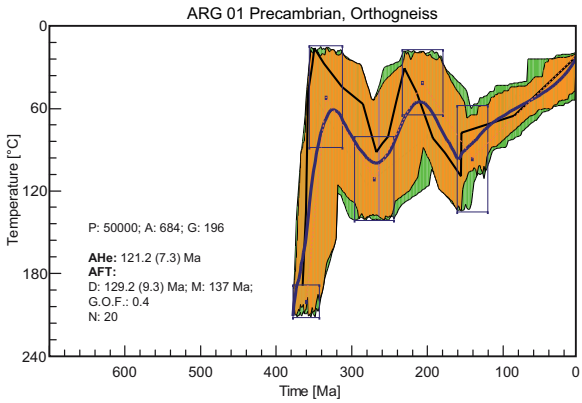

Fig. 5.18: modelled t-T history for ARG 01 (with reheating).

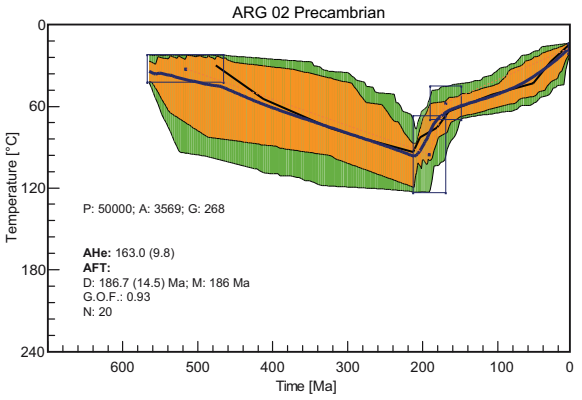

Fig. 5.19: modelled t-T history for ARG 02 (without reheating).

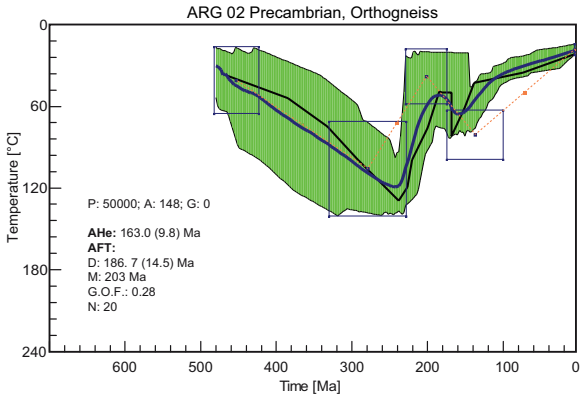

Fig. 5.20: modelled t-T history for ARG 02 (with reheating).

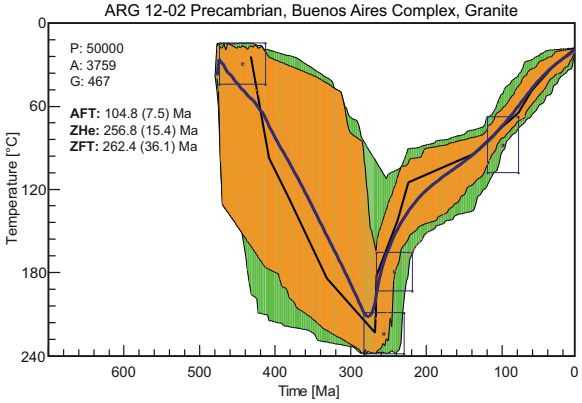

Fig. 5.21: t-T history for ARG 12-02 (without reheating).

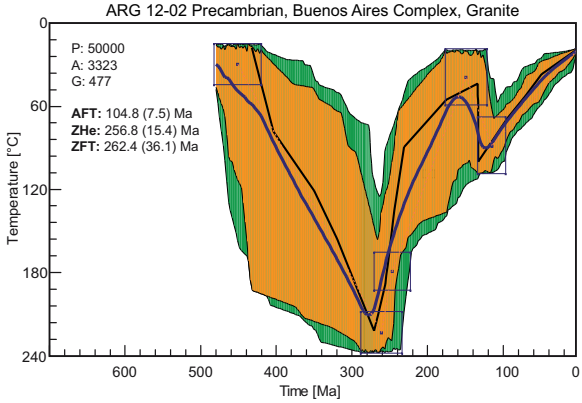

Fig. 5.22: t-T history for ARG 12-02 (with reheating).

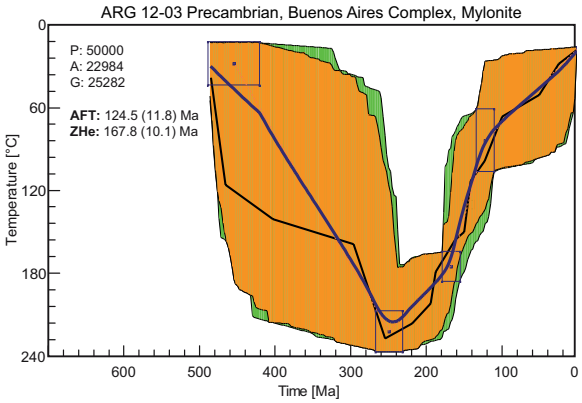

Fig. 5.23: t-T history for ARG 12-03 (without reheating).

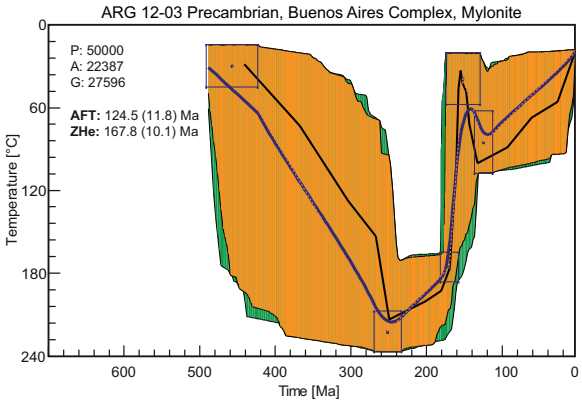

Fig. 5.24: modelled t-T history for ARG 12-03 (with reheating).

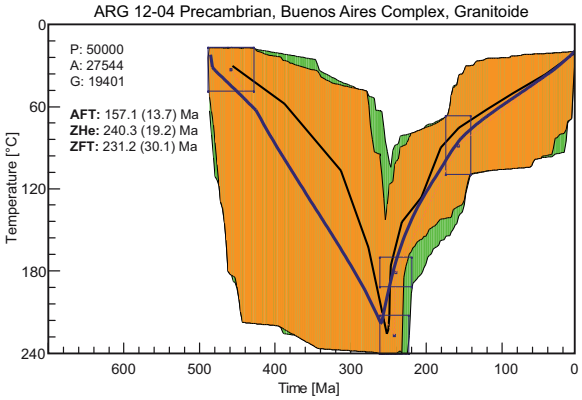

Fig. 5.25: t-T history for ARG 12-04 (without reheating).

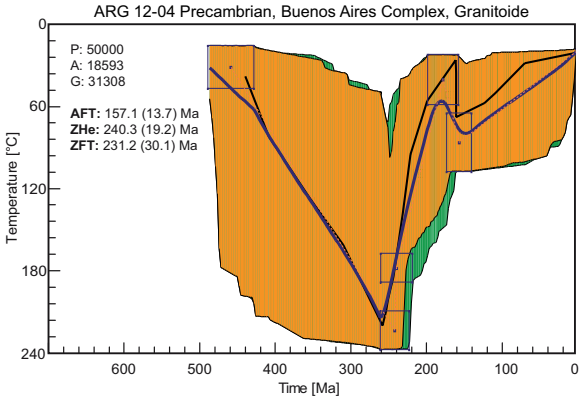

Fig. 5.26: t-T history for ARG 12-04 (with reheating).

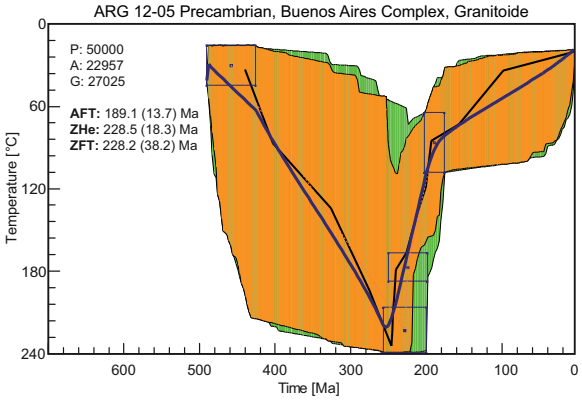

Fig. 5.27: t-T history for ARG 12-05 (without reheating).

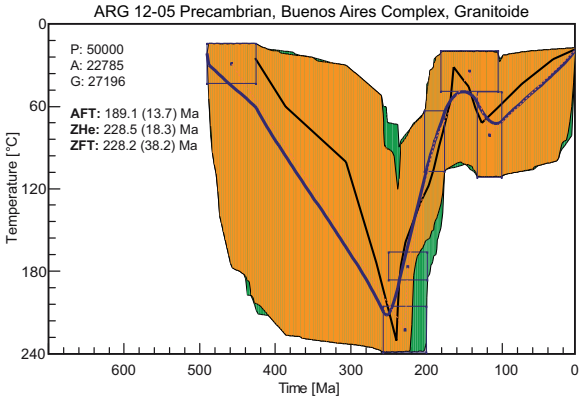

Fig. 5.28: t-T history for ARG 12-05 (with reheating).

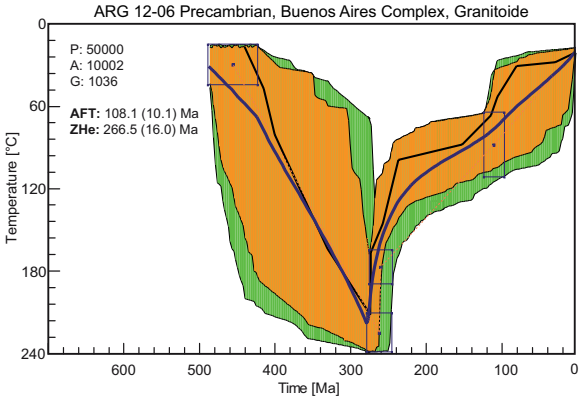

Fig. 5.29: t-T history for ARG 12-06 (without reheating).

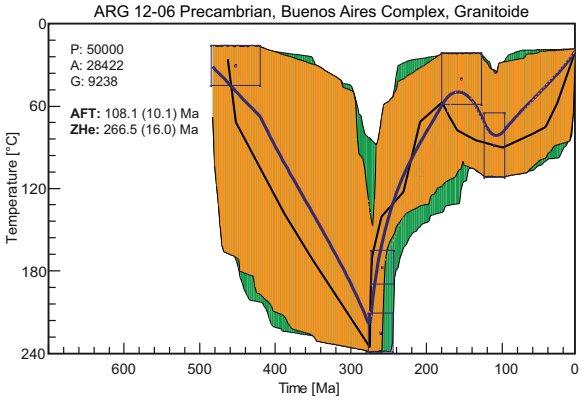

Fig. 5.30: t-T history for ARG 12-06 (with reheating).

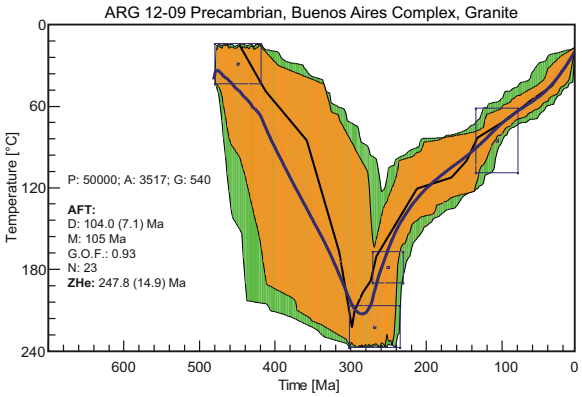

Fig. 5.31: t-T history for ARG 12-09 (without reheating).

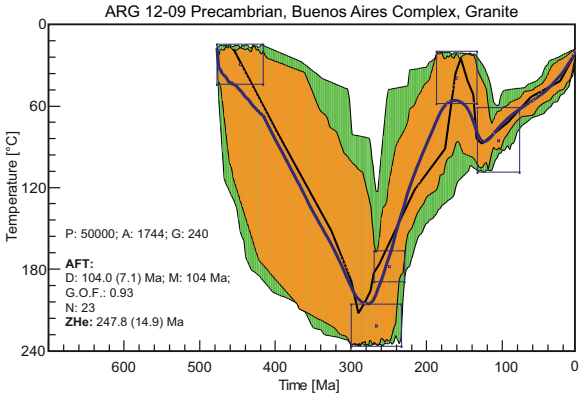

Fig. 5.32: t-T history for ARG 12-09 (with reheating).

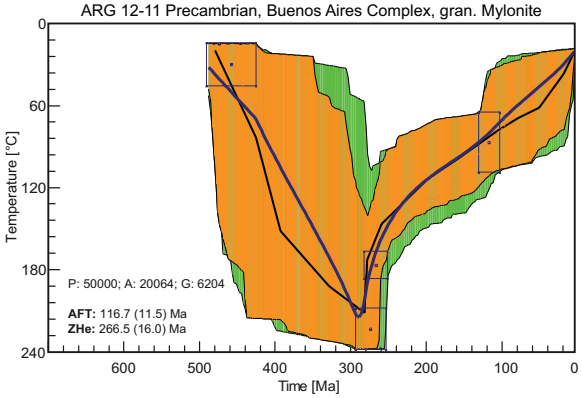

Fig. 5.33: t-T history for ARG 12-11 (without reheating).

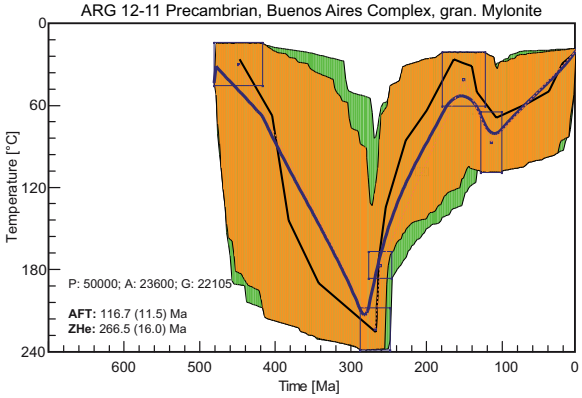

Fig. 5.34: t-T history for ARG 12-11 (with reheating).

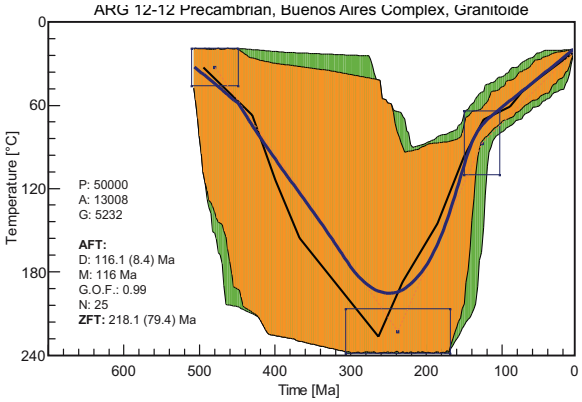

Fig. 5.35: t-T history for ARG 12-12 (without reheating).

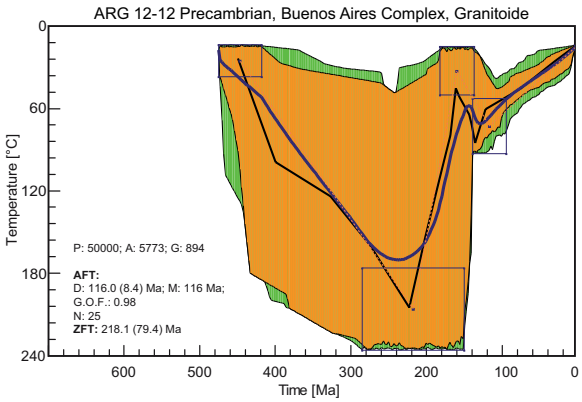

Fig. 5.36: t-T history for ARG 12-12 (with reheating).

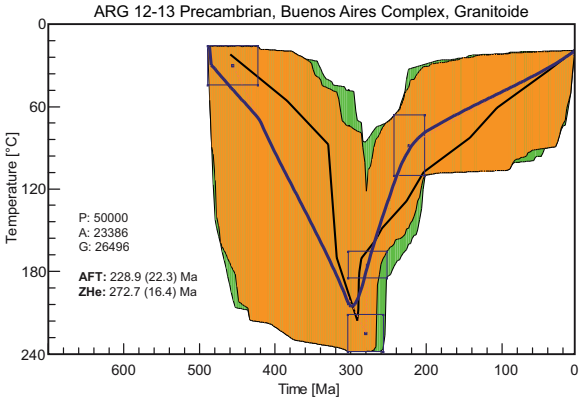

Fig. 5.37: t-T history for ARG 12-13 (without reheating).

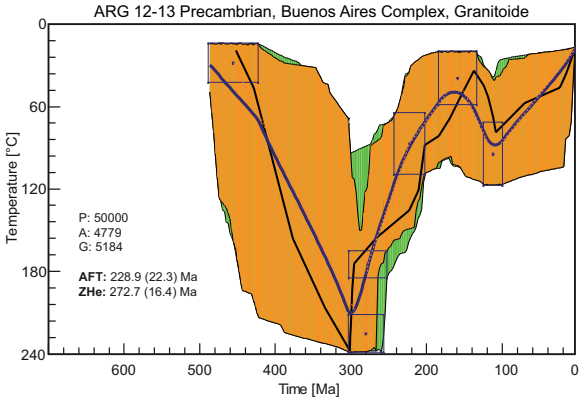

Fig. 5.38: t-T history for ARG 12-13 (with reheating).

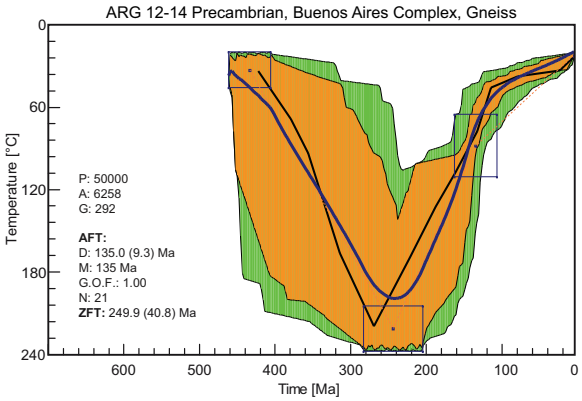

Fig. 5.39: t-T history for ARG 12-14 (without reheating).

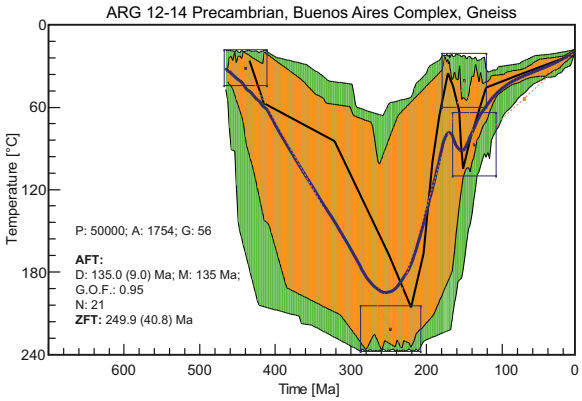

Fig. 5.40: t-T history for ARG 12-14 (with reheating).

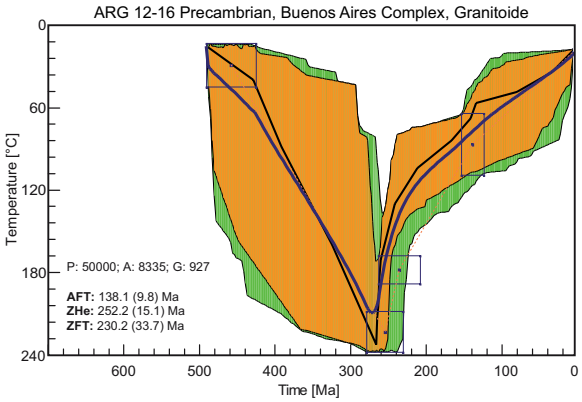

Fig. 5.41: t-T history for ARG 12-16 (without reheating).

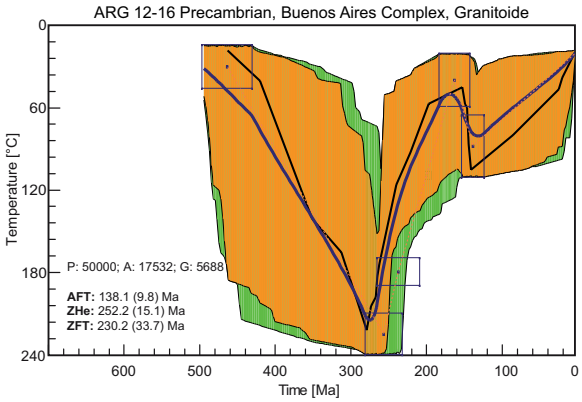

Fig. 5.42: t-T history for ARG 12-16 (with reheating).

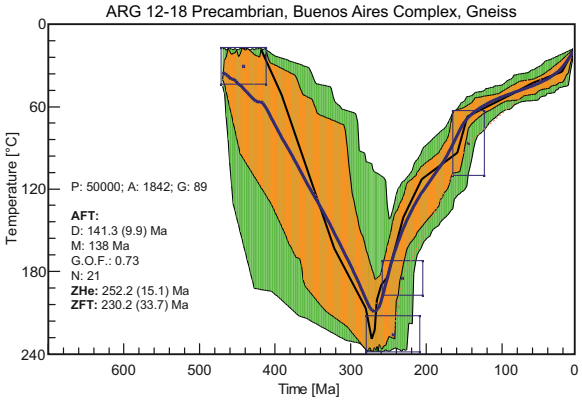

Fig. 5.43: t-T history for ARG 12-18 (without reheating).

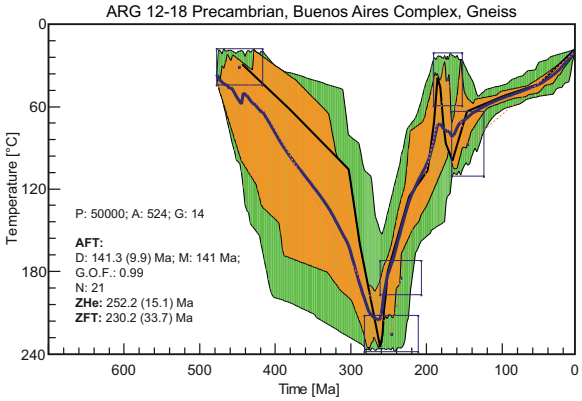

Fig. 5.44: t-T history for ARG 12-18 (with reheating).

due to the volcanic overburden (rates between 0.013 mm/a and 0.033 mm/a) and the post jurrasic to creataceous phase of cooling (rates between 0.013 mm/a and 0.021 mm/a). In General the exhumation from the Sierras Septentrionales coincides well in timing and intensity (Fig. 5.45), and support the hypothesis for a homogeneous thermal evolution and exhumation history for the Sierras Septentrionales.

Tab. 5-8: Calculated exhumation rates for the Sierras Septentrionales, based on a geothermal gradient of 30°C/km. Rates were calculated for the models with the Jurassic volcanic rocks on top.

S. no.	Elevation [m a.s.l.]	Geothe. gradient [°C/km]	Description	t-t segment [Ma]	T-T segment [°C]	Coolingrate [°C/Ma]	Exhumationrate [mm/a]	Δt	ΔT
ARG 01	153	30	cooling	370-320	230-60	3.400	0.113	50	170
		30	heating	320-260	60-95	0.583	0.019	60	35
		30	cooling	260-210	95-50	0.900	0.030	50	45
		30	heating	210-150	50-95	1.000	0.033	45	45
		30	cooling	150-0	95-20	0.500	0.017	150	75
ARG 02	273	30	heating	500-250	20-110	0.360	0.012	250	90
		30	cooling	250-190	110-60	0.833	0.028	60	50
		30	heating	190-160	60-70	0.333	0.011	30	10
		30	cooling	160-130	70-45	0.833	0.028	30	25
		30	cooling	130-0	45-20	0.192	0.006	130	25
ARG 12-02	209	30	heating	480-280	25-215	0.950	0.032	200	190
		30	cooling	280-160	215-55	1.333	0.044	120	160
		30	heating	160-120	55-90	0.875	0.029	40	35
		30	cooling	120-0	90-20	0.583	0.019	120	70
ARG 12-03	224	30	heating	480-250	30-220	0.913	0.030	230	210
		30	cooling	250-175	220-190	0.400	0.013	75	30
		30	cooling	175-140	190-65	3.571	0.119	35	125
		30	heating	140-115	65-85	0.800	0.027	25	20
		30	cooling	115-0	85-20	0.565	0.019	115	65
ARG 12-04	191	30	heating	480-260	30-220	0.864	0.029	220	190
		30	cooling	260-180	220-60	2.000	0.067	80	160
		30	heating	180-150	60-80	0.667	0.022	30	20
		30	cooling	150-0	80-20	0.400	0.013	150	60
ARG 12-05	191	30	heating	490-250	30-220	0.913	0.030	230	210
		30	cooling	250-150	220-55	1.938	0.065	80	155
		30	heating	150-105	55-75	0.382	0.013	170	65
		30	cooling	105-0	75-20	0.382	0.013	170	65
ARG 12-06	237	30	heating	490-280	30-220	0.905	0.030	210	190
		30	cooling	280-160	220-50	1.417	0.047	120	170
		30	heating	160-110	50-80	0.600	0.020	50	30
		30	cooling	110-0	80-20	0.545	0.018	110	60
ARG 12-09	280	30	heating	480-265	25-220	0.907	0.030	215	195
		30	cooling	265-160	220-60	1.524	0.051	105	160
		30	heating	160-130	60-90	1.000	0.033	30	30
		30	cooling	130-0	90-20	0.538	0.018	130	70
ARG 12-11	210	30	heating	490-290	35-220	0.925	0.031	200	185
		30	cooling	290-155	220-50	1.259	0.042	135	170
		30	heating	155-110	50-80	0.667	0.022	45	30
		30	cooling	110-0	80-20	0.545	0.018	110	60
ARG 12-12	201	30	heating	480-240	25-200	0.729	0.024	240	175
		30	cooling	240-150	200-70	1.444	0.048	90	130
		30	heating	150-135	70-85	1.000	0.033	15	15
		30	cooling	135-0	85-20	0.481	0.016	135	65
ARG 12-13	239	30	heating	480-300	30-215	1.028	0.034	180	185
		30	cooling	300-165	215-50	1.222	0.041	135	165
		30	heating	165-110	50-90	0.727	0.024	55	40
		30	cooling	110-0	90-20	0.636	0.021	110	70
ARG 12-14	239	30	heating	480-260	30-200	0.773	0.026	220	170
		30	cooling	260-175	200-75	0.676	0.023	185	125
		30	heating	175-150	75-90	0.600	0.020	25	15
		30	cooling	150-0	90-20	0.467	0.016	150	70
ARG 12-16	174	30	heating	490-270	30-220	0.955	0.032	220	210
		30	cooling	270-165	220-60	1.684	0.056	95	160
		30	heating	165-130	60-75	0.429	0.014	35	15
		30	cooling	130-0	75-20	0.423	0.014	130	55
ARG 12-18	136	30	heating	480-270	35-220	0.881	0.029	210	185
		30	cooling	270-180	220-70	1.667	0.056	90	150
		30	heating	180-160	70-80	0.500	0.017	20	10
		30	cooling	160-0	80-20	0.375	0.013	160	60

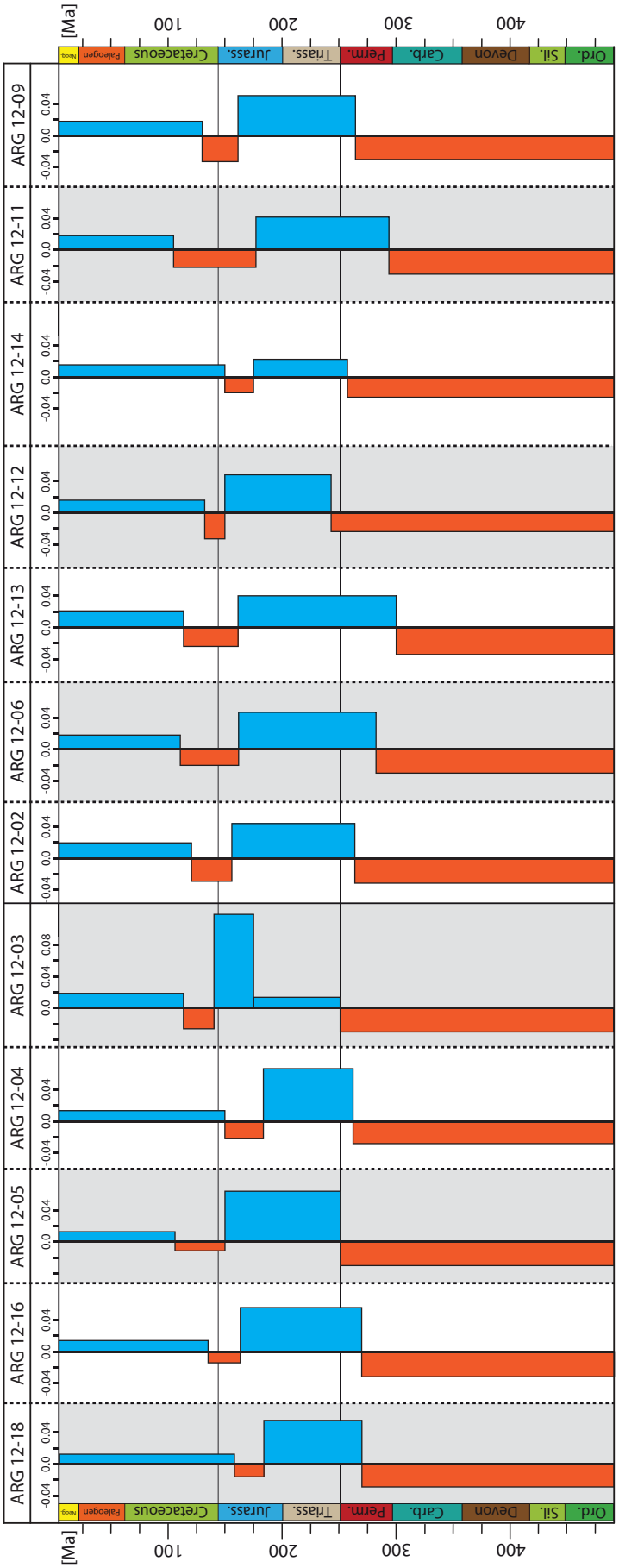

Fig. 5.45: Summary and comparison of calculated rates for the Sierras Septentrionales against the geological time line. The calculated values are based on the models with the late Mesozoic reheating. Exhumation rates are given in mm/a.

5.3 Sierras Australes (east of the Sauce Grande Wrench) and the Claromeco basin

5.3.1 Ages - Lengths - Dpar

Determined ages (detailed spread sheets of the fission-track data are listed in the appendix) from the eastern part of the Sierras Australes are summarized in (Tab. 5-9) & (Tab. 5-11) & (Tab. 5-11) & (Fig. 5.31). Sample ARG 04 (139 m a.s.l) was taken from the Permian Tunas in the Claromeco basin. The ZHe-age (160.7 (12.9) Ma) and AFT-age (157.8 (10.7) Ma) are within error, indicating a fast cooling history during the Upper Jurassic to Lower Cretaceous.

All samples (ARG 14- ARG 17) from the Sierras Australes, east of the SGW, are characterized by similar AFT-ages in the range of 155 Ma. The ZHe-ages are older and range from 236.7 (18.9) Ma to 198.7 (15.9) Ma.

Apatite (U-Th-Sm)/He-ages of two samples from the Permian Tunas Formation range from 107.4 (3.5) Ma (ARG 14) to 120.8 (7.3) Ma (ARG 15) and, therefore, are within the 1 σ-error.

The measured lengths for ARG 12 reveal a CT mean of 11.3 (1.8) µm with a positive skewness of 0.224. In total 52 lengths and 55 Dpars were measured.

ARG 15 is characterized by a CT mean of 13.1 (1.4) µm and a negative skewness of -0.639, out of 79 measured lengths and 70 measured Dpars.

Tab. 5-9: Summary of apatite (U-Th-Sm)/He data of the Sierras Australes (east of the Sauce Grande Wrench). M: mass, contributing U, Th, Sm,and He concentration, eU = [U] + 0.235 [Th] (concentration in weight %), Ft: α ejection factor for apatite and zircon calculated after Farley et al. (1996), Raw (raw) ages and 1σ error for α-ejection with accordant 1σ error. The brown marked grain was the grains of our choice.

S.-No.	Lithology	U [µg/g]	Th [µg/g]	Sm [µg/g]	eU	Th/U	He [nmol/g]	M (µg)	Ft	raw Age	± 1σ raw age	Age [Ma]	± 1σ [Ma]
East of Sauce Grande wrench													
aARG14-1	Sandstone	51.8	22.3	26.8	57.1	0.43	22.4	2.31	0.68	72.1	4.3	105.8	6.3
aARG14-2	Sandstone	39.0	34.7	66.7	47.3	0.89	15.7	1.28	0.61	60.9	3.7	99.4	5.9
aARG14-3	Sandstone	20.0	22.4	11.7	25.2	1.12	8.4	0.82	0.56	59.8	1.9	107.4	3.5
aARG15-1	Sandstone	11.4	18.7	14.3	15.8	1.64	13.1	2.56	0.68	150.9	9.1	220.9	13.2
aARG15-2	Sandstone	5.4	14.7	47.5	9.0	2.75	14.7	1.00	0.58	290.2	17.4	503.8	30.2
aARG15-3	Sandstone	56.4	39.0	49.1	65.6	0.69	29.1	2.34	0.67	81.3	4.9	120.8	7.3

Tab. 5-10: Apatite fission-track data of the Sierras Australes (east of the Sauce Grande Wrench). U: uranium concentration in µg/g, n: number of counted grains, ρS: density of spontaneous tracks (x 105/cm²), Ns: number of spontaneous tracks, ρI: density of induced tracks (x 105/cm²), NI: number of induced tracks, P(χ^2) is the probability that single grain ages are consistent and belong to the same population. Test is passed if P(χ^2) > 5% (Galbraith, 1981). Ages calculated using a ζ- value of 336.83 (19.51) a/cm² for apatite, Nd =15148 tracks.

S.-No.	Elev. [m.a.s.l.]	Formation age	U (std) [µg/g]	n	Sp. Tracks ρ_s	N_s	Ind. Tracks ρ_i	N_i	χ^2 [%]	Central age (1σ) [Ma]
Claromeco basin										
ARG 04	139	Tunas Fm.	35.6 (14.6)	20	25.684	1370	38.713	2065	100	157.8 (10.7)
East of Sauce Grande wrench										
ARG 12	319	Piedra Azul Fm.	41.3 (17.3)	20	26.872	714	44.260	1176	99.8	141.9 (10.7)
ARG 15	399	Tunas Fm.	26.4 (14.8)	20	19.796	1084	27.430	1502	4.22	169.8 (13.1)
ARG 16	381	Sauce Grande Fm.	18.6 (10.6)	17	13.684	839	20.257	1242	35.11	156.0 (11.7)
ARG 17	416	Tunas Fm.	29.2 (15.2)	20	22.433	869	32.088	1243	33.64	161.4 (12.3)

Tab. 5-12: Summary of zircon (U-Th-Sm)/He data from the Sierras Australes (east of the Sauce Grande Wrench). M: mass, contributing U, Th, Sm,and He concentration, eU = [U] + 0.235 [Th] (concentration in weight %), Ft: α-ejection factor for apatite and zircon calculated after Farley et al. (1996), Raw (raw) ages and 1σ error for α-ejection with accordant 1σ error. Zircon-He data from the Sierras Septentrionales. The brown marked grains were chosen for continuative laboratory work.

S.-No.	Lithology	U [ppm]	Th [ppm]	Sm [ppm]]	eU	Th/U	He [nmol/g]	M (ug)	Ft	raw Age	± 1 σ raw age	Age [Ma]	± 1 σ [Ma]
Claromeco basin													
zARG04-1	Sandst.	465.7	192.9	27.0	510.2	0.41	410.4	6.52	0.76	147.0	11.8	192.6	15.4
zARG04-2	Sandst.	493.9	242.5	5.8	549.7	0.49	395.2	5.35	0.74	131.6	10.5	176.6	14.1
zARG04-3	Sandst.	186.3	121.9	2.3	214.4	0.65	133.1	3.31	0.71	113.7	9.1	160.7	12.9
East of Sauce Grande wrench													
zARG10-1	Pebble from Diamiktite	399.4	615.3	7.6	541.1	1.54	493.4	6.41	0.75	165.8	13.3	221.8	17.7
zARG10-3	Pebble from Diamiktite	1037.4	1268.7	39.9	1329.7	1.22	874.9	5.34	0.74	120.2	9.6	161.7	12.9
zARG14-1	Sandst.	415.9	123.1	12.4	444.3	0.30	351.8	10.64	0.80	144.8	11.6	181.1	14.5
zARG14-2	Sandst.	485.2	152.0	1.9	520.2	0.31	446.7	5.20	0.74	156.9	12.5	212.2	17.0
zARG14-3	Sandst.	207.7	82.1	1.0	226.6	0.40	231.5	9.63	0.79	186.0	14.9	236.7	18.9
zARG15-1	Sandst.	346.7	109.0	2.1	371.8	0.31	310.2	3.90	0.72	152.5	12.2	211.4	16.91
zARG15-2	Sandst.	175.6	148.9	0.8	209.9	0.85	177.5	5.36	0.74	154.2	12.3	207.1	16.57
zARG15-3	Sandst.	60.8	45.0	1.4	71.1	0.74	62.9	4.82	0.74	161.2	12.9	218.2	17.45
zARG16-1	Diamiktite	161.7	170.8	2.8	201.0	1.06	148.7	2.62	0.66	135.0	10.8	204.7	16.38
zARG16-2	Diamiktite	69.2	56.5	1.2	82.2	0.82	64.8	3.97	0.70	143.8	11.5	206.6	16.53
zARG16-3	Diamiktite	388.8	214.8	5.5	438.2	0.55	402.5	4.98	0.74	167.5	13.4	226.9	18.16
zARG17-1	Sandst.	137.0	51.6	1.2	148.8	0.38	126.7	8.37	0.78	155.4	12.4	198.7	15.90
zARG17-2	Sandst.	231.5	75.5	1.5	248.9	0.33	228.0	8.66	0.79	167.2	13.4	212.5	17.00
zARG17-3	Sandst.	230.4	75.8	0.8	247.9	0.33	231.8	6.77	0.77	170.6	13.6	221.4	17.71

Tab. 5-11: Zircon fission-track data of the Sierras Australes (east of the Sauce Grande Wrench). U: uranium concentration in µg/g, n: number of counted grains, ρS: density of spontaneous tracks (x 105/cm²), Ns: number of spontaneous tracks, ρI: density of induced tracks (x 105/cm²), NI: number of induced tracks, P(χ^2) is the probability that single grain ages are consistent and belong to the same population. Test is passed if P(χ^2) > 5% (Galbraith, 1981). Ages calculated using a ζ- value of 123.00 (6.08) a/cm² for apatite, Nd =15128 tracks.

S.-No.	Elev. [m.a.s.l.]	Form. age	n	U (std) [µg/g]	Sp. Tracks ρ_s N_s	Ind. Tracks ρ_i N_i	χ^2 [%]	Central age (1σ) [Ma]
East of Sauce Grande wrench								
ARG 17	416	Tunas Fm.	17	175.3 (92.9)	168.618 896	31.239 166	100.0	229.0 (22.5)

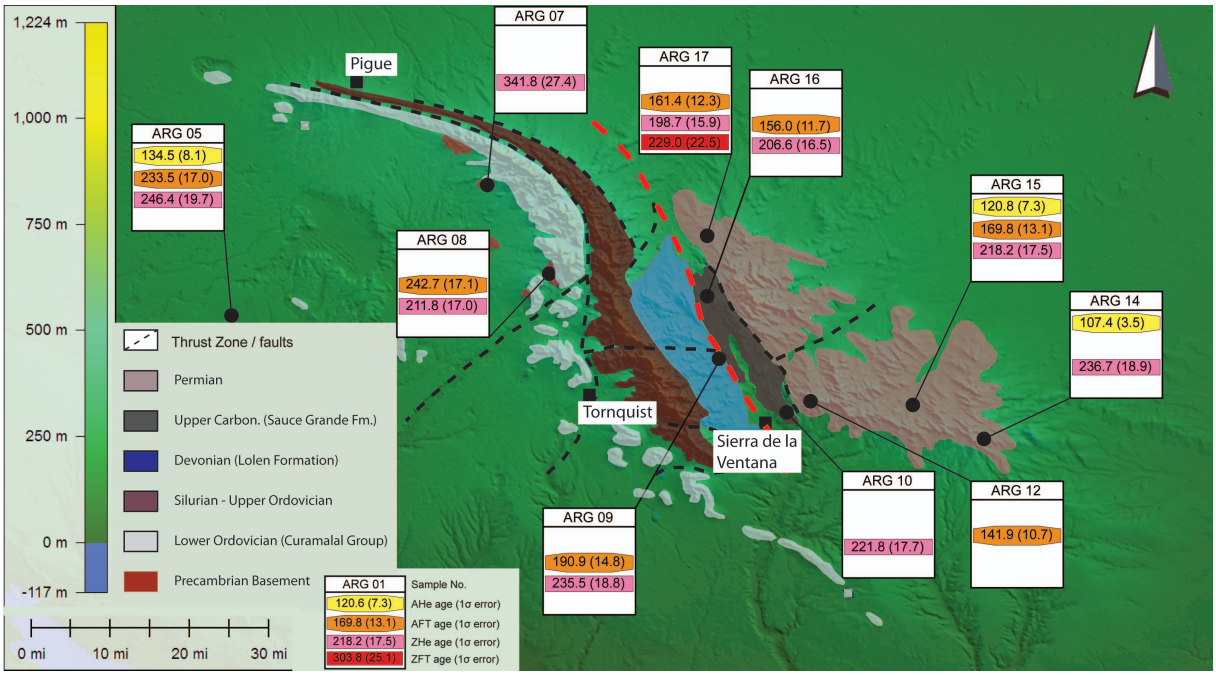

Fig. 5.46: Geological map (redrawn from Suero, 1972) and thermochronological data of the Sierras Australes. DEM-90 m by Jarvis et al., 2008).

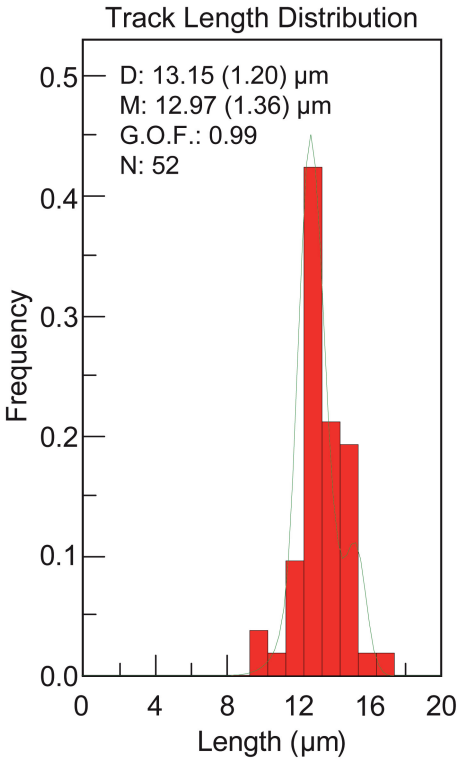

Fig. 5.47: Length distribution of ARG 12.

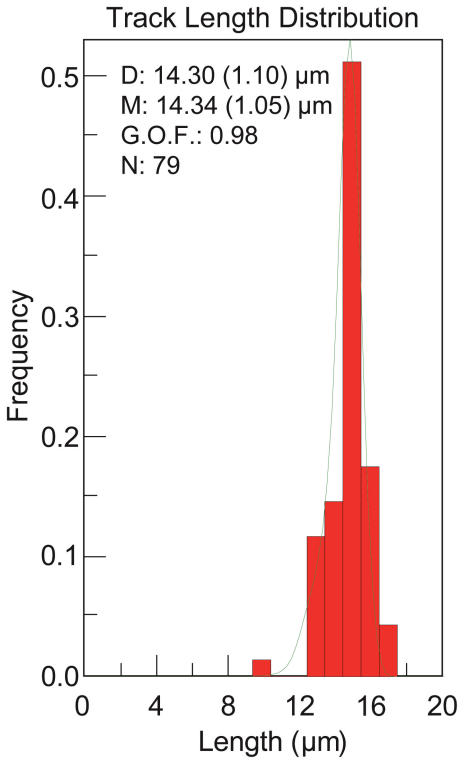

Fig. 5.48: Length distribution of ARG 15.

5.3.2 t-T models

As the geological constraints of the Mesozoic and Cenozoic evolution of the eastern part of the Sierras Australes, are minor, the available t-T constraints are limiting the t-T evolution in a broad manor (detailed spread sheets of the t-T models are listed in the appendix). From the early Permian to the Upper Triassic all numeric t-T models (Fig. 5.49, Fig. 5.50, Fig. 5.51, Fig. 5.52, Fig. 5.53 & Fig. 5.54) of the samples from the Upper Carboniferous to Permian Sauce Grande Formation (ARG 10, ARG 16), the Permian Piedra Azul Formation (ARG 12), and the Permian Tunas formation (ARG 13 – ARG 15, ARG 17) indicate a fast temperature increase of 165 °C, from surface temperature to about 180 °C at about 220 Ma. If a surface temperature of 15 °C and a geothermal gradient of 30 °C/km is assumed, the surface rocks of today were overlain by up to 5 km of sedimentary rocks in the Upper Triassic. In all models the subsidence inverted and cooling started in the Upper Triassic. Sample ARG 10 (Fig. 5.49) and ARG 14 (Fig. 5.53) cooled constantly until surface temperature was reached during the Quaternary. Sample ARG 16 and #ARG 17 cooled rapidly until 155 Ma reaching a temperature of about 90 °C and, thereafter, slower to surface temperature in Quaternary. The Permian sandstone of the Tunas formation (ARG 15) with three thermochronological ages (AHe, AFT, ZHe) cooled in three distinct steps from about 180 °C at 220 Ma to 70 °C at 185 Ma, from 70 °C to 40 °C at about 125 Ma and, thereafter to surface temperature in the Quaternary. The sandstone of the Permian Piedra Azul Fm. (ARG 12) cooled to 70 °C at 130 Ma and kept at a steady temperature up to 50 Ma and rapidly cooled to surface temperature in Quaternary.

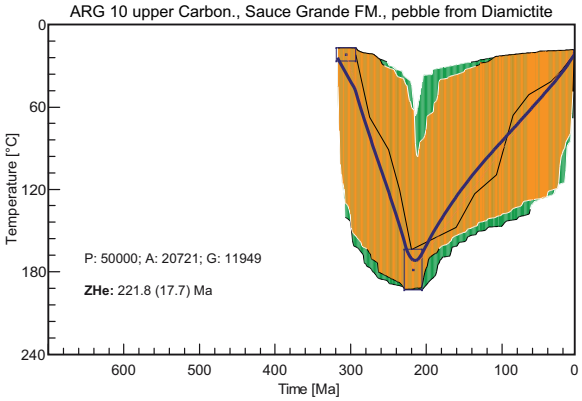

Fig. 5.49: t-T history for ARG 10.

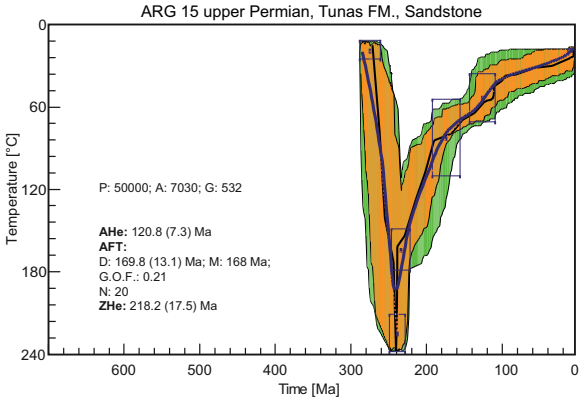

Fig. 5.50: t-T history for ARG 15.

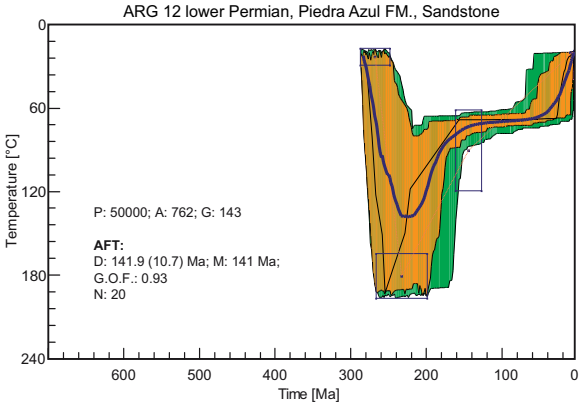

Fig. 5.51: t-T history for ARG 12.

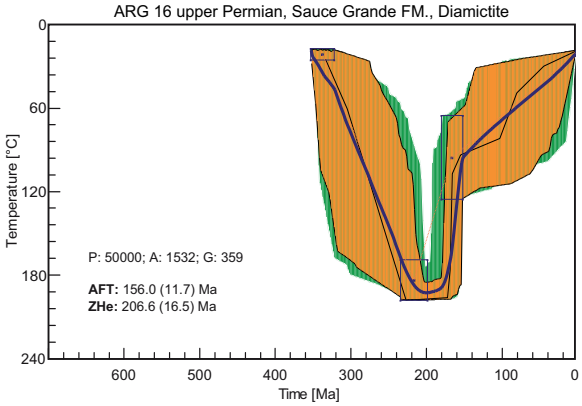

Fig. 5.52: t-T history for ARG 16.

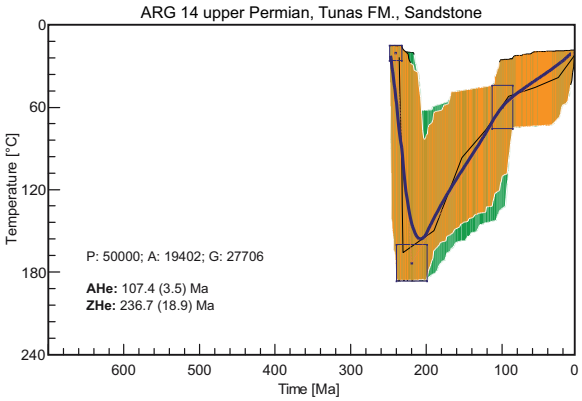

Fig. 5.53: t-T history for ARG 14.

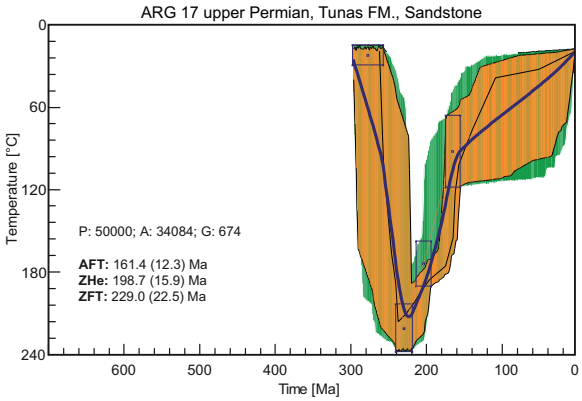

Fig. 5.54: t-T history for ARG 17.

5.4 Sierras Australes (west of the Sauce Grande Wrench)

5.4.1 Ages - Lengths - Dpar

In the western high-metamorphic part of the Sierras Australes, the determination of thermochronometers was limited(Tab. 5-13 & Tab. 5-14). The Upper Proterozoic ignimbrite (ARG 07) revealed the oldest zircon (U-Th)/He age of 341.8 (27.4) Ma. The ZHe age of the two other samples (ARG 08, a Precambrian paragneiss and ARG 09, a Upper Devonian sandstone) are younger but within error and indicate a Middle to Upper Triassic cooling age (211.8 (17.0) Ma; 235.5 (18.8) Ma, respectively). Zircon grains of a Precambrian paragneiss (ARG 08) show within error the same Upper Jurassic age of about 215 Ma (average). In comparison to the samples from the eastern side the ZHe-age lies within the error. Neoproterozoic ZHe-ages of two other zircon grains of the Devonian sandstone (ARG 09) are interpreted as detrital ages. The Devonian sandstone was sampled directly from the SGW (western section). Only the AFT-ages are significantly different. Whereas the eastern side revealed ages of around 155 Ma the AFT-age of the Devonian sandstone (ARG 09) is of 190.9 (14.8) Ma. The age of the Devonian sandstone possibly represent movement along the Sauce Grande Wrench if the cover was less than 2 km thick. Further to the west the Precambrian gneiss is characterized by an AFT-age of 242.7 (17.1) Ma, which is within error similar to the ZHe-ages of three zircon grains. This similarity in age suggests fast cooling combined with a lower He-diffusion temperature of the zircon grains.

The AFT-data plotted in the corresponding age-elevation plot, clearly shows that the AFT-ages (Fig. 5.55) east of the SGW are slightly younger than the ages from the western part. The age-elevation plot with the ZHe-ages (Fig. 5.56) from the Sierras Australes show the same tendencies of younger ages from the eastern parte and older ages from the western part.

Fig. 5.57 and Fig. 5.58 present the length distribution for samples ARG 08 and ARG 09. They are both characterized by a negative skewness of -0.118, based on 51 lengths measurements for ARG 08 and a skewness of -0.110, based on 48 lengths measurements for ARG 09. The CT mean values for both samples are nearly equal and reveal a value of 13.0 (1.6) µm for ARG 08 and a CT mean of 12.9 (1.7) µm for ARG 09. For sample ARG 08 50 Dpars and for sample ARG 09 55 Dpars were measured. The corresponding Dpar values are with a value of 1.8 µm and an error of 0.2 µm identical.

Tab. 5-13: Apatite fission-track data of the Sierras Australes (west of the Sauce Grande Wrench) and the Lopez Lecube intrusion. U: uranium concentration in µg/g, n: number of counted grains, ρS: density of spontaneous tracks (x 105/cm²), Ns: number of spontaneous tracks, ρI: density of induced tracks (x 105/cm²), NI: number of induced tracks, P(χ^2) is the probability that single grain ages are consistent and belong to the same population. Test is passed if P(χ^2) > 5% (Galbraith, 1981). Ages calculated using a ζ- value of 336.83 (19.51) a/cm² for apatite, Nd =15148 tracks.

S.-No.	Elev. [m.a.s.l.]	Form. age	U (std) [µg/g]	n	Sp. Tracks ρ_s	N_s	Ind. Tracks ρ_i	N_i	χ^2 [%]	Central age (1σ) [Ma]
West of Sauce Grande wrench										
ARG 08	426	Precambr.	36.3 (24.3)	20	39.174	1315	37.804	1269	99.88	242.7 (17.1)
ARG 09	353	Lolen Fm.	25.3 (15.2)	20	22.071	1021	27.367	1266	15.25	190.9 (14.8)
Lopez Lecube intrusion										
ARG 05	96	Permian	26.6 (7.0)	18	30.693	1056	30.655	1065	100	233.5 (17.0)

Tab. 5-14: Summary of zircon (U-Th-Sm)/He data of the Sierras Australes (west of the Sauce Grande Wrench) and the Lopez Lecube intrusion. M: mass, contributing U, Th, Sm,and He concentration, eU = [U] + 0.235 [Th] (concentration in weight %), Ft: α-ejection factor for apatite and zircon calculated after Farley et al. (1996), Raw (raw) ages and 1σ error for α-ejection with accordant 1σ error. The brown marked grains were the grains of our choice.

S.-No.	Lithology	U [µg/g]	Th [µg/g]	Sm [µg/g]	eU	Th/U	He [nmol/g]	M (µg)	Ft	raw Age	± 1σ raw age	Age [Ma]	± 1σ [Ma]
West of Sauce Grande wrench													
zARG07-1	Ignimbrite	1.1	1.6	0.1	1.5	1.37	369.2	5.02	0.71	n.d.	n.d.	n.d.	n.d.
zARG07-2	Ignimbrite	221.1	173.6	5.7	261.1	0.79	319.6	2.03	0.65	221.9	17.8	341.8	27.4
zARG07-3	Ignimbrite	285.1	212.2	4.7	334.0	0.74	307.0	1.71	0.62	167.4	13.4	269.2	21.5
zARG08-1	Paragneiss	407.4	86.8	1.5	427.4	0.21	421.2	10.17	0.80	179.7	14.4	225.8	18.1
zARG08-2	Paragneiss	258.4	64.3	1.3	273.3	0.25	252.3	9.77	0.80	168.5	13.5	211.8	17.0
zARG08-3	Paragneiss	321.5	55.6	1.9	334.3	0.17	267.0	3.70	0.72	146.1	11.7	203.6	16.3
zARG09-1	Sandstone	195.0	167.4	7.0	233.6	0.86	521.5	8.57	0.78	397.9	31.8	512.8	41.0
zARG09-2	Sandstone	227.7	104.9	5.7	251.8	0.46	255.4	8.69	0.78	184.6	14.8	235.5	18.8
zARG09-3	Sandstone	111.8	67.8	3.5	127.4	0.61	320.7	6.52	0.76	446.1	35.7	584.6	46.8
Lopez Lecube intrusion													
zARG05-1	Syenite	263.6	220.5	1.0	314.4	0.84	363.5	8.70	0.78	209.8	16.8	270.3	21.6
zARG05-2	Syenite	200.0	205.6	3.1	247.3	1.03	271.1	11.20	0.79	199.0	15.9	251.9	20.1
zARG05-3	Syenite	336.2	300.7	4.2	405.5	0.89	447.9	6.08	0.75	200.6	16.0	267.4	21.3
zARG05-1-1	Syenite	200.2	192.9	1.4	244.6	0.96	255.7	8.85	0.77	190.0	15.2	246.4	19.7
zARG05-1-2	Syenite	289.5	254.8	4.7	348.1	0.88	365.1	9.11	0.76	190.6	15.2	250.3	20.0
zARG05-1-3	Syenite	289.1	277.4	4.7	353.0	0.96	319.2	5.47	0.73	164.7	13.2	224.1	17.9

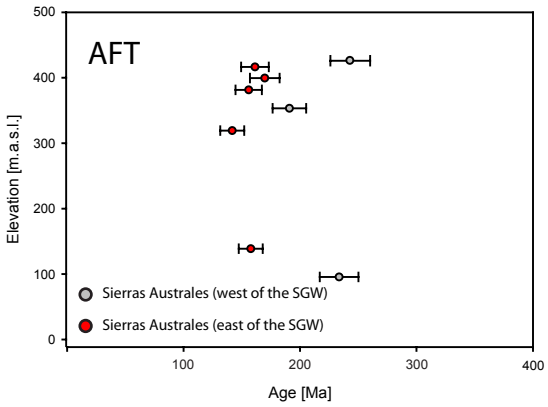

Fig. 5.55: AFT-age-elevation plot of the Sierras Australes.

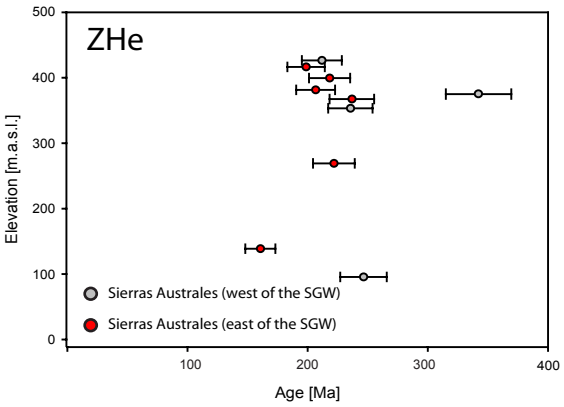

Fig. 5.56: ZHe-age-elevation plot of the Sierras Australes.

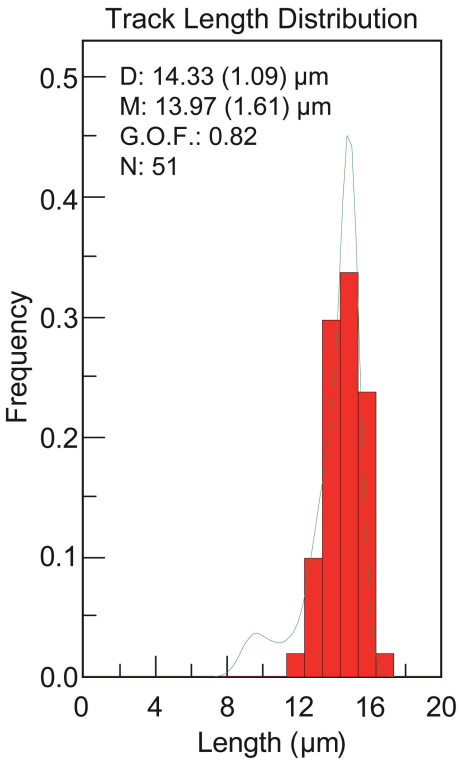

Fig. 5.57: Length distribution of ARG 08.

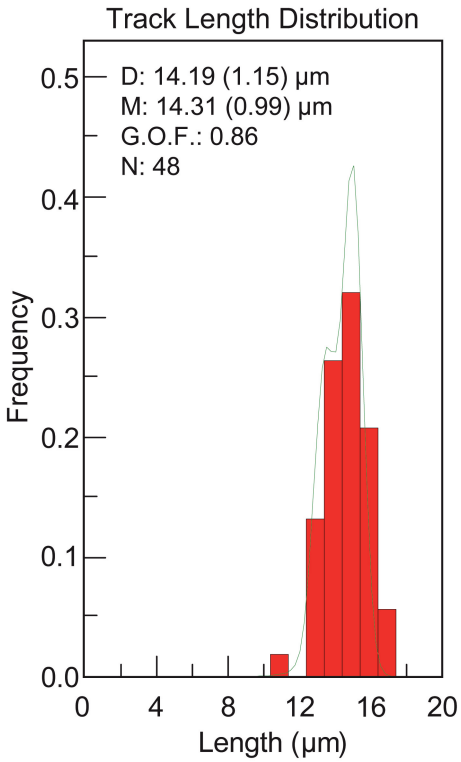

Fig. 5.58: Length distribution of ARG 09.

5.4.2 t-T models

The thermochronological age is represented by a constant cooling model starting ca 350 Ma, using the ZHe-age of the Upper Proterozoic ignimbrite (ARG 07). The t-T model (Fig. 5.59) is only constraint by the ZHe-age.

The t-T model of ARG 08 shows that a phase of constant heating is followed by a phase of constant cooling beginning on the Permian-Triassic transition (Fig. 5.60).

Testing the geological evolution of the Devonian sandstone (ARG 09) against the thermochronological data set revealed a heating from surface temperature to a temperature of 180 °C at about 240 Ma (Fig. 5.61). Assuming a surface temperature of about 15 °C and a geothermal gradient of 30 °C/km and a Carboniferous and Permian sediment thickness of about 5.0 km overlying the Upper Devonian sandstone. After the formation of the basin a period of fast cooling reaching temperatures of about 65°C at 200 Ma followed. Almost constant cooling to surface conditions in the Quaternary indicates the exhumation of nearly 2 km of rock cover. Similarly, the t-T evolution (Fig. 5.60) of the Proterozoic paragneiss (ARG 08) further to the west shows a steady temperature increase and, therefore, basin formation at near surface temperatures in the Ordovician to about 180 °C at the end of the Permian (250 Ma). The following period of rapid cooling, which is similar to the cooling event of the Devonian Sandstone (ARG 09), is changing into a stage of constant cooling from 60°C at about 225 Ma to surface temperature in the Upper Cenozoic.

Comparing these two models would suggest a late Permian to Triassic exhumation leading to the erosion of about 3 km of Carboniferous to Permian rocks in the Sierras Australes, west of the SGW.

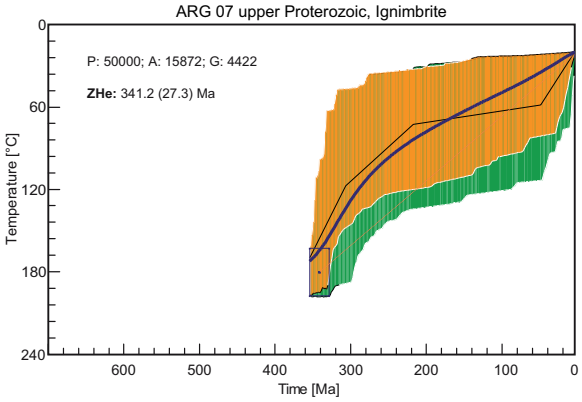

Fig. 5.59: t-T history for ARG 07.

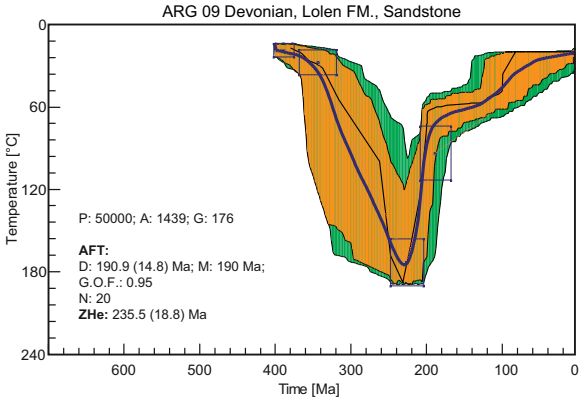

Fig. 5.61: t-T history for ARG 09.

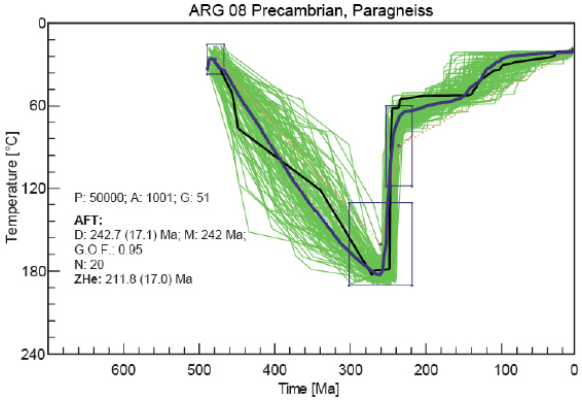

Fig. 5.60: t-T history for ARG 08.

5.5 The Lopez Lecube intrusion

5.5.1 Ages - Lengths - Dpar

West of the Sierras Australes a porphyritic syn-tectonic syenite intrusion (ARG 05) of Permian age (around 258 (2) Ma; Pankhurst et al., 2006), revealed a ZHe-age of 246.4 (19.7) Ma and an AFT-age of 233.5 (17.0) Ma. The ages indicate a fast cooling history during the Triassic followed by slow cooling thereafter (AHe 134.5 (8.1) Ma). The determined ages are presented in Tab. 5-13, Tab. 5-14 & Tab. 5-15). For sample ARG 05 56 lengths and 55 Dpars were measured. The CT mean for the lengths reveals a value of 11.7 (1.6) µm, whereas the mean Dpar value is 1.9 (0.2) µm. The mean value of the c-axes corrected confined fission-track lengths distribution of the apatite grains indicates a fast cooling below the PAZ. Out of the measured lengths a skewness of 0.074 was determined.

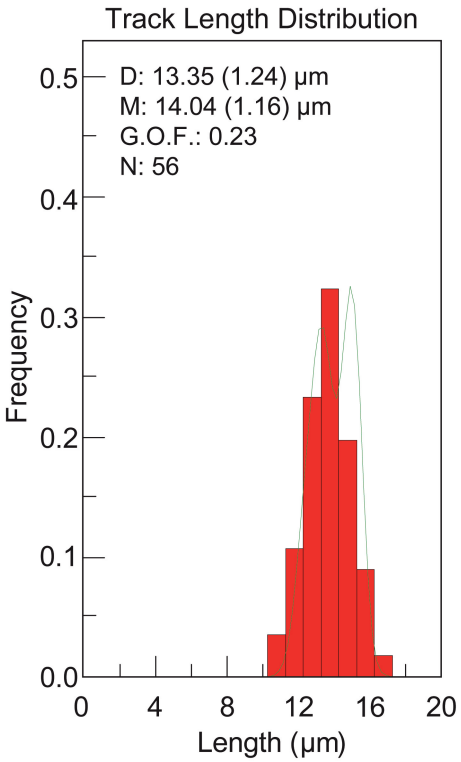

Fig. 5.63: Length distribution of ARG 05.

5.5.2 t-T model

The K/Ar cooling age of 245 (12) Ma, Rossello et al., 1997) of hornblende supports the fast cooling during the Triassic. Ages are presented in (Tab. 5-15) & (Tab. 5-14) & (Tab. 5-14). The t-T history (Fig. 5.62) indicates an extreme fast cooling in a very short time from more than 350 °C at 260 Ma to 75 °C at about 250 Ma. During the Mesozoic the temperature is almost steady until 130 Ma. Thereafter, the cooling rate increases. Surface temperature might already be reached at 50 Ma. Assuming a paleo-geothermal gradient of 30 °C/km and a paleo-surface-temperature of 15°C the temperature of 75 °C at 240 Ma might represent

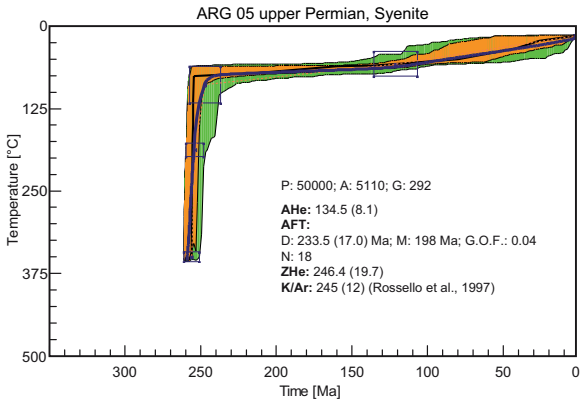

Fig. 5.62: t-T history for ARG 05

Tab. 5-15: Summary of apatite (U-Th-Sm)/He data of the Lopez Lecube intrusion. M: mass, contributing U, Th, Sm,and He concentration, eU = [U] + 0.235 [Th] (concentration in weight %), Ft: α ejection factor for apatite and zircon calculated after Farley et al. (1996), Raw (raw) ages and 1σ error for α-ejection with accordant 1σ error. The brown marked grain was the grains of our choice.

S.-No.	Lithology	U [µg/g]	Th [µg/g]	Sm [µg/g]	eU	Th/U	He [nmol/g]	M (µg)	Ft	raw Age	± 1σ raw age	Age [Ma]	± 1σ [Ma]
Lopez Lecube intrusion													
aARG05-1	Syenite	12.0	87.7	26.3	32.4	7.29	18.3	9.92	0.77	102.4	6.1	132.6	7.9
aARG05-2	Syenite	21.0	67.0	87.3	36.9	3.19	14.6	3.15	0.69	71.6	4.3	103.3	6.2
aARG05-3	Syenite	10.2	65.3	16.7	25.4	6.39	14.6	8.63	0.78	104.5	6.3	134.5	8.1

the temperature of the surrounding rocks and, therefore, indicate an intrusion depth of about 2 km. The large K-feldspar crystals in a medium-grained matrix might propose a shallow intrusion depth as well.

5.6 Correlation of exhumation rates from the Sierras Australes

Based on the t-T models and an average geothermal gradient of 30°C/km, exhumation- and subsidence rates were calculated (Tab. 5-16)& (Tab. 5-17). To get a better overview, the exhumation- and subsidence rates from both sides of the Sauce Grande Wrench, the Lopez Lecube intrusion and the Colorado basin were combined in one figure, with rates plotted against the geological time-line (Fig. 5.64).

Additionally the timing of the thrusting and wrenching along the Sauce Grande Wrench at the Permian-Triassic border and the timing of the basaltic flows (Jurrasic-Cretaceous) were marked with black lines.

By comparing the rates from both sides of the SGW it is obvious that both sides behaved differently. The changeover from subsidence to exhumation did not take place simultaneously. The initiation of exhumation in the area west of the SGW was prior earlier to the eastern part. The exhumation in the western part started on the Permian-Triassic transition at about 250 Ma, whereas the eastern part was exhumed a bit later, in the Upper Triassic. The rates for the Lopez Lecube intrusion show a complete different pattern. It shows the typical trend for intrusive samples with a fast cooling/exhumation at the beginning, slowing down towards the surface. The slight increase of the exhumation rate in the lower Cretaceous is more likely related to a tectonic uplift.

A comparison of the rates with the published sedimentation rates from the Colorado basin is difficult, due to different scales and resolutions in time and vertical position. The relatively middle-rated sedimentation rates from the Colorado basin match the fact that the eastern part of the Sierras Australes is exhuming and therefore provides material for the offshore part of the Colorado basin. The AFT-data plotted in the corresponding age-elevation plot clearly shows that the AFT-ages (Fig. 5.55) east of the SGW are slightly younger than the ages from the western part. The age-elevation plot with the ZHe-ages (Fig. 5.56) from the Sierras Australes show the same tendencies of younger ages from the eastern parte and older ages from the western part.

Tab. 5-16: Calculated exhumation rates for the Sierras Australes (east of the SGW), based on a geothermal gradient of 30°C/km.

Sample number	Elevation [m a.s.l.]	Cooling	t-t segment [Ma]	T-T segment [°C]	Cooling gradient [°C/Ma]	Geothe. gradient [°C/km]	Exhumation rate [mm/a]	Δt	ΔT
East of the Sauce Grande wrench									
ARG 12	319	heating	280-250	20-240	7.33	30	-0.244	30	220
		cooling	250-130	240-70	1.38	30	0.047	120	170
		nearly stable t-T-conditions	130-50	70-65	1.17	30	0.002	80	5
		cooling	50-0	40-65	0.20	30	0.017	50	25
ARG 14	367	heating	250-220	20-185	5.50	30	-0.183	30	165
		cooling	220-0	185-20	0.75	30	0.025	220	165
ARG 15	399	heating	270-220	20-190	3.40	30	-0.113	50	170
		cooling	220-185	190-70	3.43	30	0.114	35	120
		cooling	185-125	70-40	0.50	30	0.017	60	30
		cooling	125-0	40-20	0.16	30	0.005	125	20
ARG 16	381	heating	320-200	20-185	1.38	30	-0.046	120	165
		stable t-T-conditions	200-160	185-184	0.03	30	0.001	40	1
		cooling	160-155	184-85	4.95	30	0.008	20	5
		cooling	155-0	85-20	0.46	30	0.037	140	155
ARG 17	416	heating	280-250	20-100	2.33	30	-0.078	30	80
		heating	250-215	100-210	3.14	30	-0.105	35	110
		cooling	215-155	210-90	2.00	30	0.067	60	120
		cooling	155-0	90-20	0.58	30	0.015	155	70

Tab. 5-17: Calculated exhumation rates for the Sierras Australes (west of the SGW) and the Lopez Lecube intrusion, based on a geothermal gradient of 30°C/km.

Sample number	Elevation [m a.s.l.]	Cooling	t-t segment [Ma]	T-T segment [°C]	Cooling gradient [°C/Ma]	Geothe. gradient [°C/km]	Exhumation rate [mm/a]	Δt	ΔT
West of the Sauce Grande wrench									
ARG 07	375	cooling	340-280	190-110	0.50	30	0.017	160	80
		cooling	280-0	110-20	0.32	30	0.011	280	90
ARG 08	426	heating	480-250	25-190	0.72	30	0.024	230	165
		cooling	250-225	190-60	5.2	30	0.173	25	130
		cooling	225-150	60-50	0.13	30	0.004	75	10
		cooling	150-100	50-25	0.5	30	0.017	50	25
		cooling	100-0	25-20	0.05	30	0.002	100	5
ARG 09	353	heating	400-240	20-180	1.00	30	0.033	160	160
		cooling	240-200	180-65	2.88	30	0.096	40	115
		cooling	200-135	65-55	0.15	30	0.005	65	10
		cooling	135-95	55-25	0.75	30	0.025	40	30
		cooling	95-0	25-20	0.05	30	0.002	95	5
Lopez Lecube intrusion									
ARG 05	96	cooling	260-250	370-75	29.50	30	0.983	10	295
		cooling	250-130	75-60	0.13	30	0.004	120	15
		cooling	130-0	60-20	0.46	30	0.015	130	40

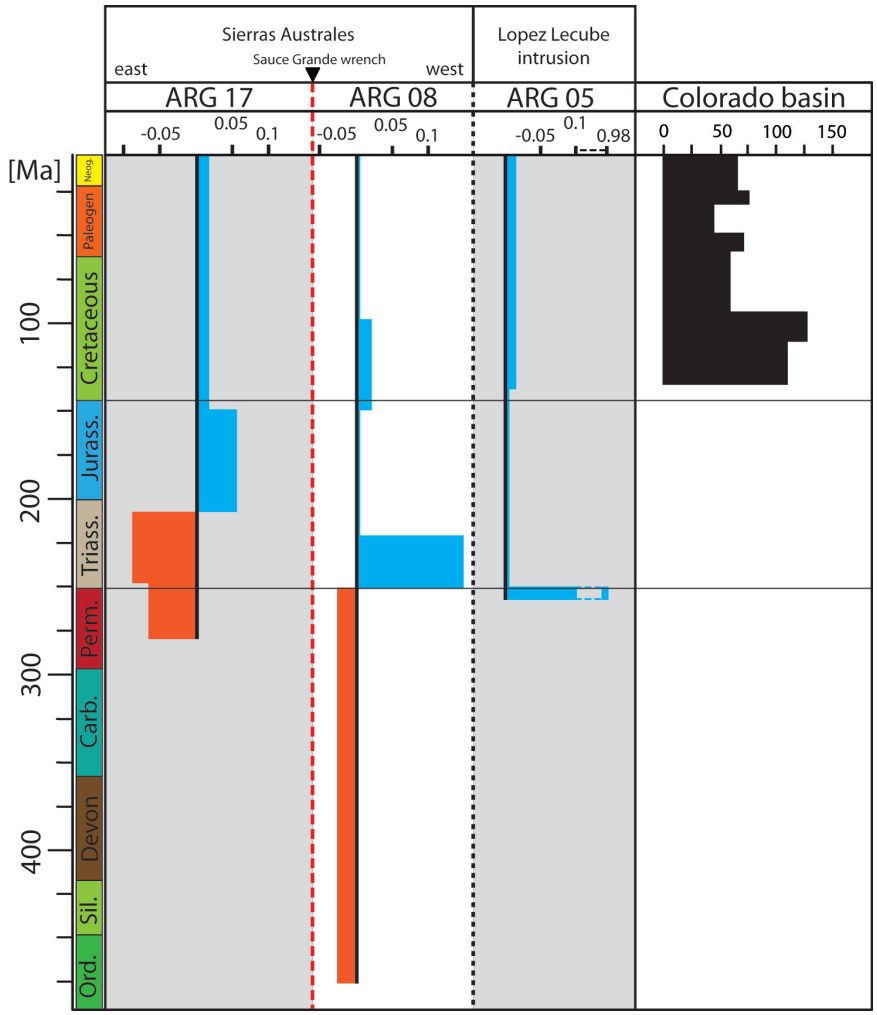

Fig. 5.64: Summary and comparison of calculated rates for the Sierras Australes, the Lopez Lecube intrusion and the Colorado basin (Loegering et al., 2013) against the geological time line. Exhumation rates are given in mm/a. Sedimentation rates are given in m/Ma.

5.7 Uruguay

5.7.1 Ages - Lengths - Dpar

All measured AFT-ages ((Fig. 5.43) & (Tab. 5-18)) are younger than the corresponding crystallisation ages (detailed spread sheets of the fission-track data are listed in the appendix). They range from 200.2 (19.3) Ma from the Paleoproterozoic Isla Mala granodiorite (2074 (6) Ma, U-Pb on zircon: Hartmann et al., 2000) about 15 km north of Florida to 325.7 (24.8) Ma from the Paleoproterozoic Mahoma Gabbro (1998 (35) Ma, Rb-Sr: Umpierre and Halpern, 1971) in the western Piedra Alta Terrane. That indicates that both, the youngest and the oldest AFT-age of the dataset are from the Piedra Alta Terrane. U 11 next to the town of Florida is dated 298.3 (22.3) Ma. The Tandilia Terrane shows ages of 245.0 (24.3) Ma from a Paleoproterozoic orthoamphibolite (U 43) and 227.3 (43.1) Ma from a pegmatite of probable Paleoproterozoic age (U 47). From the southern Cuchilla Dionisio Terrane, only one AFT-age exists. U 42 reveals an age of 219.1 (2.3) Ma from an orthogneiss of the Cerro Olivo Complex in Punta del Este (1001 (17) Ma, U-Pb on zircon: Basei et al., 2011). Sample U 37 from the Sierra Ballena Shear Zone located between the Nico Perez Terrane and the Cuchilla Dionisio Terrane shows an AFT-age of 238.8 (20.3) Ma in a foliated granite at the eastern section of the shear zone.

Four samples (U 06, U 11, U 37, U 43) provided enough length to apply the measurements of lengths and Dpars© for 2D thermokinematic HeFTy-modelling (Tab. 5-2). The mean lengths distribution ranges between 10.8 µm (1.39 µm) in U 43 and 12.2 µm (1.5). As these length distributions do not vary much, a consistent t-T-evolution for all 4 samples consequentially is reasonable. The measured mean Dpar©-values range between 1.3 µm (0.2 µm) and 1.6 µm (0.2 µm) and therefore do not propose differing chemical compositions of the analysed grains (big Dpar©-values indicates chlorine rich grains and low Dpar©-values indicate fluorine rich grains). The

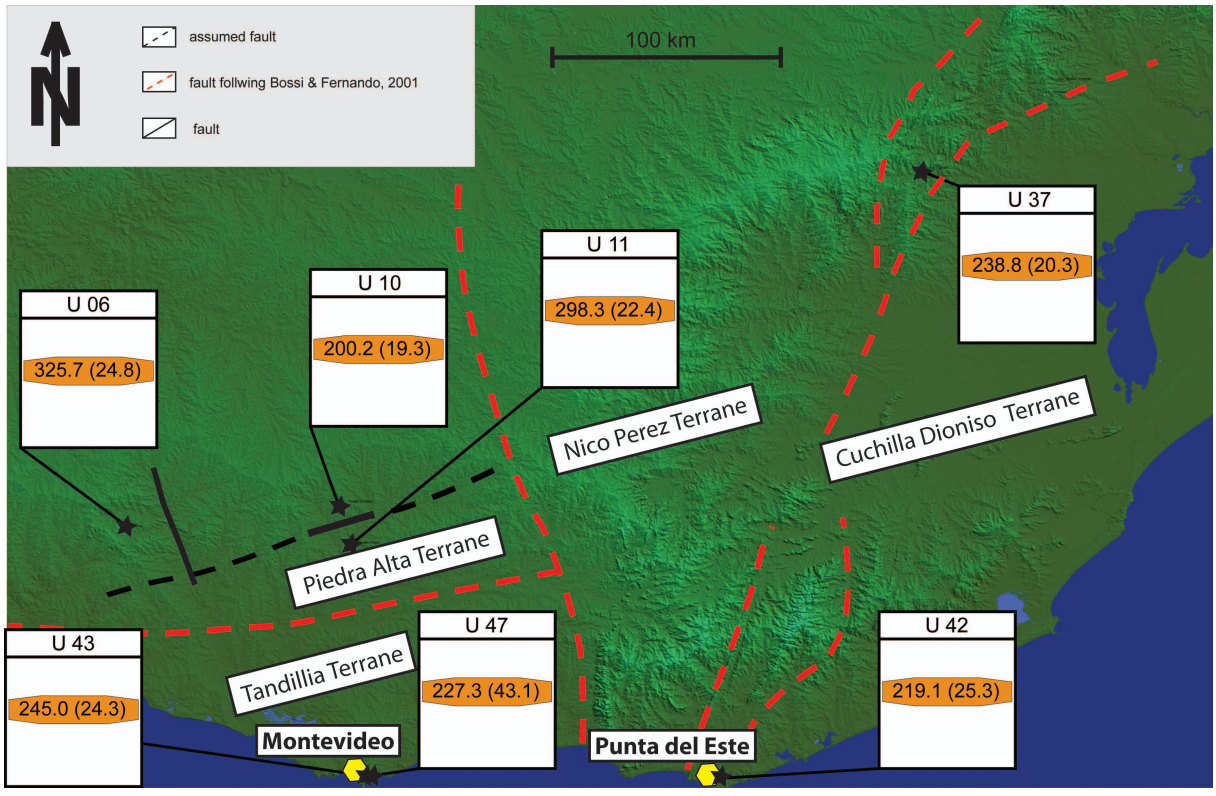

Fig. 5.65: AFT-ages from south-eastern Uruguay (plotted on the DEM-90 m by Jarvis et al., 2008).

corresponding length distributions are characterized by 65 lenghts measurements for U 06, 95 measured lengths for U 11, 70 measured lengths for U 37 and 50 measured lengths for U 43. The measured Dpars range between 95 and 110 for each sample. U 06 and U 43 are characterized by a negative skewness of -0.072, respectively -0.055 and corresponding CT mean values of 12.2 (1.5) µm, respectively 10.8 (1.4) µm. Samples U 11 and U 37 reveal a positive skewness of 0.202, respectively 0.101. The determined CT mean values of 11.2 (1.2) µm and 11.0 (1.7) µm are nearly equal. The age-elevation plot of the AFT-ages from Uruguay provides only few additional information. Again a vertical movement along faults could be detected, due to differing ages on nearly the same topographic altitude levels (Fig. 5.69; Fig. 5.65). The black circle marks a possible cooling path for the area. This cooling path reveals an average exhumation rate of 2.3 m/Ma (0.023 mm/a). Comparing this averaged value from the age-elevation plot with the calculated rates (Tab. 5-19), it is obvious that it is well suitable.

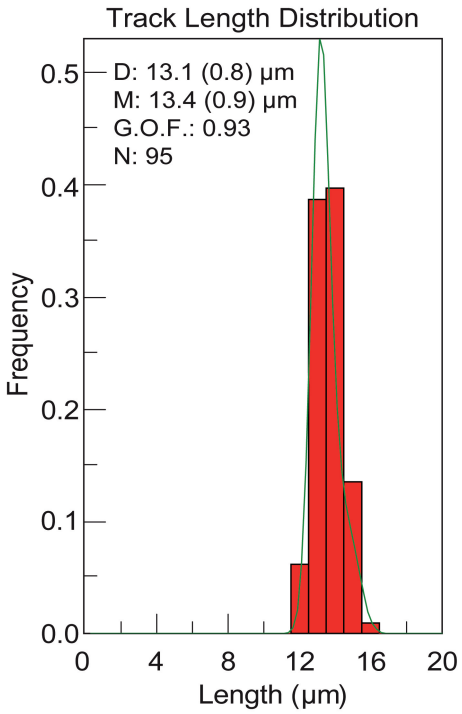

Fig. 5.66: Length distribution of U 11.

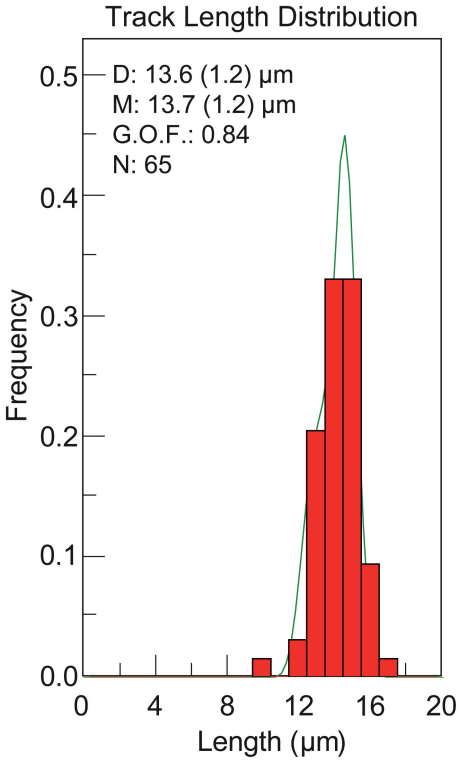

Fig. 5.67: Length distribution of U 06.

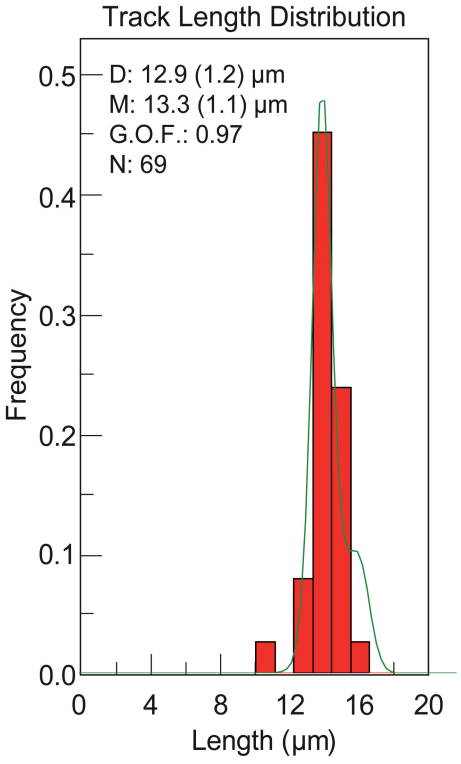

Fig. 5.68: Length distribution of U 37.

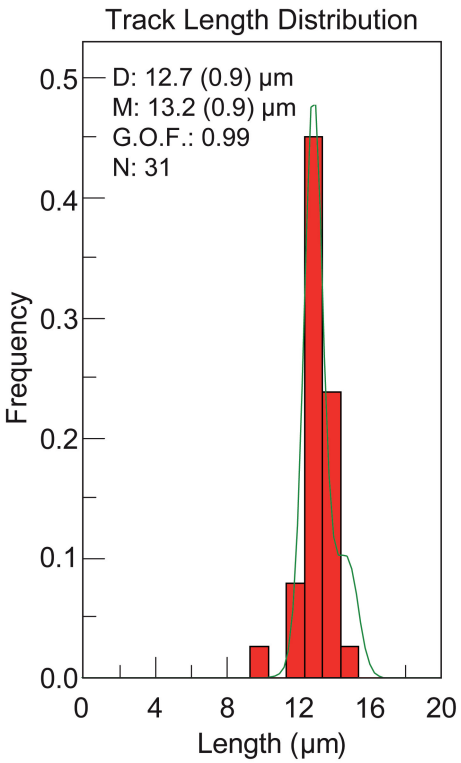

Fig. 5.69: Length distribution of U 43.

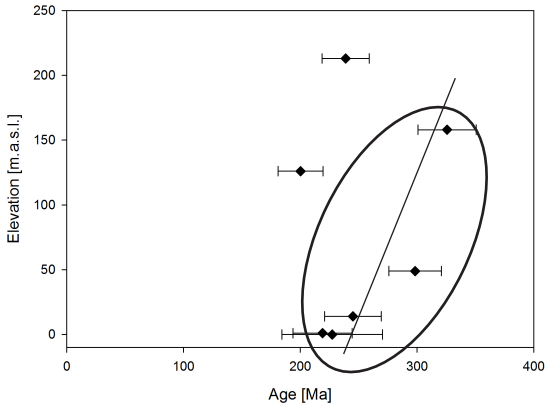

Fig. 5.70: AFT-age-elevation plot of NE-Uruguay. The black circle marks a possible cooling path for the region, the black line the partial regression line.

Tab. 5-18: Apatite fission-track data of Uruguay. U: uranium concentration in µg/g, n: number of counted grains, ρS: density of spontaneous tracks (x 105/cm²), Ns: number of spontaneous tracks, ρI: density of induced tracks (x 105/cm²), NI: number of induced tracks, P(χ^2) is the probability that single grain ages are consistent and belong to the same population. Test is passed if P(χ^2) > 5% (Galbraith, 1981). Ages calculated using a ζ- value of 336.83 (19.51) a/cm² for apatite, Nd =15148 tracks.

Sample No.	Altitude [m.a.s.l.]	Form. age	U (std) [µg/g]	n	Sp. Tracks ρ_s	Sp. Tracks N_s	Ind. Tracks ρ_i	Ind. Tracks N_i	χ^2 [%]	Central age (1σ) [Ma]
U 06	158	Precambrian	15.1 (6.02)	20	25.267	1012	18.226	730	100.00	325.7 (24.8)
U 10	126	Precambrian	14.9 (8.4)	18	13.868	314	16.517	374	100.00	200.2 (19.3)
U 11	49	Precambrian	36.7 (12.5)	20	54.429	1032	43.406	823	100.00	298.3 (22.4)
U 37	213	Precambrian	19.2 (6.0)	19	22.294	645	22.709	657	100.00	238.8 (20.3)
U 42	1	Precambrian	11.36 (5.1)	11	13.621	192	15.181	214	99.76	219.1 (25.3)
U 43	14	Precambrian	13.1 (4.8)	16	15.938	314	15.939	314	100.00	245.0 (24.3)
U 47	0	Precambrian	11.7 (10.2)	2	12.99	59	14.091	64	67.83	227.3 (43.1)

5.7.2 t-T models and exhumation rates

The measured AFT-ages and the corresponding length-distributions were used to model particular time-temperature-histories (Fig. 5 – Fig. 8) with the computer code HeFTy (Ketcham, 2009). Boxes (constraints) were chosen to test the data set versus a certain t-T history. At the beginning the t-T histories were modelled without any constraints except of the AFT-constraint. For a constant cooling up to recent surface conditions no solutions were found (detailed spread sheets of the t-T models are listed in the appendix).

According to the local stratigraphy, the Jurassic and lower cretaceous is missing in the region but younger units are deposited, suggesting a reheating scenario. Reported Jurassic volcanic units in the Salado basin (Carol et al., 2010) support this t-T evolution. Two boxes forced the t-T paths to reach nearly surface conditions during Jurassic and early cretaceous times. The following reheating represents a scenario of a basalt layer with a thickness of about 2000 m. This scenario correlates the data set. Additionally, work done by Stoakes et al. (1991) shows that offshore Uru-

guay in the Punta del Este basins, a volcanic rift-sequence is visible in two wells penetrating the basin-filling. These volcanic rocks are probably Early Cretaceous in age, coeval with continental flood basalts of the Arapey Formation.

During the analytical work length measurements for four samples were possible, whereas the model for U 43 is only based on a data-set of 31 lengths.

The data-set for each sample was tested against the geological scenario described above. The primary, self-governed reheating the model created was constrained by a box for middle- to upper-cretaceous times down to 70°C.

Subsidence- and exhumation rates were calculated. Based on the t-T models and a assumed geothermal gradient, heating- and cooling rates were evaluated. The rates are presented in (Tab. 5-19) and in (Fig. 5.75). The exhumation rates can be summarized in 4 different clusters. An initial period of cooling represents exhumation rates between 0.006 mm/a and 0.012 mm/a. The following phase of almost stable conditions (with a first tendency to a reheating event) reveals a homogeneous rate of 0.003 mm/a. The actual reheating event shows rates between 0.007 mm/a and 0.026 mm/a and is followed by a final phase of cooling (exhumation rates between 0.012 mm/a and 0.021 mm/a).

In general the HeFTy models and calculated exhumation rates for Uruguay correlate well with each other (Fig. 5.75). The timing of the changeover from cooling to the reheating event is simultaneously. The changeover from reheating to the final phase of cooling is also nearly isochronal. By comparing the calculated rates with the published sedimentation rates from the neighbouring Pelotas basin emphasizes that the tendency of rates from the on- and offshore data fits only partially. Considering a lag-time the onshore erosion fits to the offshore sediment supply. A more detailed correlation of both data-sets is not possible, due to the differing resolutions.

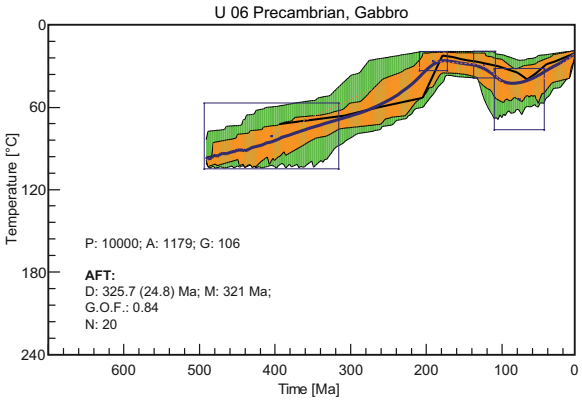

Fig. 5.71: t-T history for U 06.

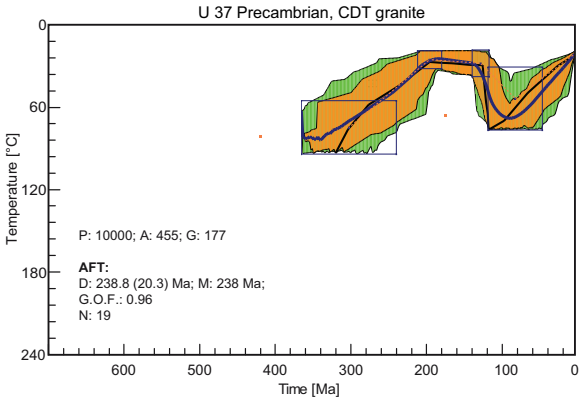

Fig. 5.72: t-T history for U 37.

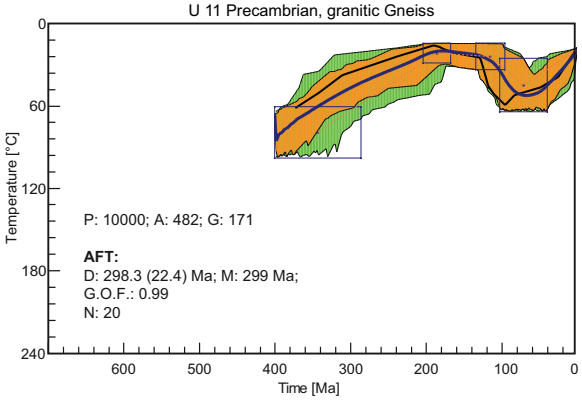

Fig. 5.73: t-T history for U 11.

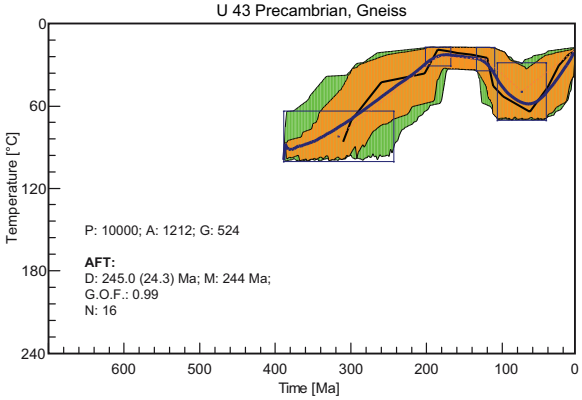

Fig. 5.74: t-T history for U 43.

Tab. 5-19: Calculated exhumation- and subsidence rates for Uruguay (based on a geothermal gradient of 30°C/km).

sample number	Altitude [m.a.s.l.]	Description	t-t Segment [Ma]	T-T Segment [°C]	Heating- / Coolingrate [°C/Ma]	Subsidence- / Exhumationrate [mm/a]	Δt	ΔT
U 06	158	cooling	450-280	90-60	0.176	0.006	170	30
		cooling	280-180	60-25	0.350	0.012	100	35
		nearly stable	180-125	25-30	0.091	0.003	55	5
		heating	125-80	30-40	0.222	0.007	45	10
		cooling	80-0	40-20	0.348	0.012	115	40
U 11	49	cooling	370-180	80-25	0.289	0.010	190	55
		nearly stable	180-120	25-30	0.083	0.003	60	5
		heating	120-60	30-55	0.417	0.014	60	25
		cooling	60-0	55-20	0.583	0.019	60	35
U 37	213	cooling	350-180	80-25	0.324	0.011	170	55
		nearly stable	180-125	25-30	0.091	0.003	55	5
		heating	125-80	30-65	0.778	0.026	45	35
		cooling	80-0	65-20	0.563	0.019	80	45
U 43	14	cooling	370-180	95-25	0.368	0.012	190	70
		nearly stable	180-130	25-30	0.100	0.003	50	5
		heating	130-65	30-60	0.462	0.015	65	30
		cooling	65-0	60-20	0.615	0.021	65	40

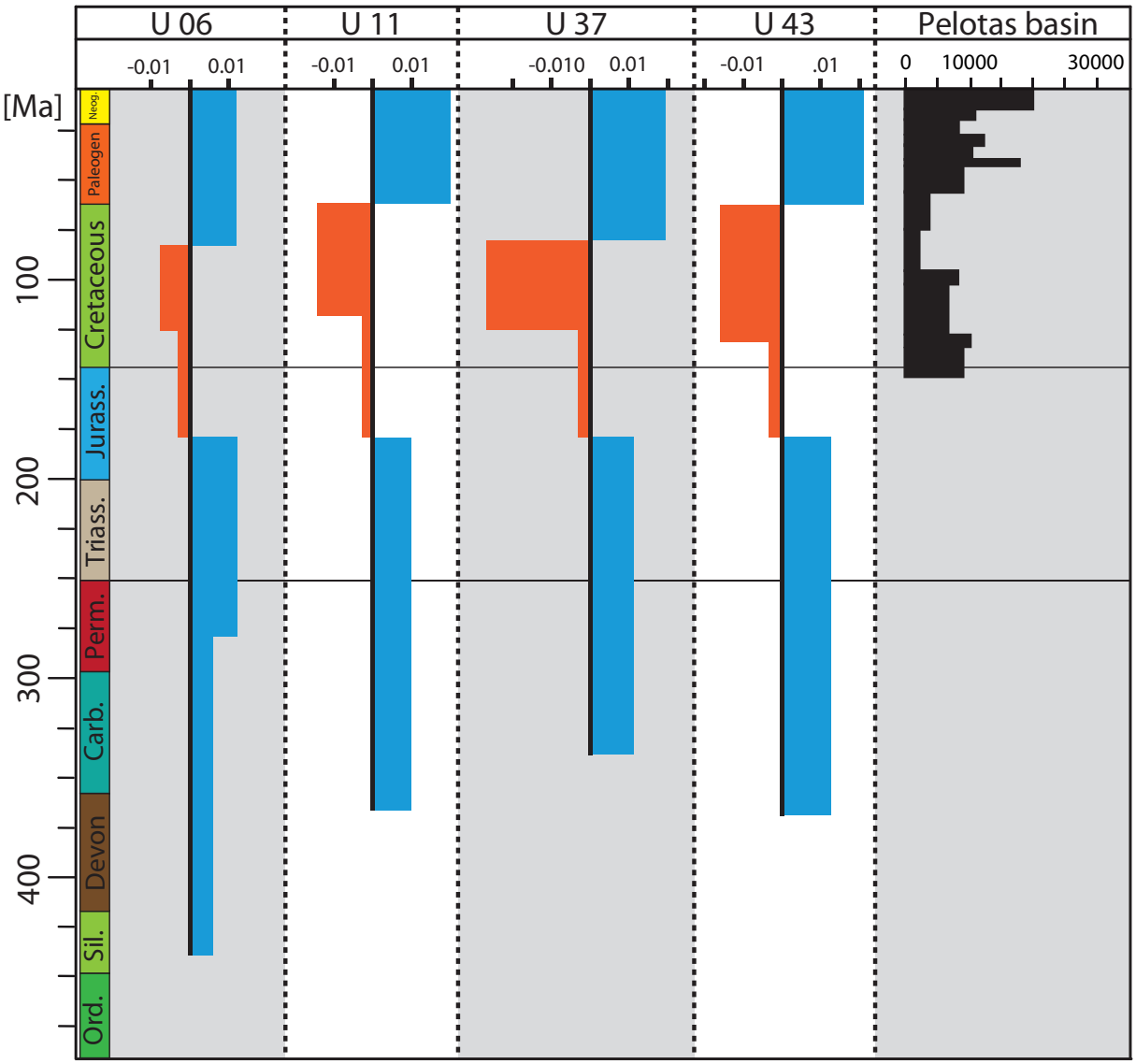

Fig. 5.75: Summary and comparison of calculated rates for SE-Uruguay and the Pelotas basin (Loegering et al., 2013) against the geological time line. Exhumation rates are given in mm/a. Sedimentation rates are given in m/Ma.

6

Discussion - Subsidence, inversion and exhumation

Contents

The following chapter will transfer the thermochronological data and the t-T models into subsidence and inversion history, and discuss the exhumation rates in selected time steps. The schematic illustration (Fig. 6.1) of the initial tectonic and geological set-up of the research area is based on cross-sections published by Rapela et al., 2003 (Sierras Australes), Cingolani, 2010 (Sierras Septentrionales and Alesandretti, 2013 (Claromeco Basin).

6.1 Argentina

6.1.1 Sierras Australes - Interpretation and exhumation rates

6.1.1.1 Ordovician to Permian (Gondwanide basin evolution and orogeny)

The Ordovician to Permian is characterized by the evolution of a sedimentary basin that overlaid the Precambrian metamorphic and intrusive basement throughout the whole area. In Permian time this basin was deformed and partially metamorphosed. In the neighbouring Sierras Australes the SGW zone separates a western area with lower greenschist facies metamorphic sedimentary rocks of Ordovician to Devonian age from the eastern part, which is characterized by diagenetic to anchizonal Carboniferous to Permian sedimentary rocks.

The thermochronological data and the thermokinematic modelling of samples from the Sierras Septentrionales indicate a Late Devonian to Early Carboniferous fast exhumation (rate: 0.113 mm/a), followed by subsidence with a rate of 0.019 mm/a (Fig. 28). The exhumation history leads to approximately 5.000 m of eroded rocks. Considering a surface temperature of 15°C, a geothermal gradient of 30 °C/km (Zeil, 1980) and the subsidence rate, the basin was filled with 2.500 m of sedimentary rocks at the end of Permian.

At the same time, west of the Sauce Grande wrench, subsidence with a rate of 0.024 mm/a also leads to the accumulation of 2.500 m of sedimentary rocks. In Permian, east of the SGW subsidence with a subsidence rate of 0.078 mm/a almost 3.000 m of sedimentary rocks were accumulated.

At the end of Permian the Lopez Lecube syenite intruded into the Precambrian metamorphic rocks and cooled extremely fast from magmatic temperature to about 75 °C within 10 Ma. We interpret the low temperature as an indication for the temperature of the Precambrian metamorphic rocks at the intrusion depth; indicating an intrusion depth of 2.000 to 3.000 m depending on the geothermal gradient in the area.

6.1.1.2 Permian to Jurassic (Post Gondwanides)

The timing of the tectonic and long-term landscape evolution of the western and the eastern part of the SGW is significantly different. During the Triassic the western part (Fig. 28, #ARG 08) exhumed rapidly (up to 0.173 mm/a). This vertical movement induced the erosion of more than 5.000 m of sedimentary rocks. The exhumation rate decreased significantly in the middle Triassic and continued with this rate until the end of the Jurassic. During the whole Triassic east of the SGW the Permian subsidence continued and the subsidence rate increased significantly (0.105 mm/a). This lead to a pile of more than 3.500 m of sedimentary rocks of Triassic age. Subsidence was terminated at the end of Triassic and changed to an exhumation with a rate of 0.067 mm/a (erosion of > 3.000 m of sedimentary rocks) until the end of the Jurassic. The spatial relationship between the strong exhumation of the western part (west of the SGW) and the strong subsidence of the eastern part (east of the SGW) indicates a sediment transport from west to east (Fig. 6.1). Therefore, the western Sierras Australes is a possible source area for the sediments of the eastern Sierras Australes. Furthermore, the westerly dipping SGW thrust zone, might be an indication for a tectonically induced subsidence of the eastern side, due to the thrusting of the western area towards the east. The timing of the thrust movement is widely thought to have occurred on the Permian-Triassic transition (e.g. Tomezzoli & Vilas,

1999 and literature cited therein). Unfortunately, the data does not provide any information on the timing of tectonic uplift versus erosion.

6.1.1.3 Jurassic to recent (Syn- and Post- South Atlantic rift evolution)

This time interval is of fundamental importance for the evolution of the South Atlantic, as rifting is followed by the formation of "passive margins". One aim of this thermochronological study was to evaluate the influence of the tectonic processes related to the rifting, the opening and the post-rift stage of the plate tectonic evolution. West of the SGW the Lower Cretaceous is characterized by an increase in exhumation velocity from 0.004 mm/a (Jurassic) to 0.017 mm/a. This exhumation of rocks is followed by the erosion of about 400 m of sedimentary rocks. Furthermore, the exhumation rate (0.015 mm/a) of the Lopez Lecube syenite increases as well.

During the Upper Cretaceous the sedimentation rate of the offshore part of the Colorado Basin is in the range of 0.125 mm/a (Loegering et al., 2013; Kuhlmann et al., 2010). Considering a lag time from erosion to sedimentation it seams reasonable, that the eastern part of the Sierras Australes is a possible source for the sediments.

6.1.2 Sierras Septentrionales - Interpretation and exhumation rates

6.1.2.1 Ordovician to Permian (Gondwanides basin evolution and orogeny)

The modeled t-T histories and the published geological facts lead to the assumption that the Ordovician to Permian period is characterized and influenced by the evolution of a sedimentary basin, which overlaid the Precambrian metamorphic and intrusive basement throughout the area of the today's Sierras Australes, the Claromecco basin and the Sierras Septentrionales.

Assuming a surface temperature of about 15°C and a geothermal gradient of 30 °C/km (Zeil, 1980) the intracratonic Claromeco basin was filled with at least 6000 m of sedimentary rocks at the end of the Permian. The subsidence rate between the early Ordovician and the Permian varied slightly with values between 0.024 mm/a and 0.034 mm/a, and therefore was relatively high.

6.1.2.2 Permian to Jurassic (Post Gondwanides)

The tectonic activity along the Sauce Grande Wrench, lead to an exhumation of the neighbouring Sierras Australes on the Permian-Triassic transition. This exhumation provided the source rocks for Triassic sediments, that were accumulated in the Claromeco basin. The overlaying Triassic sediments induced a phase of subsidence in the basin.

In the Upper Triassic the region (Sierras Australes, Claromeco basin and Sierras Septentrionales) was affected by a new phase of exhumation. The exhumation in the Sierras Australes, as well as in the Sierras Septentrionales, was quite fast (exhumation rates up to 0.067 mm/a). This exposure of rocks lead to the erosion of nearly the whole sedimentary body, which was lying on top of the metamorphic and intrusive basement.

6.1.2.3 Upper Jurassic and Cretaceous

The exhumation in the Sierras Septentrionales was abruptly interrupted by the deposition of a massive volcanic sequence. Volcanic activity influenced the area of the Sierras Septentrionales (Fig. 6.1)and today's Salado basin (max. thickness up to 2 km, depending on the estimated thermal gradient) . By estimating a thermal gradient of 30°C/km the maximum thickness would be a bit less, but by considering an increased heat-flow going along with the massive volcanic activity, a 2000 m-overburden is comprehensible. The deposition of the volcanic units in the Claromeco basin could not be determined by the data, so that it seems that the Sierras Septentrionales represent the most southern point, influenced by the basaltic flows. In the Sierras Septentrionales, these extrusive successions acted against the previous exhumation, inferring a change of the tectonic setting with the consequence of subsidence. The volcanic rocks were not only distributed in the Si-

erras Septentrionales, but also in the neighbouring Salado basin. The subsidence and the initial opening of the South Atlantic Ocean finally resulted in the formation of the Salado basin.

6.1.2.4 Cretaceous to recent

Due to the prolonged exhumation in the Sierras Septentrionales the accumulated Jurassic extrusive layers were exhibited to weathering and climatic impacts. Continuing exhumation as well as exposition to climate and weathering resulted in the erosion of material in the Sierras Australes and Sierras Septentrionales and the accumulation in the Claromeco basin. The Jurassic extrusive rocks from the Sierras Septentrionales were eroded completely and distributed most likely to the Claromeco basin, as well as the Salado basin. It is hard to quantify the amount of input from the Sierras Septentrionales to the Salado basin and the Claromeco basin (as well as the amount of input from the Sierras Australes to the Colorado basin and the Claromeco basin), due to the fact that all three basin in the research area are operating as a sink for multiple source areas. Following the 2D-models, the tectonic setting from cretaceous times to recent times has not changed and both mountain ranges are still exhuming, while the neighbouring basins are still subsiding.

6.2 Uruguay

6.2.1. Interpretation and exhumation rates

The combination of AFT-ages, age-elevation-plots and t-T models give new insights into the thermal history of south-eastern Uruguay. Differing ages (with respect to the error) from similar topographic altitudes indicate vertical fault movement between both localities, whereas same ages (with respect to the errors) from different topographic altitudes indicate a fast exhumation. However, the topographic variation is very small throughout the region, the age-elevation-plot shows remarkable patterns.

The relative positions of some samples to each other indicate movements along faults as they show different ages of similar topographic height (e.g. U 06/U 10 ; U 11/U 10 ; U 37/U 06 ; U 47,U 43/U 11 ; U 42/U 11). These movements could be along the borders separating the different terranes, but also smaller faults could be responsible. U 11 and U 10 are located very close to each other, so in this case a fault, which was active at about 200 Ma, separating both sample localities. The mafic dyke swarm between these samples may represent a zone of weakness in the crust. The ages of U 06 and U 10 indicate tectonic movement between them, due to the age-spread of more than 100 Ma and only a topographic variation of around 30 m. These cases show how powerful thermochronology can be to identify new faults and tectonic movements. The AFT-ages from the Tandillia Terrane are also quite remarkable. With respect to the error the two AFT-ages (U 43, U 47) are in the range of 250 Ma. Pfister et al (2015) and Kollenz et al (2015) were able to show a tectonic relationship between the Argentinean Sierras Septentrionales (=Sierras de Tandil) and the Sierras Australes. The thrust-belt of the Sierras Australes was active at the Permian-Triassic border (Rossello et al., 1997 and literature cited therein) at about 250 Ma. Those strong tectonics also controlled the thermal evolution of the neighbouring Sierras Septentrionales, so that the thermochronological data-set of the dated zircons show ages of about 250 Ma. The ages of U 43 and U 47 point to a tectonic link between the Sierras the Tandil in Argentina and the Tandilia Terrane in Uruguay, as postulated by Bossi et al. (2005) and Bossi and Cingolani (2009). By comparing the ages from the Tandilia Terrane with the neighbouring U 11 (AFT: 298.3 (22.4)) from the Piedra Alta Terrane tectonic movement at the border of both terranes could be detected. This movement took place at about 250 Ma so that it is possibly also linked and controlled by the Permo-Triassic wrenching from the Sierras Australes. The calculated exhumation rates (calculated with a geothermal gradient of 30°C/km) show a constant exhumation in all modelled time-temperature-solutions until ~130 Ma with rates between

0,003 mm/a and 0,012 mm/a. The following reheating indicates burial rates between 0,007 mm/a and 0.026 mm/a. The latest phase of exhumation starts in all models between 60 and 80 Ma, until the time-temperature paths reach the recent surface conditions. The examined rocks were exhumed with calculated rates between 0,012 mm/a and 0,021 mm/a. By comparing the exhumation rates it is obvious that the rates before the Cretaceous reheating and the rates after this event are similar. This reheating due to the deposition of the Parana basalts intercepts the constant cooling history. The published sedimentation data done by Contreras (2011) shows a decrease in sedimentation from 130 Ma in the northern Pelotas basin. The average sedimentation here starts to increase again after passing its nick point at about 65 Ma. The trend of this sedimentation period between 130 Ma and recent times fits the modeled time-temperature history for this period. However, the sedimentation data is from the northern part of the Pelotas basin, which does not necessarily represent the passive continental margin of Uruguay and is used representatively as no sedimentation data for the southern part of the basin is known. The modeled scenarios were set up with a parana-basalt-cover. The models worked well for this t-T history and also the sedimentary history and rates fit this model. Although the first data set is limited (7 AFT-ages and 4 2D thermokinematic models) it supports the hypothesis of a Parana-basalt cover in southern Uruguay. Post-rift tectonic fault-reactivation or movements could not be identified, although movements along smaller faults could be detected and previously unknown faults on the Piedra Alta Terrane could be identified. Also vertical movement between the Piedra Alta Terrane and Tandilia Terrane could be verified with the age-elevation plot.

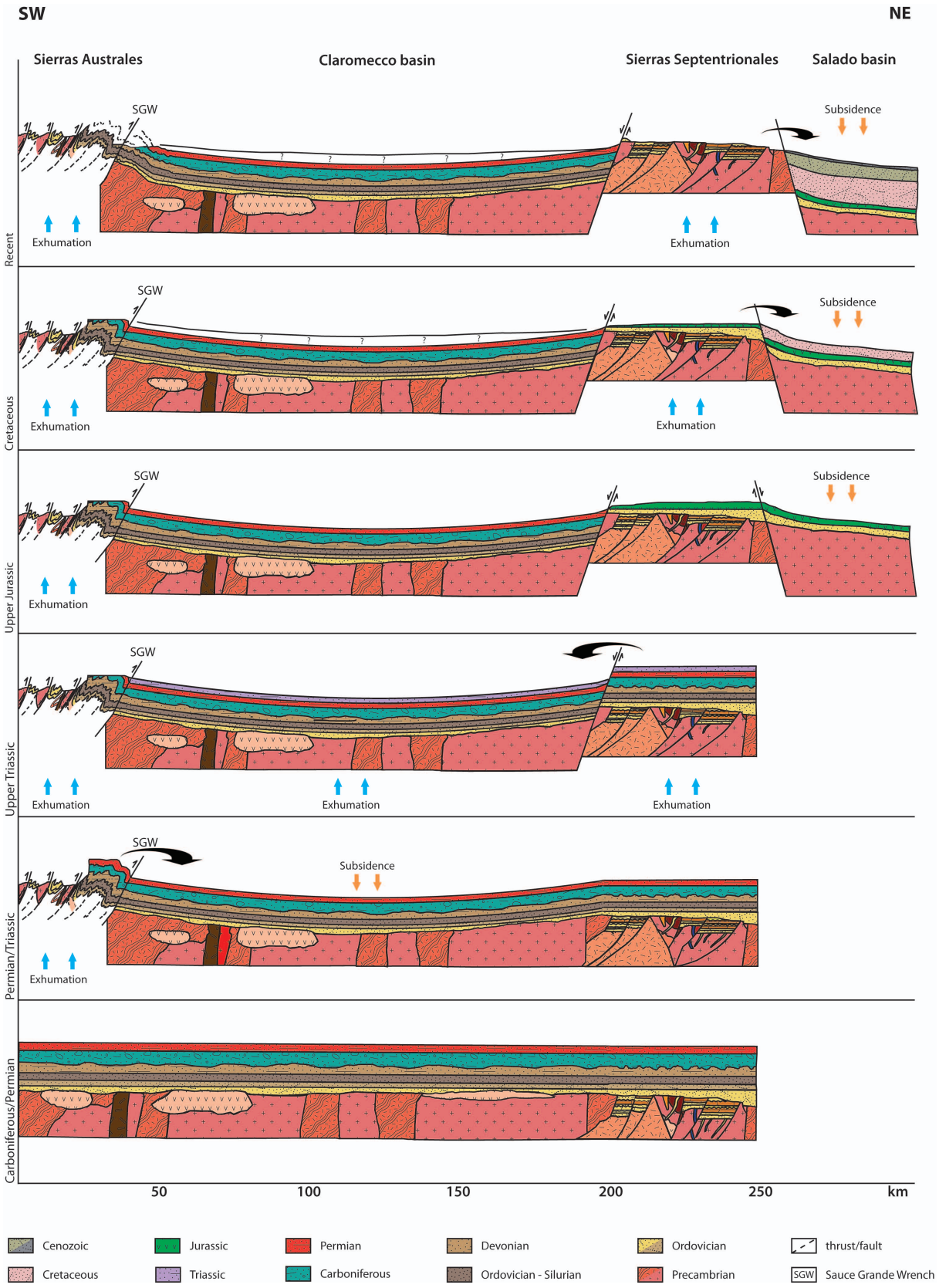

Fig. 6.1: Schematic illustration of the tectonic evolution of the research area.

7

Conclusions

In conclusion, the described thermochronological study clearly indicated that the area of investigation has a complex subsidence and exhumation history since the Ordovician. The thermochronological archive stored information on the pre-, syn-, and post orogenetic history of the Gondwanides in Argentina. Interesting enough the major west-dipping thrust zone , the "Sauce Grande Wrench" in the Sierras Australes, must have been active during the Permian and Triassic. This activation caused exhumation (and accompanying erosion) of the western part and deposition and subsidence in the eastern part. It is very likely, that the east-oriented thrusting process might have induced the subsidence of this easter portion of the mountain range. The major exhumation of the eastern side occurred during the Jurassic and might have been the source for the first strong sedimentation rate in the offshore Colorado basin. All exhumation rates are constant during the Cenozoic but vary related to the location of the samples.

Also, the new data of the Sierras Septentrionales provides new insights into the onshore evolution of the north-eastern Argentinean continental margin. The tectonic movements during Permo-Triassic Variscan orogeny can be clearly approved. Additionally the whole area of the Sierras Septentrionales and the neighbouring Salado basin seemed to be influenced by overlaying Jurassic lavas. The fact that this prominent volcanic layers have extended so far to the south, was not reported or recognized before, and is one of the biggest outcome of this study.

Also the tectonic link between the Uruguay and the Sierras Septentrionales could be proved.

The southernmost Uruguayan Terrane, the Tandilia Terrane, shows a very similar evolution as the Sierras Septentrionales (Tandilia range). The ages fit perfectly to the thermochronological data from the Sierras Septentrionales with ZHe- and ZFT-ages around 250 Ma (Kollenz et al., 2015 and Pfister et al. 2014).

Tectonic movements along faults could be clearly identified with the age-elevation-plot. However, this tectonic activation took place before the initial rifting of the South Atlantic Ocean, and is therefore part of the pre-rift history and gives no insight of the younger post-rift evolution of the research area.

The modelled time-temperature histories from Uruguay also support a history with thick overlaying basalts. The AFT-data-set and the 2D-models shows an excellent fit for a scenario with a this overburden.

The calculated exhumation-rates show a very good fit with the published sedimentation-data from the Pelotas basin (Contreras, 2011).

As concluding remarks for the Uruguayan passive margin some important aspects and outcomes have to be mentioned.

1. The southernmost Uruguayan Terrane, the Tandilia Terrane, shows a similar evolution as the Sierras Septentrionales (Tandilia range). The two AFT ages from the Tandilia Terrane are within error in the range of 250 Ma. This ages fit perfectly with the thermochronological data-set of the Sierras Septentrionales with ZHe- and ZFT-ages around 250 Ma.

2. Tectonic movements along faults could be clearly identified with the age-elevation-plot. However, this tectonic activation took place before the initial rifting of the South Atlantic Ocean, and is therefore part of the pre-rift history and gives no insight of the younger post-rift evolution of the research area.

3. The modelled time-temperature histories for 4 samples from the area points to larger regional extension of the Paraná-basalts. The AFT-data-set and the 2D-models showed an excellent fit for a scenario with a thick overburden.

4. The modelled t-T-history and the calculated exhumation-rates and paths show a very good fit with the published sedimentation-data from the Pelotas basin (Contreras, 2011).

Finally, to refer to the initial questions we can say that all thermochronological ages were reset and that the tectonics from the Sierras Australes also influenced to evolution of the Sierras Septentrionales. The recent differences of both pas-

sive Atlantic margins, are based on the differing post-rift evolution and varying influences from the younger onshore history. Both margins share a part of there history, but also were affected by lot of different influences, that lead to two different continental margins. The exhumation throughout in NE-Argentina and SE-Uruguay are characterized by a very heterogeneous and a homogeneous exhumation history at the same time. The lower mountain ragnes shared some tectonic features throughout their history, but also reveal periods with a differing thermal evolution.

8

References

Abre, P., Bossi, J., Cingolani, C., Gaucher, C., Piñeyro, D., Blanco, G. 2014. El Terreno Tandilia en Uruguay y Argentina. In: Bossi, J., Gaucher, C. (Eds.) Geología del Uruguay. Tomo 1: Predevónico. Polo, Montevideo, pp. 89-119.

Alessandretti, L., Philipp, R.P., Chemale Jr., F., Brückmann, M.P., Zvirtes, G., Matte, V., Ramos, V.A., 2013. Provenance, volcanic record, and tectonic setting of the Paleozoic Ventania Fold Belt and the Claromecó Foreland Basin: Implications on sedimentation and volcanism along the southwestern Gondwana margin. Journal of South American Earth Sciences, Vol. 47, pp. 12-31.

Almeida, F.F.M. de, Hasui, Y. and Brito Neves, B.B.de, 1976. The Upper Precambrian of South America. Boletim Instituto Geociencias, Universidade de Sao Paulo, 7, 45-80.

Basei, M.A.S., Frimmel, H.E., Nutman, A.P., Preciozzi, F., Jacob, J. 2005. A connection between the Neoproterozoic Dom Feliciano (Brazil/Uruguay) and Gariep (Namibia/South Africa) orogenic belts – evidence from a reconnaissance provenance study. Precambrian Research, 139: 195–221.

Basei, M.A.S., Peel, E., Sánchez Bettucci, L., Preciozzi, F., Nutman, A.P., 2011. The basement of the Punta del Este Terrane (Uruguay): an African Mesoproterozoic fragment at the eastern border of the South American Río de la Plata Craton. International Journal of Earth Sciences, 100, 289-304.

Benedetto, J.L., 2010. El continente de Gondwana a través del tiempo. Una introducción a la Geología Histórica. Academia Nacional de Ciencias, Córdoba, 384 p.

Bishop, P., 2007. Long-term landscape evolution: linking tectonics and surface processes. Earth Surf. Process. Landforms 32, p 329–365. Published online in Wiley InterScience.

Blanco, G., Rajesh, H.M., Gaucher, C., Germs, G.J.B., Chemale Jr., F. 2009. Provenance of the Arroyo del Soldado Group (Ediacaran to Cambrian, Uruguay): Implications for the paleogeographic evolution of southwestern Gondwana. Precambrian Research, 171, 57-73.

Bossi, J. , Preciozzi, F., Campal, N. 1993. Predevoniano del Uruguay - Parte I: Terreno Piedra Alta. 50 pp., 37 fig., DINAMIGE, Montevideo.

Bossi, J. , Ferrando, L., Montaña, J., Campal, N., Morales, H., Gancio, F., Schipilov, A., Piñeyro, D., Sprechmann, P., 1998. Carta geológica del Uruguay. Escala 1:500.000. Geoeditores, Montevideo.

Bossi, J. & Ferrando,L. 2001. Carta Geologica del Uruguay. Escala 1:500 000.Version digital. Geoeditores, Montevideo.

Bossi, J., Gaucher, C. 2004. The Cuchilla Dionisio Terrane, Uruguay: an allochthonous block accreted in the Cambrian to SW-Gondwana. Gondwana Research, 7 (3), 661-674.

Bossi, J., Piñeyro, D., Cingolani, C.A., 2005. El límite sur del Terreno Piedra Alta (Uruguay). Importancia de la faja milonítica sinistral de Colonia. Actas XVI Congreso Geológico Argentino, 1, 173-180.

Bossi, J., Schipilov, A. 2007. Rocas ígneas básicas del Uruguay. Facultad de Agronomía,

Montevideo, pp. 1-364.

Bossi, J., Cingolani, C.A. 2009. Extension and general evolution of the Río de la Plata Craton. In: Gaucher, C., Sial, A.N., Halverson, G.P., Frimmel, H.E. (Eds.), Neoproterozoic-Cambrian tectonics, global change and evolution: a focus on southwestern Gondwana. Developments in Precambrian Geology 16: 73–85.

Bossi, J., Gaucher, C. 2014a. Estratigrafía del Predevónico del Uruguay. In: Bossi, J., Gaucher, C. (Eds.) Geología del Uruguay. Tomo 1: Predevónico. Polo, Montevideo, pp. 19-42.

Bossi, J., Gaucher, C. 2014b. Terreno Cuchilla Dionisio: bloque meridional. In: Bossi, J., Gaucher, C. (Eds.) Geología del Uruguay. Tomo 1: Predevónico. Polo, Montevideo, pp. 355-376.

Bossi, J., Piñeyro, D. 2014. Terreno Piedra Alta. In: Bossi, J., Gaucher, C. (Eds.) Geología del Uruguay. Tomo 1: Predevónico. Polo, Montevideo, pp. 45-86.

Bracaccini, I.O., 1980. Cuenca del Salado. En J.C.M. Turner (Ed.) Segundo Simposio de Geología Regional Argentina. Academia Nacional de Ciencias de Córdoba, II: 879-918.

Braun, J., van der Beek, P., 2004. Evolution of passive margin escarpments: What can we learn from low-temperature thermochronology? Journal of Geophysical Research: Earth Surface (2003–2012). Volume 9, Issue F4.

Braun, J., van der Beek, P., Batt, Geoffrey, 2006. Quantitative Thermochronology: Numerical Methods for the Interpretation of Thermochronological Data. Cambridge University Press. ISBN-10: 0521830575

Brix, M. R., Stockhert, B., Seidel, E., Theye, T., Thomson, S. N., Küster, M., 2002. Thermobarometric data from a fossil zircon partial annealing zone in high pressure–low temperature rocks of eastern and central Crete, Greece. Tectonophysics 349, p. 309–326.

Buggisch, W., 1987. Stratigraphy and Very Low Grade Metamorphism of the Sierras Australes de la Provincia de Buenos Aires (Argentina) and implications to Gondwana correlation. In: Zbl. Geol. Paläont. Teil I (1987), Nr. (7/8), S. 819-837.

Bushnell, D.C., Baldi, J.E., Bettini, F.H., Franzin, H., Kovas, E., Marinelli, R., and Wartenburg, G.J., 2000. Petroleum systems analysis of the eastern Colorado Basin, offshore northern Argentina. Petroleum systems of South Atlantic margins: AAPG Memoir, 73: 403–415.

Carol E., Kruse E., Pousa J., 2010. Eco-hydrological role of deep aquifers in the Salado sedimentary basin in the Province of Buenos Aires, Argentina. Environmental Earth Science, 60: 749–756.

Cernuschi, F., Dilles, J.H., Kent, A.J.R., Schroer, G., Raab, A.K., Conti, B., Muzio, R., 2014. Geology, geochemistry and geochronology of the Cretaceous Lascano East intrusive complex and magmatic evolution of the Laguna Merín basin, Uruguay. Gondwana Research. Doi: 10.1016/j.gr.2014.07.007

Cingolani, C.A., 2010. The Tandilia System of Argentina as a southern extension of the Rio de la Plata craton: an overview. Int. J. Earth Sci. (Geol Rundsch), 100: 221–242.

Cobbold, P.R., Massabie, A.C. y Rossello, E.A., 1986. Hercynianwrenching and thrusting in the Sierras Australes Foldbelt, Argentina. Hercynica, 2(2): 135-148.

Cogné, N., Gallagher, K., Cobbold, P.R., Riccomini, C., Gautheron, C., 2012. Post break-up tectonics in southeast Brazil from thermochronological data and combined inverseforward thermal history modeling. Journal of Geophysical Research 117, B11413.

Contreras, J., 2011. Seismostratigraphy and numerical basin modeling of the southern Brazilian continental margin (Campos, Santos, and Pelotas Basins). PhD Thesis, Heidelberg University.

Corvetto, C.B., Novara, I. L., Introcaso, A., 2007. A stretching model to explain the Salado basin (Argentina): Boletin del Instituto de Fisiografia y Geologia, 77.

D'Angiola, M., Echeveste, H. J., Risi, D., Vinciguerra P., 1992. Analisisestructural de la faja milonıtica del flanco norte del Cerro Albion, Sierras de Tandil. In: Prov. de Buenos Aires. Jornadas Geologicas Bonaerenses, pp 63–67.

Dalla Salda, L.H., 1975. Geologia y petrologia del basamento cristalino en el area del Cerro El Cristo e Isla Martın Garcıa. Provincia de Buenos Aires, Republica Argentina. Tesis doctoral, Facultad de Ciencias Naturales y Museo. Univ. Nacional de La Plata.

Delpino, S.H. 1993. Mecanismos de deformacio´n y transformaciones mineralo´gicascomo indicadores del regimen de deformacio´n operante sobre las rocasdel basamento del faldeo occidental del Cerro del Corral, Sierras Australesde Buenos Aires. In: XII Congreso Geologico Argentino y II Congreso de Exploracion de Hidrocarburos, Mendoza, Actas, III, 21–31.

deSanta Ana, H., Veroslavsky, G., 2003. La tectosecuencia volcanosedimentaria de la Cuenca Norte de Uruguay. Edad Jurásico-Cretácico Temprano. In: Veroslavsky, G, Ubilla, M, Martínez, S eds. (2003) Cuencas Sedimentarias de Uruguay: Geología, Paleontología y Recursos Naturales – Mesozoico. DIRAC, Facultad de Ciencias, Universidad de la República, Montevideo, pp. 51-74

deSanta Ana, H., Goso, C., Daners, G., 2006a. Cuenca Norte: estratigrafía del Carbonífero-Pérmico. In: Veroslavsky, G, Ubilla, M, Martínez, S eds. (2006) Cuencas Sedimentarias de Uruguay: Geología, paleontología y recursos naturales – Paleozoico. DIRAC, Facultad de Ciencias, Universidad de la República, Montevideo, pp. 147-208

deSanta Ana, H., Veroslavsky, G., Fulfaro, V., Rossello, E. A., 2006b. Cuenca Norte: Evolución tectónica y sedimentaria del Carbonífero-Pérmico. In: Veroslavsky, G, Ubilla, M, Martínez, S eds. (2006) Cuencas Sedimentarias de Uruguay: Geología, Paleontología y Recursos Naturales – Paleozoico. DIRAC, Facultad de Ciencias, Universidad de la República, Montevideo, pp. 209-256

Dodson, M.H., 1973. Closure temperature in geochronological and petrological systems. Contrib Mineral Petrol 40: 259–274.

Donelick, R.A., 1993. A method of fission track analysis utilizing bulk chemical etching of apatite. Patent number 5,267,274, U.S.A.

Donelick, R.A., 1995. A method of fission track analysis utilizing bulk chemical etching of apatite. Patent number 658,800, Australia.

Donelick, R.A., Ketcham, R.A., and Carlson, W.D., 1999, Variability of apatite fission track annealing kinetics II: Crystallographic orientation effects. American Mineralogist, v. 84, pp. 1224-1234.

Donelick, R.A., O'Sullivan, P.B.& Ketcham, R.A., 2005. Apatite fission-track analysis. In: Reiners, P. W. & Ehlers, T. A. (eds.) Low-Temperature Thermochronology: Techniques, Interpretations, and Applications: Rev. Mineral. Geochem., 58, 49-94.

Dunkl, I., 2002. Trackkey: a Windows program for calculation and graphical presentation of fission track data. Comput. Geosci., 28:3–12.

Farley, K.A., Wolf, R.A., and Silver, L.T., 1996. The effects of long alpha-stopping distances on (U-Th)/He dates, Geochim. et Cosmochim. Acta, 60, 4223-4229.

Du Toit, A.L., 1937. Our Wandering Continents; An Hypothesis of Continental Drifting. Oliver & Boyd, London, UK: 366.

Farley, K.A., 2000. Helium diffusion from apatite: general behavior as illustrated byDurango fluorapatite. Journal of Geophysical Research 105, p. 2903–2914.

Farley, K.A., 2002. (U-Th)/He dating: Techniques, calibrations, and applications. Reviews in Mineralogy & Geochemistry, 47, p. 819-844.

Farley, K.A., 2007. He diffusion systematics in minerals: Evidence from synthetic monazite and zircon structure phosphates. Geochim. Cosmochim. Acta, 71, 4015-4024.

Féraud, G., Bertrand, H., Martínez, M., Ures, C., Schipilov, A., Bossi, J. 1999. ^{40}Ar-^{39}Ar age and geochemistry of the southern extension of Paraná traps in Uruguay. In: Actas II Simposio Sudamericano de Geología Isotópica, Córdoba (Argentina), p. 57-59.

Flowers, R. M., Shuster, D. L., Wernicke, B. P. and Farley, K. A., 2007. Radiation damage control on apatite (U–Th)/He dates from the Grand Canyon region, Colorado Plateau. Geology 35, 447–450.

Flowers, R.M., Ketcham, R., Shuster, D.L., Farley, K.A., 2009. Apatite (U/Th)/He thermochronometry using a radiation damage accumulation and annealing model. Geochimica et Cosmochimica Acta, 73, p. 2347-2365.

Franco-Magalhães, A. O. B., Hackspacher, P. C., Glasmacher, U. A., Saad, A. R., 2010. Rift to post-rift evolution of a —passivell continental margin: The Ponta Grossa Arch, SE Brazil. International Journal of Earth Sciences (Geologische Rundschau) 99, p. 1599–1613.

Franke, D. , Neben, S., Ladage, S., Schreckenberger, B., Hinz, K., 2007. Margin segmentation and volcano-tectonic architecture along the volcanic margin of Argentina/Uruguay, South Atlantic. Marine geology, 244, p. 46–67.

Frimmel, H.E., Basei, M.A.S., Gaucher, C., 2011. Neoproterozoic geodynamic evolution of SW-Gondwana: a southern African perspective. International Journal of Earth Sciences, 100,

p. 323-354.

Frimmel, H.E., Basei, M.A.S., Correa, V.X., Mbangula, N., 2013. A new lithostratigraphic subdivision and geodynamic model for the Pan-African western Saldania Belt, South Africa. Precambrian Research, 231, p. 218– 235.

Fryklund, B., Marshal, A. and Stevens, J., 1996. Cuenca del Colorado. In: V.A.T. Ramos,M.A., (Editor), Geologia y recursos naturales de la plataforma continental Argentina,relatario XIII. Congreso Geologico Argentino y III. Congreso de Exploracion de Hidrocarboros,. Associacion Geologica Argentina & Inst. Argentino del Petroleo, Buenos Aires, p. 135–158.

Gallagher, K., Brown, R.W., Johnson, C., 1998. Fission track analysis and its application to geological problems. Annual Review of Earth and Planetary Science 26, p 519-572.

Garver, J.I., 2002. Discussion: "Metamictization of natural zircon: accumulation versus thermal annealing of radioactivity-induced damage; "Contributions to Mineralogy and Petrology, 143, p 756-757.

Garver, J.I., and Kamp, P.J.J., 2002, Integration of zircon color and zircon fission track zonation patterns in Orogenic belts: Application of the Southern Alps, New Zealand; Tectonophysics, V. 349, n. 1-4, p 203-219.

Garver, J.I., 2003. Etching age standards for fission track analysis. Radiation Measurements 37 (1), p 47–54.

Garver, J.I., Reiners, P.R., Walker, L.J., Ramage, J.M., Perry, S.E., 2005, Implications for timing of Andean uplift based on thermal resetting of radiation-damaged zircon in the Cordillera Huayhuash, northern Perú, Journal of Geology, v. 113, n. 2, p. 117-138.

Gaucher, C., Blanco, G., Chiglino, L. Poiré, D.G., Germs, G.J.B., 2008a. Acritarchs of Las Ventanas Formation (Ediacaran, Uruguay): implications for the timing of coeval rifting and glacial events in western Gondwana. Gondwana Research, 13, p 488-501.

Gaucher, C., Finney, S.C., Poiré, D.G., Valencia, V.A., Grove, M., Blanco, G., Pamoukaghlián, K., Gómez Peral, L., 2008b. Detrital zircon ages of Neoproterozoic sedimentary successions in Uruguay and Argentina: insights into the geological evolution of the Río de la Plata Craton. Precambrian Research, 167, p. 150-170.

Gaucher, C.; Frimmel, H.E., Germs, G.J.B. 2009. Tectonic events and palaeogeographic evolution of southwestern Gondwana in the Neoproterozoic and Cambrian. In: Gaucher, C., Sial, A.N., Halverson, G.P., Frimmel, H.E. (Eds): Neoproterozoic-Cambrian Tectonics, Global Change and Evolution: a focus on southwestern Gondwana. Developments in Precambrian Geology, 16, Elsevier, p. 295-316.

Gaucher, C., Frei, R., Chemale Jr., F., Frei, D., Bossi, J., Martínez, G., Chiglino, L., Cernuschi, F. 2011. Mesoproterozoic evolution of the Río de la Plata Craton in Uruguay: at the heart of Rodinia? International Journal of Earth Sciences, 100, p. 273-288.

Gaucher, C., Sial, A.N., Frei, R., Ferreira, V.P., Frei, D., Bossi, J., Cabrera, J. 2014. Magmatismo Anorogénico Ediacárico. In: Bossi, J., Gaucher, C. (Eds.) Geología del Uruguay. Tomo 1: Predevónico. Polo, Montevideo, p. 283-298.

Glasmacher, U. A., Zentilli, M., Grist, A.M., 1998. Apatite fission-track thermochronology of Palaeozoic sandstones and the Hill-Intrusion, Northern Linksrheinisches Schiefergebirge, Germany. In: van den Haute, P., de Corte, F. (Eds.). Advances in Fission-Track Geochronology. Solid Earth Sciences Library, 10, p. 151-172.

Gleadow, A.J.W., Duddy, I.R., 1981. A natural long term track annealing experiment for apatite. Nucl. Tracks, 5, p. 169-174.

Gleadow, A. J. W., Duddy, I. R., Green, P. F. and Lovering, J. F., 1986. Confined fission track lengths in apatite: a diagnostic tool for thermal history analysis. Contrib. Mineral. Petrol. 94, 405) 15.

Green, P. F., and Durrani, S.A. 1977. Annealing studies of tracks in crystals. Nuclear Track Detection, l, p. 33-39.

Green, P. F,. 1981. A new look at statistics in fission-track dating. Nuclear Tracks, 5 (1/2), p. 77–86.

Green, P.F., Duddy, I.R., Gleadow, A.J.W., Tingate, P.R., Laslett, G.M., 1986. Thermal annealing of fission tracks in apatite 1. A qualitative description. Chem. Geol., 59: 237–253

Green, P. F. 1988. The relationship between track shortening and fission track age reduction in apatite: combined influences of inherent instability, annealing and anisotropy, length bias, and system calibration, Earth and Planetary Science Letters, 89 , p. 335–352.

Green, P.F., Lidmar-Bergström, K, Japsen, P., Bonow, J.M., Chalmers, J.A., 2013. Stratigraphic landscape analysis, thermochronology and the episodic development of elevated, passive continental margins. Geological survey of Denmark and Greenland Bulletin 30.

Grist, A.M., Ravenhurst, C.E., 1992a. Mineral separation techniques used at Dalhousie University. In: Zentilli M, Reynolds PH (eds). Short course handbook on low temperature thermochronology. Mineral Associ. Can. Short Course Handb. 20 Append. 2, p. 203–209.

Grist, A.M., Ravenhurst, C.E., 1992b. A step-by-step laboratory guide to fission track thermochronology at Dalhousie University. In: Zentilli, M., Reynolds, P.H. (eds), Short course handbook on low temperature thermochronology. Mineral Associ. Can. Short Course Handb. 20 Append. 1, p. 190–201.

Guenthner, W.R., Barbeau, D.L., Reiners, P.W., and Thomson, S.N., 2010. Slab window migration and terrane accretion preserved by low-temperature thermochronology of a magmatic arc, northern Antarctic Peninsula: Geochemistry Geophysics Geosystems, v.11, doi:10.1029/2009GC002765.

Guenthner, W.R., Reiners, P.W., Ketcham, R.A., Nasdala, L., and Giester, G., 2013. Helium diffusion in natural zircon: Radiation damage, anisotropy, and the interpretation of zircon (U-Th)/He thermochronology: American Journal of Science, v. 313, p. 145-198.

Halls, H.C., Campal, N., Davis, D.W., Bossi, J., 2001. Magnetic studies and U-Pb geochronology of the Uruguayan dyke swarm, Rio de la Plata craton, Uruguay:paleomagnetic and economic implications. Journal of South American Earth Sciences, 14, p. 349-361.

Harrington, H.J., 1955. The Permian Eurydesma fauna of eastern Argentina. Journal of Paleontology 29, p. 112–128.

Hartmann, L. A., Piñeyro, D., Bossi, J., Leite, J. A. D., McNaughton, N. J., 2000. Zircon U-Pb dating of Isla Mala granitic magmatism in the Rio de La Plata Craton, Uruguay. Jour. South Amer. Earth Sci. 13, p. 105–113.

Hartmann, L.A., Campal, N., Santos, J.O., Mac Naughton, N. J., Schipilov, A. 2001. Archean crust in the Río de la Plata Craton, Uruguay: SHRIMP U-Pb reconnaissance geochronology. Journal of South American Earth Sciences, 14, p. 557-570.

Hartmann, L.A., Santos, J.O.S., Cingolani, C.A., McNaughton, N.J. 2002b. Two Paleoproterozoic Orogenies in the Evolution of the Tandilia Belt, Buenos Aires, as evidenced by zircon U-Pb SHRIMP geochronology. International Geology Review, 44, p. 528-543.

Hiruma, S.T., Riccomini, C., Modenesi-Gauttieri, M.C., Hackspacher, P.C., Neto, J.C.H.,Franco-Magalhaes, A.O.B., 2010. Denudation history of the Bocaina Plateau, Serra do Mar, southeastern Brazil: relationships to Gondwana breakup and passive margin development. Gondwana Research 18, p. 674–687.

Huismans, R.S. Beaumont, C., 2011. Depth-dependent extension, two-stage breakup and cratonic underplating at rifted margins, Nature, 473, doi:10.1038/nature09988.

Huismans, R.S. Beaumont, C., 2015. Effect of Lithospheric Stratification on Extensional Styles and Rift Basin Geometry. GCSSEPM Conference Proceedings.

Hurford, A.J., Green, P.F., 1982. A user's guide to fission-track dating calibration. Earth Planet. Sci. Lett., 59, p. 343–354.

Hurford, A.J., Green, P.F., 1983. The Zeta age calibration of fission-track dating. Isot. Geosci., 1, p. 285–317.

Hubbard, R.J., 1984. Seismic stratigraphic framework and depositional sequences in the Santos Basin, Brazil. Marine Petroleum Geol, 1, p. 90–104.

Hurford, A.J., 1986. Standardization of fission track dating calibration: results of questionnaire distributed by international union of geological sciences subcommission on geochronology. Nuclear tracks and radiation measurements, 11, p. 329–333.

Introcaso, A. & Ramos, V., 1984. La cuenca del Salado: un modelo de evolución aulacogénica. IX Congreso Geológico Argentino, Actas III: p. 27-46. Bariloche.

Japsen, P., Bonow, J.M., Green, P.F., Chalmers, J.A., and Lidmar-Bergström, K., 2006. Elevated, passive continental margins: Long-term highs or Neogene uplifts? New evidence from West Greenland: Earth Planet. Sci. Lett., 248, 315-324.

Jarvis, A., H.I. Reuter, A. Nelson, E. Guevara, 2008, Hole-filled SRTM for the globe Version 4, available from the CGIAR-CSI SRTM 90m Database.

Juez-Larre, A.J., 2003. Post Late Paleozoic tectonothermal evolution of the northeastern margin of Iberia, assessed by fission-track and (U-T)/He analysis: a case history from the

Catalan Coastal Ranges. Ph.D. thesis, Free University of Amsterdam. 200 pp.

Karl, M., Glasmacher, U.A., Kollenz, S., Franco-Magalhaes, A.O.B., Stockli, D.F., Hackspacher, P. 2013. Evolution of the South Atlantic passive continental margin in southern Brazil derived from zircon and apatite (U–Th–Sm)/He and fission-track data. Tectonophysics, Volume 604, p. 224–244.

Keidel, J., 1913. Über das Alter, die Verbreitung und die gegenseitigen Beziehungen der verschiedenen tektonischen strukturen in den argentinischen Gebirgen. 12° Session du Congrés Géologique International (Toronto), Compte Rendus, p. 671–687.

Keidel, J., 1916. La geología de las Sierras de la Provincia de Buenos Aires y sus relaciones con las montañas de Sudáfrica y Los Andes. Ministerio de Agricultura de la Nación, Sección Geología, Mineralogía y Minería, Anales 11, p. 1–78.

Keidel, J., 1921. Sobre la distribución de los depósitos glaciares del Pérmico conocidos en la Argentina y su significación para la estratigrafía de la serie del Gondwana y la paleogeografía del Hemisferio Austral. Academia Nacional de Ciencias, Boletín 25, p. 239–368.

Ketcham, R.A., 2005. Forward and Inverse Modelling of low-temperature thermochronometry data. Rev. Min. Geoch. 58, p. 275-314.

Ketcham, R.A. Carter, A., Donelick, R.A., Barbarand, J. and Hurford, A.J., 2007a. Improved modeling of fission-track annealing in apatite. American Mineralogist, 92: 789-798.

Ketcham, R.A., Carter, A., Donelick, R.A., Barbarand, J., Hurford, A.J., 2007b. Improved measurement of fission-track annealing in apatite using c-axis projection. American Mineralogist. 92, p. 789-798.

Ketcham, R.A., Donelick, R.A., Balestrieri, M.L., Zattin, M., 2009. Reproducibility of apatite fission-track length data and thermal history reconstruction. Earth and Planetary Science Letters, 284, p. 504–515.

Ketcham, R.A., 2009. HeFTy version 1.6.7, Manual.

Kirstein, L., Peate, D.W., Hawkesworth, C.J., Turner, S.P., Harris, C., Mantovani, M.S.M., 2000. Early Cretaceous basaltic and rhyolitic magmatism in southern Uruguay associated with the opening of the South Atlantic. J Petrol 41: pp. 1413-1438

Kollenz, S., Pfister, S., Glasmacher, U.A., Rossello, E.A., Oriolo, S., Stockli, D.F., 2015. Thermal history and long-term landscape evolution of the Sierras Septentrionales, NE Argentina (in preperation).

Kooi, K. and Beaumont, C., 1994. Insights derived from a surface processes model that combines diffusion, advection, and reaction. Journal of Geophysical Research 99.

Kooi, K. and Beaumont, C., 1996. Large-scale geomorphology: Classical concepts reconciled and integrated with contemporary ideas via a surface processes model. Journal of Geophysical Research: Solid Earth (1978–2012). Volume 101, Issue B2, p. 3361–3386.

Kostadinoff, J., and Font, G., 1985. Cuenca interserrana bonaerense, Argenting, V. Congr. Latinoam. Geol., Vol. 4, 1982, p. 105-121.

Kostadinoff, J., 1993. Geophysical evidence of a Paleozoic basin in the interhilly area of Buenos Aires Province, Argentina, Congr. Internat. Strat. et Geol. du Carbonifere et Permien, Comptes Rendus XII, ICC-P, Vol. 1, p. 397-404.

Kuhlmann, G., Adams, S., Campher, C., van der Spuy, D., di Primio, R., Horsfield, B., 2010. Passive margin evolution and its controls on natural gas leakage in the southern Orange Basin, blocks 3/4, offshore South Africa. Marine and Petroleum Geology, 27, 973–992.

Kusznir, N.J. & Park, R.G., 1987. The extensional strength of the continental lithosphere: its dependence on geothermal gradient, crustal composition and thickness. In: Continental extensional tectonics, Geol. Soc. Lond. Spec. Publ. No. 26, pp. 35-52.

Kusznir, N.J. & Ziegler, P.A. 1992. "The mechanics of continental extension and sedimentary basin formation: a simple-shear/pure-shear flexural cantilever model. Tectonophysics, 215, pp. 117-131.

Laslett, G.M., Gleadow, A.J.W., and Duddy, I.R.1984. The relationship between fission track length and track density in apatite. Nucl. Tracks 9, 29-38.

Laslett, G.M., Green, P.F., Duddy, I.R., and Gleadow, A.J.W., 1987. Thermal Annealing of Fission Tracks in Apatite: 2 - A Quantitative Analysis. Chem. Geol. (Isot. Geosci. Sect.) 65, 1-13.

Lenz, C., Fernandes, L.A.D., McNaughton, N.J., Porcher, C.C., Masquelin, H. 2011. U–Pb SHRIMP ages for the Cerro Bori Orthogneisses, Dom Feliciano Belt in Uruguay: Evidences of a ~800Ma magmatic and ~650Ma metamorphic event. Precambrian Research, 185, p. 149–163.

Lisker F, Ventura B, Glasmacher UA (2009) Apatite thermochronology in modern geology. Geol Soc London Spec Publ 324, p. 1-23.

Loegering, M.J., Anka, Z., Autin, J., di Primio, R., Marchal, D., Rodriguez, J.F., Franke, D., Vallejo, E., 2013: Tectonic evolution of the Colorado Basin, offshore Argentina, inferred from seismo-stratigraphy and depositional rates analysis. Tectonophysics, Volume 604, p. 245-263.

Lopez-Gamundi, O.R., Rossello, E.A., 1998. Basin fill evolution and paleotectonic patterns along the Samfrau geosyncline: the Sauce Grande basin–Ventana foldbelt (Argentina) and Karoo basin–Cape foldbelt (South Africa) revisited. Geol. Rundsch., 86, p. 819-834.

Lustrino, M., Melluso, L., Brotzu, P., Gomes, G.B., Morbidelli, L., Muzio, R., Ruberti, E., Tassinari, C.C.G., 2005. Petrogenesis of the early Cretaceous Valle Chico igneous complex (SE Uruguay): relationships with Paraná-Etendeka magmatism. Lithos 82: pp. 407-434

McKenzie, D.P. 1978. Some remarks on the development of sedimentary basins. Earth and Planetary Science Letters 40, p. 25-32.

Mitchell, S. G., Reiners, P. W., 2003. Influence of wildfires on apatite and zircon (U-Th)/He ages. Geology 31, p.1025–1028.

Muzio R., 2000. Evolução petrológica e geocronologia do Maciço Alcalino Valle Chico, Uruguai. Unpublished PhD dissertation, Universidad Estadual Paulista, Rio Claro, SP, 171 pp

Nasdala, L., 2009. Pb+ irradiation of synthetic zircon (ZrSiO4): infrared spectroscopic investigation—discussion. American Mineralogist 94, p. 853–855.

Ollier, C. D., 1985. Morphotectonics of continental margins with great escarpments,in M. Morisawa and J. T. Hack (eds), Tectonic Geomorphology, Allen and Unwin, Boston, p. 3–25.

Osmundsen, P.T. and Redfield, T.F., 2011. Crustal taper and topography at passive continental margins. Terra Nova, 00, p.1–13.

Oyhantçabal, P.B., Siegesmund, S., Wemmer, K., Presnyakov, S., Layer, P. 2009. Geochronological constraints on the evolution of the southern Dom Feliciano Belt (Uruguay). Journal of the Geological Society of London, 166, p. 1075-1084.

Oyhantçabal, P.B., Wagner-Eimer, M., Wemmer, K., Schulz, B., Frei, R., Siegesmund, S., 2012. Paleo- and Neoproterozoic magmatic and tectonometamorphic evolution of the Isla Cristalina de Rivera (Nico Pérez Terrane, Uruguay). International Journal of Earth Sciences, 101, p. 1745-1762.

Pamoukaghlián, K. 2012. Sedimentología y estratigrafía de la Formación Piedras de Afilar, Terreno Tandilia, Uruguay. Tesis doctoral, Universidad Nacional de La Plata, La Plata, p. 1-284.

Panario, D., Gutierrez, O., Sanchez Bettucci, L., Peel, E., Oyhantcabal, P., Rabassa, J., 2014. Ancient landscapes of Uruguay. In: Jorge Rabassa, Clifford Ollier (Eds), Gondwana Landscapes of Southern South America. Serie: Springer Earth Sytem Sciences.

Pangaro, F., Ramos, V.A., 2012. Paleozoic crustal blocks of onshore and offshore central Argentina: New pieces of the southwestern Gondwana collage and their role in the accretion of Patagoniaand the evolution of Mesozoic south Atlantic sedimentary basins. Marine and Petroleum Geology 37 (2012) 162-183.

Pankhurst, R.J., Rapela, C.W., Fanning, C.M., Márquez, M., 2006. Gondwandine continental collision and the origin of Patagonia. Earth-Science Reviews, 76, p. 235–257.

Perez-Diaz, L. And Eagles, G., 2014. Constraining South Atlantic growth with seafloor spreading data. Tectonics, 33, p. 1848-1873.

Pfister, S., Kollenz, S., Glasmacher, U.A., Rossello, E.A., Oriolo, S., Stockli, D.F., 2015. Thermal history and long-term landscape evolution of the Sierras Septentrionales based on apatite fission-track dating, NE Argentina (in preperation).

Poire, D.G., Spalletti, L.A., del Valle, A., 2003. The Cambrian Ordovician siliciclastic platform of the Balcarce Formation (Tandilia System, Argentina): facies, trace fossils, palaeoenvironments and sequence stratigraphy. Geologica Acta, 1, p. 41-60.

Poiré, D., Gaucher, C. 2009. Lithostratigraphy. Neoproterozoic-Cambrian evolution of the Río de la Plata Palaeocontinent. En: Gaucher, C., Sial, A.N., Halverson, G.P., Frimmel, H.E. (Eds.), Neoproterozoic-Cambrian tectonics, global change and evolution: a focus on southwestern Gondwana. Developments in Precambrian Geology, 16, Elsevier, p. 87-101.

Rahn, M.K., Brandon, M.T., Batt, G.E., and Garver, J.I.,2004, A zero-damage model for fission-track annealing in zircon. American Mineralogist, V. 89, n. 3.

Ramos, V.A., Turic, M.A., 1996. Geologia y Recursos Naturales de la Plataforma Continental Argentina, Asociacion Geol. Arg. e Inst. Arg. Petr., pp 452, Buenos Aires.

Rapela, C.W., Pankhurst, R.J. Fanning, C.M. and Grecco, L.E., 2003. Basement evolution of the Sierra de la Ventana Fold Belt: new evidence for Cambrian continental rifting along the southern margin of Gondwana. Journal of the Geological Society, 160, p. 613–628.

Rapela, C.W., Pankhurst, R.J., Casquet, C., Fanning, C.M., Baldo, E.G., Gonzalez-Casado, J.M., Galindo, C., Dahlquist, J., 2007. The Rio de la Plata craton and the assembly of SW Gondwana. Earth-science reviews, 83, p. 49-82.

Rapela, C.W., Fanning, C.M., Casquel, C., Pankhurst, R.J., Spalletti, L., Poiré, D., Baldo, E.G. 2011. The Río de la Plata craton and the adjoining Pan-African/brasiliano terranes: their origins and incorporation into south-west Gondwana. Gondwana Research 20, p. 673-690.

Reiners, P.W., Farley, K.A,. 2001. Influence of crystal size on apatite (U-Th)/He thermochronology: an example from the Bighorn Mountains, Wyoming, Earth Planet. Sci. Lett., 188, 413-420.

Reiners, P.W., Farley, K.A., and Hickes, H.J., 2002. He diffusion and (U-Th)/He thermochronometry of zircon: Initial results from Fish Canyon Tuff and Gold Butte, Nevada, Tectonophysics, v. 349, p. 297-308.

Reiners, P.W., Spell, T.L., Nicolescu, S., Zanetti, K.A., 2004. Zircon (U–Th)/He thermochronometry: He diffusion and comparisons with 40Ar/39Ar dating. Geochimica et Cosmochimica Acta v. 68, p. 1857–1887.

Reiners, P.W., 2005. Zircon (U-Th)/He Thermochronometry. Reviews in Mineralogy & Geochemistry, 58, p. 151-179.

Reiners, P.W, Brandon, M.T., 2006. Using Thermochronology to understand orogenic erosion. Annu. Rev. Earth Planet. Sci. 34, p 419-66.

Rossello, E.A., Massabie A.C., Lopez-Gamundi, O.R., Cobbold P.R., Gapais, D., 1997. Late Paleozoic transpression in Buenos Aires and northeast Patagonia ranges, Argentina. Journal of South American Earth Sciences, 10, p. 389-402.

Sacek, V., Braun, J., van der Beek, P., 2012. The influence of rifting on escarpment migration on high elevation passive continental margins. Journal of Geophysical Research: Solid Earth (1978–2012). Volume 117, Issue B4.

Santos, J.OS., Hartmann, L.A., Bossi, J., Campal, N., Schipilov, A., Piñeyro, D., McNaughton, N.J., 2003. Duration of the Transamazonian and its correlation within South America based on U-Pb SHRIMP geochronology of the la Plata Craton, Uruguay. International Geological Review 45, p. 27-48.

Schobbenhaus, C. & Bellizzia, A., 2001 (coord.). Geological map of South America,

1:5000000, CGMW - CPRM - DNPM – UNESCO, Brasilia.

Shuster, D.L., Flowers, R.M., Farley, K.A., 2006. The influence of natural radiation damage on helium diffusion kinetics in apatite. Earth Planet. Sci. Lett. 249, p. 148–161.

Shuster, D. L., Farley, K. A., 2009. The influence of artificial radiation damage and thermal annealing on helium diffusion kinetics in apatite, Geochimica et Cosmochimica Acta, 73(1), p. 183-196.

Sobel, E.R., Seward, D., 2010. Influence of etching conditions on apatite fission-track etch pit diameter. Chemical Geology 271, 59–69.

Sprechmann P., Bossi J., Da Silva J., 1981. Cuencas del Jurásico y Cretácico del Uruguay. In: VolkheimerW,Musacchio EA (eds) Cuencas sedimentarias del Jurásico y Cretácico de América del Sur. Comité Sudamericano del Jurásico y Cretácico, Buenos Aires, 1, p 239–270.

Stewart, K., Turner, S., Kelley, S., Hawkesworth, C., Kirstein, L., Mantovani, M., 1996. 3-D, 40Ar–39Ar geochronology in the Paraná continental flood basalt province. Earth Planet Sci Lett 143: pp. 95-109.

Stoakes, F.A., Campbell, C.V., Cass, R., Ucha, N. 1991. Seismic stratigraphic analysis of the Punta del Este Basin, offshore Uruguay, South America. American Association Petroleum Geologists Bulletin, 75, p. 219-240.

Summerfield, M.A. (ed.), 2000. Geomorphology and Global Tectonics. Wiley: Chichester. 386 pp.

Suero, T., 1972.Compilación geológica de las Sierras Australes de la provincia de Buenos Aires. LEMIT (la Plata), Anales 3, 135-147.

Teixeira W., Renne, P., Bossi. J., Campal, N., D'Agrella, F., 1999. $^{40}Ar/^{39}Ar$ and Rb/Sr geochronology of the Uruguayan dike swarm, Río de la Plata Craton and implications for Proterozoic intraplate activity in western Gondwana. Precambrian Research, 93, p. 153-180.

Tomezzoli, R.N. and Vilas J.F., 1999. Palaeomagnetic constraints on the age of deformation of the Sierras Australes thrust and fold belt, Argentina. Geophys. J. Int., 138, p 857–870.

Tomezzoli, R. N., 2001. Further palaeomagnetic results from the Sierras Australes fold and thrust belt, Argentina. Geophys. J. Int., 147, p. 356–366.

Ubilla M., Perea D., Goso Aguilar C., Lorenzo, N., 2004. Late Pleistocene vertebrates from northern Uruguay: tools for biostratigraphic, climatic and environmental reconstruction. Quatern Int 114(1):129–142

Umpierre, M., Halpern, M., 1971. Edades Rb-Sr del sur de la República Oriental del Uruguay. Revista de la Asociación Geológica Argentina, 26, p. 133-155.

Vayssaire, A., Prayitno, W., Figueroa, D., Quesada, S., 2007. Petroleum Systems of Colorado and Malvinas Basins, Deep Water Argentina, South Atlantic Petroleum Systems. Geol. Soc. London, London, p. 10.

Vermeesch, P., Seward, D., Latkoczy, C., Wipf, M., Gunther, D., Baur, H., 2007. Alpha-emitting mineral inclusions in apatite, their effect on (U–Th)/He ages, and how to reduce it. Geochim. Cosmochim. Acta, 31, p. 1737–1746.

Veroslavsky G (1999) Geologia da Bacia de Santa Lucía-Uruguai. Unpublished PhD dissertation, Universidad Estadual Paulista, Rio Claro, SP, 152 pp

Von Gosen,W.,Buggisch,W.,Dimieri,L.V.,1990.Structuralandmetamorphicevolutionof the Sierras Australes, Buenos Aires province, Argentina. Geologisthe Rundschau 79, 797-821.

Von Gosen, W., Buggisch, W. & Krumm, S. 1991. Metamorphism and deformation mechanisms in the Sierras Australes fold and thrust belt (Buenos Aires Province, Argentina). Tectonophysics, 185, p. 335–356.

Wagner, G. A. and Reimer, G. M., 1972. Fission-track tectonics: the tectonic interpretation of fission track apatite ages. Earth and Planet. Sci. Lett., 14, p. 263-268.

Wagner, G. A., van den Haute, P., 1992. Fission Track dating. Kluwer Verlag, Enke Publisher 285 pp.

Wernicke, B. 1985. Uniform-sense normal simple shear of the continental lithosphere. Canadian Journal of Earth Sciences 22, p. 108-125.

Will, T.M., Frimmel, H.E., Gaucher, C., Bossi, J., 2014. Geochemical and isotopic composition of Pan-African metabasalts from southwestern Gondwana: Evidence of Cretaceous South Atlantic opening along a Neoproterozoic back-arc. Lithos, 202-203, p. 363-381.

Wolf R. W., Farley K. A. and Silver L. T. , 1996. Helium diffusion and low temperature thermochronometry of apatite. Geochim. Cosmochim. Acta 60 4231–4240

Yamada, R., Tagami, T, Nishimura, S, Ito, H., 1995. Annealing kinetics of fission tracks in zircon: an experimental study. Chemical Geology (Isotope Geoscience Section), 122, p. 249-258.

Zambrano, J.J. & Urien, C.M. 1970. Geological outline of the basins in southern Argentina and their offshore extension. Journal of Geophysical Research 75(8), p. 1363-1396.

Zambrano J.J., 1974. Cuencas Sedimentarias en el subsuelo de la provincia de Buenos Aires y zonas adyacentes. Revista de la Asociación Geológica Argentina 29(4), p. 443-449.

Zeil, W., 1980. Brinkmanns Abriß der Geologie, erster Band: Allgemeine Geologie. 12. Auflage. Ferdinand Enke Verlag, Stuttgart

Zhang, M., Boatner, L., Salje, E.K.H., Honda, S., Ewing, R.C., 2008a. Pb+ irradiation of synthetic zircon (ZrSiO4): infrared spectroscopic investigation. American Mineralogist 93, p. 1418–1423.

Zhang, M., Boatner, L., Salje, E.K.H., Honda, S., Ewing, R.C., 2008a. Pb+ irradiation of synthetic zircon (ZrSiO4): infrared spectroscopic investigation. American Mineralogist 93, 1418–1423.

Zhang, M.L., Salje, E.K.H., Ewing, R.C., Daniel, P., Weber, W.J., Zhang, Y., Farnan, I.,

2008b. Micro-Raman and micro-infrared spectroscopic studies of Pb- and Au-irradiated ZrSiO4: optical properties, structural damage, and amorphisation. Physical Review B77, 144110.

Ziegler, P. A. y Cloething, S. 2004. Dynamic processes controlling evolution of rifted basins. Earth Science Reviews 64, p. 1-50.

Zimmermann, U., Poire, D.G. and Gomez Peral, L., 2010. Neoproterozoic to lower Palaeozoic successions of the Tandilia sytem in argentina: implication for the palaeotectonic framework of southwest gondwana. Int. J. Earth Sci., 100, p. 489-510.

9

Appendix

Contents

9.1 Argentina - data sheets AFT

9.1.1 Sierras Septentrionales

ARG 01.apa --- TRACKKEY 4.2.g --- *counted: 26 Mrz. 12 printed: 26 Mrz. 12*

Apatite | Argentina, ARG 01 | Precambr./ Arcean Orthogneis | SK Leitz

Cryst.: 20 ***Area:*** 37133
Ns: 867 ***RhoS:*** 23.349
Ni: 1616 ***RhoI:*** 43.519

Pooled:	0.537	129.2 ± 9.3
Mean:	0.543	130.7 ± 6.0
Central:	0.536	129.2 ± 9.3
Weigh.I:	0.562	135.3
Weigh.II:	0.55	131.2

Chi-sq.: 17.72 ***P (%):*** 54.13
Dispersion: 0.02
a: -4.57 ***b:*** 0.655 ***r:*** 0.93
Irr.: ARG1234 ***Glass:*** CN_5
Nd: 15148 ***RhoD:*** 14.44
Zeta: 336.83 ± 19.51 ***U.:*** 38.47 (± 44 %)
Goodness: n. d.

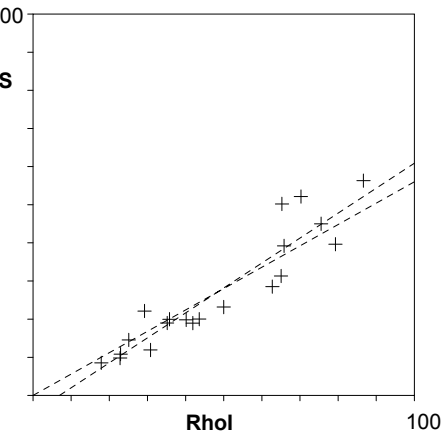

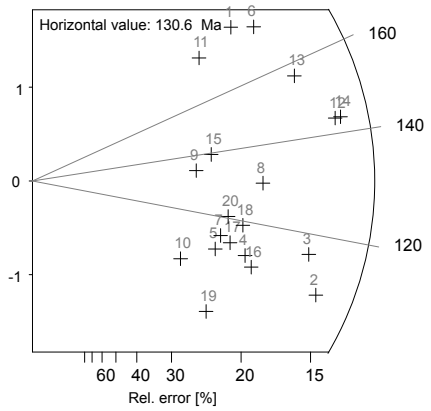

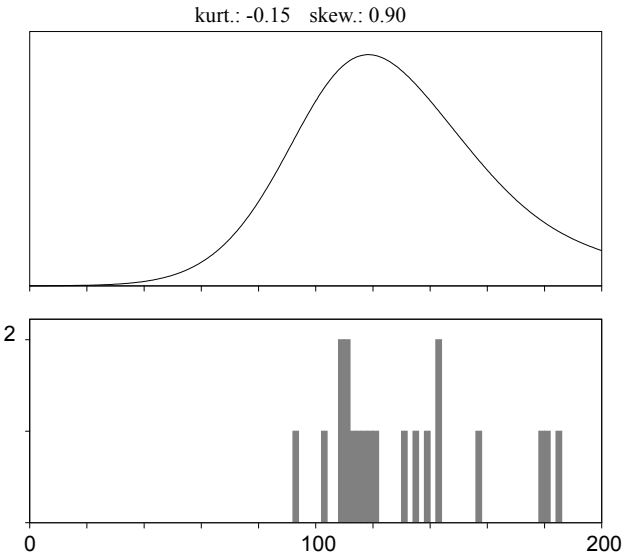

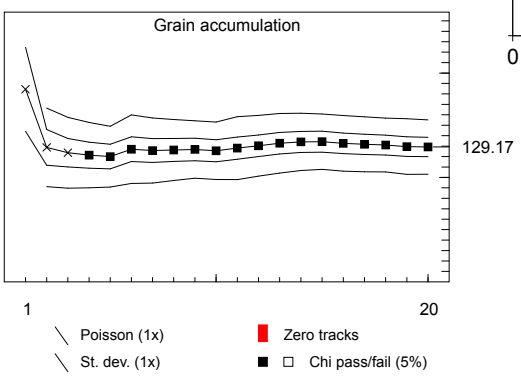

ARG 02.apa --- TRACKKEY 4.2.g --- *counted: 16 Mrz. 12 printed: 16 Mrz. 12*

Apatite

Argentina	Precambrian	SK
ARG 02	Orthogneis	Leitz

Cryst.: ***Area:***
20 45280
Ns: ***RhoS:***
678 14.974
Ni: ***RhoI:***
866 19.125

Pooled:	0.783	186.7 ± 14.5
Mean:	0.826	196.9 ± 6.6
Central:	0.783	186.7 ± 14.5
Weigh.I:	0.798	190.3
Weigh.II:	0.81	193.2

Chi-sq.: 9.57 ***P (%):*** 96.27
Dispersion: 0.00
a: 1.411 ***b:*** 0.737 ***r:*** 0.89
Irr.: ARG12345 ***Glass:*** CN_5
Nd: 15148 ***RhoD:*** 14.37
Zeta: 336.83 ± 19.51 ***U.:*** 14.79 (± 38 %)
Goodness: n. d.

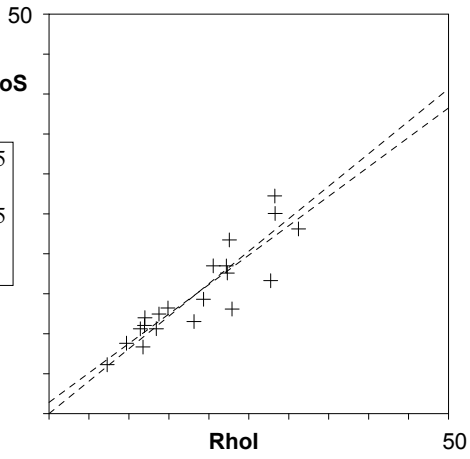

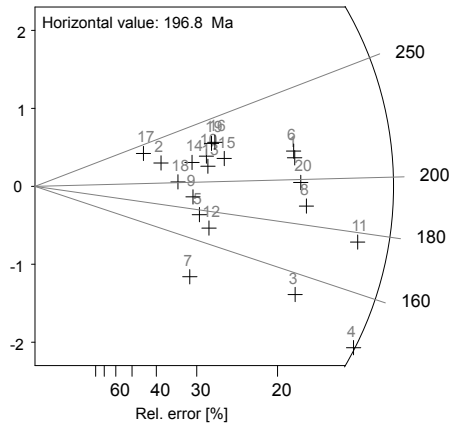

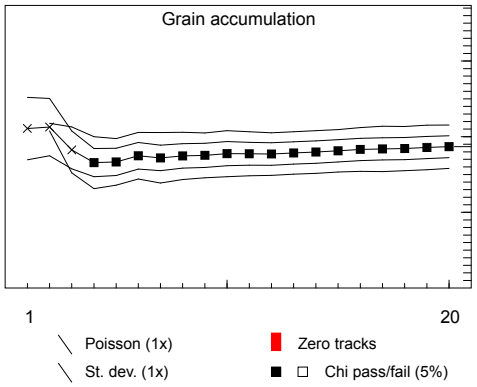

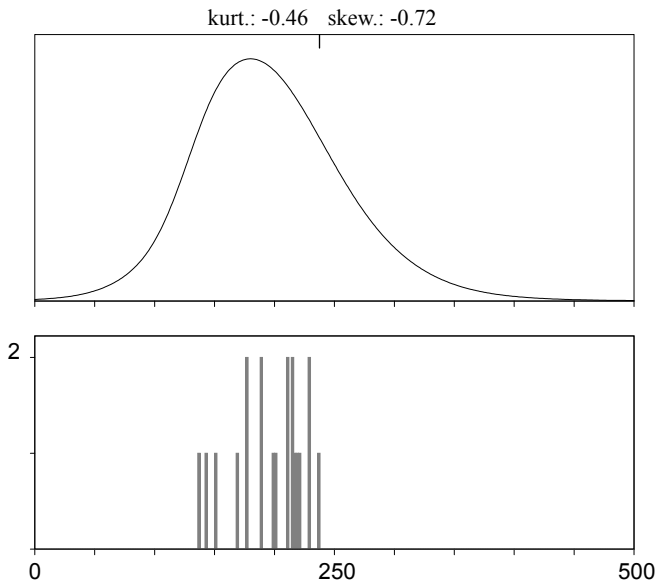

ARG 12-02SP.apa — TRACKKEY 4.2g — *printed: 4 Nov. 13*

Apatite | ARG / ARG 12-02 | Proterozoikum / Granit | SP / Leitz

Cryst.: 20 *Area:* 26126
Ns: 645 *RhoS:* 24.888
Ni: 1288 *Rhoi:* 49.209

Pooled:	0.501	104.8 ± 7.5
Mean:	0.507	106.2 ± 3.1
Central:	0.501	104.8 ± 7.5
Weigh.I:	0.5	104.6
Weigh.II:	0.51	106.1

Chi-sq.: 7.44 *P (%):* 99.15
Dispersion: 0.00
a: 1.828 *b:* 0.469 *r:* 0.93
Irr.: SabArg13 *Glass:* CN_5
Nd: 16077 *RhoD:* 12.88
Zeta: 327.74 ± 16.93 *U.:* 51.06 (± 37 %)
Goodness: n. d.

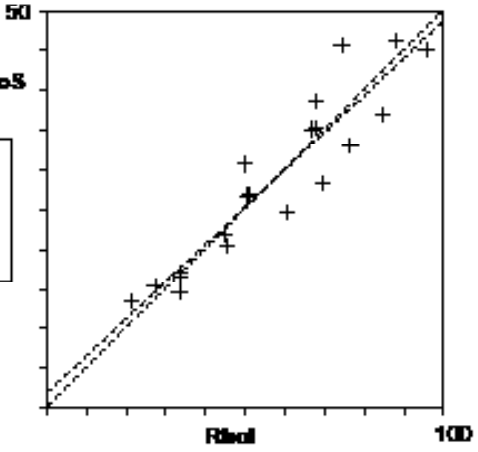

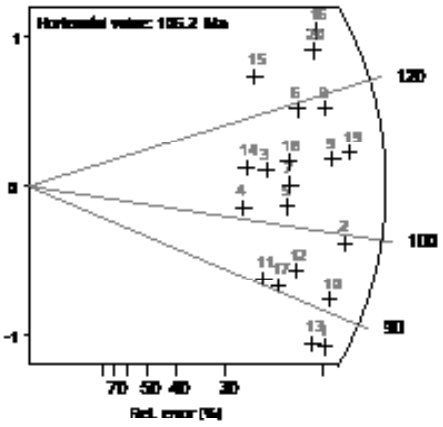

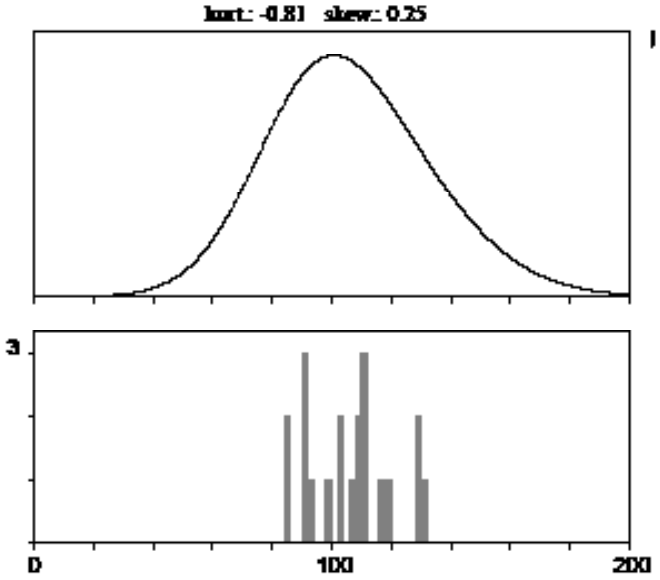

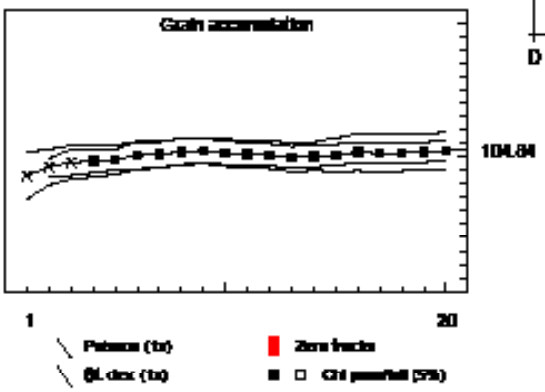

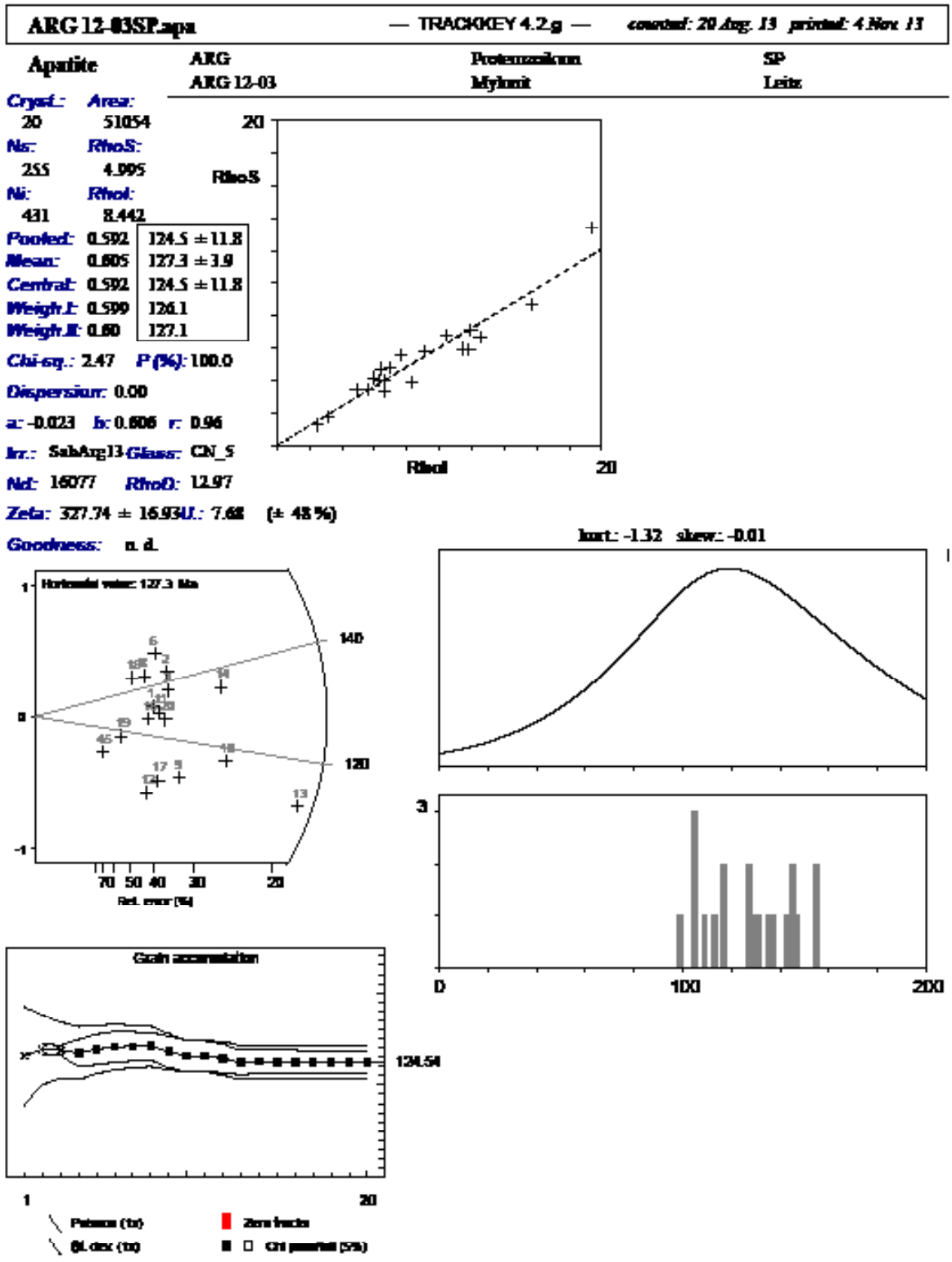
ARG 12-03SP.apa
— TRACKKEY 4.2.g —
counted: 20.Aug. 13 printed: 4.Nov. 13
Apatite
ARG
ARG 12-03
Proterozoikum
Mylonit
SP
Leitz
Cryst.: Area:
20 51054
Ns: RhoS:
255 4.995
Ni: RhoI:
431 8.442
Pooled: 0.592 124.5 ± 11.8
Mean: 0.605 127.3 ± 3.9
Central: 0.592 124.5 ± 11.8
Weigh.I: 0.599 126.1
Weigh.II: 0.60 127.1
Chi-sq.: 2.47 P (%): 100.0
Dispersion: 0.00
a: -0.023 b: 0.606 r: 0.96
Irr.: SahArg13 Glass: CN_5
Nd: 16077 RhoD: 12.97
Zeta: 327.74 ± 16.93 U.: 7.68 (± 48 %)
Goodness: n. d.
RhoS
RhoI
20
Horizontal value: 127.3 Ma
140
120
70 50 40 30 20
Rel. error [%]
kurt.: -1.32 skew.: -0.01
3
0
100
200
Grain accumulation
124.54
1
20

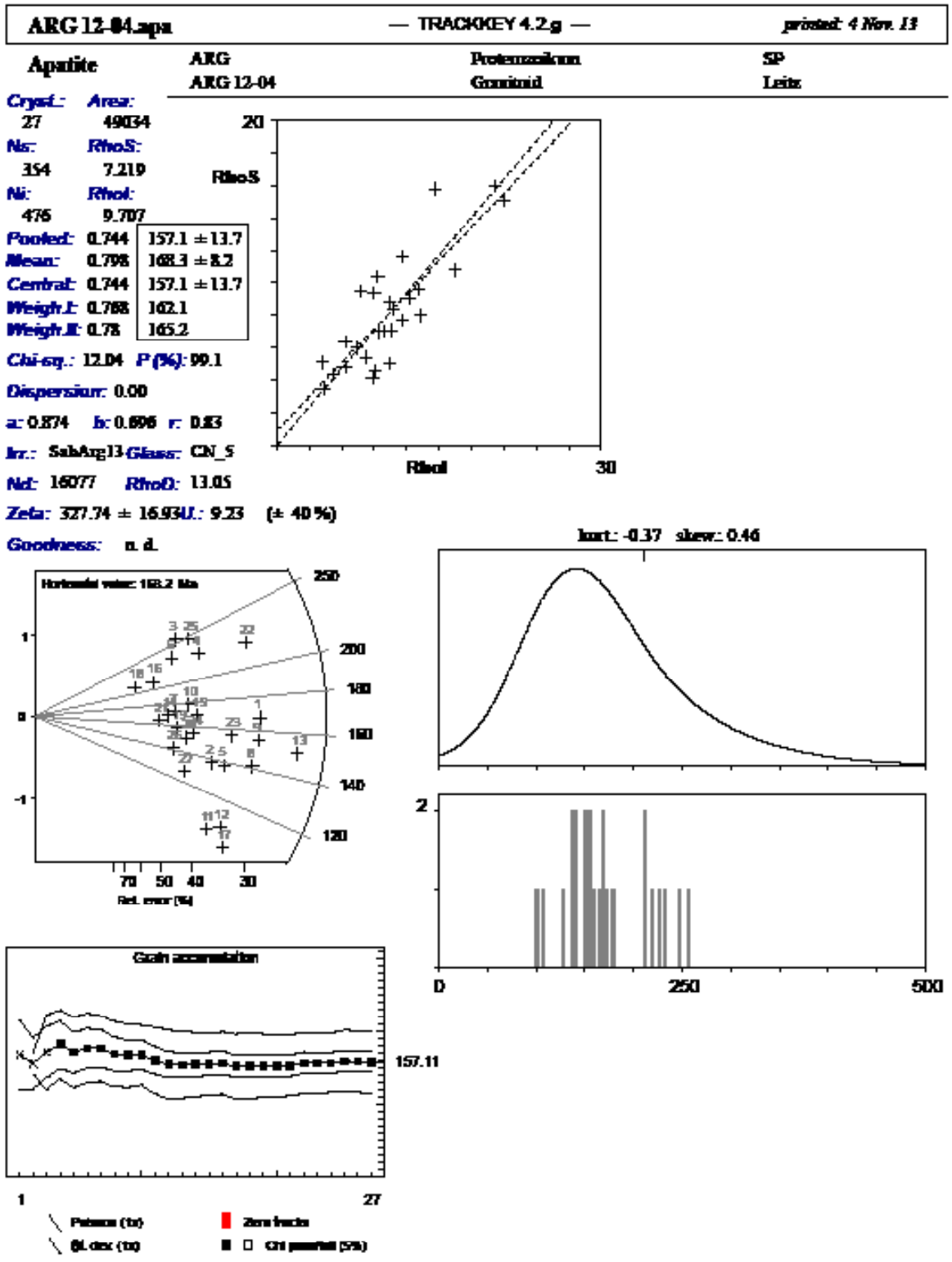
ARG 12-04.apa
— TRACKKEY 4.2g —
printed: 4 Nov. 13
Apatite
ARG
ARG 12-04
Proterozoikum
Granitoid
SP
Leitz
Cryst.: 27
Area: 49034
Ns: 354
RhoS: 7.219
Ni: 476
RhoI: 9.707
Pooled: 0.744 157.1 ± 13.7
Mean: 0.798 168.3 ± 8.2
Central: 0.744 157.1 ± 13.7
Weigh.I: 0.788 162.1
Weigh.II: 0.78 165.2
Chi-sq.: 12.04 P (%): 99.1
Dispersion: 0.00
a: 0.874 b: 0.896 r: 0.83
Irr.: SahArg13 Glass: CN_5
Nd: 16077 RhoD: 13.05
Zeta: 327.74 ± 16.93 U.: 9.23 (± 40 %)
Goodness: n. d.
RhoS
RhoI
20
30
kurt.: -0.37 skew.: 0.46
250
200
180
160
140
120
70
50
40
30
Grain accumulation
157.11
1
27
0
250
500

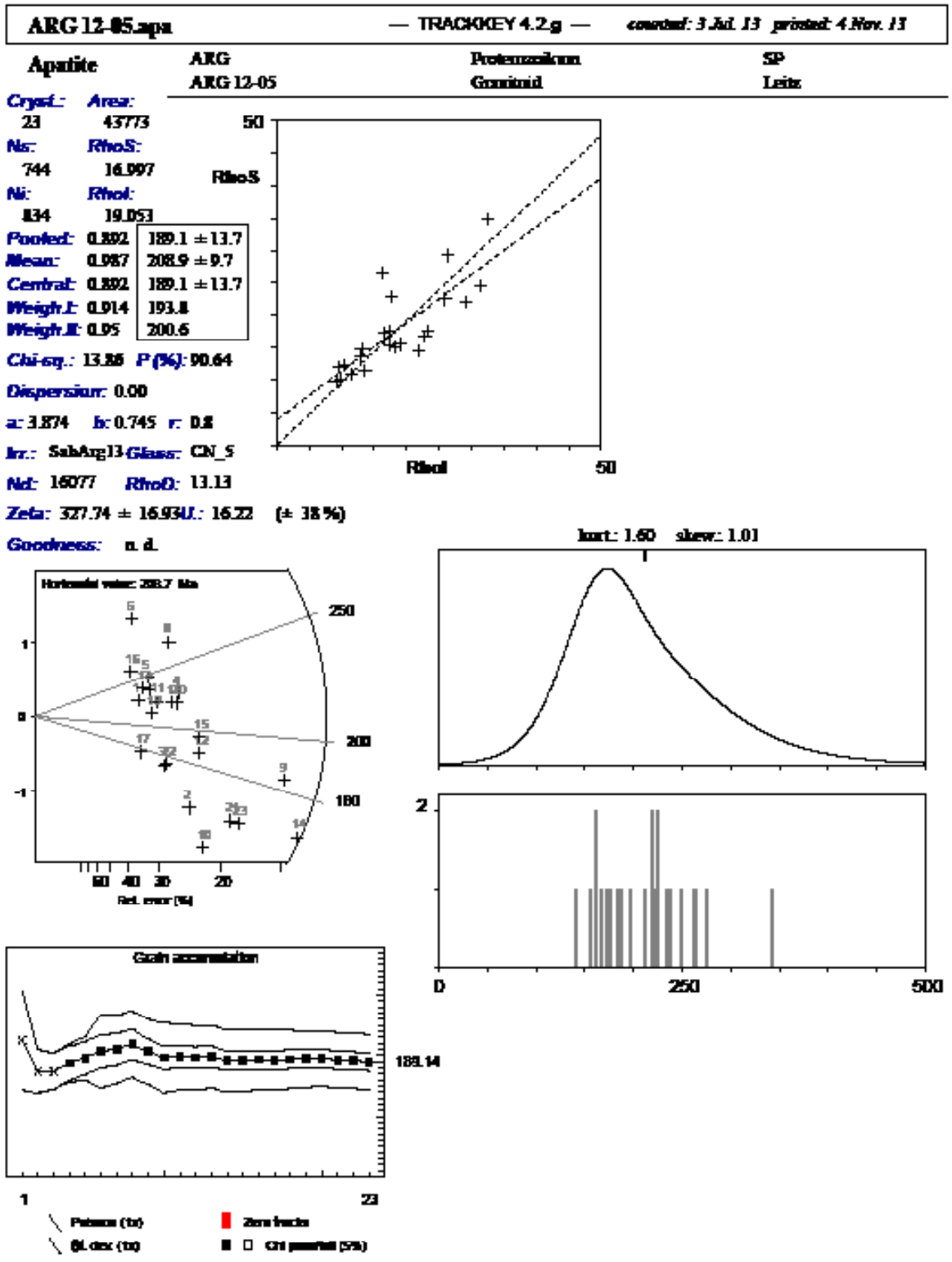
ARG 12-05.apa
— TRACKKEY 4.2.g —
counted: 3 Jul. 13 printed: 4 Nov. 13
Apatite
ARG
ARG 12-05
Proterozoikum
Granitoid
SP
Leitz
Cryst.: 23
Area: 43773
Ns: 744
RhoS: 16.997
Ni: 834
RhoI: 19.053
Pooled: 0.892 189.1 ± 13.7
Mean: 0.987 208.9 ± 9.7
Central: 0.892 189.1 ± 13.7
Weigh.I: 0.914 193.8
Weigh.II: 0.95 200.6
Chi-sq.: 13.88 P (%): 90.64
Dispersion: 0.00
a: 3.874 b: 0.745 r: 0.8
Irr.: SahArg13 Glass: CN_5
Nd: 16077 RhoD: 13.13
Zeta: 327.74 ± 16.93 U.: 16.22 (± 38 %)
Goodness: n. d.
RhoS
RhoI
50
50
kurt.: 1.60 skew.: 1.01
250
200
180
Rel. error (%)
Grain accumulation
189.14
1
23
2
0
250
500

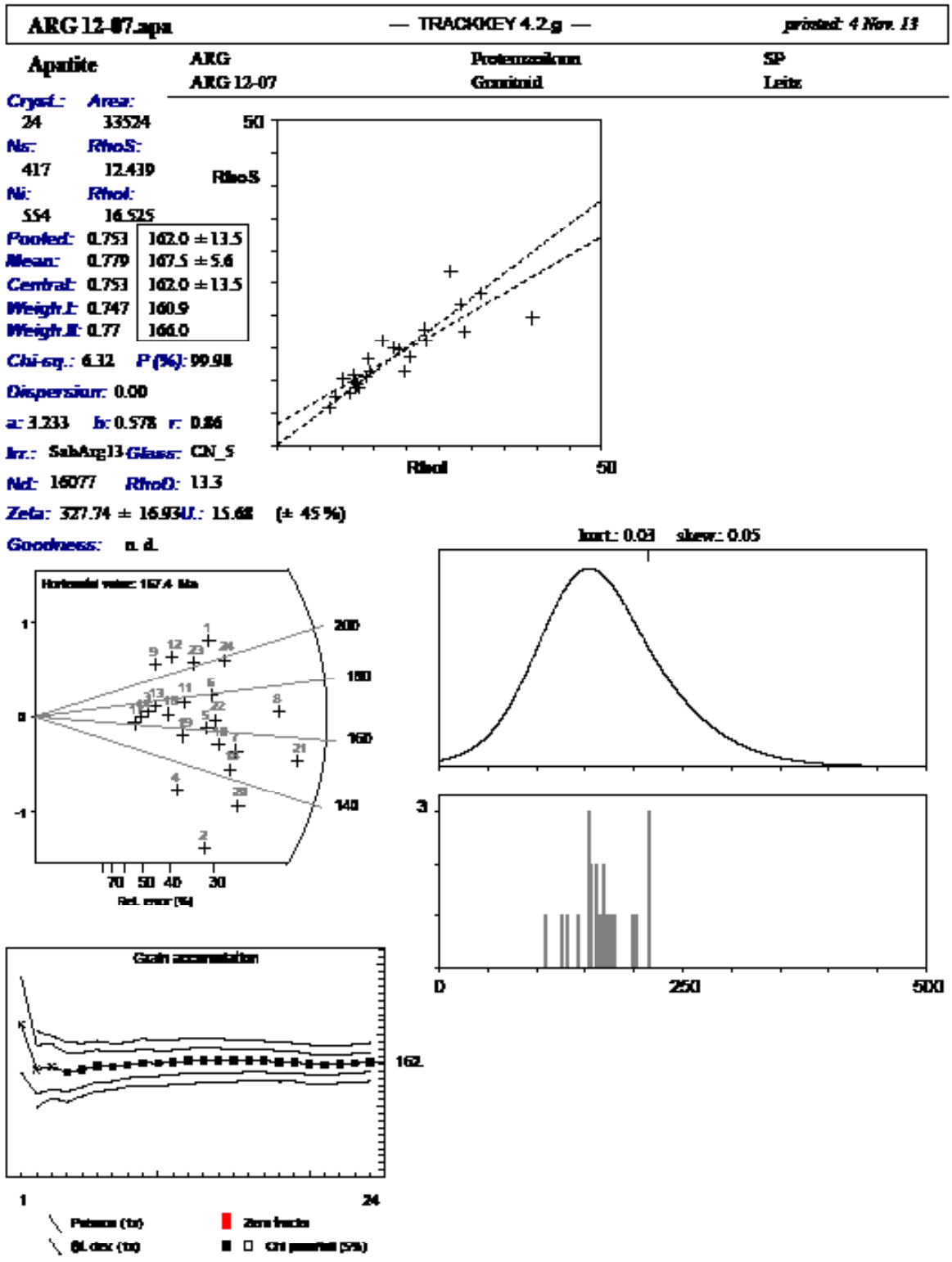
ARG 12-07.apa
— TRACKKEY 4.2g —
printed: 4 Nov. 13
Apatite
ARG
ARG 12-07
Proterozoikum
Granitoid
SP
Leitz
Cryst.: 24
Area: 33524
Ns: 417
RhoS: 12.439
Ni: 554
RhoI: 16.525
Pooled: 0.753 162.0 ± 13.5
Mean: 0.779 167.5 ± 5.6
Central: 0.753 162.0 ± 13.5
Weigh.I: 0.747 160.9
Weigh.II: 0.77 166.0
Chi-sq.: 6.32 P (%): 99.98
Dispersion: 0.00
a: 3.233 b: 0.578 r: 0.86
Irr.: SahArg13 Glass: CN_5
Nd: 16077 RhoD: 13.3
Zeta: 327.74 ± 16.93 U.: 15.68 (± 45 %)
Goodness: n. d.
RhoS
RhoI
50
50
kurt.: 0.03 skew.: 0.05
200
180
160
140
70 50 40 30
Grain accumulation
162.
1
24
0
250
500
3

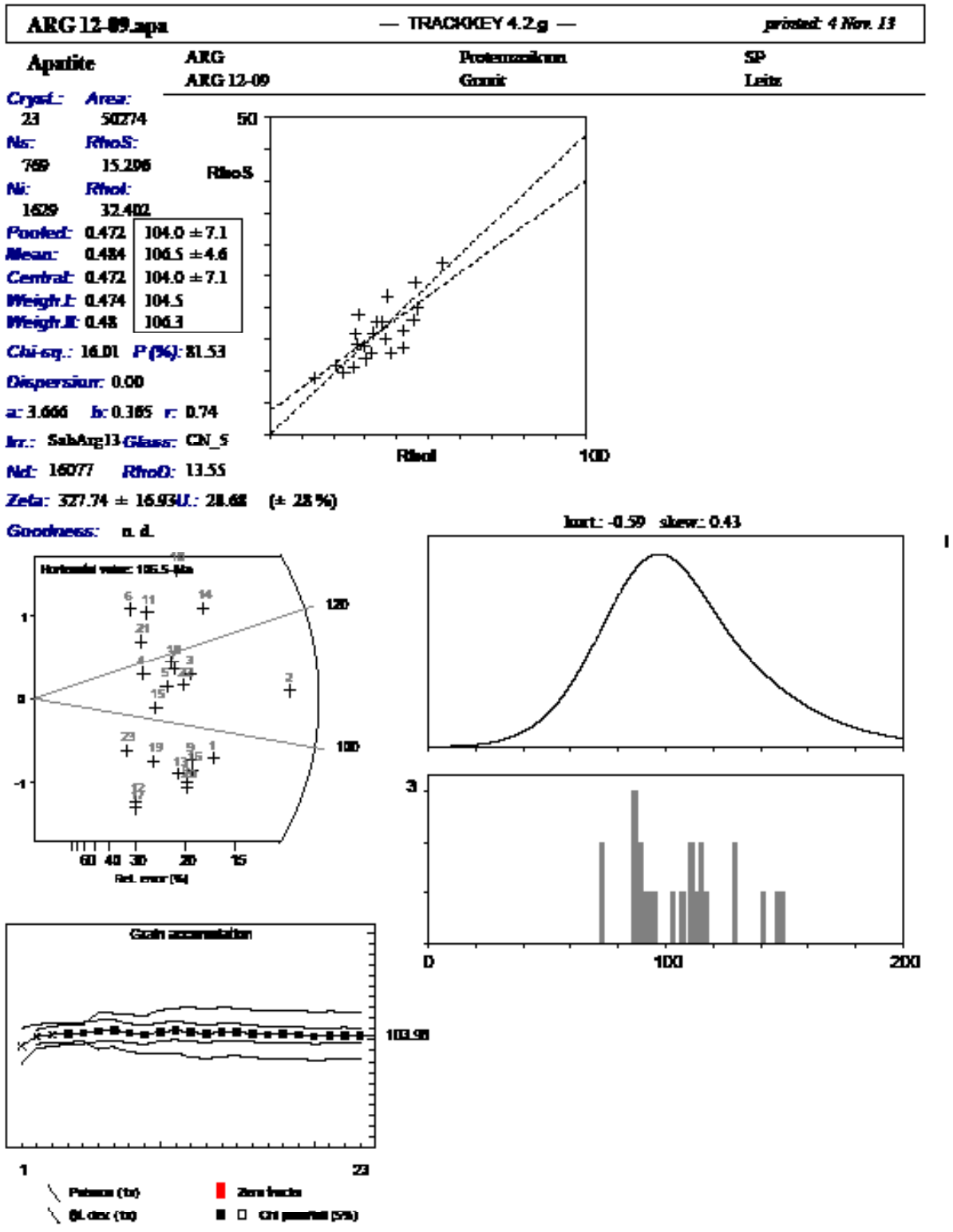
ARG 12-09.apa
— TRACKKEY 4.2g —
printed: 4 Nov. 13
Apatite
ARG
ARG 12-09
Proterozoikum
Granit
SP
Leitz
Cryst.: 23
Area: 50274
Ns: 769
RhoS: 15.296
Ni: 1629
RhoI: 32.402
Pooled: 0.472 104.0 ± 7.1
Mean: 0.484 106.5 ± 4.6
Central: 0.472 104.0 ± 7.1
Weigh.I: 0.474 104.5
Weigh.II: 0.48 106.3
Chi-sq.: 16.01 P (%): 81.53
Dispersion: 0.00
a: 3.666 b: 0.385 r: 0.74
Irr.: SahArg13 Glass: CN_5
Nd: 16077 RhoD: 13.55
Zeta: 327.74 ± 16.93 U.: 28.68 (± 28 %)
Goodness: n. d.
RhoS
RhoI
50
100
kurt.: -0.59 skew.: 0.43
120
100
60 40 30 20 15
Rel. error [%]
Grain accumulation
103.98
1
23
0
100
200
3

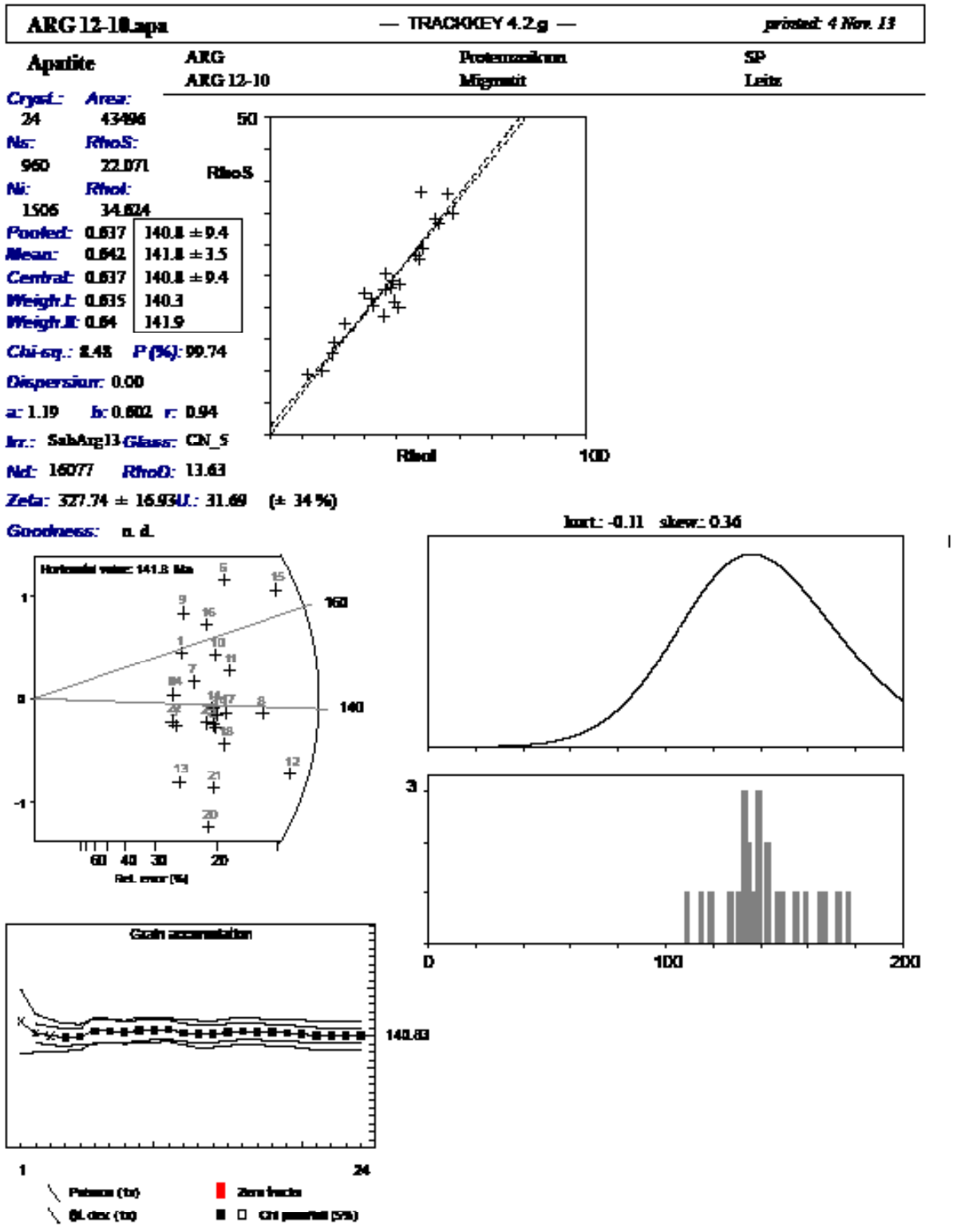
ARG 12-18.apa
— TRACKKEY 4.2g —
printed: 4 Nov. 13
Apatite
ARG
ARG 12-10
Proterozoikum
Migmatit
SP
Leitz
Cryst.: 24
Area: 43496
Ns: 960
RhoS: 22.071
Ni: 1506
RhoI: 34.624
Pooled: 0.637 140.8 ± 9.4
Mean: 0.642 141.8 ± 3.5
Central: 0.637 140.8 ± 9.4
Weigh.I: 0.635 140.3
Weigh.II: 0.64 141.9
Chi-sq.: 8.48 P (%): 99.74
Dispersion: 0.00
a: 1.19 b: 0.802 r: 0.94
Irr.: SubArg13 Glass: CN_5
Nd: 16077 RhoD: 13.63
Zeta: 327.74 ± 16.93 U.: 31.69 (± 34 %)
Goodness: n. d.
RhoS
RhoI
50
100
kurt.: -0.11 skew.: 0.36
160
140
120
60
40
30
20
Rel. error [%]
Grain accumulation
140.83
1
24
0
100
200
3

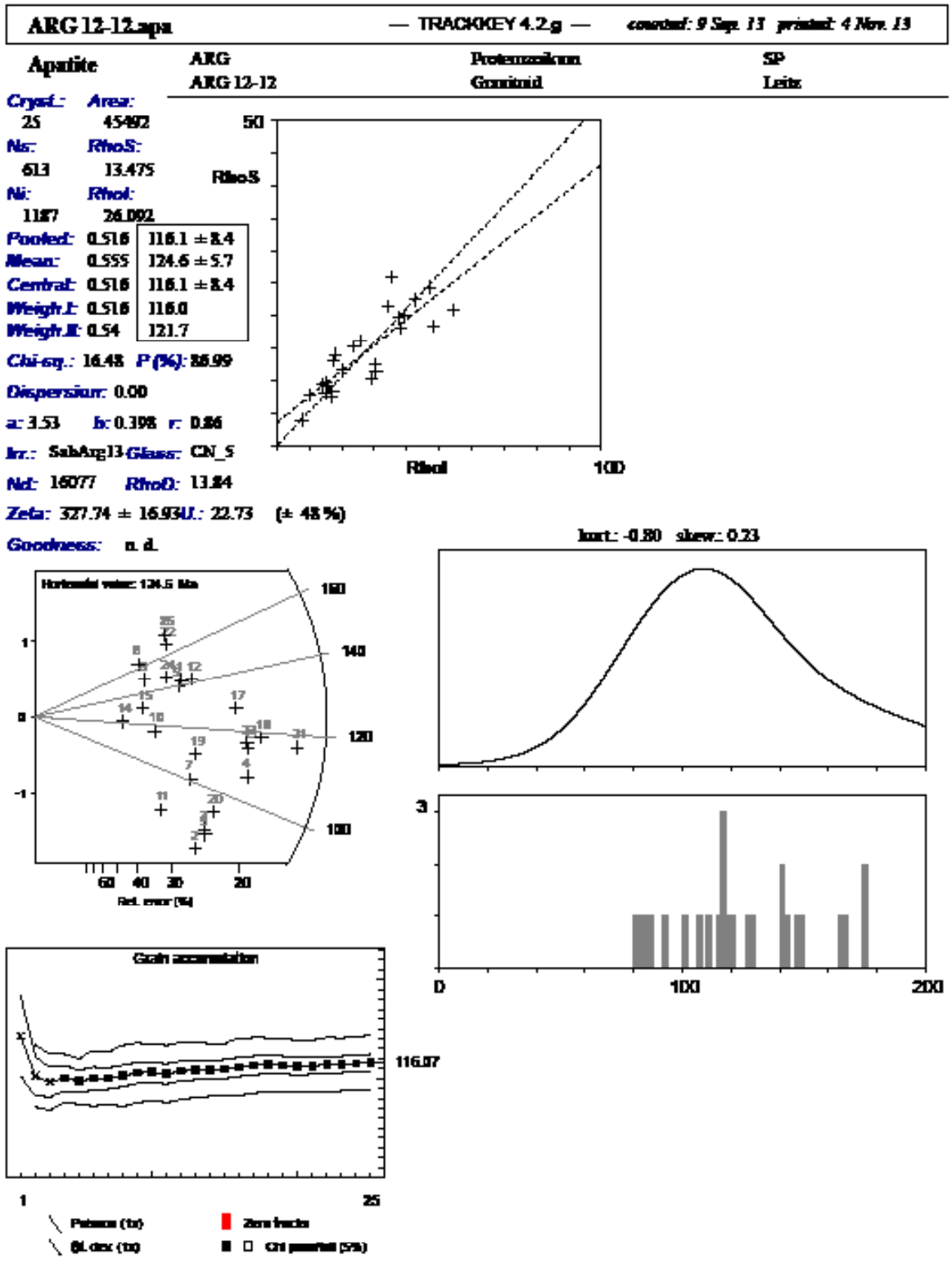
ARG 12-12.apa
— TRACKKEY 4.2.g —
counted: 9 Sep. 13 printed: 4 Nov. 13
Apatite
ARG
ARG 12-12
Proterozoikum
Granitoid
SP
Leitz
Cryst.: 25
Area: 45492
Ns: 613
RhoS: 13.475
Ni: 1187
RhoI: 26.092
Pooled: 0.516 116.1 ± 8.4
Mean: 0.555 124.6 ± 5.7
Central: 0.516 116.1 ± 8.4
Weigh.I: 0.516 116.0
Weigh.II: 0.54 121.7
Chi-sq.: 16.48 P (%): 88.99
Dispersion: 0.00
a: 3.53 b: 0.398 r: 0.86
Inr.: SahArg13 Glass: CN_5
Nd: 16077 RhoD: 13.84
Zeta: 327.74 ± 16.93 U.: 22.73 (± 48 %)
Goodness: n. d.
RhoS
RhoI
50
100
kurt.: -0.80 skew.: 0.23
160
140
120
100
60
40
30
20
Rel. error [%]
Grain accumulation
116.07
1
25
3
0
100
200

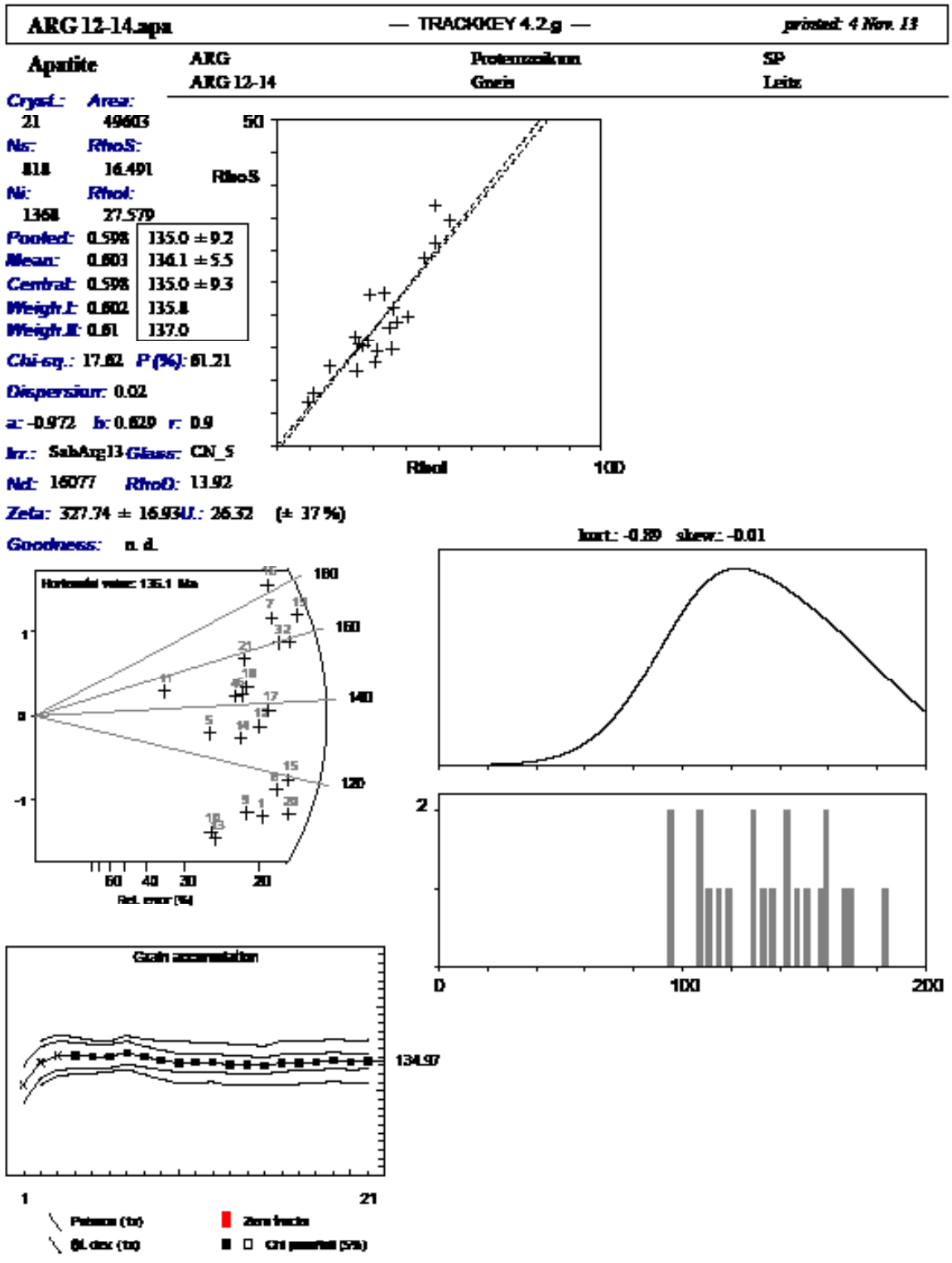
ARG 12-14.apa
— TRACKKEY 4.2g —
printed: 4 Nov. 13
Apatite
ARG
ARG 12-14
Proterozoikum
Gneis
SP
Leitz
Cryst.: 21
Area: 49603
Ns: 818
RhoS: 16.491
Ni: 1368
RhoI: 27.579
Pooled: 0.598 135.0 ± 9.2
Mean: 0.603 136.1 ± 5.5
Central: 0.598 135.0 ± 9.3
Weigh.I: 0.602 135.8
Weigh.II: 0.61 137.0
Chi-sq.: 17.62 P (%): 61.21
Dispersion: 0.02
a: -0.972 b: 0.629 r: 0.9
Irr.: SubArg13 Glass: CN_5
Nd: 16077 RhoD: 13.92
Zeta: 327.74 ± 16.93 U.: 26.32 (± 37 %)
Goodness: n. d.
RhoS
RhoI
50
100
kurt.: -0.89 skew.: -0.01
Horizontal value: 135.1 Ma
180
160
140
120
60
40
30
20
Rel. error [%]
2
0
100
200
Grain accumulation
134.97
1
21

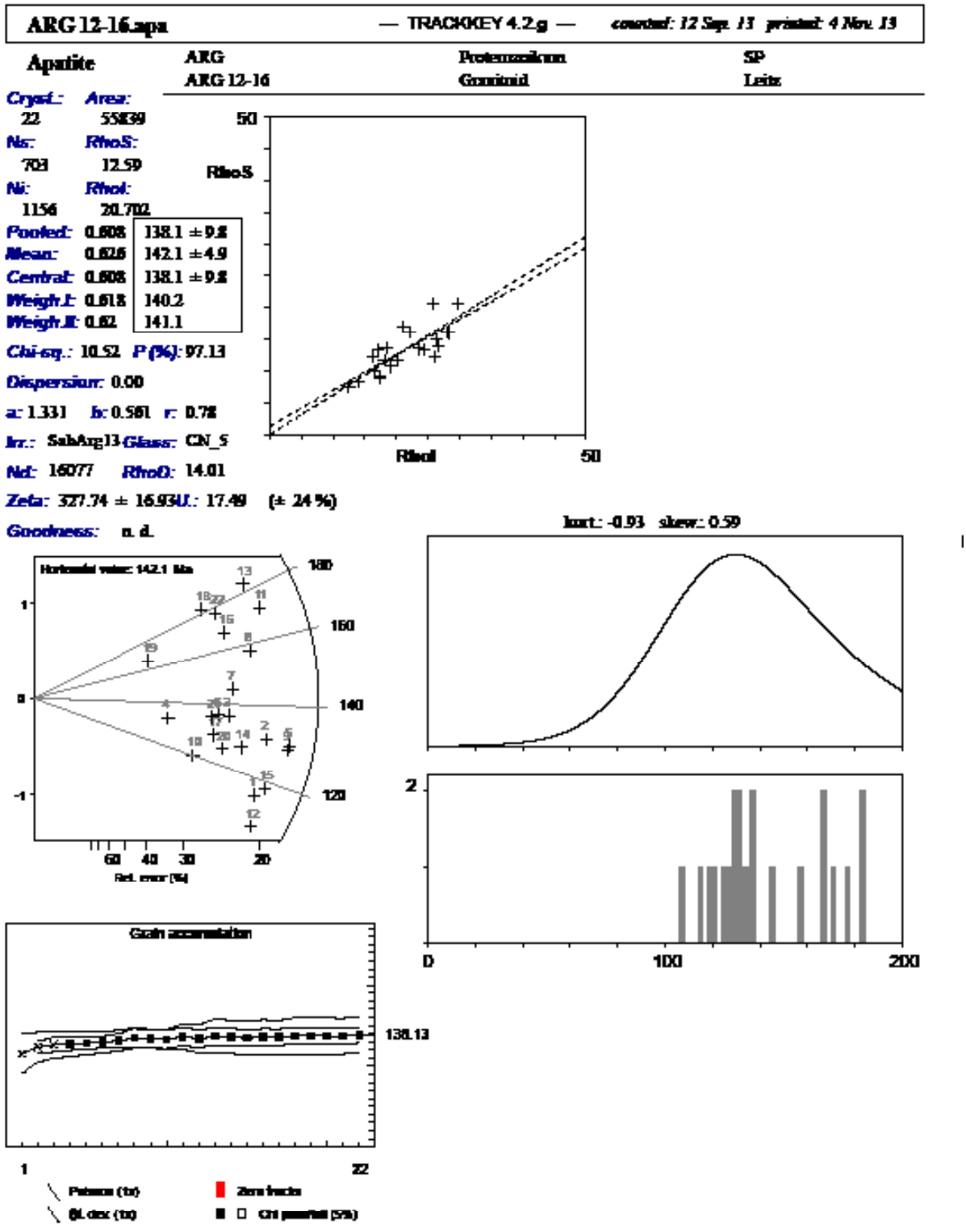
ARG 12-16.apa
— TRACKKEY 4.2.g —
counted: 12 Sep. 13 printed: 4 Nov. 13
Apatite
ARG
ARG 12-16
Proterozoikum
Granitoid
SP
Leitz
Cryst.: 22
Area: 55839
Ns: 703
RhoS: 12.59
Ni: 1156
RhoI: 20.702
Pooled: 0.608 138.1 ± 9.8
Mean: 0.626 142.1 ± 4.9
Central: 0.608 138.1 ± 9.8
Weigh.I: 0.618 140.2
Weigh.II: 0.62 141.1
Chi-sq.: 10.52 P (%): 97.13
Dispersion: 0.00
a: 1.331 b: 0.581 r: 0.78
Irr.: SubArg13 Glass: CN_S
Nd: 16077 RhoD: 14.01
Zeta: 327.74 ± 16.93 U.: 17.49 (± 24 %)
Goodness: n. d.
RhoS
RhoI
50
50
kurt.: -0.93 skew.: 0.59
Horizontal value: 142.1 Ma
180
160
140
120
60
40
30
20
Rel. error [%]
2
0
100
200
Grain accumulation
138.13
1
22
Poisson (1σ)
Zero tracks
ML conc (1σ)
CN1 pooled (5%)

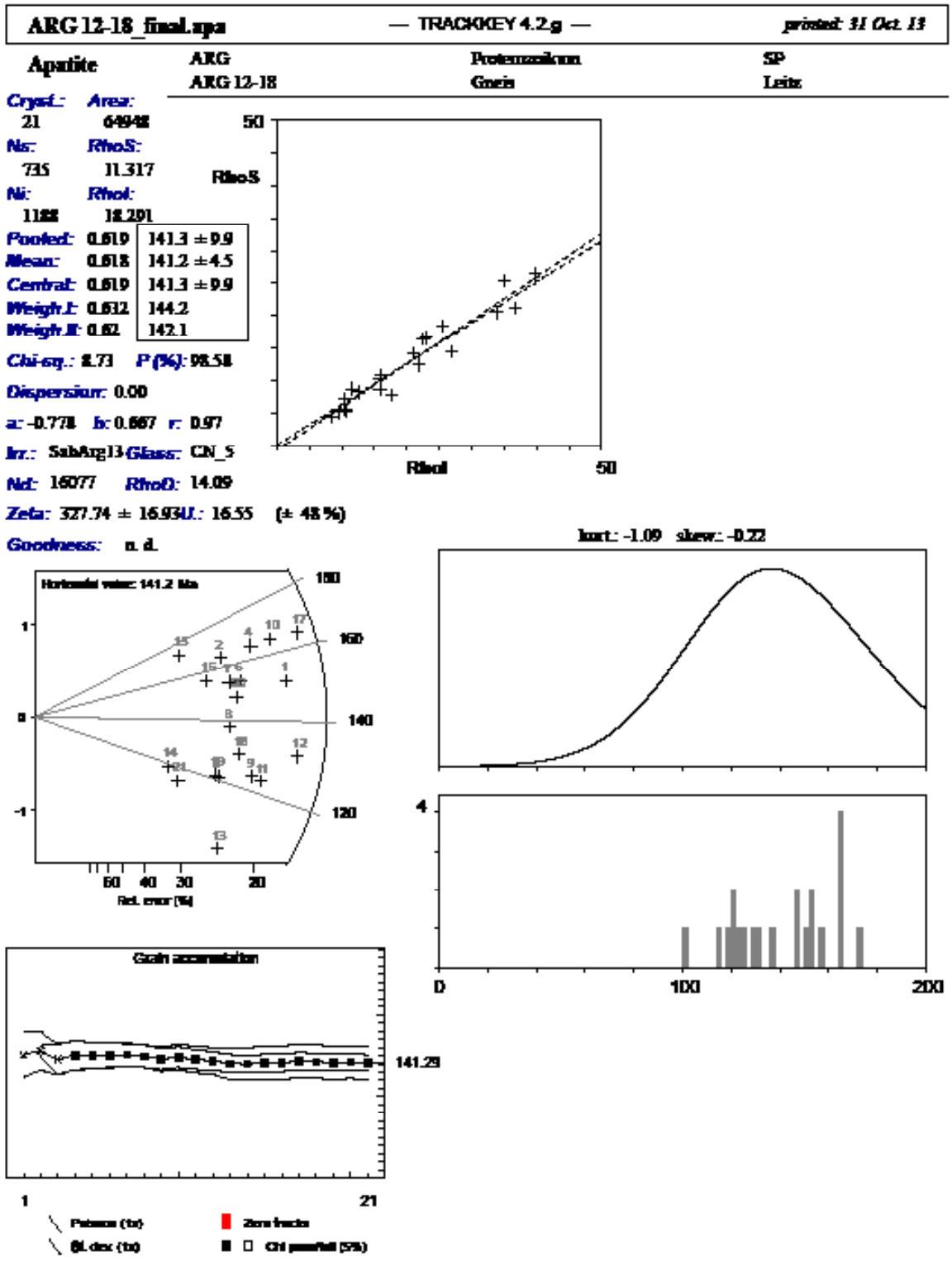
ARG 12-18_final.apa
— TRACKKEY 4.2g —
printed: 31 Oct. 13
Apatite
ARG
ARG 12-18
Proterozoikum
Gneis
SP
Leitz
Cryst.: 21
Area: 64948
Ns: 735
RhoS: 11.317
Ni: 1188
RhoI: 18.291
Pooled: 0.619 141.3 ± 9.9
Mean: 0.618 141.2 ± 4.5
Central: 0.619 141.3 ± 9.9
Weigh.I: 0.632 144.2
Weigh.II: 0.62 142.1
Chi-sq.: 8.73 P (%): 98.58
Dispersion: 0.00
a: -0.778 b: 0.667 r: 0.97
Irr.: SubArg13 Glass: CN_5
Nd: 16077 RhoD: 14.09
Zeta: 327.74 ± 16.93 U.: 16.55 (± 48 %)
Goodness: n. d.
RhoS
RhoI
50
50
kurt.: -1.09 skew.: -0.22
Horizontal value: 141.2 Ma
Rel. error [%]
Grain accumulation
141.29
1
21
0
100
200
4

9.1.2 Sierras Australes

ARG 04.apa --- TRACKKEY 4.2.g --- *counted: 16 Mrz. 12 printed: 16 Mrz. 12*

Apatite

Argentina	Permian	SK
ARG 04	Sand- /Siltstone	Leitz

Cryst.: 20 ***Area:*** 53341
Ns: 1370 ***RhoS:*** 25.684
Ni: 2065 ***Rhol:*** 38.713

Pooled:	0.663	157.8 ± 10.7
Mean:	0.673	160.0 ± 2.6
Central:	0.663	157.8 ± 10.7
Weigh.I:	0.673	160.2
Weigh.II:	0.67	159.0

Chi-sq.: 3.33 ***P (%):*** 100.0
Dispersion: 0.00
a: -1.301 ***b:*** 0.706 ***r:*** 0.99
Irr.: ARG1234 ***Glass:*** CN_5
Nd: 15148 ***RhoD:*** 14.3
Zeta: 336.83 ± 19.51 ***U.:*** 35.57 (± 41 %)
Goodness: n. d.

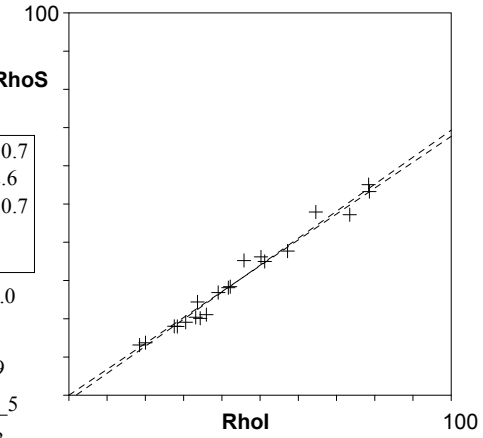

kurt.: -0.29 skew.: -0.07

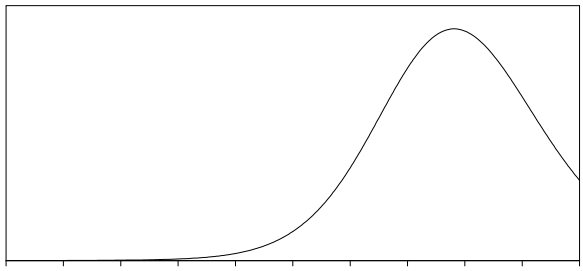

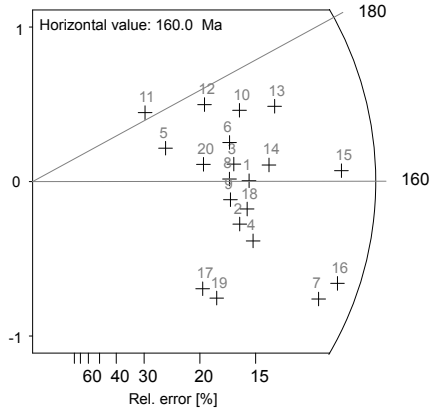

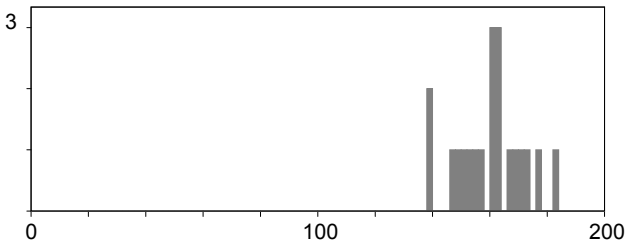

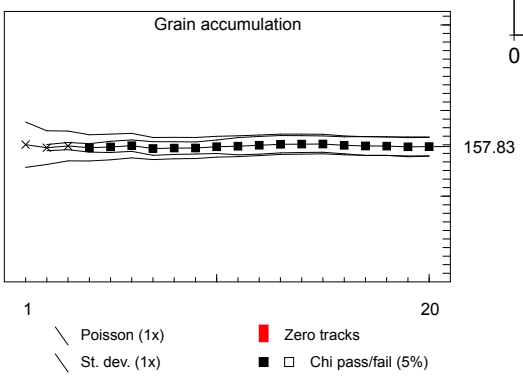

ARG 05.apa --- TRACKKEY 4.2.g --- *counted: 16 Mrz. 12 printed: 16 Mrz. 12*

Apatite

Argentina	upper Permian	SK
ARG 05	Syenite	Leitz

Cryst.: 20 ***Area:*** 37177
Ns: 1149 ***RhoS:*** 30.906
Ni: 1171 ***RhoI:*** 31.498

Pooled:	0.981	231.1 ± 16.6
Mean:	0.997	234.7 ± 6.9
Central:	0.981	231.1 ± 16.6
Weigh.I:	0.988	232.8
Weigh.II:	0.99	233.4

Chi-sq.: 7.65 ***P (%):*** 98.98
Dispersion: 0.00
a: 2.536 ***b:*** 0.917 ***r:*** 0.88
Irr.: ARG12345 ***Glass:*** CN_5
Nd: 15148 ***RhoD:*** 14.24
Zeta: 336.83 ± 19.51 ***U.:*** 26.78 (± 26 %)
Goodness: n. d.

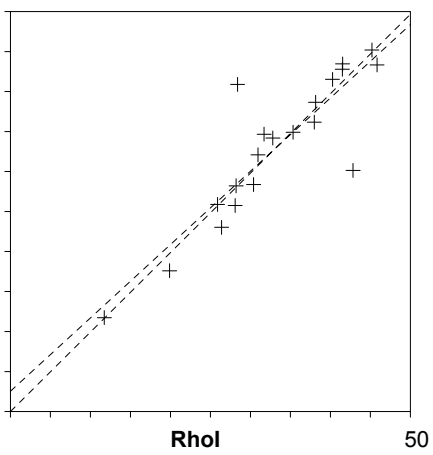

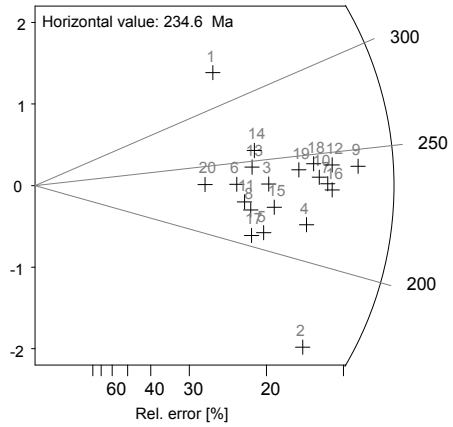

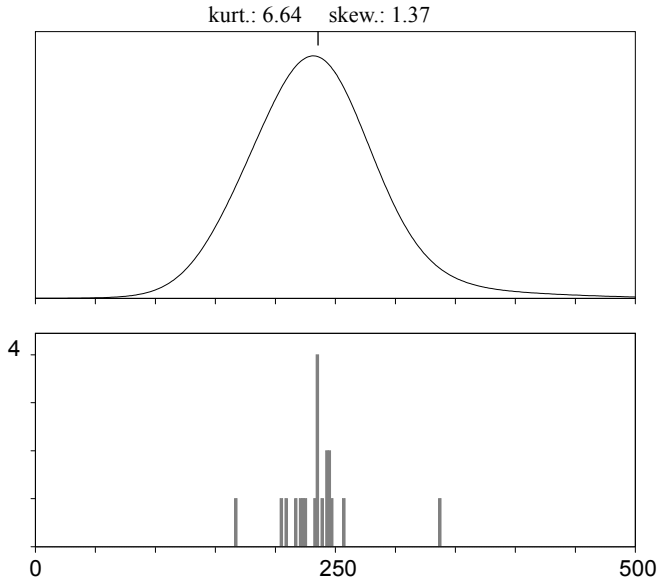

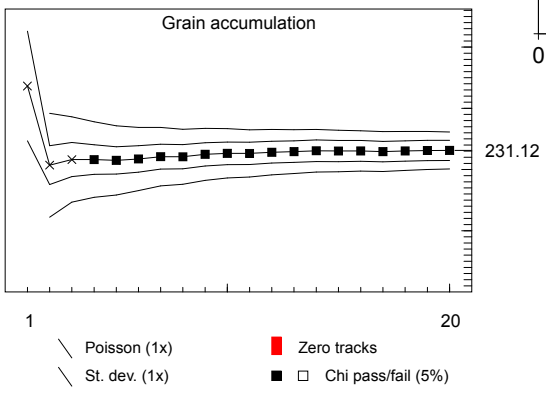

ARG 08.apa --- TRACKKEY 4.2.g --- *counted: 16 Mrz. 12 printed: 16 Mrz. 12*

Apatite

Argentina	Precambrian	SK
ARG 08	Paragneis	Leitz

Cryst.: ***Area:***
20 33568
Ns: ***RhoS:***
1315 39.174
Ni: ***RhoI:***
1269 37.804

Pooled:	1.036	242.7 ± 17.1
Mean:	1.077	252.0 ± 10.2
Central:	1.036	242.7 ± 17.1
Weigh.I:	1.028	240.7
Weigh.II:	1.05	246.4

Chi-sq.: 5.53 ***P (%):*** 99.88
Dispersion: 0.00
a: 3.514 ***b:*** 0.959 ***r:*** 0.99
Irr.: ARG12345 ***Glass:*** CN_5
Nd: 15148 ***RhoD:*** 14.17
Zeta: 336.83 ± 19.51 ***U.:*** 36.27 (± 67 %)
Goodness: n. d.

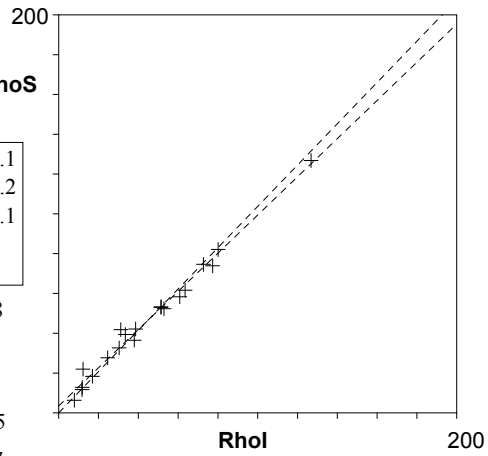

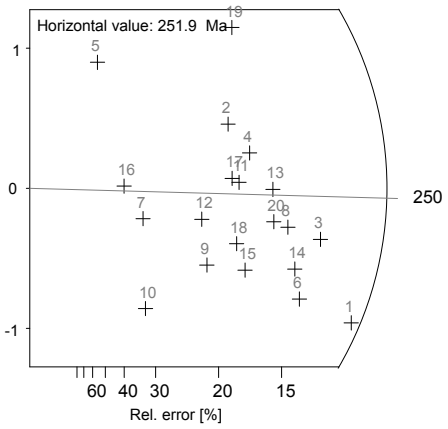

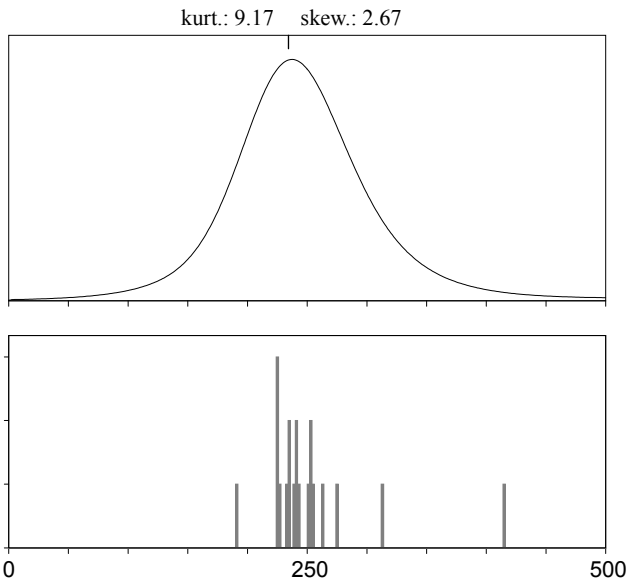

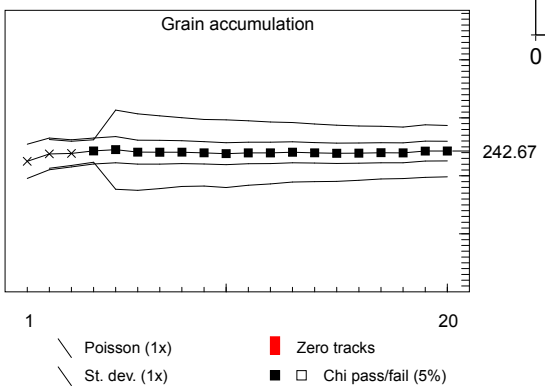

ARG 09.apa --- TRACKKEY 4.2.g --- *counted: 20 Mrz. 12 printed: 20 Mrz. 12*

Apatite

Argentina	Dev. /Carb.	SK
ARG 09	Sandstone	Leitz

Cryst.: 20 ***Area:*** 46261
Ns: 1021 ***RhoS:*** 22.071
Ni: 1266 ***RhoI:*** 27.367

Pooled:	0.806	188.7 ± 13.6
Mean:	0.864	202.0 ± 11.2
Central:	0.816	190.9 ± 14.8
Weigh.I:	0.816	190.9
Weigh.II:	0.85	197.7

Chi-sq.: 25.25 ***P (%):*** 15.25
Dispersion: 0.11
a: 2.062 ***b:*** 0.764 ***r:*** 0.9
Irr.: ARG12345 ***Glass:*** CN_5
Nd: 15148 ***RhoD:*** 14.1
Zeta: 336.83 ± 19.51 ***U.:*** 25.34 (± 60 %)
Goodness: n. d.

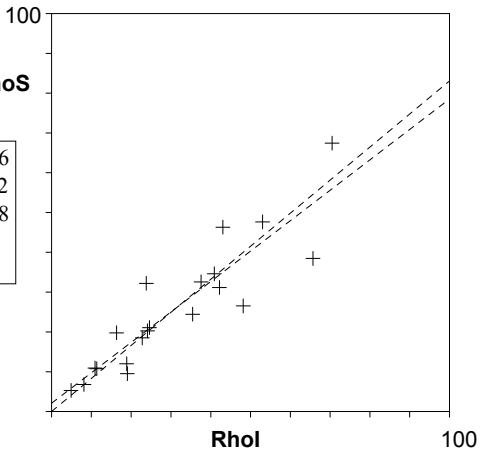

kurt.: 0.10 skew.: 0.32

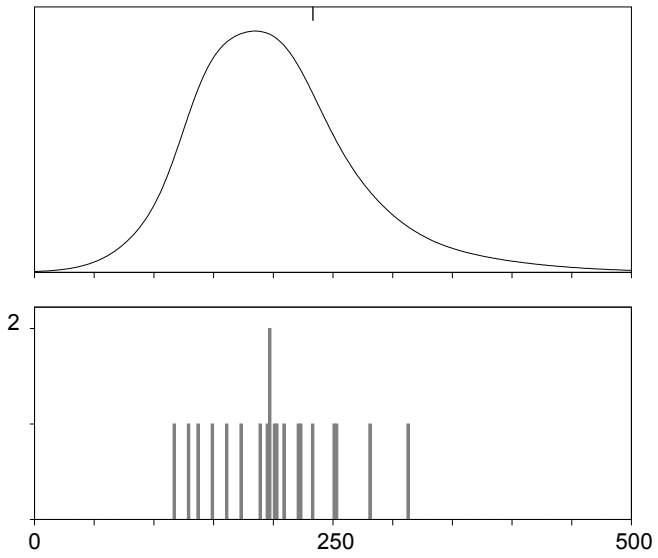

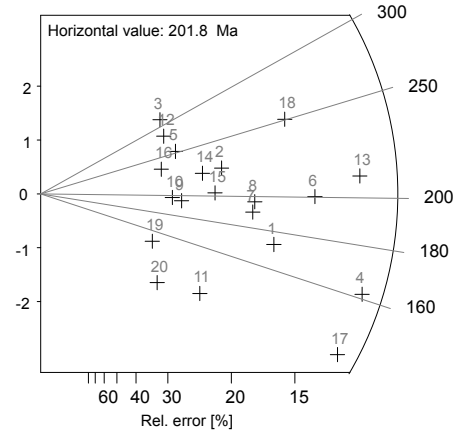

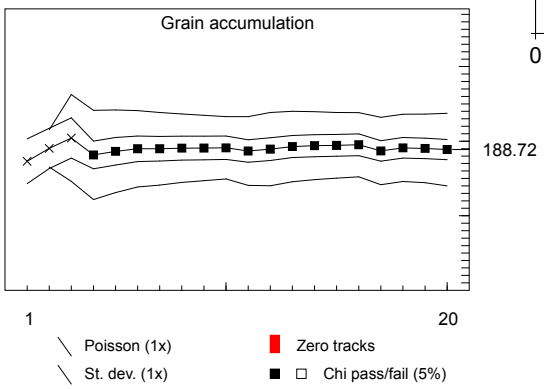

ARG 12.apa --- TRACKKEY 4.2.g --- *counted: 28 Mrz. 12 printed: 28 Mrz. 12*

Apatite

Argentina | Carbon./Perm. | SK
ARG 12 | Sandstone | Leitz

Cryst.:	Area:
20	26570
Ns:	**RhoS:**
714	26.872
Ni:	**RhoI:**
1176	44.26

Pooled:	0.607	141.9 ± 10.7
Mean:	0.599	140.0 ± 4.0
Central:	0.607	141.9 ± 10.7
Weigh.I:	0.61	142.6
Weigh.II:	0.61	141.6

Chi-sq.: 5.96 **P (%):** 99.8

Dispersion: 0.00

a: -2.114 **b:** 0.647 **r:** 0.97

Irr.: ARG1234 **Glass:** CN_5

Nd: 15148 **RhoD:** 14.03

Zeta: 336.83 ± 19.51 **U.:** 41.26 (± 42 %)

Goodness: n. d.

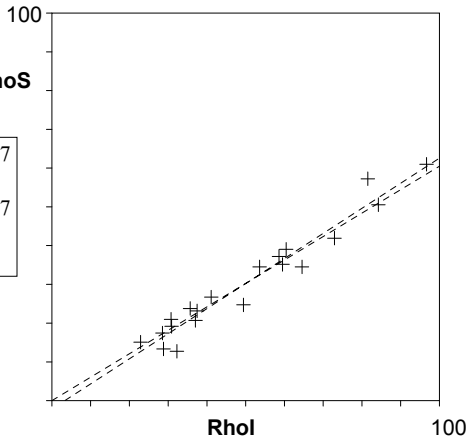

kurt.: 1.49 skew.: -1.27

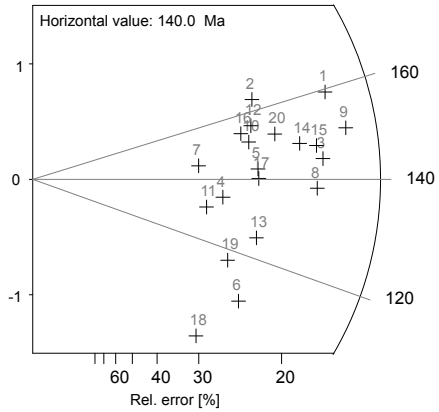

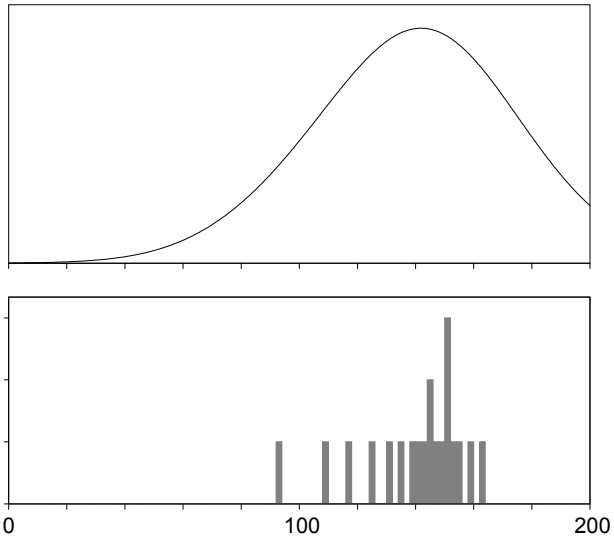

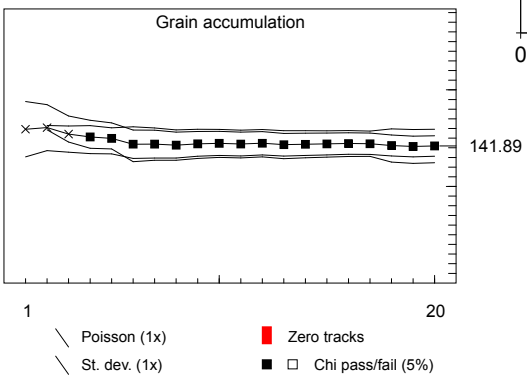

ARG 15.apa --- TRACKKEY 4.2.g --- *counted: 20 Mrz. 12 printed: 20 Mrz. 12*

Apatite

Argentina	Permian	SK
ARG 15	Sandstone	Leitz

Cryst.: ***Area:***
20 54758
Ns: ***RhoS:***
1084 19.796
Ni: ***RhoI:***
1502 27.43

Pooled:	0.722	167.5 ± 11.9
Mean:	0.768	178.1 ± 9.5
Central:	0.732	169.8 ± 13.1
Weigh.I:	0.716	166.2
Weigh.II:	0.76	175.3

Chi-sq.: 30.83 ***P (%):*** 4.22
Dispersion: 0.13
a: 2.868 ***b:*** 0.636 ***r:*** 0.89
Irr.: ARG12345 ***Glass:*** CN_5
Nd: 15148 ***RhoD:*** 13.96
Zeta: 336.83 ± 19.51 ***U.:*** 26.44 (± 56 %)
Goodness: n. d.

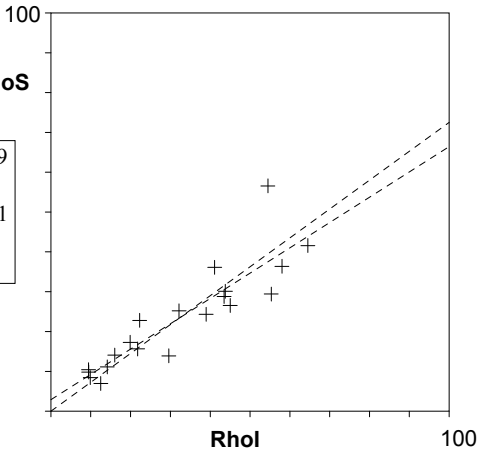

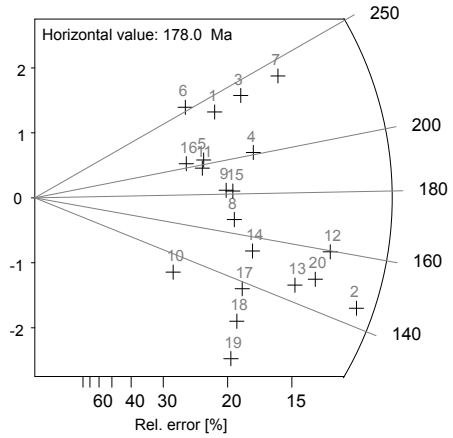

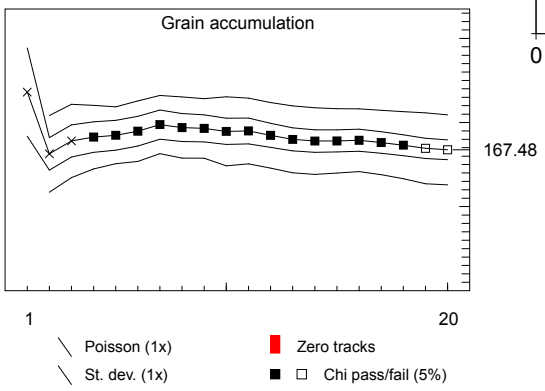

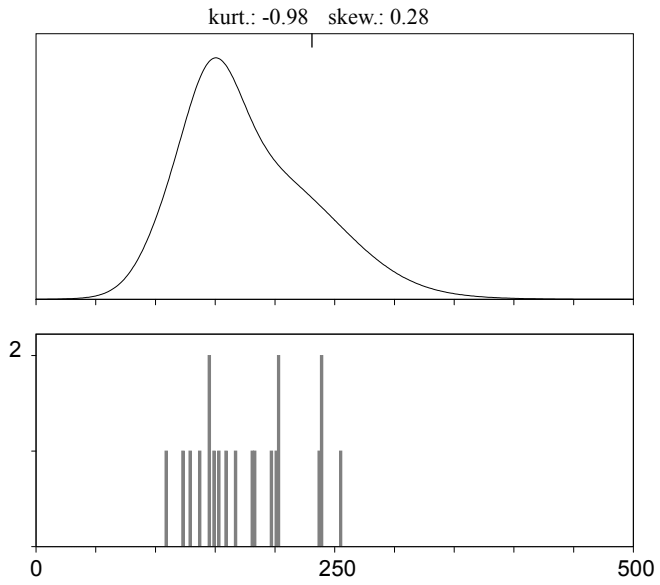

ARG 16.apa --- TRACKKEY 4.2.g --- *counted: 28 Mrz. 12 printed: 28 Mrz. 12*

Apatite Argentina up. Carbon./Perm. SK
ARG 16 Diamiktite Leitz

Cryst.: 17	***Area:*** 61312	
Ns: 839	***RhoS:*** 13.684	
Ni: 1242	***Rhol:*** 20.257	
Pooled:	0.676	156.2 ± 11.5
Mean:	0.666	154.1 ± 7.6
Central:	0.675	156.0 ± 11.7
Weigh.I:	0.679	156.9
Weigh.II:	0.68	157.3

Chi-sq.: 17.55 ***P (%):*** 35.11

Dispersion: 0.05

a: -0.419 ***b:*** 0.683 ***r:*** 0.95

Irr.: ARG12345 ***Glass:*** CN_5

Nd: 15148 ***RhoD:*** 13.9

Zeta: 336.83 ± 19.51 ***U.:*** 18.63 (± 57 %)

Goodness: n. d.

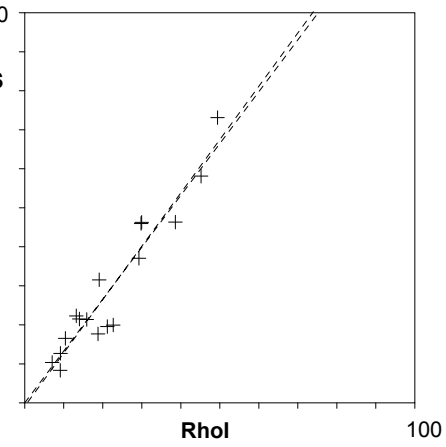

kurt.: -1.01 skew.: -0.60

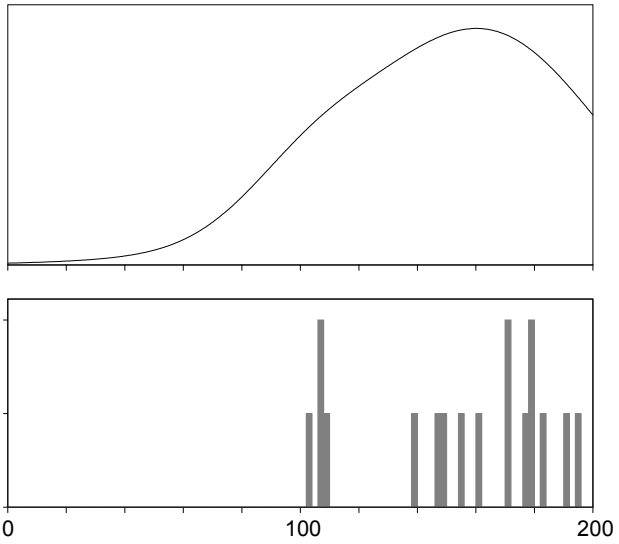

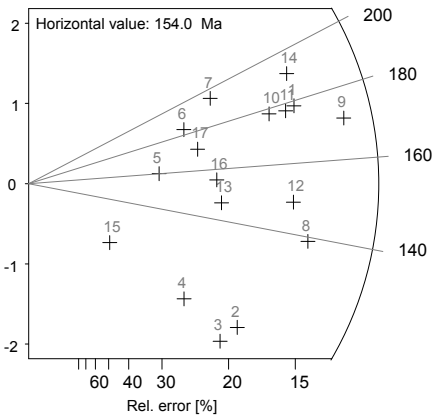

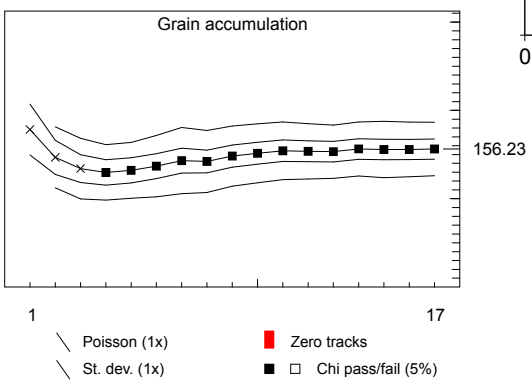

ARG 17.apa --- TRACKKEY 4.2.g --- *counted: 26 Mrz. 12 printed: 26 Mrz. 12*

Apatite

Argentina	Permian(Tunas Fm)	SK
ARG 17	Sandstone	Leitz

Cryst.: 20 ***Area:*** 38738
Ns: 869 ***RhoS:*** 22.433
Ni: 1243 ***RhoI:*** 32.088

Pooled:	0.699	160.8 ± 11.8
Mean:	0.732	168.3 ± 7.9
Central:	0.702	161.4 ± 12.3
Weigh.I:	0.694	159.7
Weigh.II:	0.72	166.4

Chi-sq.: 21.01 ***P (%):*** 33.64
Dispersion: 0.08
a: 4.42 ***b:*** 0.577 ***r:*** 0.9
Irr.: ARG12345 ***Glass:*** CN_5
Nd: 15148 ***RhoD:*** 13.83
Zeta: 336.83 ± 19.51 ***U.:*** 29.23 (± 52 %)
Goodness: n. d.

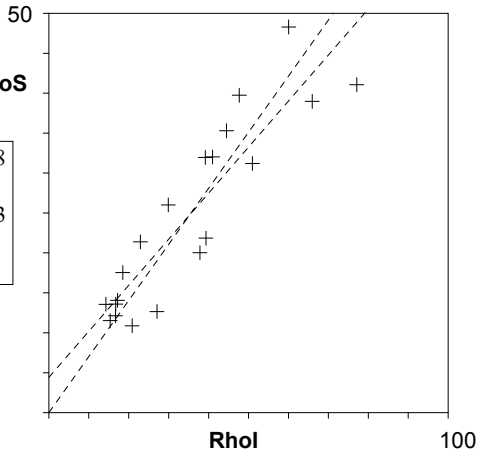

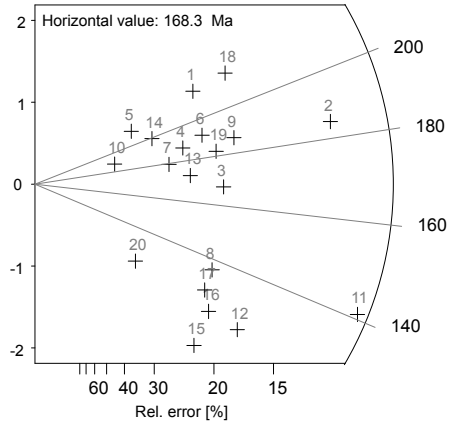

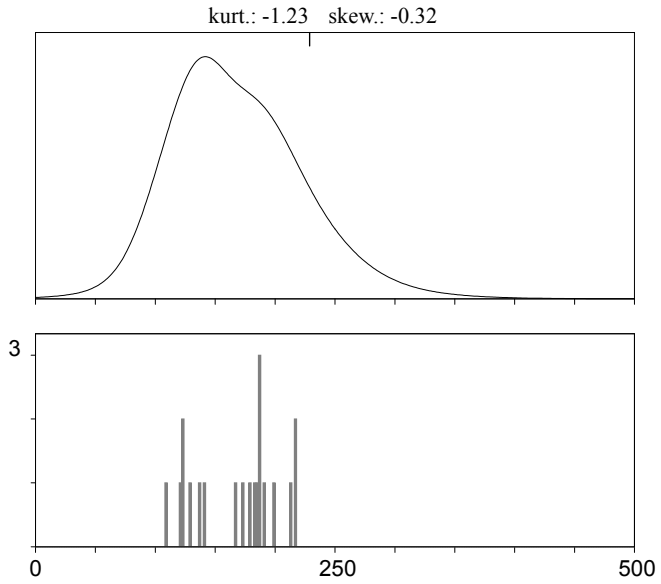

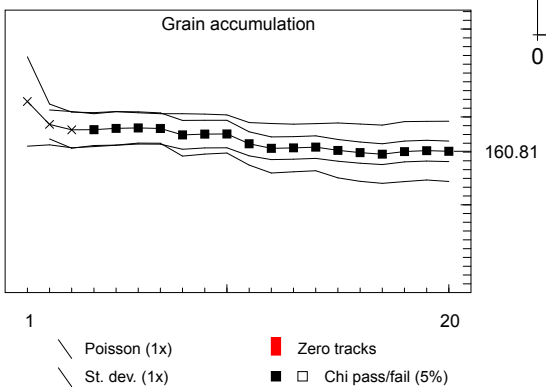

9.2 Argentina - data sheets ZFT

9.2.1 Sierras Septentrionales

ARG 12-02Ur.zir --- TRACKKEY 4.2.g --- *counted: 22 Jan. 14 printed: 22 Jan. 14*

Zircon ARG 12-02 SK Leitz

Cryst.:	***Area:***	
11	1706	
Ns:	***RhoS:***	
478	280.148	
Ni:	***RhoI:***	
70	41.026	
Pooled:	6.829	262.4 ± 36.1
Mean:	6.889	264.7 ± 6.0
Central:	6.829	262.4 ± 36.1
Weigh.I:	6.733	258.8
Weigh.II:	6.86	263.5

Chi-sq.: 0.34 ***P (%):*** 100.0

Dispersion: 0.00

a: 959.125 ***b:*** -2.812 ***r:*** -0.74

Irr.: ARGZR12 ***Glass:*** CN_1

Nd: 7558 ***RhoD:*** 6.37684

Zeta: 123 ± 6.08 ***U.:*** 215.09 (± 35 %)

Goodness: n. d.

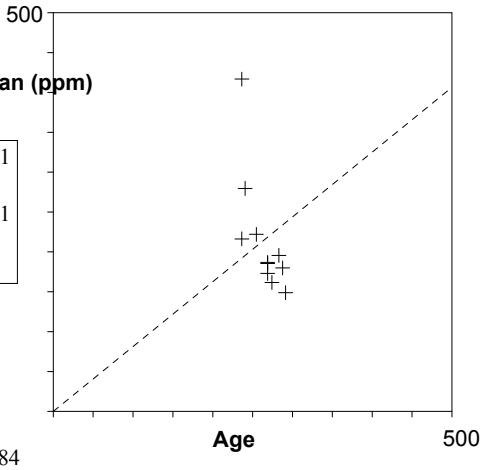

kurt.: -1.26 skew.: -0.33

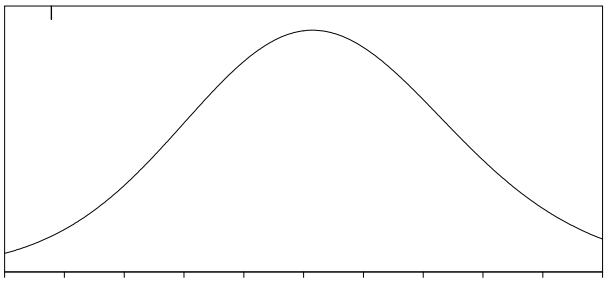

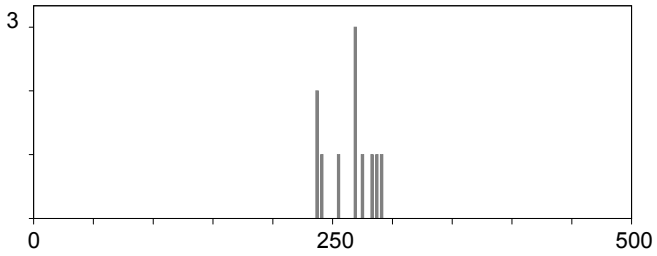

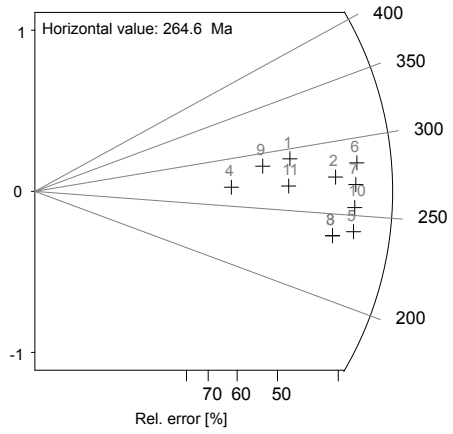

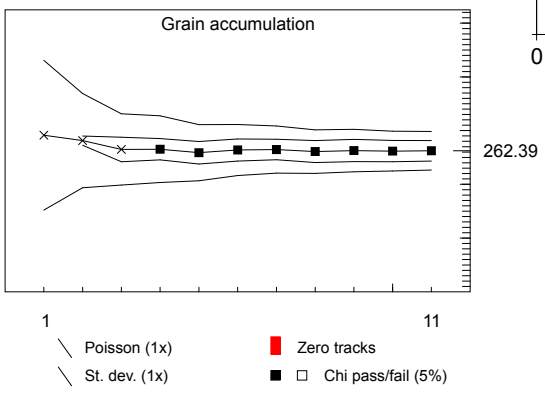

ARG 12-04-02.zir --- TRACKKEY 4.2.g --- *counted: 22 Jan. 14 printed: 22 Jan. 14*

Zircon

Argentina
ARG 12-04-02

SK
Leitz

Cryst.:	***Area:***	
9	1527	
Ns:	***RhoS:***	
482	315.585	
Ni:	***RhoI:***	
81	53.034	
Pooled:	5.951	231.2 ± 30.1
Mean:	6.223	241.5 ± 9.2
Central:	5.951	231.2 ± 30.1
Weigh.I:	5.932	230.5
Weigh.II:	6.06	235.5

Chi-sq.: 0.28 ***P (%):*** 100.0

Dispersion: 0.00

a: 1177.662 ***b:*** -3.769 ***r:*** -0.46

Irr.: ARGZR12 ***Glass:*** CN_1

Nd: 7558 ***RhoD:*** 6.43157

Zeta: 123 ± 6.08 ***U.:*** 267.41 (± 84 %)

Goodness: n. d.

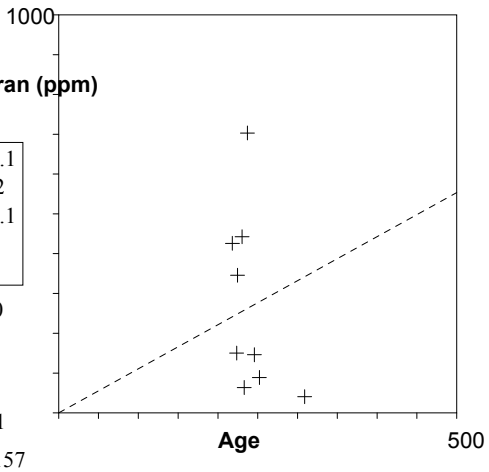

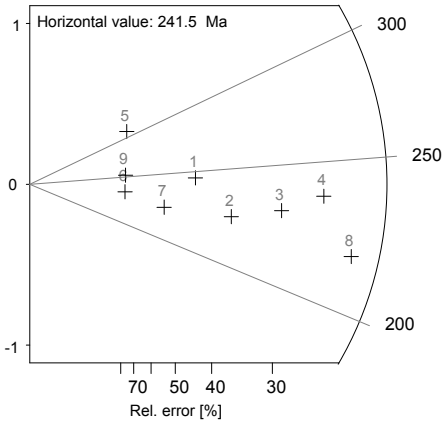

kurt.: 5.33 skew.: 2.17

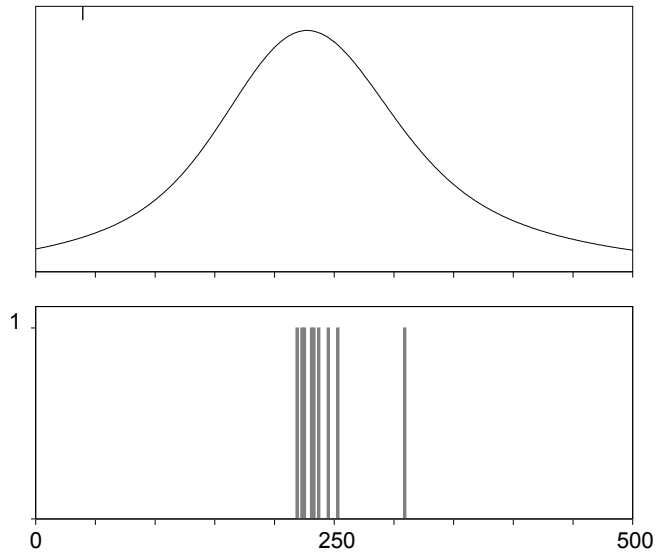

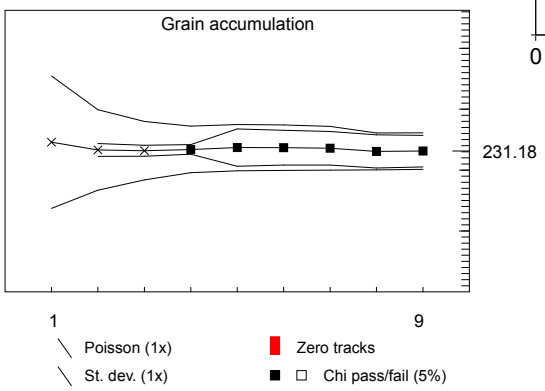

ARG 12-05.zir --- TRACKKEY 4.2.g --- *counted: 22 Jan. 14 printed: 22 Jan. 14*

Zircon SK

ARG 12-05 Leitz

Cryst.:	***Area:***	
8	967	
Ns:	***RhoS:***	
273	282.442	
Ni:	***RhoI:***	
46	47.591	
Pooled:	5.935	228.2 ± 38.2
Mean:	6.146	236.2 ± 7.8
Central:	5.935	228.2 ± 38.2
Weigh.I:	5.822	223.9
Weigh.II:	6.04	232.0

Chi-sq.: 0.3 ***P (%):*** 99.99

Dispersion: 0.00

a: 1993.332 ***b:*** -7.131 ***r:*** -0.73

Irr.: ARGZR12 ***Glass:*** CN_1

Nd: 7558 ***RhoD:*** 6.36421

Zeta: 123 ± 6.08 ***U.:*** 309.31 (± 69 %)

Goodness: n. d.

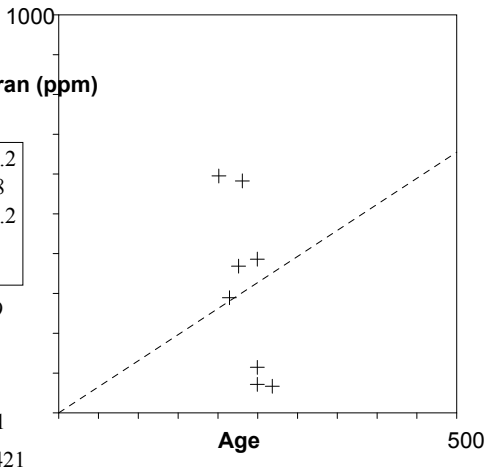

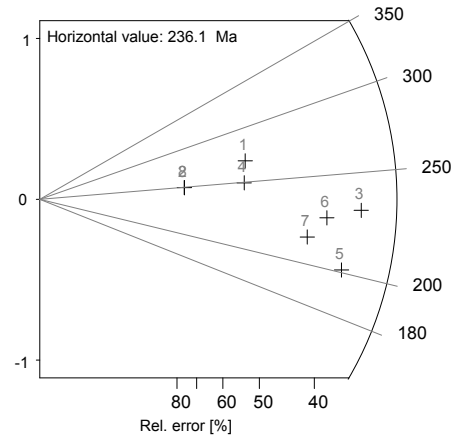

kurt.: -0.69 skew.: -0.25

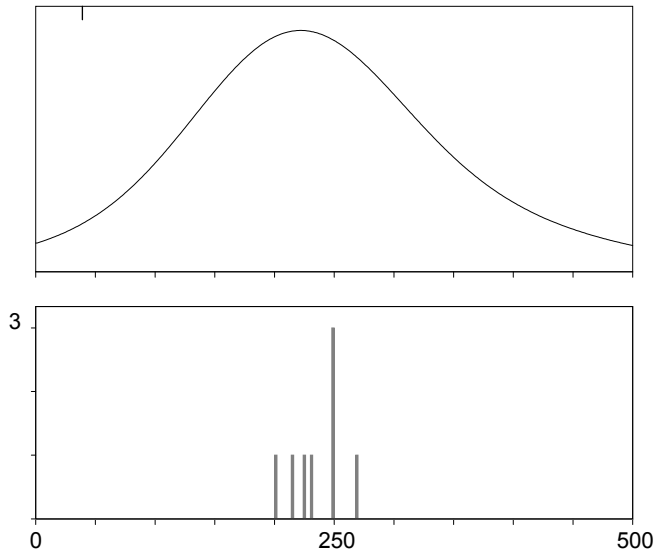

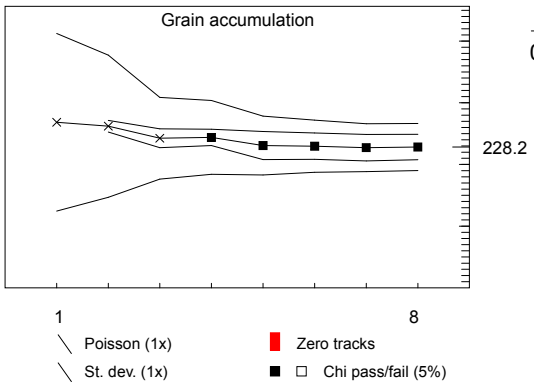

Poisson (1x) Zero tracks

St. dev. (1x) Chi pass/fail (5%)

ARG 12-07.zir --- TRACKKEY 4.2.g --- *counted: 22 Jan. 14 printed: 22 Jan. 14*

Zircon

ARG 12-07

Cryst.:	***Area:***	
10	2972	
Ns:	***RhoS:***	
377	126.83	
Ni:	***RhoI:***	
65	21.867	
Pooled:	5.8	223.7 ± 32.1
Mean:	5.966	230.0 ± 10.5
Central:	5.8	223.7 ± 32.1
Weigh.I:	6.205	239.0
Weigh.II:	5.92	228.1

Chi-sq.: 2.0 ***P (%):*** 99.14

Dispersion: 0.00

a: -171.536 ***b:*** 1.454 ***r:*** 0.37

Irr.: ARGZR12 ***Glass:*** CN_1

Nd: 7558 ***RhoD:*** 6.38105

Zeta: 123 ± 6.08 ***U.:*** 162.75 (± 80 %)

Goodness: n. d.

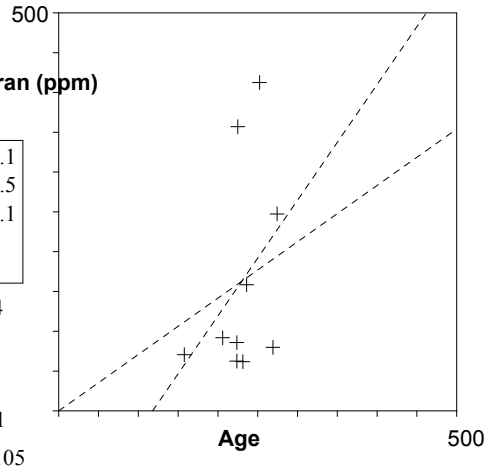

kurt.: 1.75 skew.: -0.88

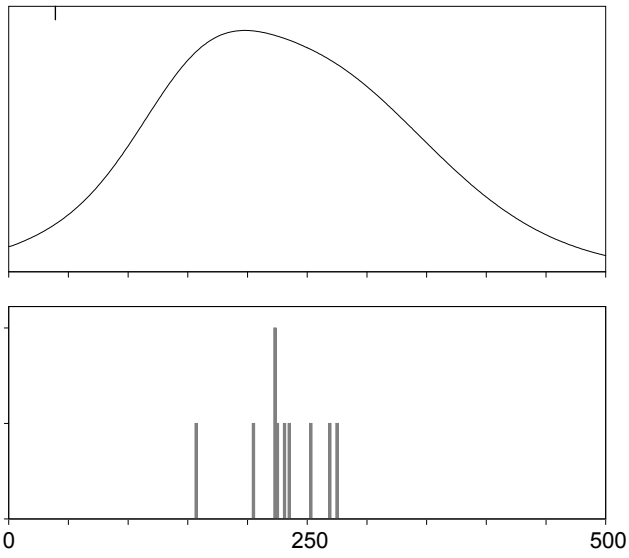

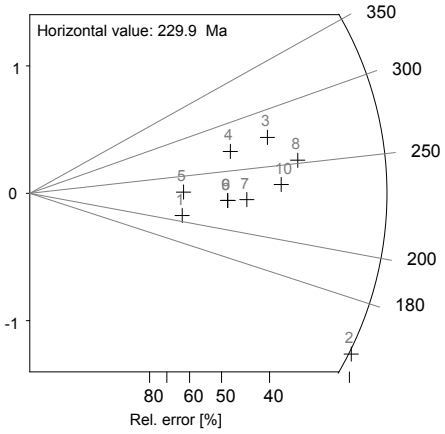

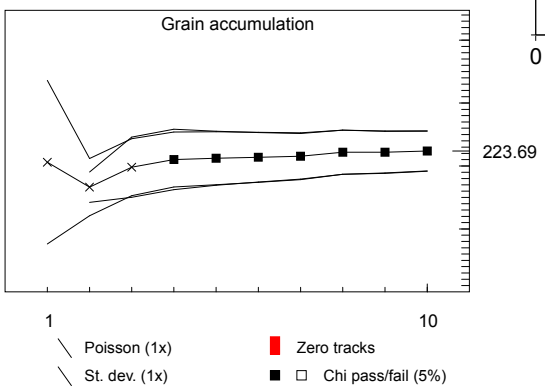

ARG12-12.zir --- TRACKKEY 4.2.g --- *counted: 22 Jan. 14 printed: 22 Jan. 14*

Zircon ARG12-12

Cryst.:	***Area:***	
2	244	
Ns:	***RhoS:***	
53	217.347	
Ni:	***RhoI:***	
9	36.908	
Pooled:	5.889	218.1 ± 79.4
Mean:	5.925	219.4 ± 0.0
Central:	5.889	218.1 ± 79.4
Weigh.I:	5.866	217.3
Weigh.II:	5.91	218.8

Chi-sq.: 0.02 ***P (%):*** 87.96

Dispersion: 0.00

a: 659.336 ***b:*** -2.132 ***r:*** -1.0

Irr.: ARGZR12 ***Glass:*** CN_1

Nd: 7558 ***RhoD:*** 6.1251

Zeta: 123 ± 6.08 ***U.:*** 191.66 (± 19 %)

Goodness: n. d.

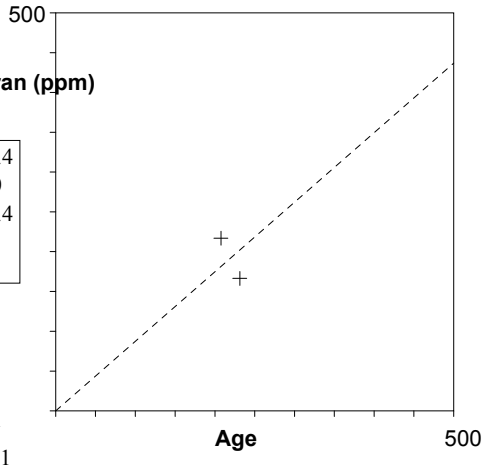

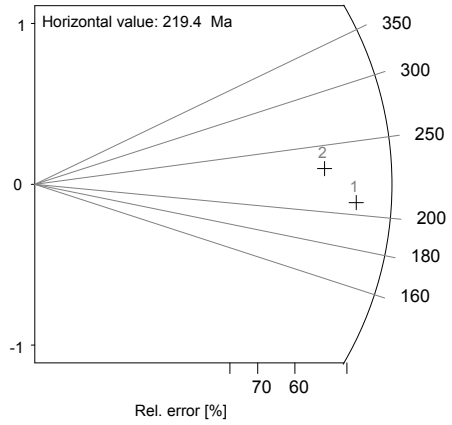

kurt.: 1.75 skew.: -0.88

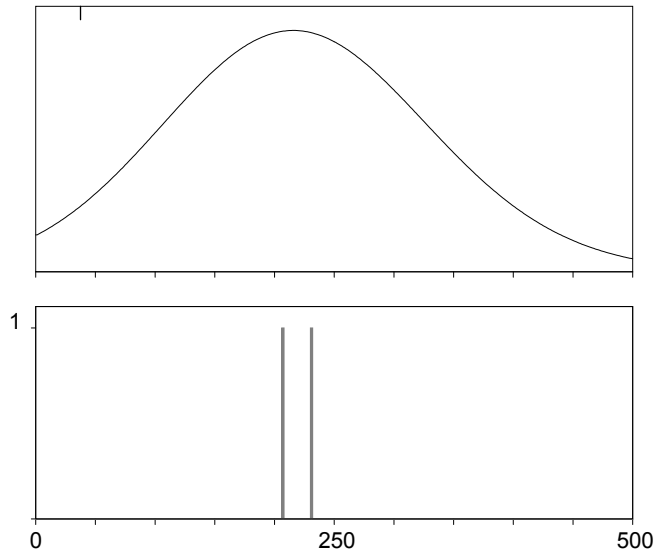

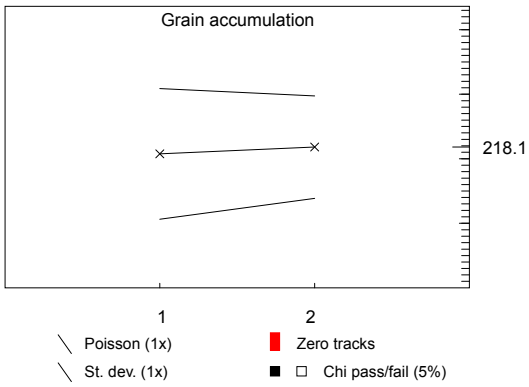

Poisson (1x) Zero tracks
St. dev. (1x) Chi pass/fail (5%)

ARG12-14.zir --- TRACKKEY 4.2.g --- *counted: 22 Jan. 14 printed: 22 Jan. 14*

Zircon ARG12-14

Cryst.:	***Area:***	
9	1090	
Ns:	***RhoS:***	
310	284.357	
Ni:	***RhoI:***	
48	44.029	
Pooled:	6.458	249.9 ± 40.8
Mean:	6.523	252.3 ± 16.4
Central:	6.458	249.9 ± 40.8
Weigh.I:	6.296	243.7
Weigh.II:	6.49	250.9

Chi-sq.: 1.52 ***P (%):*** 99.24

Dispersion: 0.00

a: 474.912 ***b:*** -0.882 ***r:*** -0.42

Irr.: ARGZR12 ***Glass:*** CN_1

Nd: 7558 ***RhoD:*** 6.41473

Zeta: 123 ± 6.08 ***U.:*** 252.45 (± 41 %)

Goodness: n. d.

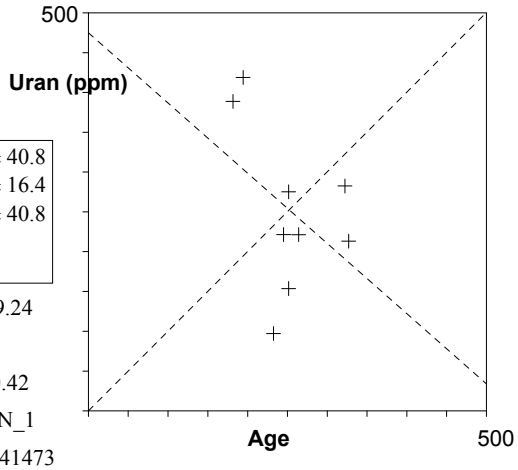

kurt.: -0.41 skew.: 0.27

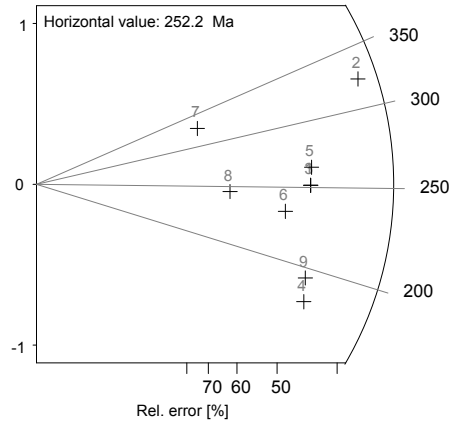

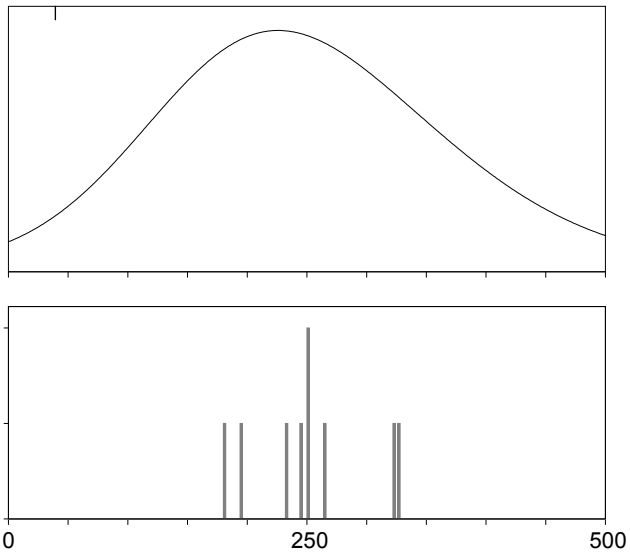

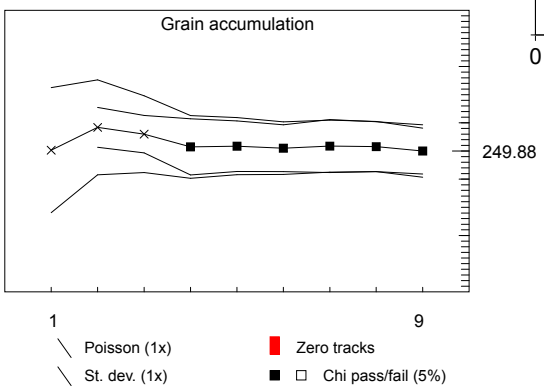

ARG12-16.zir --- TRACKKEY 4.2.g --- *counted: 22 Jan. 14 printed: 22 Jan. 14*

Zircon

ARG12-16

Cryst.:	***Area:***	
11	1853	
Ns:	***RhoS:***	
370	199.682	
Ni:	***RhoI:***	
62	33.46	
Pooled:	5.968	230.2 ± 33.7
Mean:	6.025	232.3 ± 8.2
Central:	5.968	230.2 ± 33.7
Weigh.I:	6.116	235.8
Weigh.II:	6.00	231.4

Chi-sq.: 0.59 ***P (%):*** 100.0

Dispersion: 0.00

a: -91.169 ***b:*** 1.295 ***r:*** 0.35

Irr.: ARGZR12 ***Glass:*** CN_1

Nd: 7558 ***RhoD:*** 6.38526

Zeta: 123 ± 6.08 ***U.:*** 209.54 (± 48 %)

Goodness: n. d.

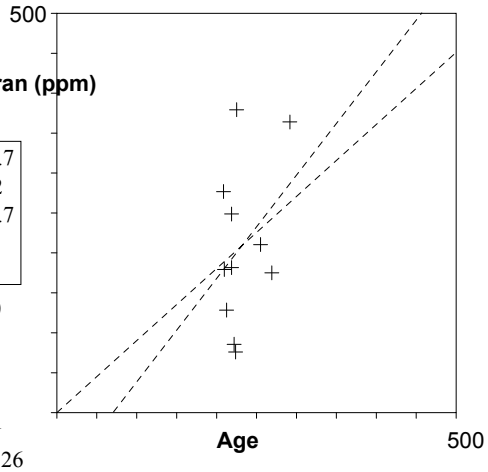

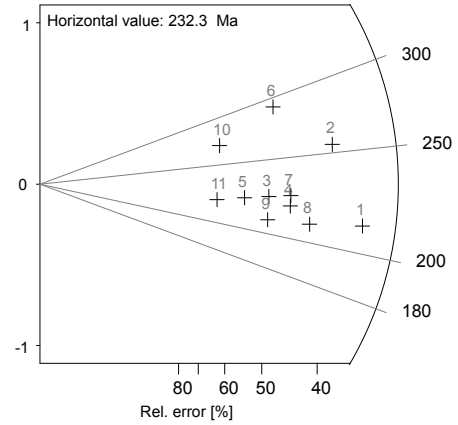

kurt.: 0.88 skew.: 1.38

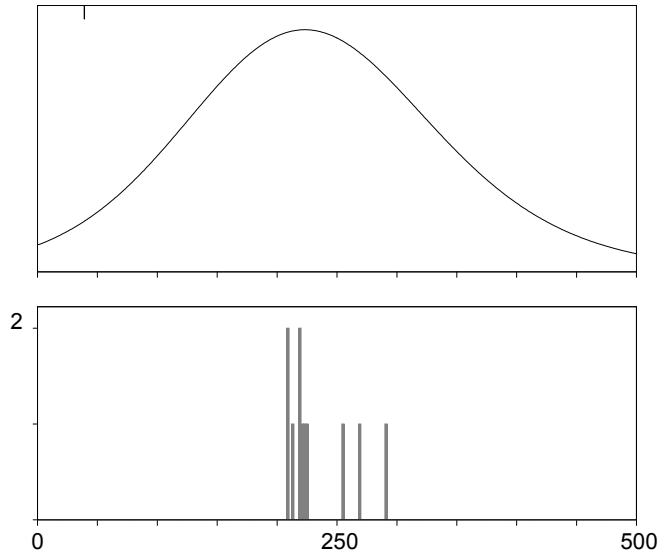

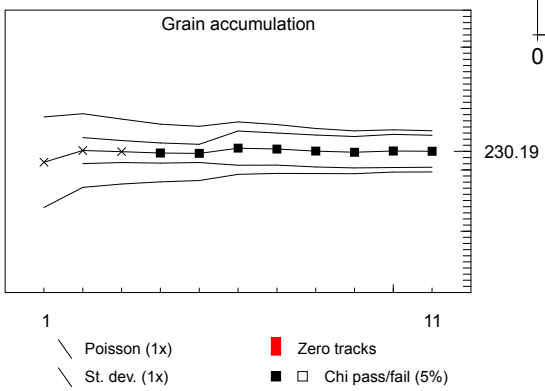

ARG12-18.zir --- TRACKKEY 4.2.g --- *counted: 22 Jan. 14 printed: 22 Jan. 14*

Zircon SK

ARG12-18 Leitz

Cryst.: ***Area:***
3 681
Ns: ***RhoS:***
156 229.183
Ni: ***RhoI:***
25 36.728

Pooled:	6.24	240.0 ± 53.1
Mean:	6.591	253.3 ± 0.0
Central:	6.24	240.0 ± 53.1
Weigh.I:	6.179	237.7
Weigh.II:	6.37	245.0

Chi-sq.: 0.08 ***P (%):*** 96.27

Dispersion: 0.00

a: 1137.856 ***b:*** -3.791 ***r:*** -1.0

Irr.: ARGZR12 ***Glass:*** CN_1

Nd: 7558 ***RhoD:*** 6.37263

Zeta: 123 ± 6.08 ***U.:*** 178.01 (± 64 %)

Goodness: n. d.

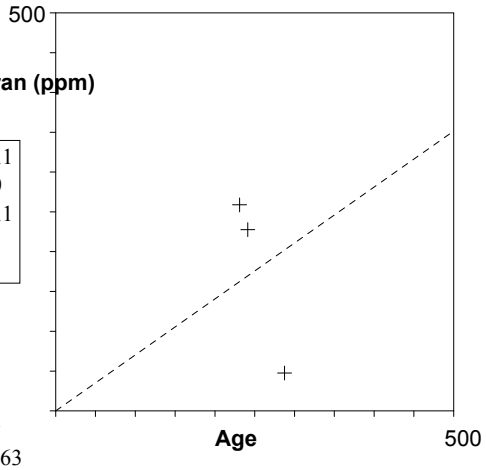

kurt.: 0.88 skew.: 1.38

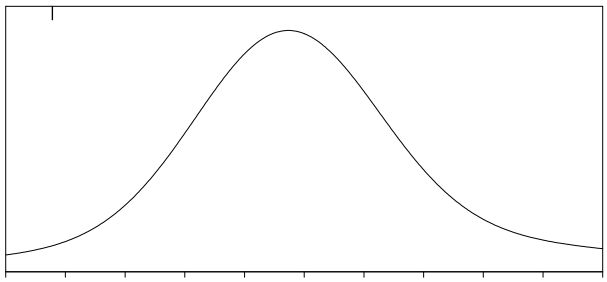

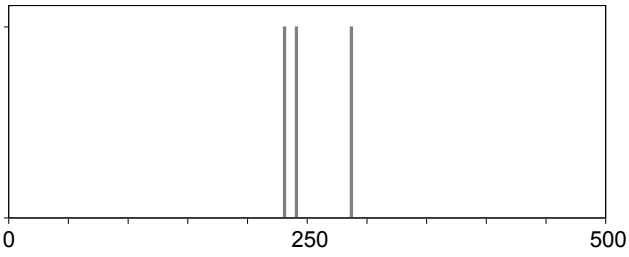

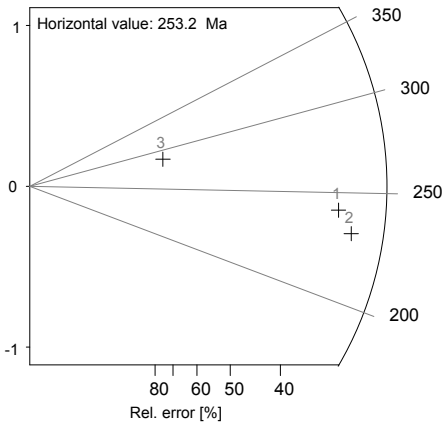

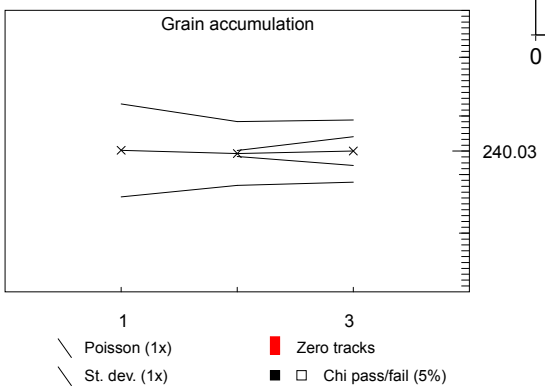

9.2.2 Sierras Australes

ARG17.zir --- TRACKKEY 4.2.g --- *counted: 13 Aug. 12 printed: 13 Aug. 12*

Zircon | Argentina | Tunas (permian) | SK
ARG 17 | Sandstone | Leitz

Cryst.:	***Area:***	
17	5314	
Ns:	***RhoS:***	
896	168.618	
Ni:	***RhoI:***	
166	31.239	
Pooled:	5.398	229.0 ± 22.5
Mean:	5.399	229.1 ± 6.3
Central:	5.398	229.0 ± 22.5
Weigh.I:	5.291	224.6
Weigh.II:	5.40	229.1

Chi-sq.: 1.27 ***P (%):*** 100.0

Dispersion: 0.00

a: 19.197 ***b:*** 4.789 ***r:*** 0.98

Irr.: ZirkARG ***Glass:*** CN_1

Nd: 15128 ***RhoD:*** 7.024

Zeta: 123 ± 6.08 ***U.:*** 175.25 (± 53 %)

Goodness: n. d.

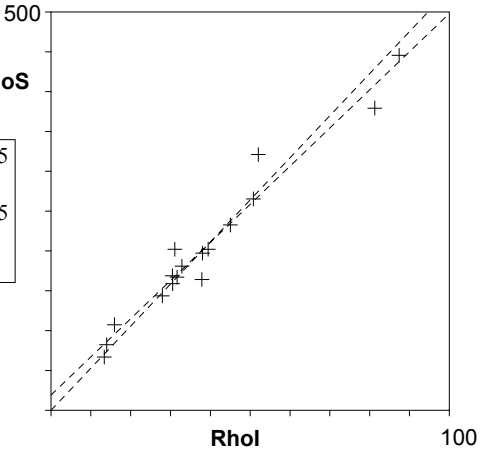

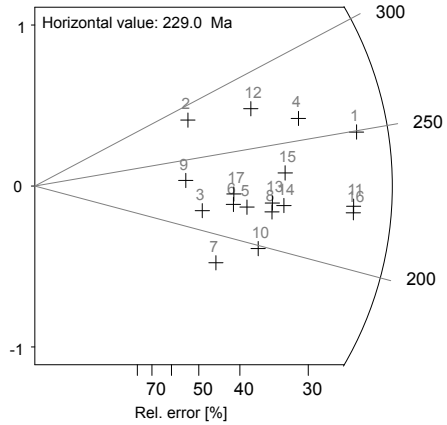

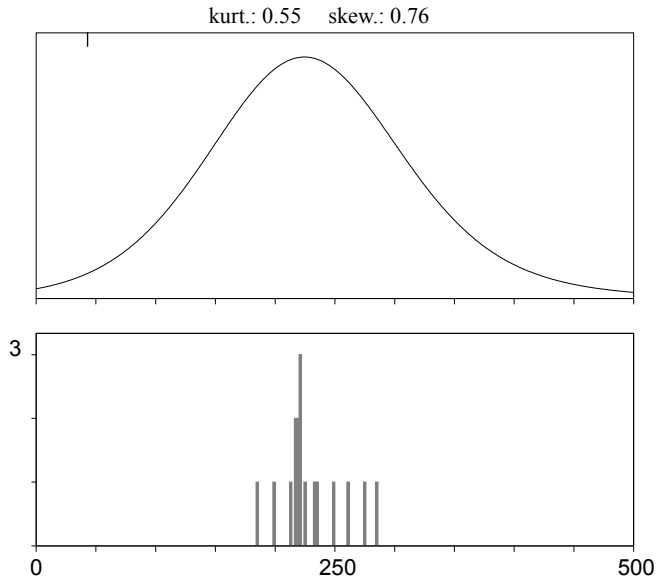

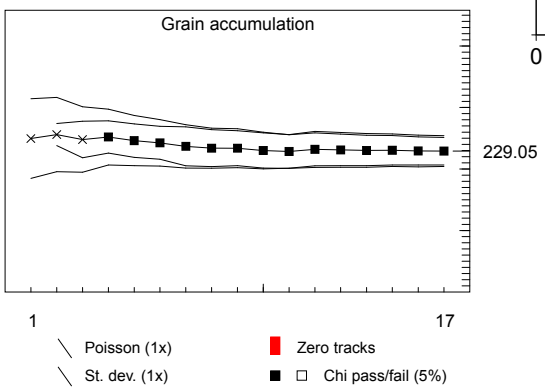

9.3 URUGUAY - DATA SHEETS AFT

12-06.apa --- TRACKKEY 4.2.g --- *counted: 12 Mrz. 14 printed: 12 Mrz. 14*

Apatite U12-06 SK Leitz

Cryst.: ***Area:***
20 40053
Ns: ***RhoS:***
1012 25.267
Ni: ***Rhol:***
730 18.226

Pooled:	1.386	325.7 ± 24.8
Mean:	1.395	327.7 ± 5.1
Central:	1.386	325.7 ± 24.8
Weigh.I:	1.393	327.3
Weigh.II:	1.39	327.1

Chi-sq.: 1.78 ***P (%):*** 100.0
Dispersion: 0.00
a: 0.342 ***b:*** 1.381 ***r:*** 0.98
Irr.: UruApati ***Glass:*** CN_5
Nd: 10042 ***RhoD:*** 14.307
Zeta: 336.83 ± 19.51 ***U.:*** 15.05 (± 40 %)
Goodness: n. d.

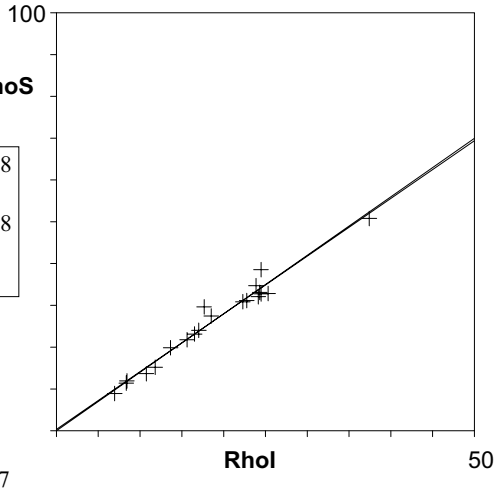

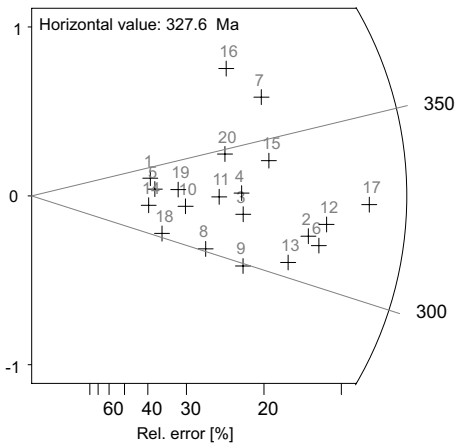

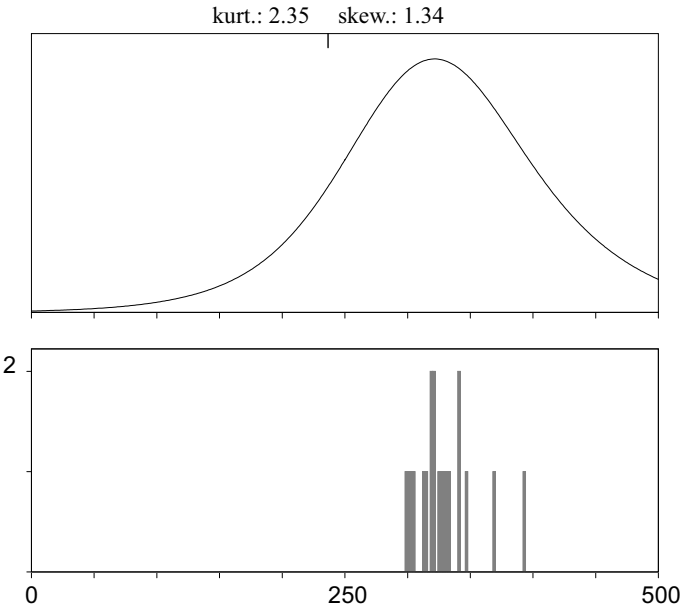

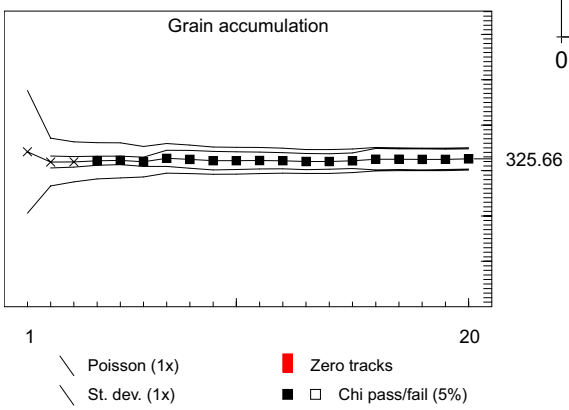

12-10.apa --- TRACKKEY 4.2.g --- *counted: 12 Mrz. 14 printed: 12 Mrz. 14*

Apatite

SK
Leitz

U 12-10

Cryst.:	***Area:***	
18	22643	
Ns:	***RhoS:***	
314	13.868	
Ni:	***RhoI:***	
374	16.517	
Pooled:	0.84	200.2 ± 19.3
Mean:	0.808	192.7 ± 4.7
Central:	0.84	200.2 ± 19.3
Weigh.I:	0.841	200.6
Weigh.II:	0.83	196.9

Chi-sq.: 1.44 ***P (%):*** 100.0

Dispersion: 0.00

a: -1.15 ***b:*** 0.882 ***r:*** 0.98

Irr.: UruApati ***Glass:*** CN_5

Nd: 10042 ***RhoD:*** 14.381

Zeta: 336.83 ± 19.51 ***U.:*** 14.92 (± 56 %)

Goodness: n. d.

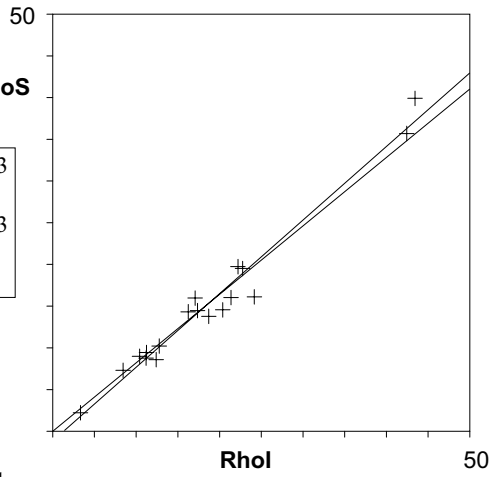

kurt.: -1.06 skew.: -0.38

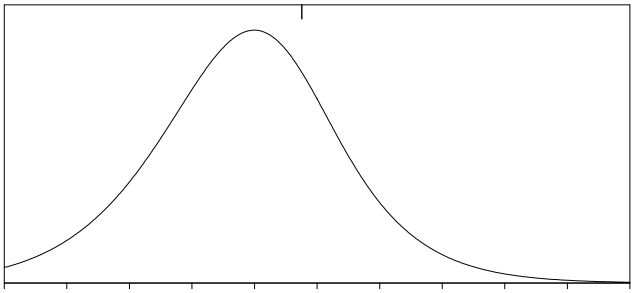

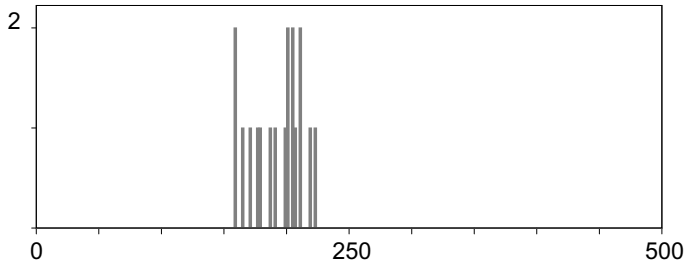

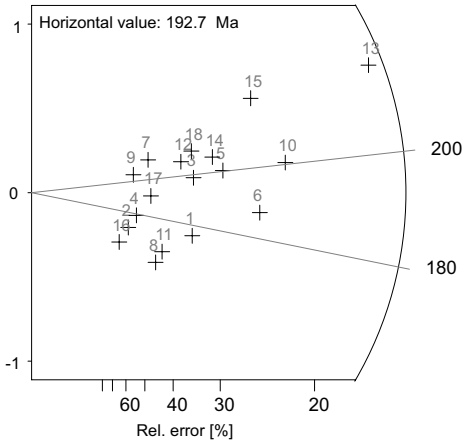

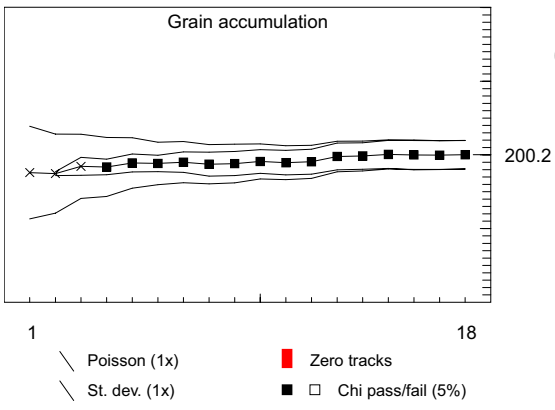

12-11.apa --- TRACKKEY 4.2.g --- *counted: 12 Mrz. 14 printed: 12 Mrz. 14*

Apatite U12-11 SK Leitz

Cryst.:	***Area:***	
20	18961	
Ns:	***RhoS:***	
1032	54.429	
Ni:	***RhoI:***	
823	43.406	
Pooled:	1.254	298.3 ± 22.4
Mean:	1.246	296.3 ± 5.3
Central:	1.254	298.3 ± 22.4
Weigh.I:	1.249	297.1
Weigh.II:	1.25	297.5

Chi-sq.: 2.95 ***P (%):*** 100.0

Dispersion: 0.00

a: 2.185 ***b:*** 1.196 ***r:*** 0.97

Irr.: UruApati ***Glass:*** CN_5

Nd: 10042 ***RhoD:*** 14.455

Zeta: 336.83 ± 19.51 ***U.:*** 36.69 (± 34 %)

Goodness: n. d.

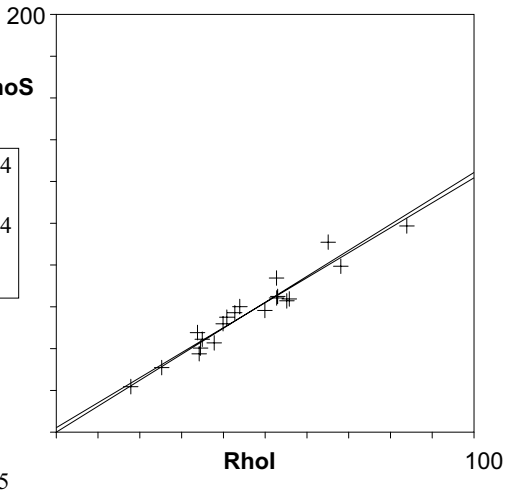

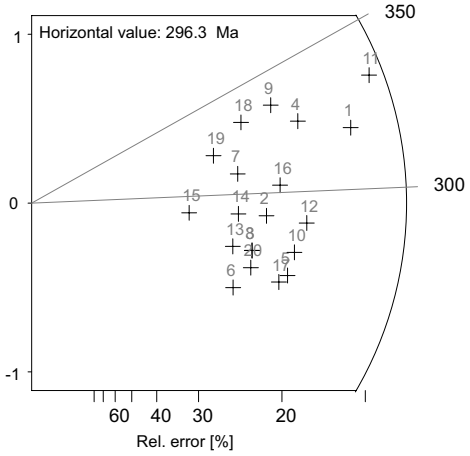

kurt.: -1.27 skew.: 0.36

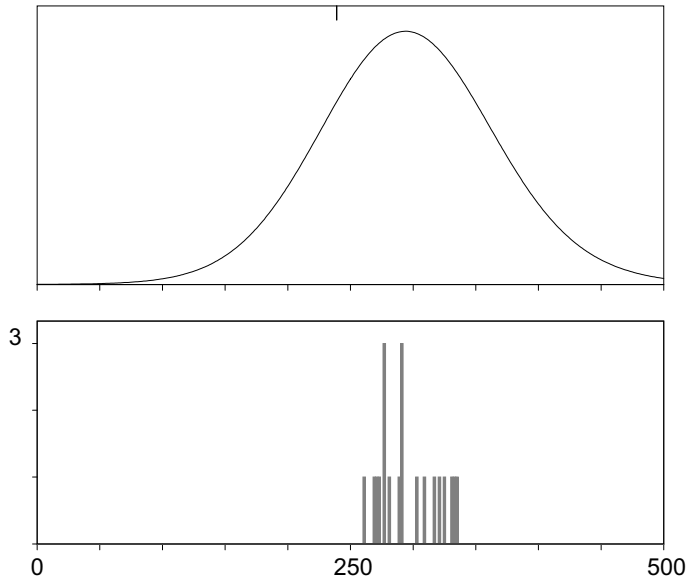

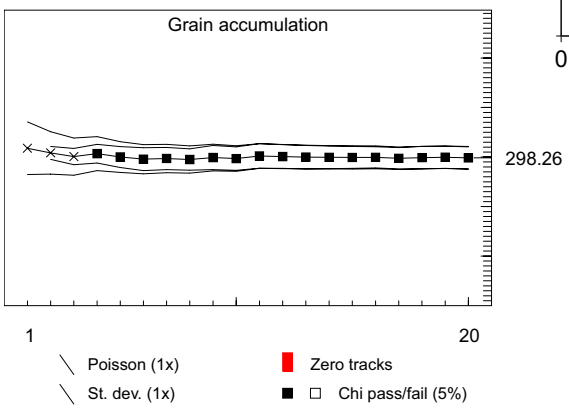

12-37.apa --- TRACKKEY 4.2.g --- *counted: 12 Mrz. 14 printed: 12 Mrz. 14*

Apatite

Kollenz
Leitz

U12-37

Cryst.:	***Area:***
19	28931
Ns:	***RhoS:***
645	22.294
Ni:	***RhoI:***
657	22.709

Pooled:	0.982	238.2 ± 19.2
Mean:	1.014	245.8 ± 12.5
Central:	0.984	238.8 ± 20.3
Weigh.I:	1.009	244.7
Weigh.II:	1.01	245.7

Chi-sq.: 19.08 ***P (%):*** 38.69

Dispersion: 0.11

a: 0.959 ***b:*** 0.966 ***r:*** 0.82

Irr.: UruApati ***Glass:*** CN_5

Nd: 10042 ***RhoD:*** 14.677

Zeta: 336.83 ± 19.51 ***U.:*** 19.19 (± 31 %)

Goodness: n. d.

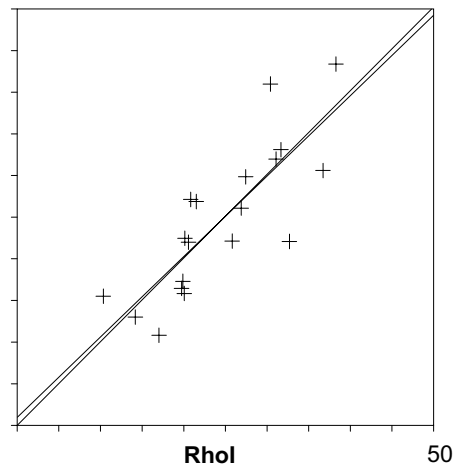

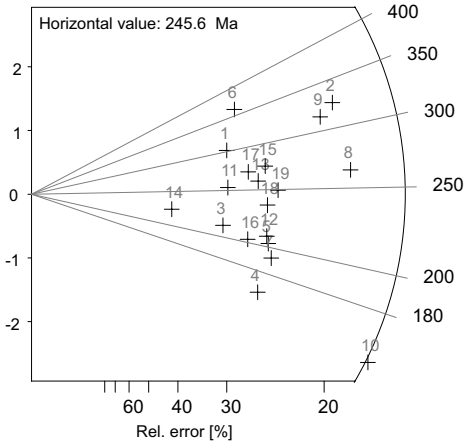

kurt.: -0.31 skew.: 0.32

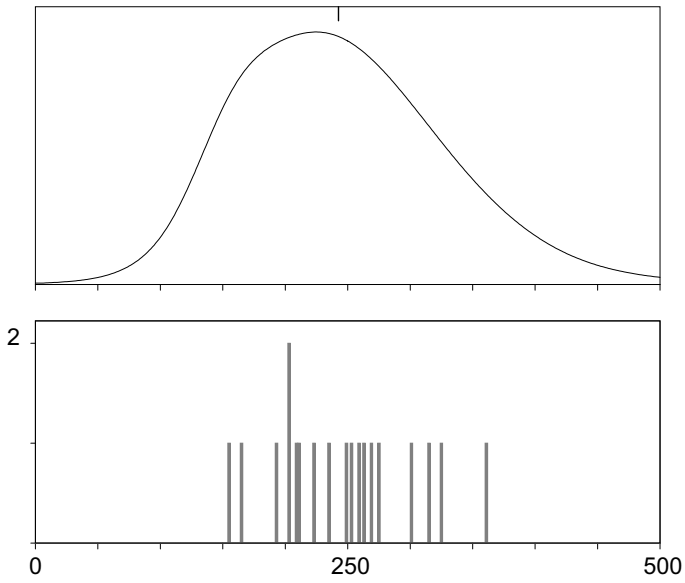

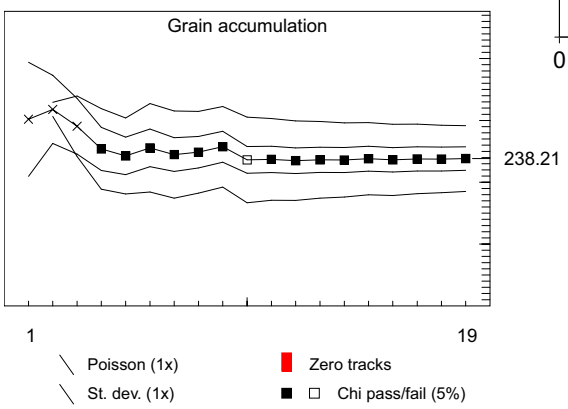

12-42.apa --- TRACKKEY 4.2.g --- *counted: 12 Mrz. 14 printed: 12 Mrz. 14*

Apatite

Uruguay
U12-42 Leitz

Cryst.:	***Area:***
11	14096
Ns:	***RhoS:***
192	13.621
Ni:	***RhoI:***
214	15.181

Pooled:	0.897	219.1 ± 25.3
Mean:	0.843	206.0 ± 9.7
Central:	0.897	219.1 ± 25.3
Weigh.I:	0.897	219.1
Weigh.II:	0.87	213.4

Chi-sq.: 1.8 ***P (%):*** 99.76

Dispersion: 0.00

a: -2.624 ***b:*** 1.043 ***r:*** 0.98

Irr.: UruApati ***Glass:*** CN_5

Nd: 10042 ***RhoD:*** 14.751

Zeta: 336.83 ± 19.51 ***U.:*** 11.36 (± 45 %)

Goodness: n. d.

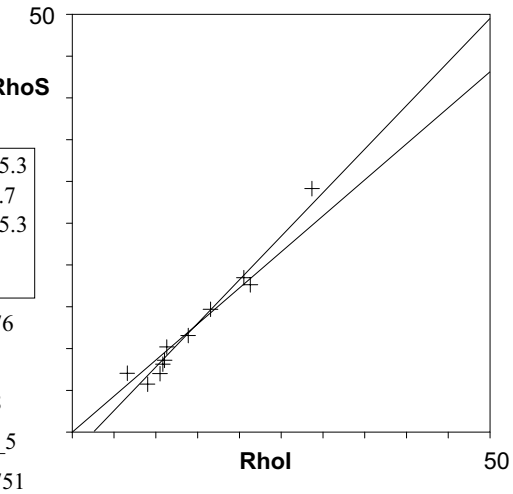

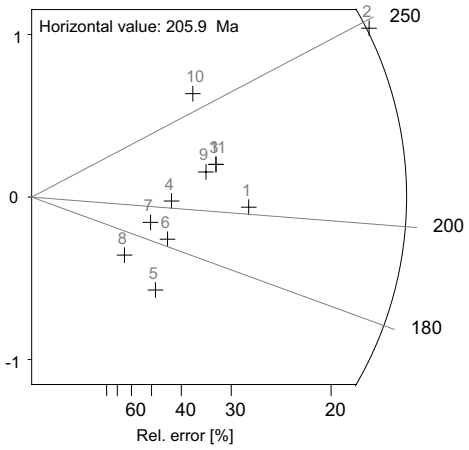

kurt.: -0.38 skew.: 0.11

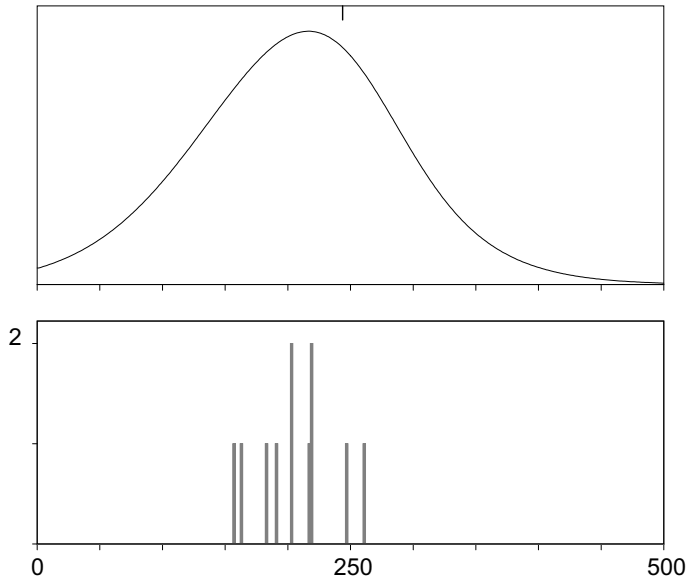

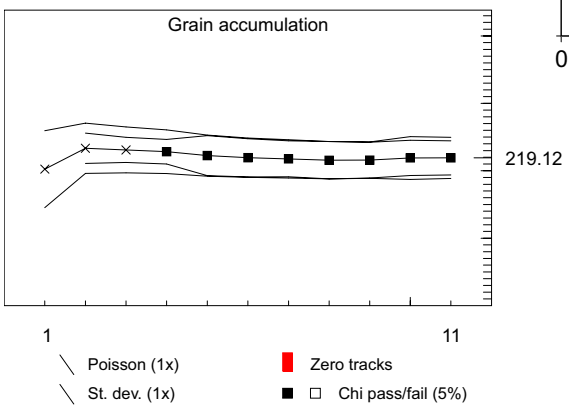

12-43.apa --- TRACKKEY 4.2.g --- *counted: 12 Mrz. 14 printed: 12 Mrz. 14*

Apatite

Kollenz
Leitz

Cryst.:	***Area:***	
16	19701	
Ns:	***RhoS:***	
314	15.938	
Ni:	***RhoI:***	
314	15.939	
Pooled:	1.0	245.0 ± 24.3
Mean:	0.988	242.1 ± 4.2
Central:	1.0	245.0 ± 24.3
Weigh.I:	1.002	245.5
Weigh.II:	1.00	243.9

Chi-sq.: 0.59 ***P (%):*** 100.0

Dispersion: 0.00

a: -1.249 ***b:*** 1.07 ***r:*** 0.99

Irr.: UruApati ***Glass:*** CN_5

Nd: 10042 ***RhoD:*** 14.825

Zeta: 336.83 ± 19.51 ***U.:*** 13.07 (± 37 %)

Goodness: n. d.

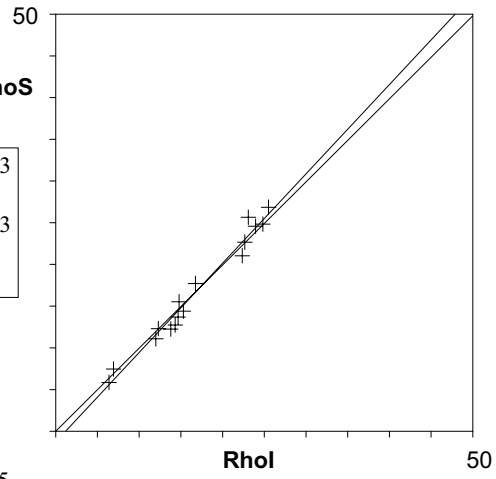

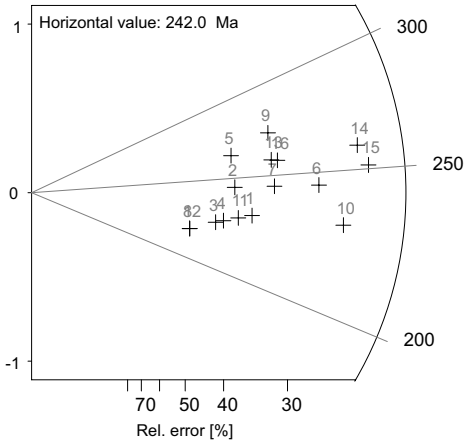

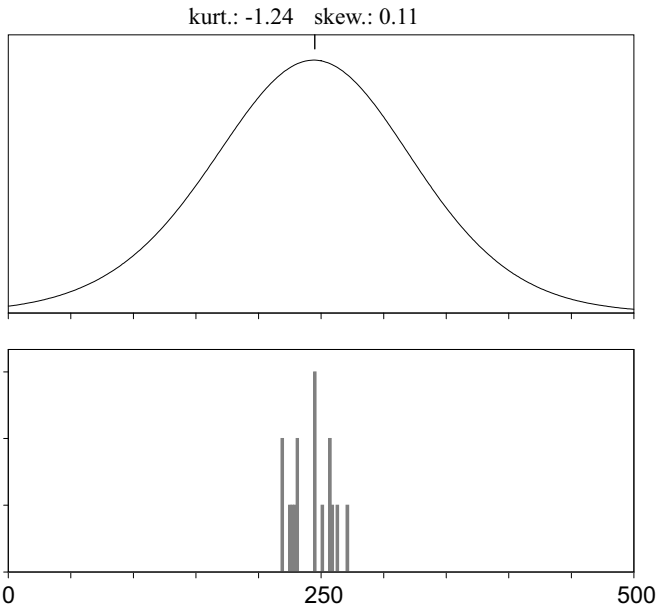

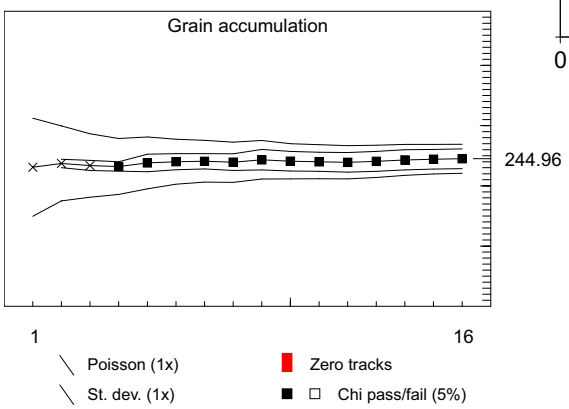

12-47.apa --- TRACKKEY 4.2.g --- *counted: 12 Mrz. 14 printed: 12 Mrz. 14*

Apatite

U12-47

Kollenz
Leitz

Cryst.:	Area:
2	4542
Ns:	**RhoS:**
59	12.99
Ni:	**RhoI:**
64	14.091

Pooled:	0.922	227.3 ± 43.1
Mean:	0.88	217.0 ± 0.0
Central:	0.922	227.3 ± 43.1
Weigh.I:	0.941	232.0
Weigh.II:	0.90	223.0

Chi-sq.: 0.17 **P (%):** 67.83

Dispersion: 0.00

a: -1.236 **b:** 1.01 **r:** 1.0

Irr.: UruApati **Glass:** CN_5

Nd: 10042 **RhoD:** 14.899

Zeta: 336.83 ± 19.51 **U.:** 11.74 (± 87 %)

Goodness: n. d.

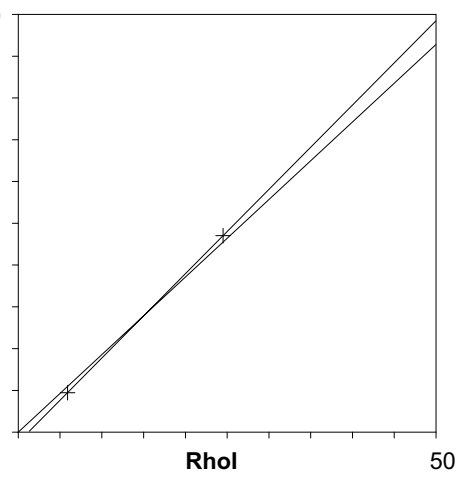

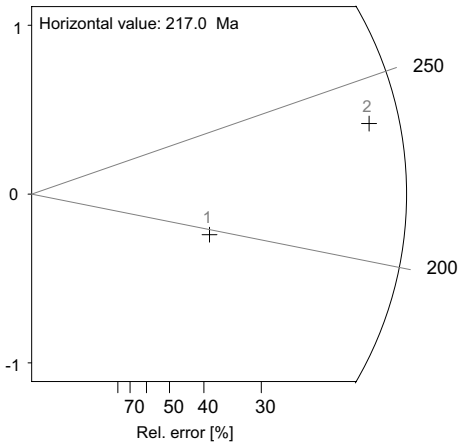

kurt.: -1.24 skew.: 0.11

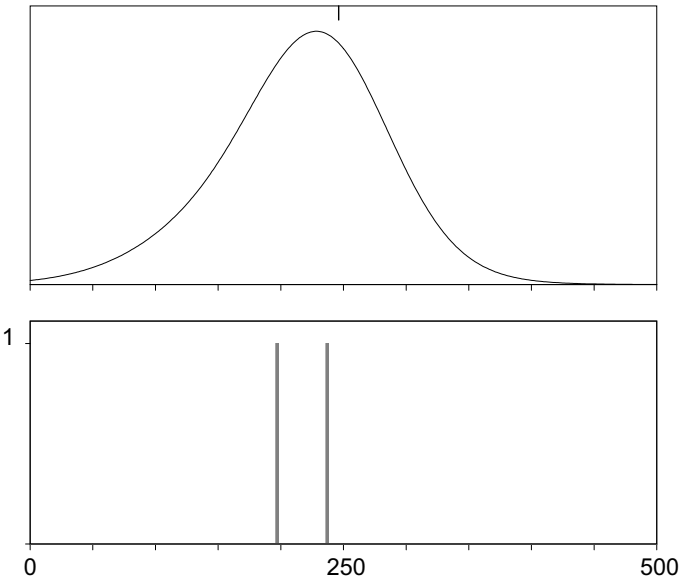

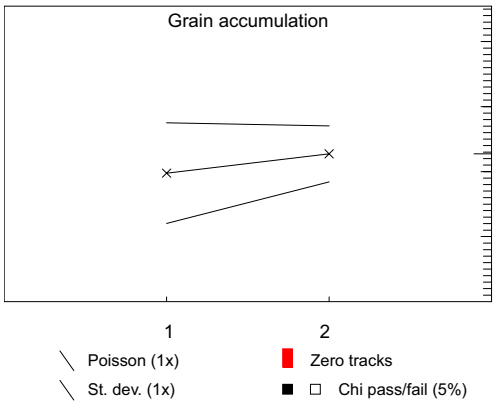

9.4 t-T models - Argentina

9.4.1 Sierras Septentrionales

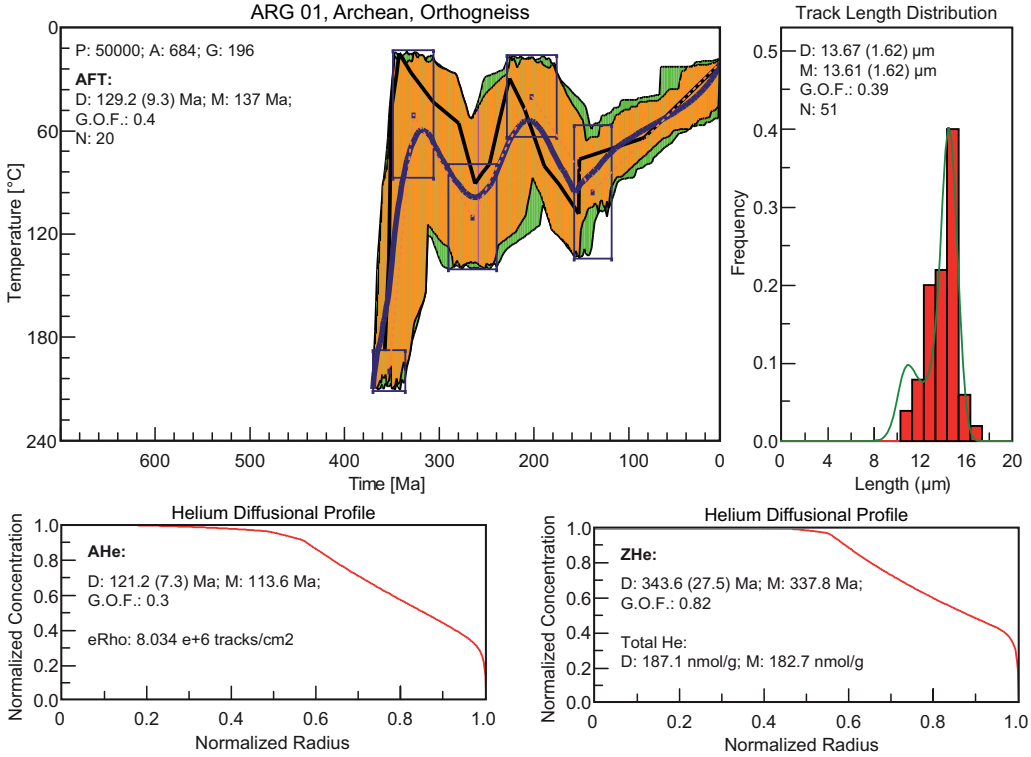

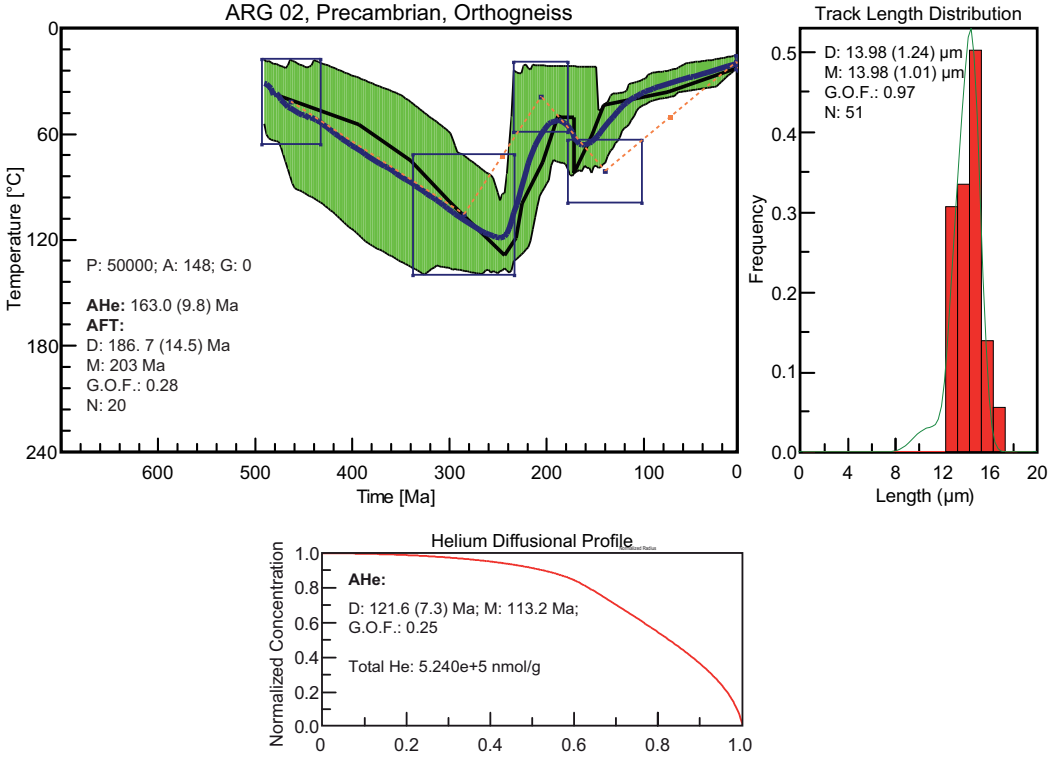

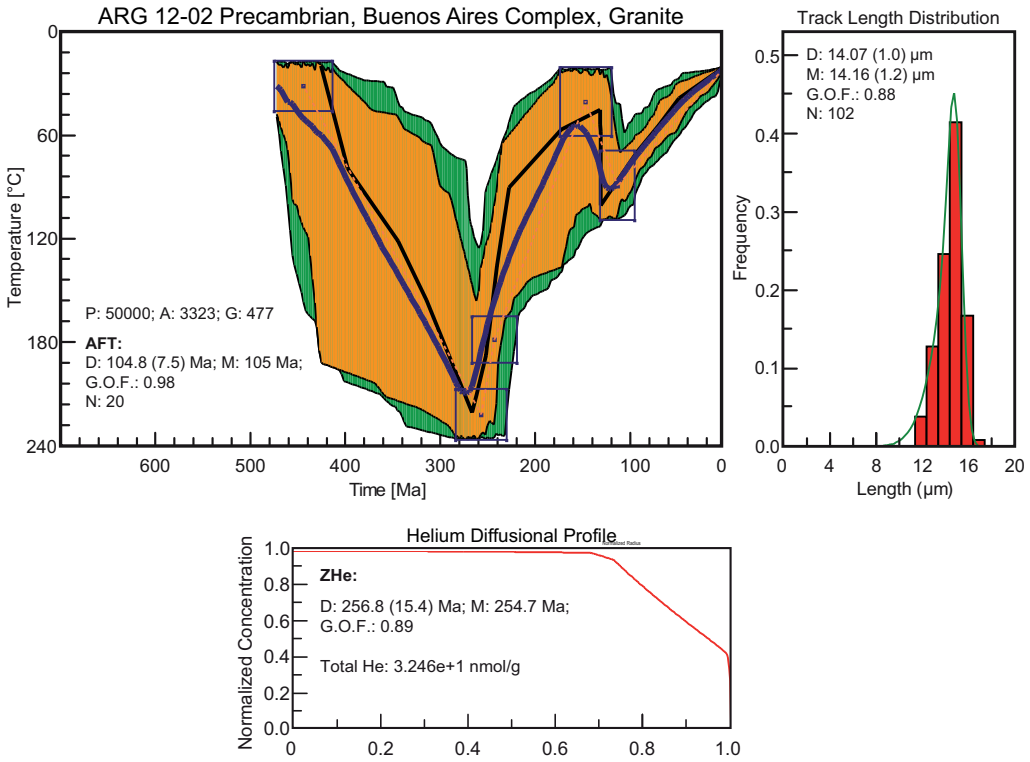
ARG 12-02 Precambrian, Buenos Aires Complex, Granite
Temperature [°C]
Time [Ma]
P: 50000; A: 3323; G: 477
AFT:
D: 104.8 (7.5) Ma; M: 105 Ma;
G.O.F.: 0.98
N: 20
Track Length Distribution
D: 14.07 (1.0) µm
M: 14.16 (1.2) µm
G.O.F.: 0.88
N: 102
Frequency
Length (µm)
Helium Diffusional Profile
Normalized Concentration
ZHe:
D: 256.8 (15.4) Ma; M: 254.7 Ma;
G.O.F.: 0.89
Total He: 3.246e+1 nmol/g

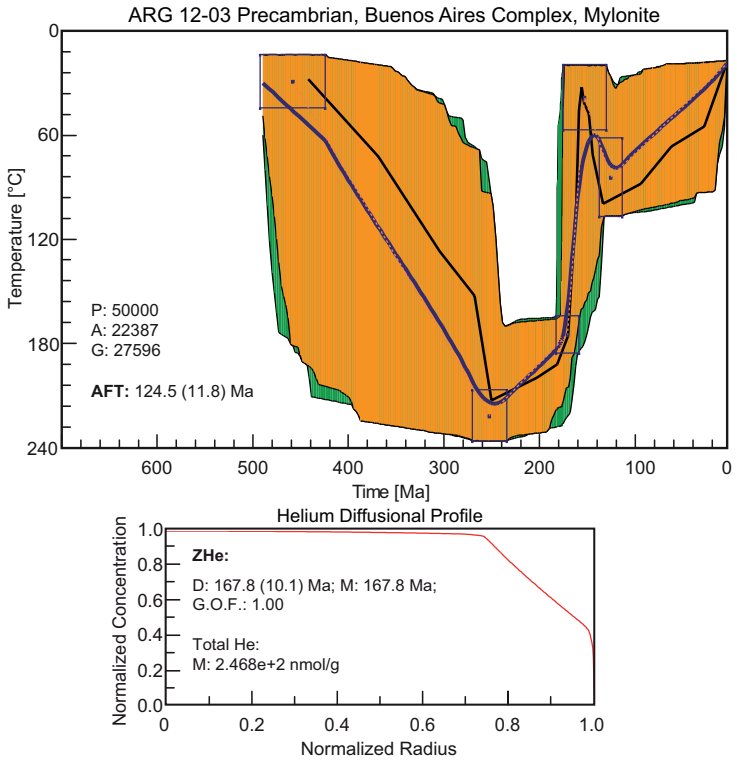
ARG 12-03 Precambrian, Buenos Aires Complex, Mylonite
Temperature [°C]
Time [Ma]
P: 50000
A: 22387
G: 27596
AFT: 124.5 (11.8) Ma
Helium Diffusional Profile
Normalized Concentration
ZHe:
D: 167.8 (10.1) Ma; M: 167.8 Ma;
G.O.F.: 1.00
Total He:
M: 2.468e+2 nmol/g
Normalized Radius

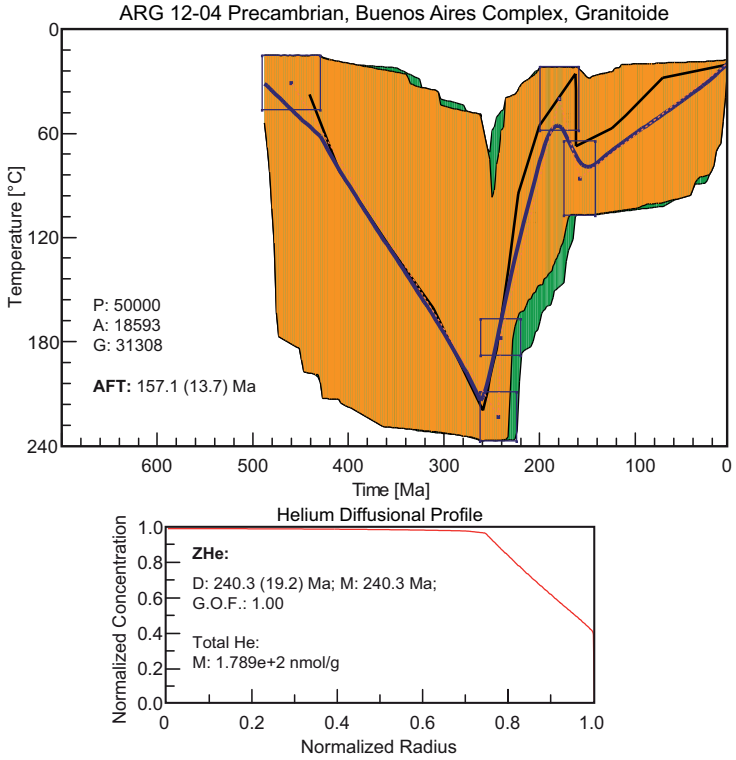
ARG 12-04 Precambrian, Buenos Aires Complex, Granitoide
Temperature [°C]
0
60
120
180
240
600
500
400
300
200
100
0
Time [Ma]
P: 50000
A: 18593
G: 31308
AFT: 157.1 (13.7) Ma
Helium Diffusional Profile
Normalized Concentration
1.0
0.8
0.6
0.4
0.2
0.0
0
0.2
0.4
0.6
0.8
1.0
Normalized Radius
ZHe:
D: 240.3 (19.2) Ma; M: 240.3 Ma;
G.O.F.: 1.00
Total He:
M: 1.789e+2 nmol/g

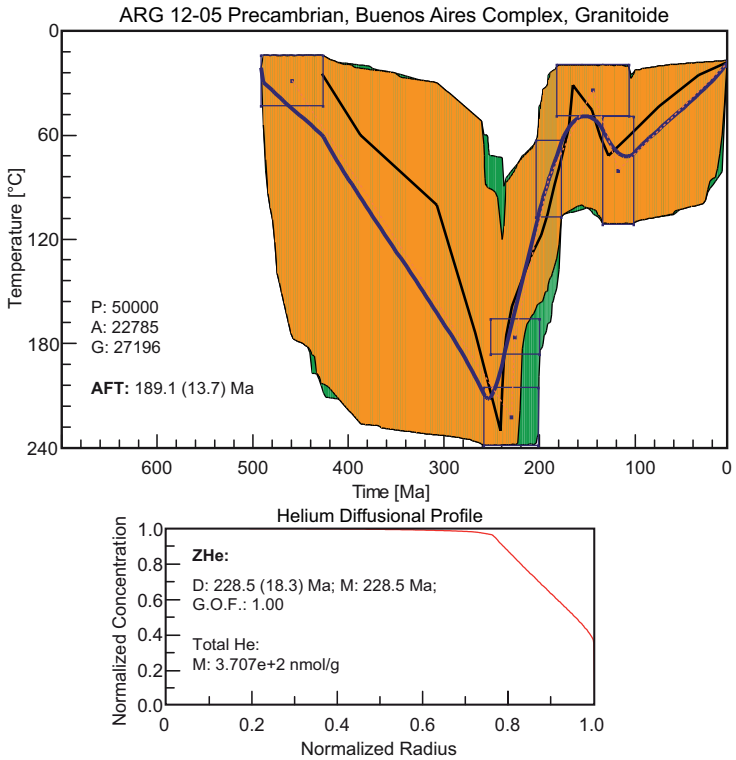
ARG 12-05 Precambrian, Buenos Aires Complex, Granitoide
Temperature [°C]
0
60
120
180
240
600
500
400
300
200
100
0
Time [Ma]
P: 50000
A: 22785
G: 27196
AFT: 189.1 (13.7) Ma
Helium Diffusional Profile
Normalized Concentration
1.0
0.8
0.6
0.4
0.2
0.0
0
0.2
0.4
0.6
0.8
1.0
Normalized Radius
ZHe:
D: 228.5 (18.3) Ma; M: 228.5 Ma;
G.O.F.: 1.00
Total He:
M: 3.707e+2 nmol/g

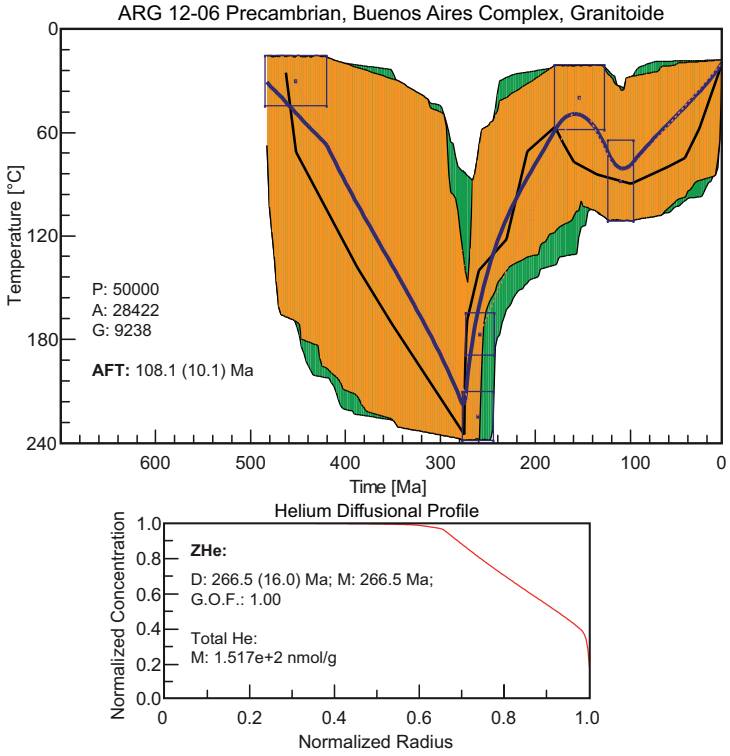
ARG 12-06 Precambrian, Buenos Aires Complex, Granitoide
Temperature [°C]
Time [Ma]
P: 50000
A: 28422
G: 9238
AFT: 108.1 (10.1) Ma
Helium Diffusional Profile
Normalized Concentration
Normalized Radius
ZHe:
D: 266.5 (16.0) Ma; M: 266.5 Ma;
G.O.F.: 1.00
Total He:
M: 1.517e+2 nmol/g

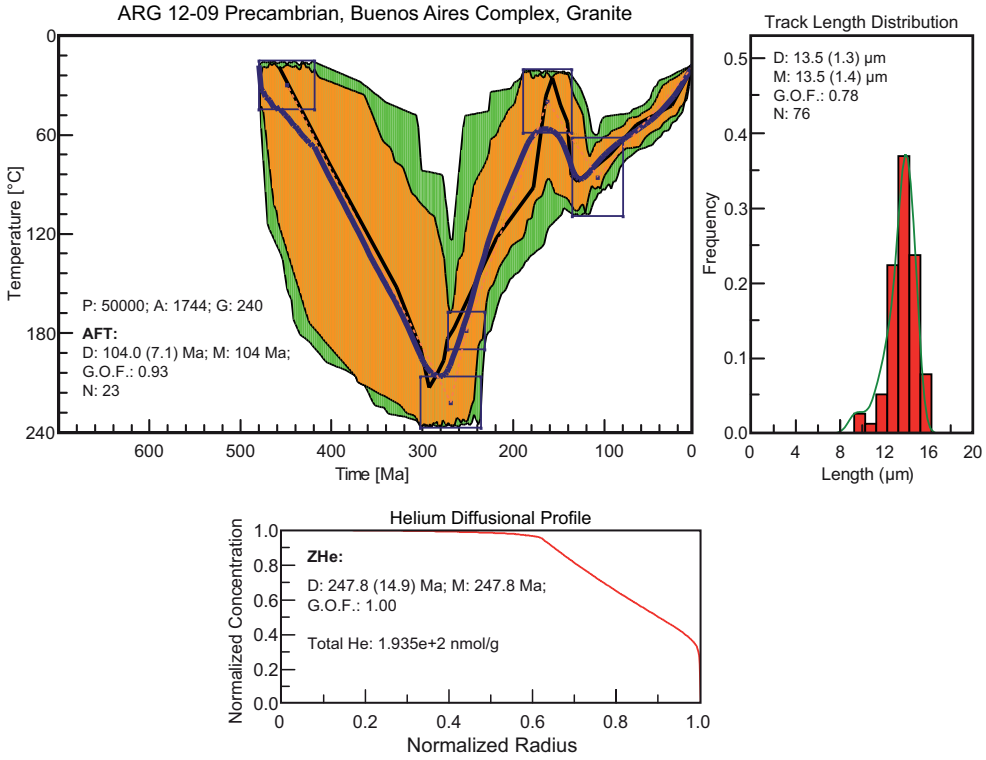
ARG 12-09 Precambrian, Buenos Aires Complex, Granite
Temperature [°C]
Time [Ma]
P: 50000; A: 1744; G: 240
AFT:
D: 104.0 (7.1) Ma; M: 104 Ma;
G.O.F.: 0.93
N: 23
Track Length Distribution
Frequency
Length (µm)
D: 13.5 (1.3) µm
M: 13.5 (1.4) µm
G.O.F.: 0.78
N: 76
Helium Diffusional Profile
Normalized Concentration
Normalized Radius
ZHe:
D: 247.8 (14.9) Ma; M: 247.8 Ma;
G.O.F.: 1.00
Total He: 1.935e+2 nmol/g

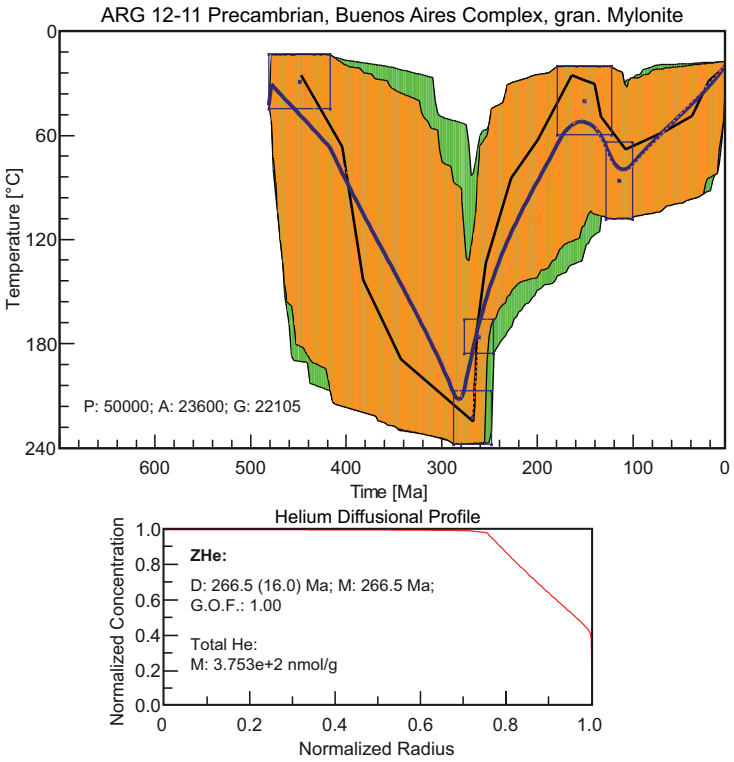
ARG 12-11 Precambrian, Buenos Aires Complex, gran. Mylonite
Temperature [°C]
Time [Ma]
P: 50000; A: 23600; G: 22105
Helium Diffusional Profile
Normalized Concentration
Normalized Radius
ZHe:
D: 266.5 (16.0) Ma; M: 266.5 Ma;
G.O.F.: 1.00
Total He:
M: 3.753e+2 nmol/g

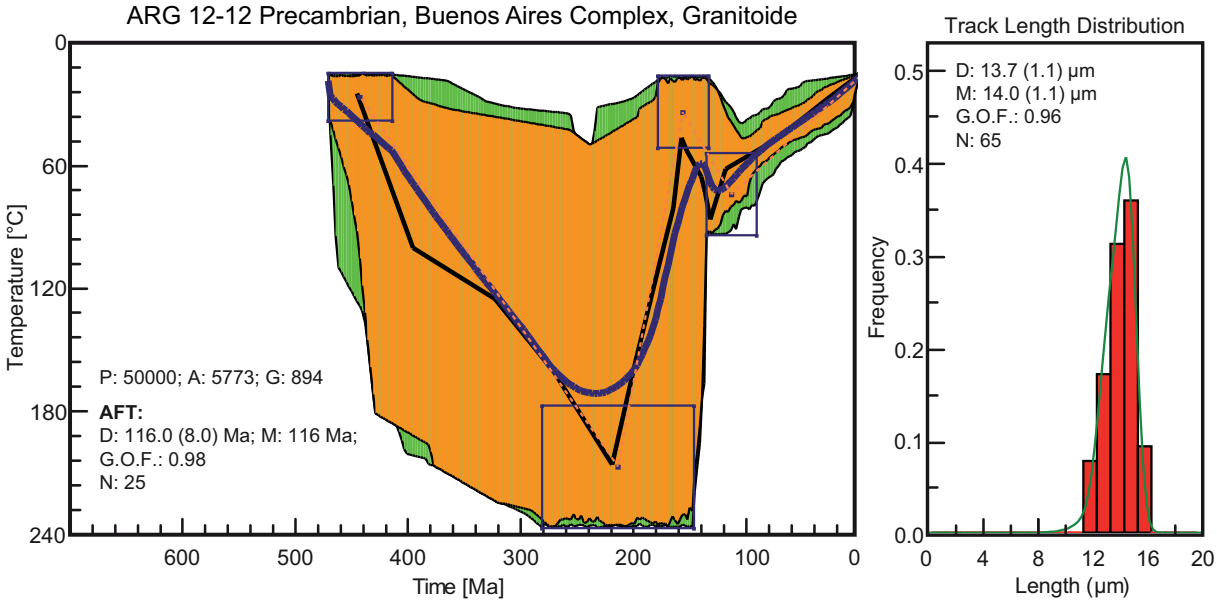
ARG 12-12 Precambrian, Buenos Aires Complex, Granitoide
Temperature [°C]
Time [Ma]
P: 50000; A: 5773; G: 894
AFT:
D: 116.0 (8.0) Ma; M: 116 Ma;
G.O.F.: 0.98
N: 25
Track Length Distribution
Frequency
Length (µm)
D: 13.7 (1.1) µm
M: 14.0 (1.1) µm
G.O.F.: 0.96
N: 65

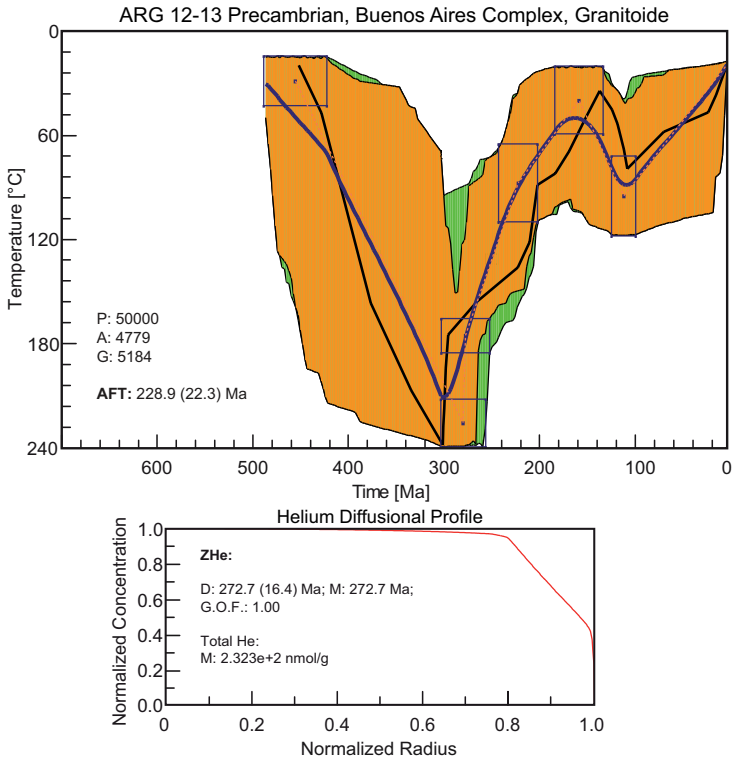
ARG 12-13 Precambrian, Buenos Aires Complex, Granitoide
Temperature [°C]
Time [Ma]
P: 50000
A: 4779
G: 5184
AFT: 228.9 (22.3) Ma
Helium Diffusional Profile
Normalized Concentration
Normalized Radius
ZHe:
D: 272.7 (16.4) Ma; M: 272.7 Ma;
G.O.F.: 1.00
Total He:
M: 2.323e+2 nmol/g

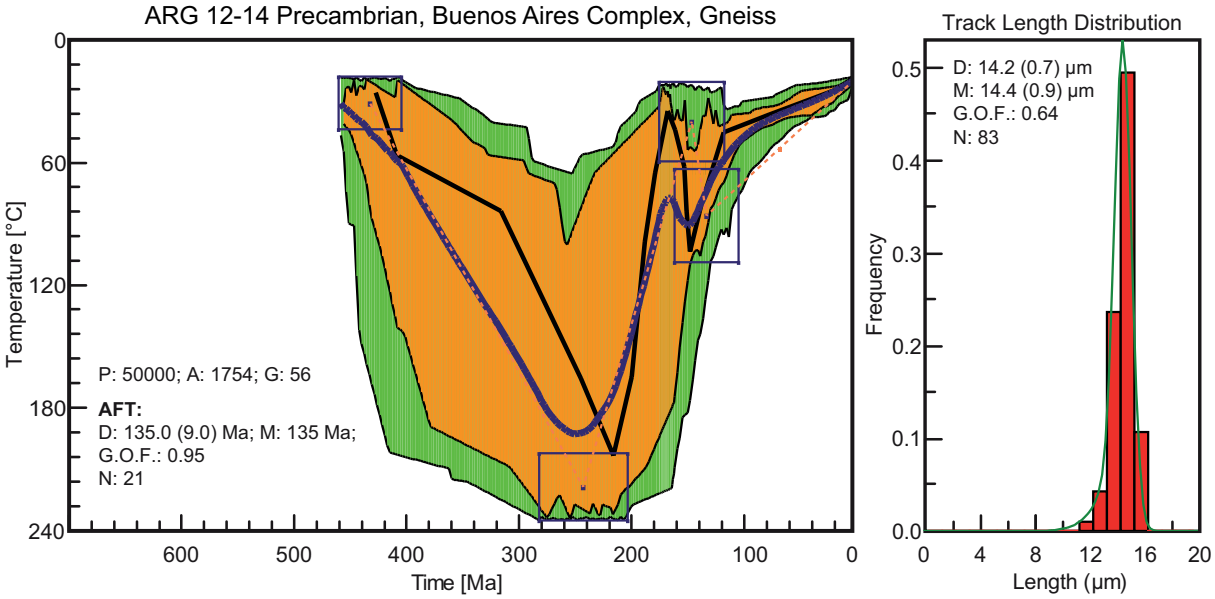
ARG 12-14 Precambrian, Buenos Aires Complex, Gneiss
Temperature [°C]
Time [Ma]
P: 50000; A: 1754; G: 56
AFT:
D: 135.0 (9.0) Ma; M: 135 Ma;
G.O.F.: 0.95
N: 21
Track Length Distribution
Frequency
Length (µm)
D: 14.2 (0.7) µm
M: 14.4 (0.9) µm
G.O.F.: 0.64
N: 83

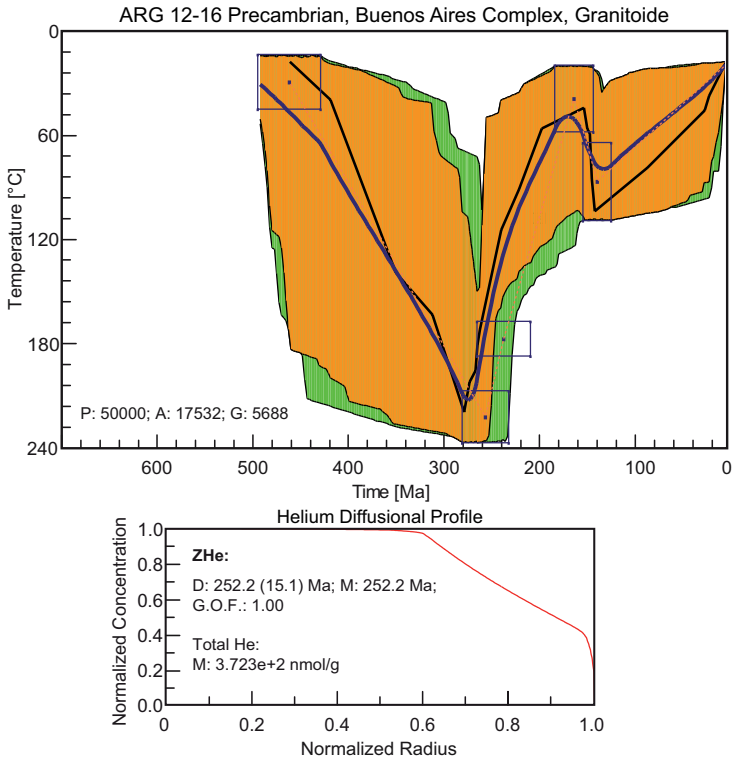
ARG 12-16 Precambrian, Buenos Aires Complex, Granitoide
Temperature [°C]
Time [Ma]
P: 50000; A: 17532; G: 5688
Helium Diffusional Profile
ZHe:
D: 252.2 (15.1) Ma; M: 252.2 Ma;
G.O.F.: 1.00
Total He:
M: 3.723e+2 nmol/g
Normalized Concentration
Normalized Radius

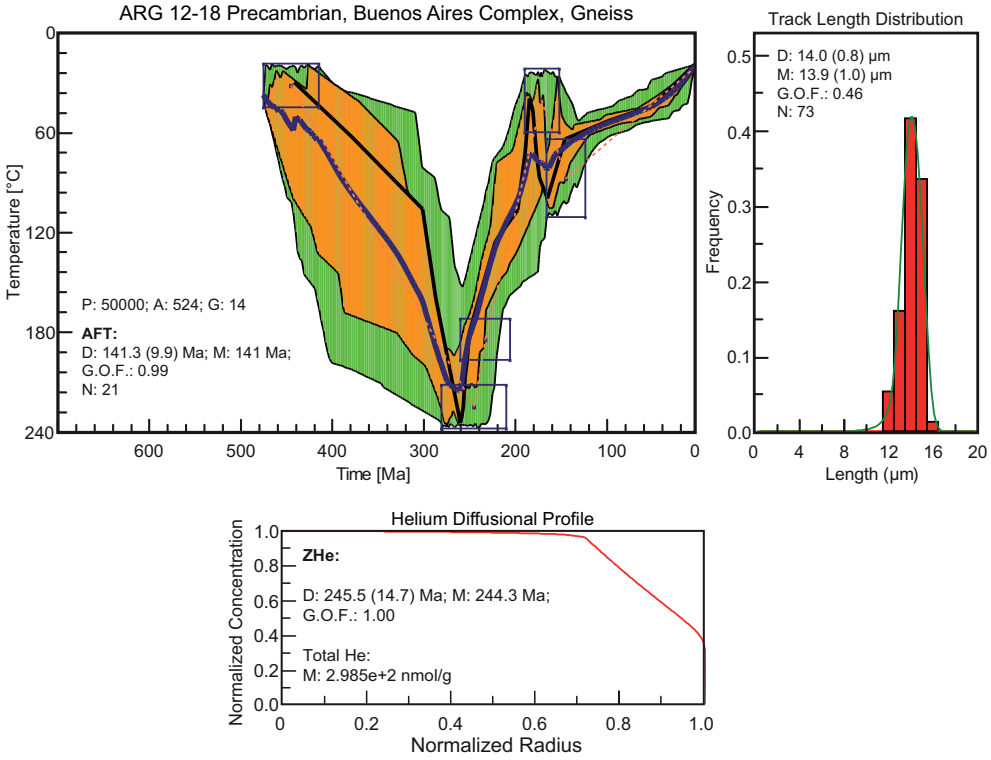
ARG 12-18 Precambrian, Buenos Aires Complex, Gneiss
Temperature [°C]
Time [Ma]
P: 50000; A: 524; G: 14
AFT:
D: 141.3 (9.9) Ma; M: 141 Ma;
G.O.F.: 0.99
N: 21
Track Length Distribution
D: 14.0 (0.8) µm
M: 13.9 (1.0) µm
G.O.F.: 0.46
N: 73
Frequency
Length (µm)
Helium Diffusional Profile
ZHe:
D: 245.5 (14.7) Ma; M: 244.3 Ma;
G.O.F.: 1.00
Total He:
M: 2.985e+2 nmol/g
Normalized Concentration
Normalized Radius

9.4.2 Sierras Australes - east of the SGW

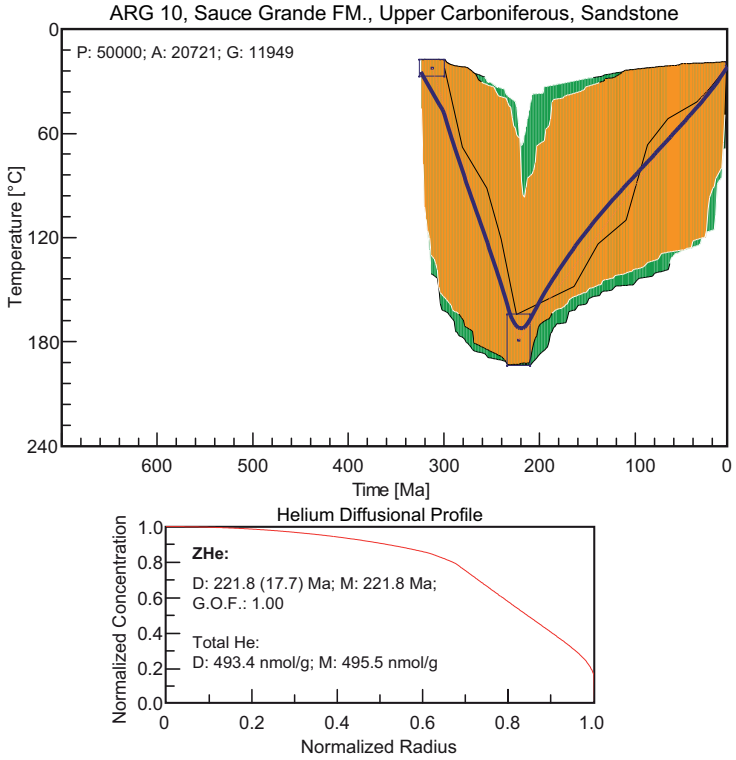

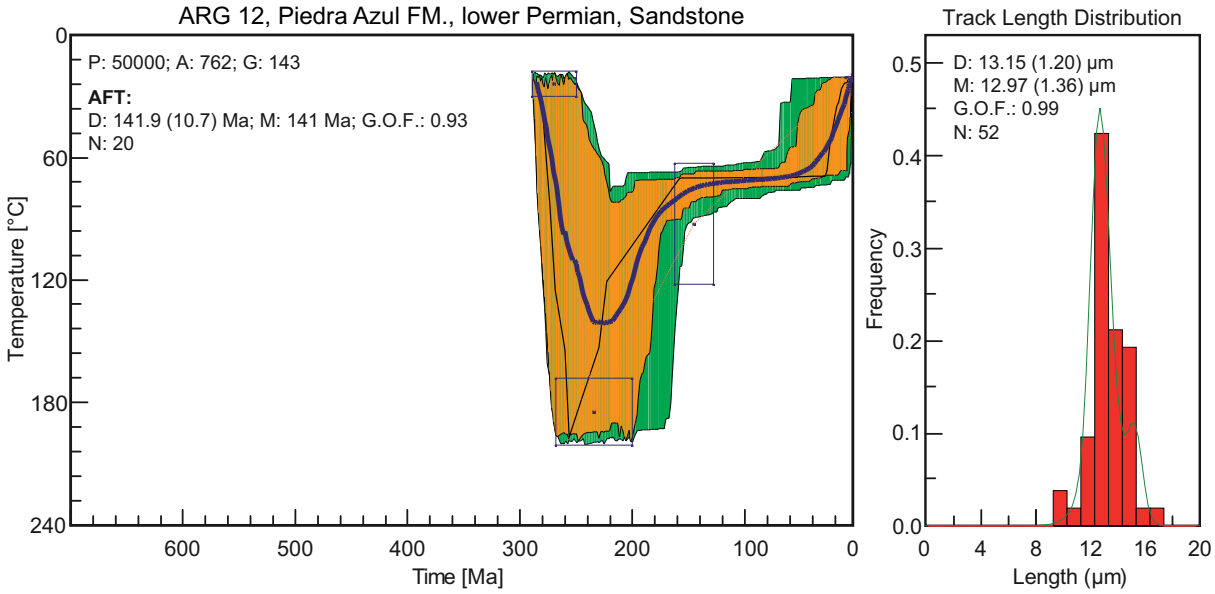

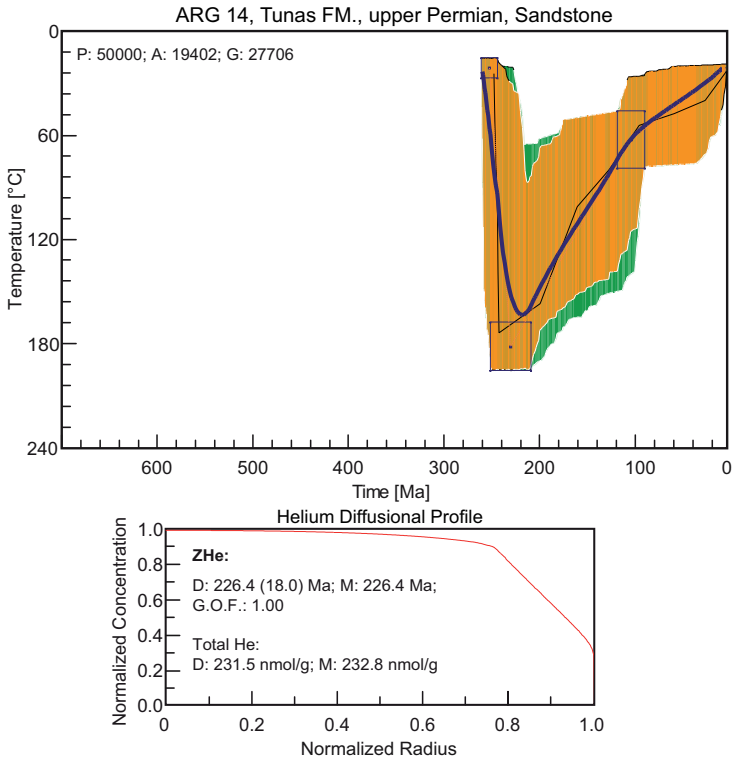
ARG 14, Tunas FM., upper Permian, Sandstone
P: 50000; A: 19402; G: 27706
Temperature [°C]
Time [Ma]
Helium Diffusional Profile
ZHe:
D: 226.4 (18.0) Ma; M: 226.4 Ma;
G.O.F.: 1.00
Total He:
D: 231.5 nmol/g; M: 232.8 nmol/g
Normalized Concentration
Normalized Radius

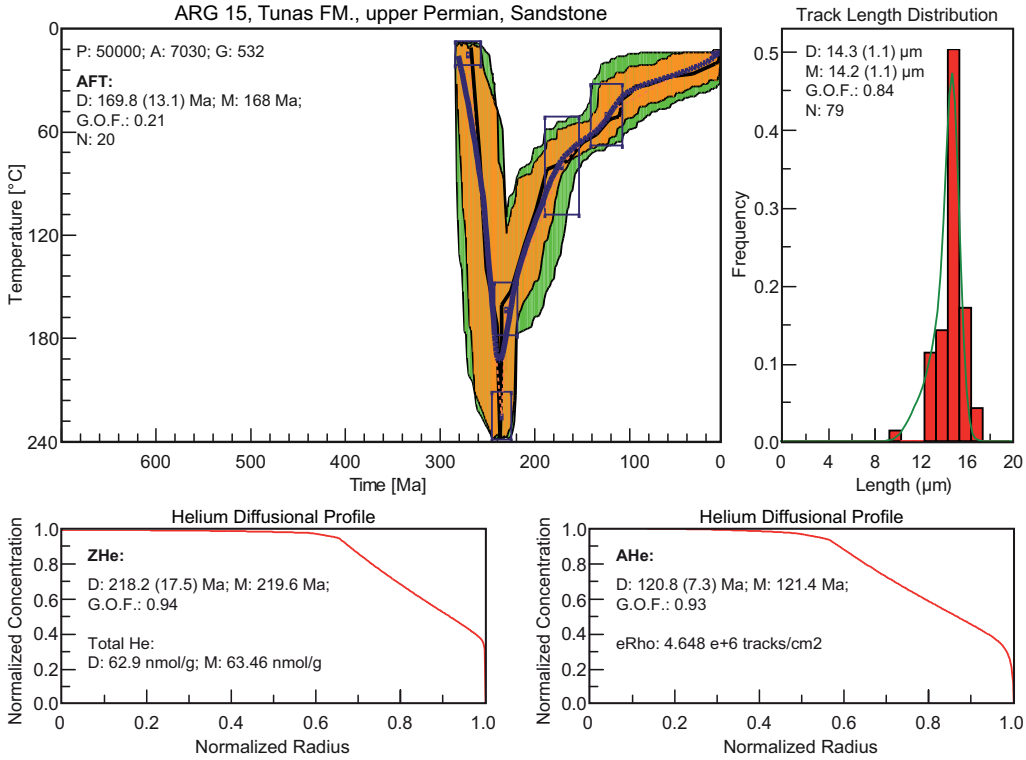
ARG 15, Tunas FM., upper Permian, Sandstone
P: 50000; A: 7030; G: 532
AFT:
D: 169.8 (13.1) Ma; M: 168 Ma;
G.O.F.: 0.21
N: 20
Temperature [°C]
Time [Ma]
Track Length Distribution
D: 14.3 (1.1) µm
M: 14.2 (1.1) µm
G.O.F.: 0.84
N: 79
Frequency
Length (µm)
Helium Diffusional Profile
ZHe:
D: 218.2 (17.5) Ma; M: 219.6 Ma;
G.O.F.: 0.94
Total He:
D: 62.9 nmol/g; M: 63.46 nmol/g
Normalized Concentration
Normalized Radius
Helium Diffusional Profile
AHe:
D: 120.8 (7.3) Ma; M: 121.4 Ma;
G.O.F.: 0.93
eRho: 4.648 e+6 tracks/cm2
Normalized Concentration
Normalized Radius

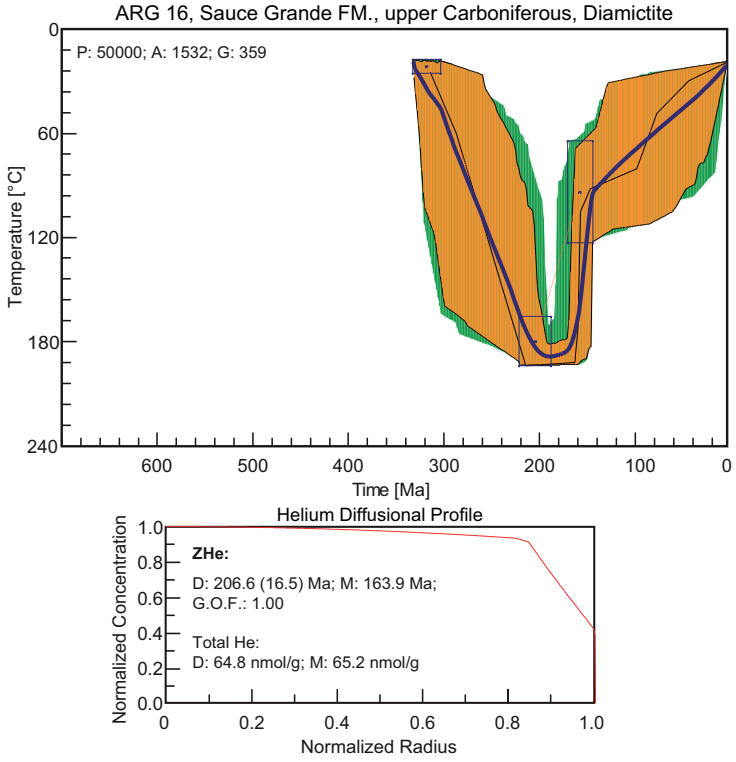
ARG 16, Sauce Grande FM., upper Carboniferous, Diamictite
P: 50000; A: 1532; G: 359
Temperature [°C]
Time [Ma]
Helium Diffusional Profile
ZHe:
D: 206.6 (16.5) Ma; M: 163.9 Ma;
G.O.F.: 1.00
Total He:
D: 64.8 nmol/g; M: 65.2 nmol/g
Normalized Concentration
Normalized Radius

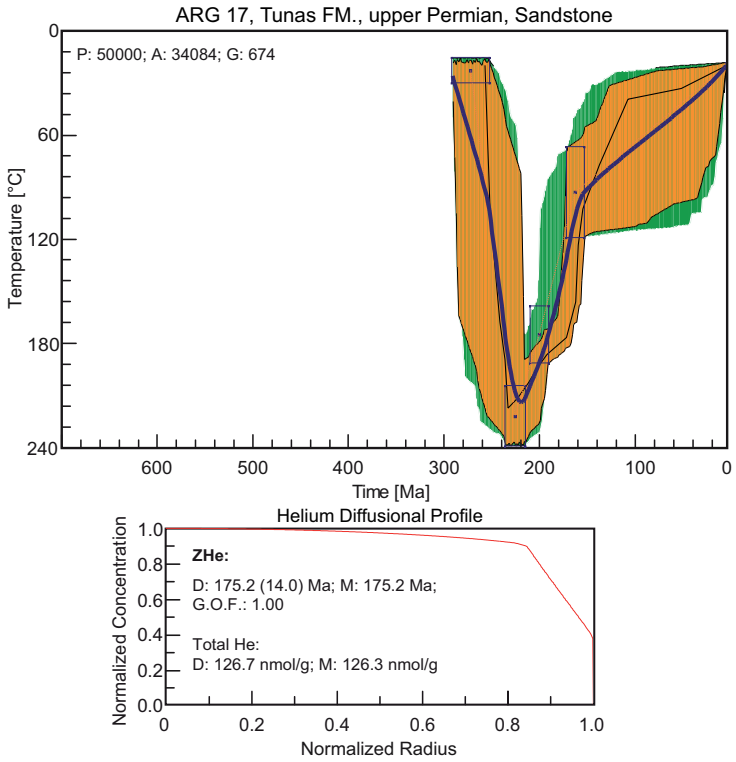
ARG 17, Tunas FM., upper Permian, Sandstone
P: 50000; A: 34084; G: 674
Temperature [°C]
Time [Ma]
Helium Diffusional Profile
ZHe:
D: 175.2 (14.0) Ma; M: 175.2 Ma;
G.O.F.: 1.00
Total He:
D: 126.7 nmol/g; M: 126.3 nmol/g
Normalized Concentration
Normalized Radius

9.4.3 Sierras Australes - west of the SGW

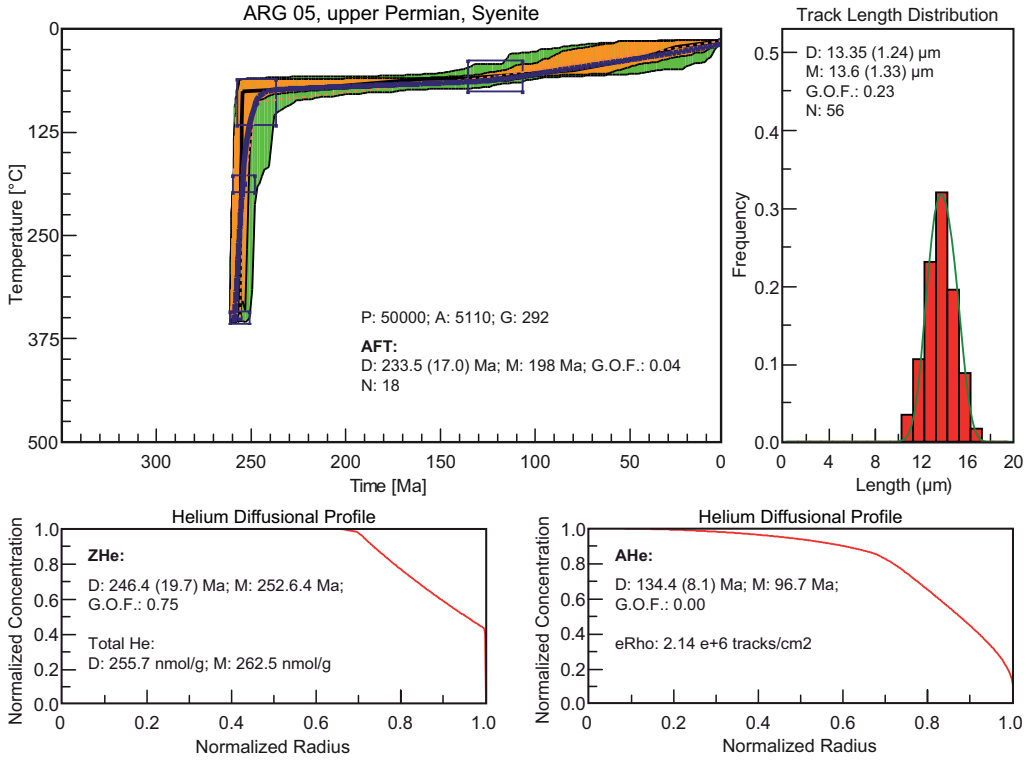

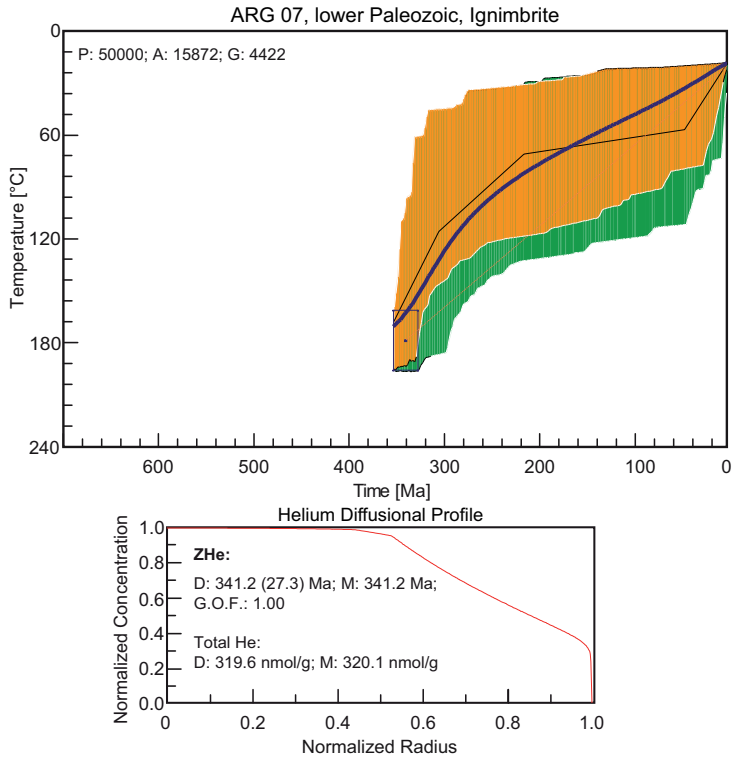

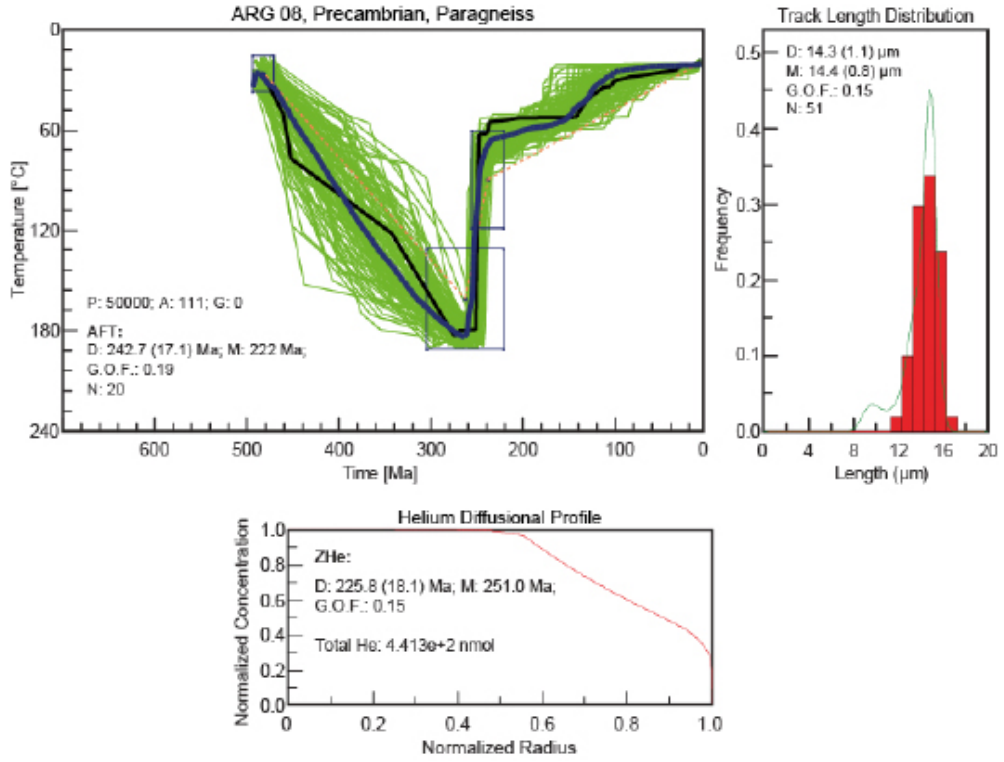
ARG 08, Precambrian, Paragneiss
Temperature [°C]
Time [Ma]
P: 50000; A: 111; G: 0
AFT:
D: 242.7 (17.1) Ma; M: 222 Ma;
G.O.F.: 0.19
N: 20
Track Length Distribution
D: 14.3 (1.1) µm
M: 14.4 (0.8) µm
G.O.F.: 0.15
N: 51
Frequency
Length (µm)
Helium Diffusional Profile
ZHe:
D: 225.8 (18.1) Ma; M: 251.0 Ma;
G.O.F.: 0.15
Total He: 4.413e+2 nmol
Normalized Concentration
Normalized Radius

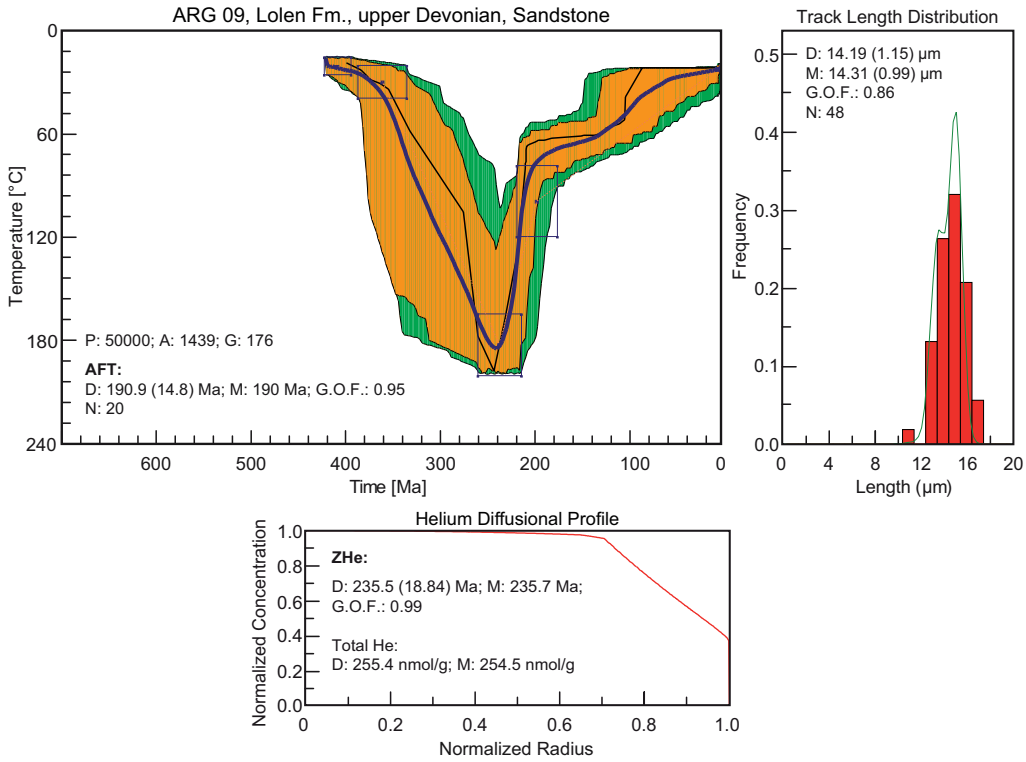
ARG 09, Lolen Fm., upper Devonian, Sandstone
Temperature [°C]
Time [Ma]
P: 50000; A: 1439; G: 176
AFT:
D: 190.9 (14.8) Ma; M: 190 Ma; G.O.F.: 0.95
N: 20
Track Length Distribution
D: 14.19 (1.15) µm
M: 14.31 (0.99) µm
G.O.F.: 0.86
N: 48
Frequency
Length (µm)
Helium Diffusional Profile
ZHe:
D: 235.5 (18.84) Ma; M: 235.7 Ma;
G.O.F.: 0.99
Total He:
D: 255.4 nmol/g; M: 254.5 nmol/g
Normalized Concentration
Normalized Radius

9.5 t-T models - Uruguay

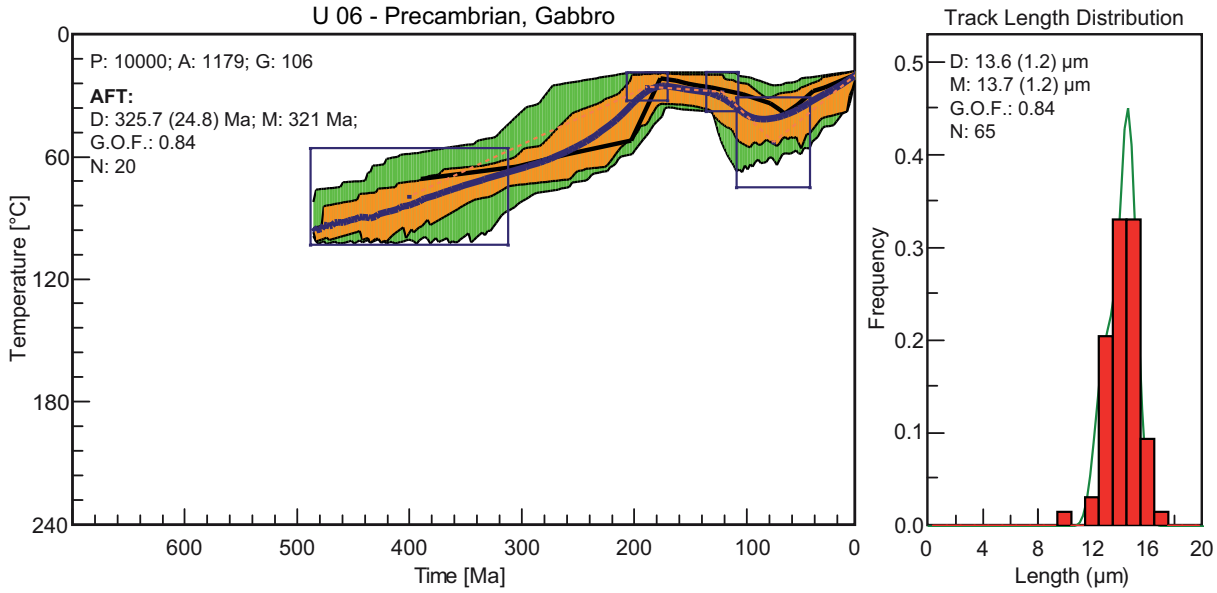

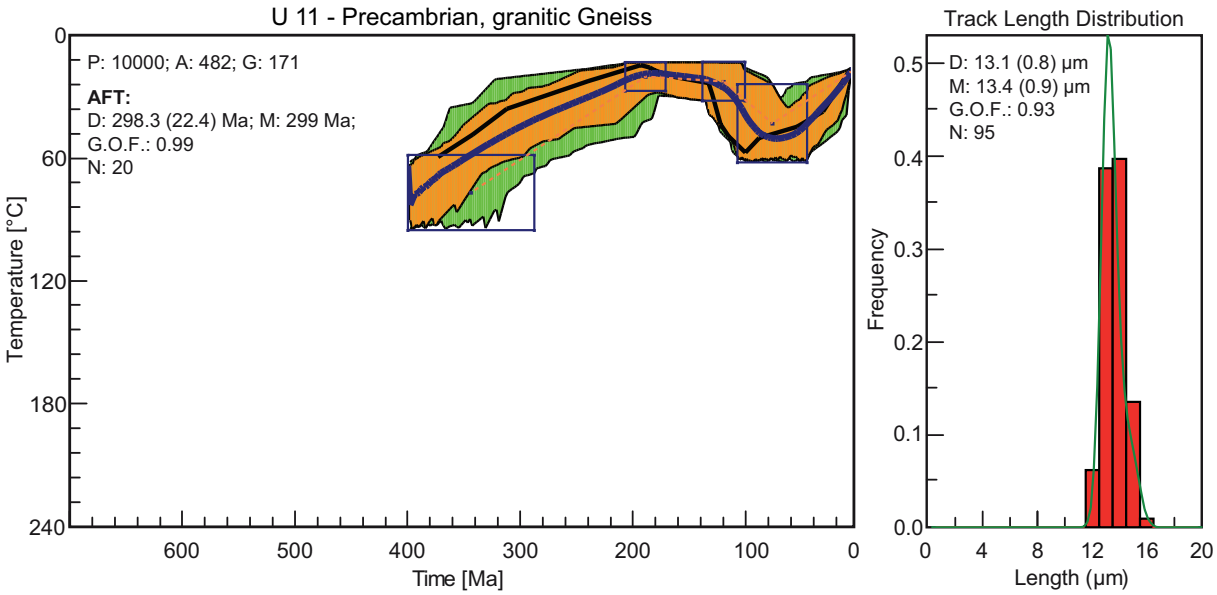

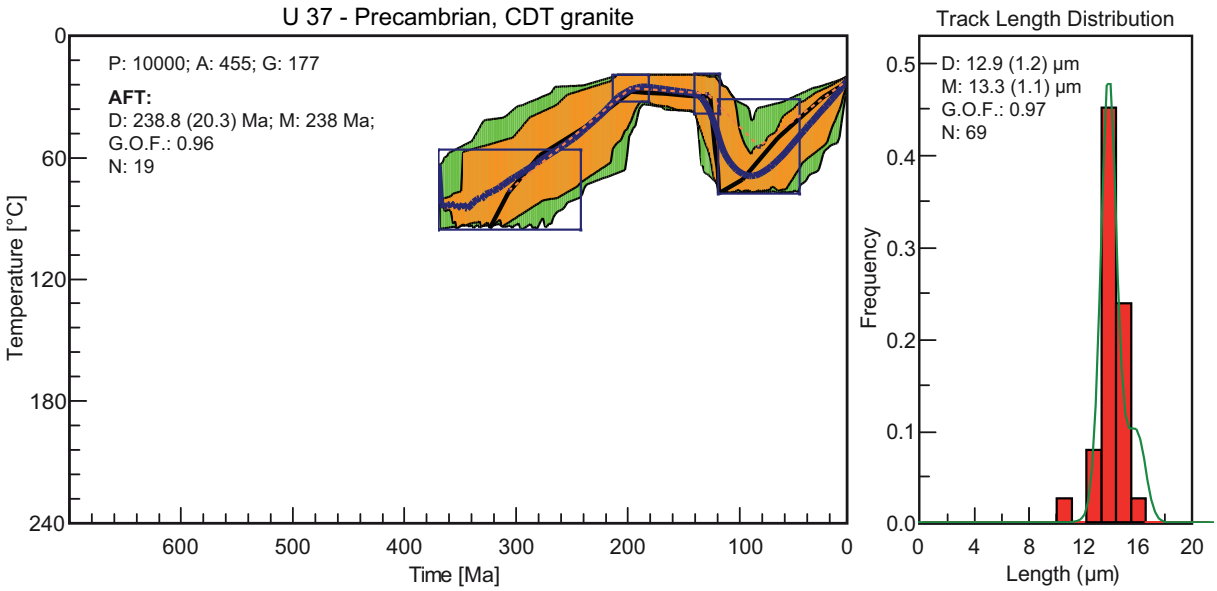
U 37 - Precambrian, CDT granite
P: 10000; A: 455; G: 177
AFT:
D: 238.8 (20.3) Ma; M: 238 Ma;
G.O.F.: 0.96
N: 19
Temperature [°C]
Time [Ma]
Track Length Distribution
D: 12.9 (1.2) µm
M: 13.3 (1.1) µm
G.O.F.: 0.97
N: 69
Frequency
Length (µm)

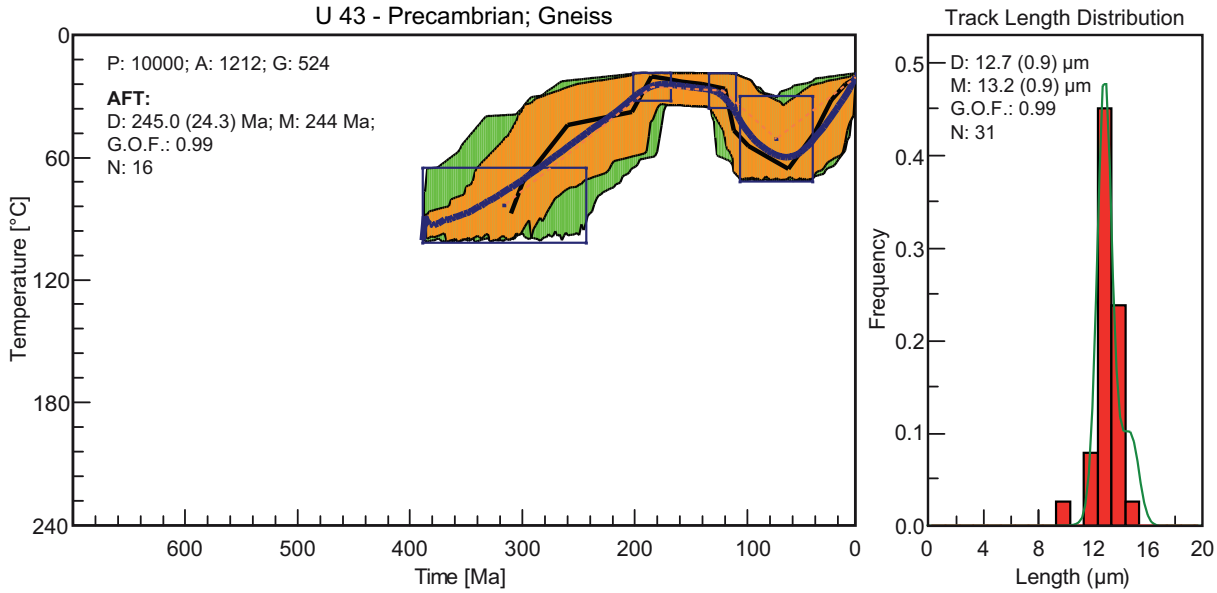
U 43 - Precambrian; Gneiss
P: 10000; A: 1212; G: 524
AFT:
D: 245.0 (24.3) Ma; M: 244 Ma;
G.O.F.: 0.99
N: 16
Temperature [°C]
Time [Ma]
Track Length Distribution
D: 12.7 (0.9) µm
M: 13.2 (0.9) µm
G.O.F.: 0.99
N: 31
Frequency
Length (µm)

9.6 Conference Contributions

22nd Colloquium on Latin American Earth Sciences (LAK)

March 30th to April 1st, 2011

Heidelberg, Germany Poster-presentation

Thermal history, exhumation, uplift, and long-term landscape evolution of the South Atlantic passive continental margin in eastern Argentina

[1]Sebastian Kollenz, [1]Ulrich A. Glasmacher, [2]Ricardo Pereyra, [3, 4]E.A. Rosello

[1]Institute of Earth Sciences, University of Heidelberg, Germany
[2]Uinversidad National de Salta, Salta, Argentina
[3]Departamento de Ciencias Geológicas, Universidad de Buenos Aires, Argentina
[4]CONICET, Universidad de Buenos Aires, Argentina

The project deals with the longterm landscape evolution of the South Atlantic passive continental margin in eastern Argentina. The eastern Argentina South Atlantic passive continental margin (SAPCM-A) is linked to a very flat topography without any escarpment. The aim is to quantify processes, like uplift-, exhumational and erosional events by using fission-track (FT) data, because the evolutional processes of the basin and the topography are only partly known.
The interpretation of the FT-ages and the thermo-kinematic modeling will lead to new conclusions on this topic and helps to understand the causes and timing of the evolution of the eastern Argentina South Atlantic passive continental margin. The SAPCM-A trends NE-SW and is linked to the SE-NW trending Salado-basin and the also SE-NW-trending Colorado-basin. These two basins are separated by the Tandill and Ventana Hills, which both also trend NE-SW. FT-data, generated from samples from the Tandill and Ventana Hills by using apatite and zircon from the different lithologies will be combined with HeFTy-models, to get new information about the kinematic processes like cooling, exhumation/inversion, uplift rates and erosional events, which have taken place and formed the topography of this region. This area is also a key area to study the influence of Fracture Zones (transform faults, transfer zones) on the evolution of the SAPCM.
Additionally we will work on data generated out of drill sites from the Colorado- and the Salado-basin, to get further information about the evolution and the geological processes of these two basins had to deal with in the past.

EGU General Assembly 2011

April 03th to April 08h, 2011

Vienna, Austria Poster-presentation

Thermal history and evolution of the South Atlantic passive continental margin in eastern Argentina

[1]Sebastian Kollenz, [1]Ulrich A. Glasmacher, [2]Ricardo Pereyra, [3, 4]E.A. Rosello

[1]Institute of Earth Sciences, University of Heidelberg, Germany
[2]Uinversidad National de Salta, Salta, Argentina
[3]Departamento de Ciencias Geológicas, Universidad de Buenos Aires, Argentina
[4]CONICET, Universidad de Buenos Aires, Argentina

Geophysical Research Abstracts Vol. 13, EGU2011-336, 2011 EGU General Assembly 2011

The project deals with the longterm landscape evolution of the South Atlantic passive continental margin in eastern Argentina. The eastern Argentina South Atlantic passive continental margin (SAPCM-A) is linked to a very flat topography without any escarpment. The aim is to quantify processes, like uplift-, exhumational and erosional events by using fission-track (FT) data, because the evolutional processes of the basin and the topography are only partly known.
The interpretation of the FT-ages and the thermo-kinematic modeling will lead to new conclusions on this topic and helps to understand the causes and timing of the evolution of the eastern Argentina South Atlantic passive continental margin. The SAPCM-A trends NE-SW and is linked to the SE-NW trending Salado-basin and the also SE-NW-trending Colorado-basin. These two basins are separated by the Tandill and Ventana Hills, which both also trend NE-SW. FT-data, generated from samples from the Tandill and Ventana Hills by using apatite and zircon from the different lithologies will be combined with HeFTy-models, to get new information about the kinematic processes like cooling, exhumation/ inversion, uplift rates and erosional events, which have taken place and formed the topography of this region. This area is also a key area to study the influence of Fracture Zones (transform faults, transfer zones) on the evolution of the SAPCM.
Additionally we will work on data generated out of drill sites from the Colorado- and the Salado-basin, to get further information about the evolution and the geological processes of these two basins had to deal with in the past.

Sample SPP 2011

June 7th to June 10th, 2011

Potsdam, Germany Poster-presentation

Thermal history and evolution of the South Atlantic passive continental margin in eastern Argentina based on different geochronometers and 2D- and 3D-modelling

[11]Sebastian Kollenz, [1]Ulrich A. Glasmacher, [2]Ricardo Pereyra, [3, 4]E.A. Rosello

[1]Institute of Earth Sciences, University of Heidelberg, Germany
[2]Uinversidad National de Salta, Salta, Argentina
[3]Departamento de Ciencias Geológicas, Universidad de Buenos Aires, Argentina
[4]CONICET, Universidad de Buenos Aires, Argentina

The project deals with the longterm landscape evolution of the South Atlantic passive continental margin in eastern Argentina. The eastern Argentina South Atlantic passive continental margin (SAPCM-A) is linked to a very flat topography without any escarpment. The aim is to quantify processes, like uplift-, exhumational and erosional events by using fission-track (FT) data, because the evolutional processes of the basin and the topography are only partly known.
The interpretation of the FT-ages and the thermo-kinematic modeling will lead to new conclusions on this topic and helps to understand the causes and timing of the evolution of the eastern Argentina South Atlantic passive continental margin. The SAPCM-A trends NE-SW and is linked to the SE-NW trending Salado-basin and the also SE-NW-trending Colorado-basin. These two basins are separated by the Tandill and Ventana Hills, which both also trend NE-SW. FT-data, generated from samples from the Tandill and Ventana Hills by using apatite and zircon from the different lithologies will be combined with HeFTy-models, to get new information about the kinematic processes like cooling, exhumation/ inversion, uplift rates and erosional events, which have taken place and formed the topography of this region. This area is also a key area to study the influence of Fracture Zones (transform faults, transfer zones) on the evolution of the SAPCM.
Additionally we will work on data generated out of drill sites from the Colorado- and the Salado-basin, to get further information about the evolution and the geological processes of these two basins had to deal with in the past.

Fragile Earth - Geological Processes from Global to Local

September 4th to September 7th, 2011

Munich, Germany Poster-presentation

Long-term landscape evolution of the South Atlantic passive continental margin, Buenos Aires, Argentina.

[1]Sebastian Kollenz, [1]Ulrich A. Glasmacher, [2]Ricardo Pereyra, [3, 4]E.A. Rosello

[1]Institute of Earth Sciences, University of Heidelberg, Germany
[2]Uinversidad National de Salta, Salta, Argentina
[3]Departamento de Ciencias Geológicas, Universidad de Buenos Aires, Argentina
[4]CONICET, Universidad de Buenos Aires, Argentina

The project deals with the evolution of the South Atlantic passive continental margin (SAPCM-A) in eastern Argentina. The aim is to quantify processes, like uplift-, exhumational and erosional events by using three different geochronometers. Combining apatite- and zircon-FT-data together with (U-Th-Sm)/He-data, it is possible to reconstruct the time-temperature-history (t-T-history) of each sample by using modeling-software. The modeling-software (HeFTy and PECUBE) leads to detailed information of the evolution of the continental margin and therefore also to information to understand the recent Topography. Passive continental margins are important geoarchives, which store information about incidents related to mantle dynamics, break-up of continents and other of exogenic and endogenic forces. The SAPCM-A trends NE-SW and is linked to the SE-NW trending Salado-basin and the also SE-NW-trending Colorado-basin. These two basins are separated by the Sierras Septentrionales and the Sierras Australes, which both also trend NE-SW. FT-data, generated from samples from the different stratigraphic Lithologies of both of the two mountain-ranges will be combined with HeFTy- and PECUBE-models, to get new insights in the kinematic processes like cooling, exhumation/inversion, uplift rates and erosional events, which have taken place and formed the recent topography of the region. This area is also a key area to study the influence of Fracture Zones (transform faults, transfer zones) on the evolution of the SAPCM. The Sierras Septentrionales is a flat mountain system and is surrounded by the Pampean plain. The hills reach their maximum of about 500 m a.s.l. near Tandil. The Sierras Septentrionales is build up of proterozoic crystalline basement covered by sedimentary rocks (Demoulin et al, 2005). The Sierras Australes is a fold belt trending in NW direction and can be sectioned in two main orographic units (Cobbold et al, 1986; Harrington, 1947). These two different units show different styles of deformation and different grades of metamorphism. The western part of the Sierras Australes is a very highly deformed unit and is build up of rocks from the lower greenschist facies (Cobbold et al, 1986). The eastern part shows much lower grades of deformation and metamorphism than the western part.

References:

Cobbold, P.R., Massabie, A.C., Rossello, E.A., 1986. Hercynian wrenching and thrusting in the Sierras Australes foldbelt, Argentina. Hercynica 2, 135–148.

Harrington, H.J., 1947. Explicacion de las Hojas Geolo gicas 33m y 34m Sierras de Curamalal y de la Ventana, Provincia de Buenos Aires. Serv. Nac. Min. Geol. Bol. 61, 46. Buenos Aires.

Gondwana 14

September 25th to September 30th, 2011

Buzios, Brazil Poster-presentation

Long-term landscape evolution of the South Atlantic passive continental margin, Buenos Aires, Argentina.

[1]Sebastian Kollenz, [1]Ulrich A. Glasmacher, [2]Ricardo Pereyra, [3, 4]E.A. Rosello

[1]Institute of Earth Sciences, University of Heidelberg, Germany
[2]Uinversidad National de Salta, Salta, Argentina
[3]Departamento de Ciencias Geológicas, Universidad de Buenos Aires, Argentina
[4]CONICET, Universidad de Buenos Aires, Argentina

The aim is to quantify processes, like uplift-, exhumational and erosional events by using three different geochronometers.
Combining apatite- and zircon-FT-data together with (U-Th-Sm)/He-data, it is possible to reconstruct the time-temperature-history (t-T-history) of each sample by using modeling-software. The modeling-software (HeFTy and PECUBE) leads to detailed information of the evolution of the continental margin and therefore also to information to understand the recent Topography. Passive continental margins are important geoarchives, which store information about incidents related to mantle dynamics, break-up of continents and other of exogenic and endogenic forces. The SAPCM-A trends NE-SW and is linked to the SE-NW trending Salado-basin and the also SE-NW-trending Colorado-basin. These two basins are separated by the Sierras Septentrionales and the Sierras Australes, which both also trend NE-SW. FT-data, generated from samples from the different stratigraphic Lithologies of both of the two mountain-ranges will be combined with HeFTy- and PECUBE-models, to get new insights in the kinematic processes like cooling, exhumation/inversion, uplift rates and erosional events, which have taken place and formed the recent topography of the region. This area is also a key area to study the influence of Fracture Zones (transform faults, transfer zones) on the evolution of the SAPCM. The Sierras Septentrionales is a flat mountain system and is surrounded by the Pampean plain.
The hills reach their maximum of about 500 m a.s.l. near Tandil. The Sierras Septentrionales is build up of proterozoic crystalline basement covered by sedimentary rocks (Demoulin et al, 2005). The Sierras Australes is a fold belt trending in NW direction and can be sectioned in two main orographic units (Cobbold et al, 1986; Harrington, 1947). These two different units show different styles of deformation and different grades of metamorphism. The western part of the Sierras Australes is a very highly deformed unit and is build up of rocks from the lower greenschist facies (Cobbold et al, 1986). The eastern part shows much lower grades of deformation and metamorphism than the western part.

References:

Cobbold, P.R., Massabie, A.C., Rossello, E.A., 1986. Hercynian wrenching and thrusting in the Sierras Australes foldbelt, Argentina. Hercynica 2, 135–148.

Harrington, H.J., 1947. Explicacion de las Hojas Geolo gicas 33m y 34m Sierras de Curamalal y de la Ventana, Provincia de Buenos Aires. Serv. Nac. Min. Geol. Bol. 61, 46. Buenos Aires.

EGU General Assembly 2012

April 22th to April 27th, 2012

Vienna, Austria Poster-presentation

Thermal history and evolution of the South Atlantic passive continental margin in eastern Argentina based on different geochronometers and 2D- and 3D-modelling

[1]S. Kollenz, [1]U. A. Glasmacher, [2]E. A. Rossello, and [3]R. Pereyra

[1]Institute of Earth Sciences, University of Heidelberg, Germany
[2]Departamento de Ciencias Geológicas, Universidad de Buenos Aires, Argentina
[3]Uinversidad National de Salta, Salta, Argentina

Geophysical Research Abstracts Vol. 14, EGU2012-4025, 2012 EGU General Assembly 2012

The eastern Argentina South Atlantic passive continental margin is distinguished by a very flat topography. Out of the so called Pampean flat two mountain ranges are arising. These mountain ranges, the Sierras Australes and the Sierras Septentrionales, are located in the State of Buenos Aires south of the capital Buenos Aires. North of the Sierras Septentrionales the Salado basin is located. The Sieras Septentrionales and the Sierras Australes are also divided by a smaller intracratonic basin. South of the Sierras Australes the Colorado basin is located. The Sierras Australes is a fold belt originated by strong phases of metamorphosis, but till now it is unclear by how many tectonic phases the area was influenced (Tomezzoli & Vilas, 1999). The recent research aim is to understand the long-term landscape evolution and to determine the exhumation rates. To fulfill this goal, thermochronological techniques such as apatite and zircon fission-track and (U-Th-Sm)/He dating has been applied to samples from the region. Furthermore, numerical modeling of the cooling history has provided the data base for the quantification of the exhumation rates.

References:

Tomezzoli, R. N. & Vilas, J. F.; Palaeomagnetic constraints on the age of deformation of the sierras Australes thrust and fold belt, Argentina; 1999; Geophys. J. Int., Vol. 138, pp. 857-870

Sample SPP 2012

June 12th to June 15th, 2012

Tutzing, Germany oral presentation

Thermal history and evolution of the South Atlantic passive continental margin in eastern Argentina based on different geochronometers and 2D- and 3D-modelling

[1]S. Kollenz, [1]U. A. Glasmacher, [2]E. A. Rossello, and [3]R. Pereyra

[1]Institute of Earth Sciences, University of Heidelberg, Germany
[2]Departamento de Ciencias Geológicas, Universidad de Buenos Aires, Argentina
[3]Uinversidad National de Salta, Salta, Argentina

The eastern Argentina South Atlantic passive continental margin is distinguished by a very flat topography. Out of the so called Pampean flat two mountain ranges are arising. These mountain ranges, the Sierras Australes and the Sierras Septentrionales, are located in the State of Buenos Aires south of the capital Buenos Aires. North of the Sierras Septentrionales the Salado basin is located. The Sieras Septentrionales and the Sierras Australes are also divided by a smaller intracratonic basin. South of the Sierras Australes the Colorado basin is located. The Sierras Australes is a fold belt originated by strong phases of metamorphosis, but till now it is unclear by how many tectonic phases the area was influenced (Tomezzoli & Vilas, 1999). The recent research aim is to understand the long-term landscape evolution and to determine the exhumation rates. To fulfill this goal, thermochronological techniques such as apatite and zircon fission-track and (U-Th-Sm)/He dating has been applied to samples from the region. Furthermore, numerical modeling of the cooling history has provided the data base for the quantification of the exhumation rates.

References:

Tomezzoli, R. N. & Vilas, J. F.; Palaeomagnetic constraints on the age of deformation of the sierras Australes thrust and fold belt, Argentina; 1999; Geophys. J. Int., Vol. 138, pp. 857-870

Thermo 2012

August 24th to August 28th, 2012

Guilin, China oral presentation

Thermal history and evolution of the South Atlantic passive continental margin in eastern Argentina based on different geochronometers

[1]S. Kollenz, [1]U. A. Glasmacher, [2]E. A. Rossello

[1]Institute of Earth Sciences, Im Neuenheimer Feld 234, University of Heidelberg, 69120 Heidelberg, Germany
[2]Depto. de Ciencias Geológicas, Facultad de Ciencias Exactas y Naturales, Universidad de Buenos Aires, Ciudad Autónoma de Buenos Aires, Argentina

The eastern Argentina South Atlantic passive continental margin is distinguished by a very flat topography. Out of the so called Pampean flat two mountain ranges are arising. These mountain ranges, the Sierras Australes and the Sierras Septentrionales, are located in the State of Buenos Aires south of the capital Buenos Aires. North of the Sierras Septentrionales the Salado basin is located. The Sieras Septentrionales and the Sierras Australes are also divided by a smaller intracratonic basin. South of the Sierras Australes the Colorado basin is located.
The Sierras Australes is a fold belt originated by strong phases of metamorphosis, but till now it is unclear by how many tectonic phases the area was influenced (Tomezzoli & Vilas, 1999[1]). The aim is to understand the long-term landscape evolution of the area by quantifiying erosion- and exhumation-rates and by dating ancient rock-uplift-events. Another goal is to analyze how processes, linked to the opening of the south atlantic, influenced the tectonic processes in the working area. To fulfill this goal, thermochronological techniques such as apatite and zircon fission-track and (U-Th-Sm)/He dating has been applied to samples from the region. Furthermore, numerical modeling of the cooling history has provided the data base for the quantification of the exhumation rates. The first data-set shows a clear reacvtivation of fault zones during mesozoic times, which supposably was linked to the opening of the South Atlantic.

References:

Renata Nela Tomezzoli and Juan Francisco Vilas (1999): Palaeomagnetic constraints on the age of deformation of the Sierras Australes thrust and fold belt, Argentina. Geophys. J. Int. (1999) 138, 857–870

EGU General Assembly 2013

April 22th to April 27th, 2013

Vienna, Austria Poster-presentation

Post-orogenic evolution of the Sierras Septentrionales and the Sierras Australes and links to the evolution of the eastern Argentina South Atlantic passive continental margin constrained by low temperature thermochronometry and 2D thermokinematic modeling

[1]S. Kollenz, [1]U. A. Glasmacher, [2]E. A. Rossello

[1]Institute of Earth Sciences, Im Neuenheimer Feld 234, University of Heidelberg, 69120 Heidelberg, Germany
[2]Depto. de Ciencias Geológicas, Facultad de Ciencias Exactas y Naturales, Universidad de Buenos Aires, Ciudad Autónoma de Buenos Aires, Argentina

Geophysical Research Abstracts, Vol. 15, EGU2013-132, 2013,EGU General Assembly 2013:

The eastern Argentina South Atlantic passive continental margin is distinguished by a very flat topography. Out of the so called Pampean flat two mountain ranges are arising. These mountain ranges, the Sierras Australes and the Sierras Septentrionales, are located in the State of Buenos Aires south of the capital Buenos Aires. North of the Sierras Septentrionales the Salado basin is located. The Sierras Septentrionales and the Sierras Australes are also divided by a smaller intracratonic basin. Further in the South the Colorado basin is located. The Sierras Australes is a variscian fold belt originated by strong phases of metamorphosis, but till now it is unclear by how many tectonic phases the area was influenced (Tomezzoli & Vilas, 1999). It consists of Proterozoic to Paleozoic rocks. The Sierras Septentrionales consists mainly of Precambrian crystalline rocks. The Precambrian sequences are overlain by younger Sediments (Cingolani, 2010). The aim is to understand the long-term landscape evolution of the area by quantifiying erosion- and exhumation-rates and by dating ancient rock-uplift-events. Another goal is to find out how the opening of the south atlantic took effect on this region. To fulfill this goal, thermochronological techniques, such as fission-track dating and (U-Th-Sm)/He dating has been applied to samples from the region. Because there was no low-temperature thermochronology done in this area, both techniques were applied on apatites and zircons. Furthermore, numerical modeling of the cooling history has provided the data base for the quantification of the exhumation rates. The first data-set shows clusters of different ages which can be linked to tectonic activities during late Paleozoic times. Also the thermokinematic modeling is leading to new insights of the evolution of both mountain ranges.

References:

Renata Nela Tomezzoli and Juan Francisco Vilas (1999): Palaeomagnetic constraints on the age of deformation of the Sierras Australes thrust and fold belt, Argentina. Geophys. J. Int. (1999) 138, 857–870.

Carlos A. Cingolani (2010): The Tandilia System of Argentina as a southern extension of the Rio de la Plata craton: an overview, Int. J. Earth. Sci. (Geol. Rundsch.) (2011) 100, 221–242.

Sample SPP 2013

August 11th to August 14th, 2013

Heidelberg, Germany Poster-presentation

Timing and rates of long-term landscape evolution in Southern Argentina

[1]S. Kollenz, [1]U. A. Glasmacher, [2]E. A. Rossello

[1]Institute of Earth Sciences, Im Neuenheimer Feld 234, University of Heidelberg, 69120 Heidelberg, Germany
[2]Depto. de Ciencias Geológicas, Facultad de Ciencias Exactas y Naturales, Universidad de Buenos Aires, Ciudad Autónoma de Buenos Aires, Argentina

The eastern Argentina South Atlantic passive continental margin is distinguished by a very flat topography. Out of the so called Pampean flat two mountain ranges are arising. These mountain ranges, the Sierras Australes and the Sierras Septentrionales, are located in the State of Buenos Aires south of the capital Buenos Aires. North of the Sierras Septentrionales the Salado basin is located. The Sierras Septentrionales and the Sierras Australes are also divided by a smaller intracratonic basin. Further in the South the Colorado basin is located. The Sierras Australes is a variscian fold belt originated by strong phases of metamorphosis, but till now it is unclear by how many tectonic phases the area was influenced (Tomezzoli & Vilas, 1999). It consists of Proterozoic to Paleozoic rocks. The Sierras Septentrionales consists mainly of Precambrian crystalline rocks. The Precambrian sequences are overlain by younger Sediments (Cingolani, 2010). The aim is to understand the long-term landscape evolution of the area by quantifiying erosion- and exhumation-rates and by dating ancient rock-uplift-events. Another goal is to find out how the opening of the south atlantic took effect on this region. To fulfill this goal, thermochronological techniques, such as fission-track dating and (U-Th-Sm)/He dating has been applied to samples from the region. Because there was no low-temperature thermochronology done in this area, both techniques were applied on apatites and zircons. Furthermore, numerical modeling of the cooling history has provided the data base for the quantification of the exhumation rates. The first data-set shows clusters of different ages which can be linked to tectonic activities during late Paleozoic times. Also the thermokinematic modeling is leading to new insights of the evolution of both mountain ranges.

References:

Renata Nela Tomezzoli and Juan Francisco Vilas (1999): Palaeomagnetic constraints on the age of deformation of the Sierras Australes thrust and fold belt, Argentina. Geophys. J. Int. (1999) 138, 857–870.

Carlos A. Cingolani (2010): The Tandilia System of Argentina as a southern extension of the Rio de la Plata craton: an overview, Int. J. Earth. Sci. (Geol. Rundsch.) (2011) 100, 221–242.

6. Deutsch-Brasilianisches Symposium zu „Nachhaltiger Entwicklung“

September 29th to October 04th, 2013

Santarem, Brazil Poster-presentation

Constraints of long-term landscape evolution and links to recent grasslands and agriculture within the pampas, Argentina

[1]S. Kollenz, [1]U. A. Glasmacher, [2]E. A. Rossello, [3]Pereyra, R., [4]Stoeckli, D.F.

[1]Institute of Earth Sciences, Im Neuenheimer Feld 234, University of Heidelberg, 69120 Heidelberg, Germany
[2]Depto. de Ciencias Geológicas, Facultad de Ciencias Exactas y Naturales, Universidad de Buenos Aires, Ciudad Autónoma de Buenos Aires, Argentina

[3]Uinversidad National de Salta, Salta, Argentina

[4]Jackson school of Geosciences, University of Texas at Austin, USA

The continental margin in the state of Buenos Aires is distinguished by a very flat topography, the so called Pampean flats. The Pampean flats are an important area for the agriculture, especially the grasslands for the cattle. The grasslands are situated within three different basins and form together with two mountain ranges a unique landscape. The geographical situation near the capital of Buenos Aires is very important for the local logistics. These mountain ranges, the Sierras Australes and the Sierras Septentrionales, show two different time-temperature histories. The evolution of the neighboring basins (Salado basin, Claromecco basin and Colorado basin) and the evolution of the mountain ranges were strongly influenced by the opening of the South Atlantic. Different thermochronometers like fission-tracks and (U-Th-Sm)/He dating will help to constrain the longterm evolution of today’s topography and morphology. The data show that the recent topography and morphology is linked to a strong phase of exhumation in Mesozoic times but also was influenced by younger tectonics and or climate change. The evolution of the basins, and therefore also the Pampean flats, is directly coupled to the evolution of the Sierras Australes and the Sierras Septentrionales and is a good example how recent space for grasslands and agriculture is linked to tectonic and climate change processes from the past.

AGU Fall Meeting

December 9th to December 13th, 2013

San Francisco, USA Poster-presentation

Timing and rates of long-term landscape evolution in Southern Argentina

[1]S. Kollenz, [1]U. A. Glasmacher

[1]Institute of Earth Sciences, Im Neuenheimer Feld 234, University of Heidelberg, 69120 Heidelberg, Germany

abstract #T23G-2667:

The eastern Argentina South Atlantic passive continental margin is distinguished by a very flat topography. Out of the so called Pampean flat two mountain ranges are arising. These mountain ranges, the Sierras Australes and the Sierras Septentrionales, are located in the State of Buenos Aires south of the capital Buenos Aires. North of the Sierras Septentrionales the Salado basin is located. The Sierras Septentrionales and the Sierras Australes are also divided by a smaller intracratonic basin. Further in the South the Colorado basin is located. The Sierras Australes is a variscian fold belt originated by strong phases of metamorphosis, but till now it is unclear by how many tectonic phases the area was influenced (Tomezzoli & Vilas, 1999). It consists of Proterozoic to Paleozoic rocks. The Sierras Septentrionales consists mainly of Precambrian crystalline rocks. The Precambrian sequences are overlain by younger Sediments (Cingolani, 2010). The aim is to understand the long-term landscape evolution of the area by quantifiying erosion- and exhumation-rates and by dating ancient rock-uplift-events. Another goal is to find out how the opening of the south atlantic took effect on this region. To fulfill this goal, thermochronological techniques, such as fission-track dating and (U-Th-Sm)/He dating has been applied to samples from the region. Because there was no low- temperature thermochronology done in this area, both techniques were applied on apatites and zircons. Furthermore, numerical modeling of the cooling history has provided the data base for the quantification of the exhumation rates. The data-set shows clusters of different ages which can be linked to tectonic activities during late Paleozoic times. Also the thermokinematic modeling is leading to new insights of the evolution of both mountain ranges and shows patterns of ongoing tectonic processes in this region. Caltculated exhumation rates show also varying cooling historys and the influence of tectonics throughout the research area.

References:

Renata Nela Tomezzoli and Juan Francisco Vilas (1999): Palaeomagnetic constraints on the age ofdeformation of the Sierras Australes thrust and fold belt, Argentina. Geophys. J. Int. (1999) 138, 857–870.

Carlos A. Cingolani (2010): The Tandilia System of Argentina as a southern extension of the Rio de la Plata craton: an overview, Int. J. Earth. Sci. (Geol. Rundsch.) (2011) 100, 221–242.

23nd Colloquium on Latin American Earth Sciences (LAK)

March 25th to March 27th, 2014

Heidelberg, Germany oral presentation

Timing and rates of long-term landscape evolution in Southern Argentina

[1]S. Kollenz, [1]U. A. Glasmacher, [2]E. A. Rossello

[1]Institute of Earth Sciences, Im Neuenheimer Feld 234, University of Heidelberg, 69120 Heidelberg, Germany
[2]Depto. de Ciencias Geológicas, Facultad de Ciencias Exactas y Naturales, Universidad de Buenos Aires, Ciudad Autónoma de Buenos Aires, Argentina

The eastern Argentina South Atlantic passive continental margin is distinguished by a very flat topography. Out of the so called Pampean flat two mountain ranges are arising. These mountain ranges, the Sierras Australes and the Sierras Septentrionales, are located in the State of Buenos Aires south of the capital Buenos Aires. North of the Sierras Septentrionales the Salado basin is located. The Sierras Septentrionales and the Sierras Australes are also divided by a smaller intracratonic basin. Further in the South the Colorado basin is located. The Sierras Australes is a variscian fold belt originated by strong phases of metamorphosis, but till now it is unclear by how many tectonic phases the area was influenced (Tomezzoli & Vilas, 1999). It consists of Proterozoic to Paleozoic rocks. The Sierras Septentrionales consists mainly of Precambrian crystalline rocks. The Precambrian sequences are overlain by younger Sediments (Cingolani, 2010). The aim is to understand the long-term landscape evolution of the area by quantifiying erosion- and exhumation-rates and by dating ancient rock-uplift-events. Another goal is to find out how the opening of the south atlantic took effect on this region. To fulfill this goal, thermochronological techniques, such as fission-track dating and (U-Th-Sm)/He dating has been applied to samples from the region. Because there was no low- temperature thermochronology done in this area, both techniques were applied on apatites and zircons. Furthermore, numerical modeling of the cooling history has provided the data base for the quantification of the exhumation rates. The data-set shows clusters of different ages which can be linked to tectonic activities during late Paleozoic times. Also the thermokinematic modeling is leading to new insights of the evolution of both mountain ranges and shows patterns of ongoing tectonic processes in this region. Caltculated exhumation rates show also varying cooling historys and the influence of tectonics throughout the research area.

References:

Renata Nela Tomezzoli and Juan Francisco Vilas (1999): Palaeomagnetic constraints on the age ofdeformation of the Sierras Australes thrust and fold belt, Argentina. Geophys. J. Int. (1999) 138, 857–870.

Carlos A. Cingolani (2010): The Tandilia System of Argentina as a southern extension of the Rio de la Plata craton: an overview, Int. J. Earth. Sci. (Geol. Rundsch.) (2011) 100, 221–242.

EGU General Assembly 2014

April 27th to May 2nd, 2014

Vienna, Austria Poster-presentation

Thermal history from both sides of the South Atlantic passive margin – A comparison: Argentinean pampa vs. South African escarpement

[1]S. Kollenz, [1]U. A. Glasmacher

[1]Institute of Earth Sciences, Im Neuenheimer Feld 234, University of Heidelberg, 69120 Heidelberg, Germany
[2]Depto. de Ciencias Geológicas, Facultad de Ciencias Exactas y Naturales, Universidad de Buenos Aires, Ciudad Autónoma de Buenos Aires, Argentina

Geophysical Research Abstracts Vol. 16, EGU2014-11777, 2014

The eastern Argentina South Atlantic passive continental margin is distinguished by a very flat topography. Out of the so called Pampean flat two mountain ranges are arising. These mountain ranges, the Sierras Australes and the Sierras Septentrionales, are located in the State of Buenos Aires south of the capital Buenos Aires. In existing literature the Sierras Australes are correlated with the South African cape fold belt (Torsvik 2009; Lopez Gamundi & Rossello 1998). Existing thermochronological data shows different post-breakup cooling histories for both areas and different AFT-ages. Published thermochronological ages (e.g. Raab et al. 2002, 2005, Gallagher et al et al. 1998)from the south African escarpement vary around 150 and 100 Ma (Gallagher et al. 1998). Only some spots in the eastern part of South Africa towards the pacific margin show older ages of 250 Ma and older than 350 Ma (Gallagher et al. 1998). New thermochronological data (AHe, AFT and ZHe) from the Sierras Australes indicate a different cooling history by revealing a range of varying ages due to younger tectonic activity. By comparing the data sets from both areas it is getting clear that the post-rift evolution of both continents is differing very strong.

References:

Gallagher, K., Brown, R. and Johnson, C. 1998. Fission track analysis and its application to geological problems. Annual review of Earth and Planetary Science, 26, 519-572.

Lopez Gamundi, O.R., Rossello, E.A. (1998): Basin fill evolution and paleotectonic patterns along the Samfrau geosyncline: the Sauce Grande basin–Ventana foldbelt (Argentina) and Karoo basin–Cape foldbelt (South Africa) revisited. Geol Rundsch 86 :819–834.

Raab, M.J., Brown, R.W., Gallagher, K., Carter, A. and Webber, K. 2002. late Cretaceous reactivation of major crustal shear zones in northern Namibia: constraints from apatite fission track analysis. Tectonophysics. 349, 75-92.

Raab, M.J., Brown, R.W., Gallagher, K., Webber, K. and Gleadow, A.J.W. 2005. denudational and thermal history of the Early Cretaceous Brandberg and Okenyenya igneous complexes on Namibia's passive margin. Tectonics. 24, TC3006, doi:10.1029/2004TC001688.

Torsvik, T.H., Rousse, S., Labails, C., Smethurst, M. A. (2009): A new scheme for the opening of the South Atlantic Ocean and the dissection of an Aptian salt basin. Geophys. J. Int. 177, 1315–1333.

EGU General Assembly 2014

April 27th to May 2nd, 2014

Vienna, Austria oral presentation

Timing and rates of long-term landscape evolution in Southern Argentina

[1]S. Kollenz, [1]U. A. Glasmacher, [2]E. A. Rossello

[1]Institute of Earth Sciences, Im Neuenheimer Feld 234, University of Heidelberg, 69120 Heidelberg, Germany
[2]Depto. de Ciencias Geológicas, Facultad de Ciencias Exactas y Naturales, Universidad de Buenos Aires, Ciudad Autónoma de Buenos Aires, Argentina

The eastern Argentina South Atlantic passive continental margin is distinguished by a very flat topography. Out of the so called Pampean flat two mountain ranges are arising. These mountain ranges, the Sierras Australes and the Sierras Septentrionales, are located in the State of Buenos Aires south of the capital Buenos Aires. North of the Sierras Septentrionales the Salado basin is located. The Sierras Septentrionales and the Sierras Australes are also divided by a smaller intracratonic basin. Further in the South the Colorado basin is located. The Sierras Australes is a variscian fold belt originated by strong phases of metamorphosis, but till now it is unclear by how many tectonic phases the area was influenced (Tomezzoli & Vilas, 1999). It consists of Proterozoic to Paleozoic rocks. The Sierras Septentrionales consists mainly of Precambrian crystalline rocks. The Precambrian sequences are overlain by younger Sediments (Cingolani, 2010). The aim is to understand the long-term landscape evolution of the area by quantifiying erosion- and exhumation-rates and by dating ancient rock-uplift-events. Another goal is to find out how the opening of the south atlantic took effect on this region. To fulfill this goal, thermochronological techniques, such as fission-track dating and (U-Th-Sm)/He dating has been applied to samples from the region. Because there was no low- temperature thermochronology done in this area, both techniques were applied on apatites and zircons. Furthermore, numerical modeling of the cooling history has provided the data base for the quantification of the exhumation rates. The data-set show clusters of different ages which can be linked to tectonic activities during late Paleozoic times. Also the thermokinematic modeling is leading to new insights of the evolution of both mountain ranges and shows patterns of ongoing tectonic processes in this region. Calculated exhumation rates show also varying cooling histories and the influence of tectonics throughout the research area.

References:

Renata Nela Tomezzoli and Juan Francisco Vilas (1999): Palaeomagnetic constraints on the age of deformation of the Sierras Australes thrust and fold belt, Argentina. Geophys. J. Int. (1999) 138, 857–870.

Carlos A. Cingolani (2010): The Tandilia System of Argentina as a southern extension of the Rio de la Plata craton: an overview, Int. J. Earth. Sci. (Geol. Rundsch.) (2011) 100, 221–242.

Sample SPP 2014

June 3rd to June 6th, 2014

Bremerhaven, Germany Poster-presentation

Timing and rates of long-term landscape evolution in Southern Argentina

[1]S. Kollenz, [1]U. A. Glasmacher

[1]Institute of Earth Sciences, Im Neuenheimer Feld 234, University of Heidelberg, 69120 Heidelberg, Germany

The eastern Argentina South Atlantic passive continental margin is distinguished by a very flat topography. Out of the so called Pampean flat two mountain ranges are arising. These mountain ranges, the Sierras Australes and the Sierras Septentrionales, are located in the State of Buenos Aires south of the capital Buenos Aires. North of the Sierras Septentrionales the Salado basin is located. The Sierras Septentrionales and the Sierras Australes are also divided by a smaller intracratonic basin. Further in the South the Colorado basin is located. The Sierras Australes is a variscian fold belt originated by strong phases of metamorphosis, but till now it is unclear by how many tectonic phases the area was influenced (Tomezzoli & Vilas, 1999). It consists of Proterozoic to Paleozoic rocks. The Sierras Septentrionales consists mainly of Precambrian crystalline rocks. The Precambrian sequences are overlain by younger Sediments (Cingolani, 2010). The aim is to understand the long-term landscape evolution of the area by quantifiying erosion- and exhumation-rates and by dating ancient rock-uplift-events. Another goal is to find out how the opening of the south atlantic took effect on this region. To fulfill this goal, thermochronological techniques, such as fission-track dating and (U-Th-Sm)/He dating has been applied to samples from the region. Because there was no low- temperature thermochronology done in this area, both techniques were applied on apatites and zircons. Furthermore, numerical modeling of the cooling history has provided the data base for the quantification of the exhumation rates. The data-set from the Sierras Australes shows clusters of different ages which can be linked to tectonic activities during late Paleozoic times. Also the thermokinematic modeling is leading to new insights of the evolution of both mountain ranges and shows patterns of ongoing tectonic processes in this region. Caltculated exhumation rates show also varying cooling historys and the influence of tectonics throughout the research area. New thermochronological constraints from the Sierras Septentrionales draw a very homogeneous picture of the thermokinematic evolution of the mountain range and a big influence by late paleozoic tectonics.

References

Cingolani, C. A. (2010): The Tandilia System of Argentina as a southern extension of the Rio de la Plata craton: an overview, Int. .Earth. Sci. (Geol. Rundsch.) (2011) 100, 221–242.

Thermo 2014

September 8th to September 12th, 2014

Chamonix, France Poster-presentation

Timing and rates of long-term landscape evolution in Southern Argentina

[1]S. Kollenz, [1]U. A. Glasmacher, [2]E. A. Rossello, [3]D. F. Stocklie

[1]Institute of Earth Sciences, Im Neuenheimer Feld 234, University of Heidelberg, 69120 Heidelberg, Germany
[2]Depto. de Ciencias Geológicas, Facultad de Ciencias Exactas y Naturales, Universidad de Buenos Aires, Ciudad Autónoma de Buenos Aires, Argentina
[3] University of Texas at Austin, Jackson School Of Geosciences, Austin, Texas , USA

The eastern Argentina South Atlantic passive continental margin is distinguished by a very flat topography. Out of the so called Pampean flat two mountain ranges are arising. These mountain ranges, the Sierras Australes and the Sierras Septentrionales, are located in the State of Buenos Aires south of the capital Buenos Aires. North of the Sierras Septentrionales the Salado basin is located. The Sierras Septentrionales and the Sierras Australes are also divided by a smaller intracratonic basin. Further in the South the Colorado basin is located. The Sierras Australes is a variscian fold belt originated by strong phases of metamorphosis, but till now it is unclear by how many tectonic phases the area was influenced (Tomezzoli & Vilas, 1999). It consists of Proterozoic to Paleozoic rocks. The Sierras Septentrionales consists mainly of Precambrian crystalline rocks. The Precambrian sequences are overlain by younger Sediments (Cingolani, 2010). The aim is to understand the long-term landscape evolution of the area by quantifiying erosion- and exhumation-rates and by dating ancient rock-uplift-events. Another goal is to find out how the opening of the south atlantic took effect on this region. To fulfill this goal, thermochronological techniques, such as fission-track dating and (U-Th-Sm)/He dating has been applied to samples from the region. Because there was no low- temperature thermochronology done in this area, both techniques were applied on apatites and zircons. Furthermore, numerical modeling of the cooling history has provided the data base for the quantification of the exhumation rates. The data-set from the Sierras Australes shows clusters of different ages which can be linked to tectonic activities during late Paleozoic times. Also the thermokinematic modeling is leading to new insights of the evolution of both mountain ranges and shows patterns of ongoing tectonic processes in this region. Caltculated exhumation rates show also varying cooling historys and the influence of tectonics throughout the research area. New thermochronological constraints from the Sierras Septentrionales draw a very homogeneous picture of the thermokinematic evolution of the mountain range and a big influence by late paleozoic tectonics.

References

Tomezzoli, R. N. and Vilas, J. F. (1999): Palaeomagnetic constraints on the age of deformation of the Sierras Australes thrust and fold belt, Argentina. Geophys. J. Int. (1999) 138, 857–870.

Cingolani, C. A. (2010): The Tandilia System of Argentina as a southern extension of the Rio de la Plata craton: an overview, Int. J.Earth. Sci. (Geol. Rundsch.) (2011) 100, 221–242.

GeoFrankfurt - Earth System Dynamics

September 21th to September 24th, 2014

Frankfurt, Germany oral presentation and Co-convener of the session

Timing and rates of long-term landscape evolution in Southern Argentina

[1]S. Kollenz, [1]U. A. Glasmacher, [2]E. A. Rossello, [3]D. F. Stocklie

[1]Institute of Earth Sciences, Im Neuenheimer Feld 234, University of Heidelberg, 69120 Heidelberg, Germany
[2]Depto. de Ciencias Geológicas, Facultad de Ciencias Exactas y Naturales, Universidad de Buenos Aires, Ciudad Autónoma de Buenos Aires, Argentina
[3] University of Texas at Austin, Jackson School Of Geosciences, Austin, Texas , USA

The eastern Argentina South Atlantic passive continental margin is distinguished by a very flat topography. Out of the so called Pampean flat two mountain ranges are arising. These mountain ranges, the Sierras Australes and the Sierras Septentrionales, are located in the State of Buenos Aires south of the capital Buenos Aires. North of the Sierras Septentrionales the Salado basin is located. The Sierras Septentrionales and the Sierras Australes are also divided by a smaller intracratonic basin. Further in the South the Colorado basin is located. The Sierras Australes is a variscian fold belt originated by strong phases of metamorphosis, but till now it is unclear by how many tectonic phases the area was influenced (Tomezzoli & Vilas, 1999). It consists of Proterozoic to Paleozoic rocks. The Sierras Septentrionales consists mainly of Precambrian crystalline rocks. The Precambrian sequences are overlain by younger Sediments (Cingolani, 2010). The aim is to understand the long-term landscape evolution of the area by quantifiying erosion- and exhumation-rates and by dating ancient rock-uplift-events. Another goal is to find out how the opening of the south atlantic took effect on this region. To fulfill this goal, thermochronological techniques, such as fission-track dating and (U-Th-Sm)/He dating has been applied to samples from the region. Because there was no low- temperature thermochronology done in this area, both techniques were applied on apatites and zircons. Furthermore, numerical modeling of the cooling history has provided the data base forthe quantification of the exhumation rates. The data-set show clusters of different ages which can be linked to tectonic activities during late Paleozoic times. Also the thermokinematic modeling is leading to new insights of the evolution of both mountain ranges and shows patterns of ongoing tectonic processes in this region. Calculated exhumation rates show also varying cooling histories and the influence of tectonics throughout the research area.

References

Tomezzoli, R. N. and Vilas, J. F. (1999): Palaeomagnetic constraints on the age of deformation of the Sierras Australes thrust and fold belt, Argentina. Geophys. J. Int. (1999) 138, 857–870.

Cingolani, C. A. (2010): The Tandilia System of Argentina as a southern extension of the Rio de la Plata craton: an overview, Int. J.Earth. Sci. (Geol. Rundsch.) (2011) 100, 221–242.

9.7 Submitted manuscript

(submitted to International Journal of Earth Sciences)

Late Palaeozoic to recent thermal history and long-term landscape evolution of the Sierras Septentrionales and Sierras Australes, NE Argentina

Sebastian KOLLENZ[1], Ulrich A. GLASMACHER[1], Eduardo A. ROSSELLO[2], Daniel F. STOCKLI[3], Ricardo E. PEREYRA[4], Sabrina PFISTER[1]

[1]Institute of Earth Sciences, University of Heidelberg, Im Neuenheimer Feld 234, 69120 Heidelberg, Germany

[2]Departamento de Ciencias Geológicas, Facultad de Ciencias Exactas y Naturales, Universidad de Buenos Aires, Ciudad Autónoma de Buenos Aires, Argentina

[3]Department of Geological Sciences, The University of Texas at Austin, 1 University Station C9000, Austin, TX 78712-0254, USA

[4]Ricardo Pereyra, Universidad Nacional de Salta (UNSa), Av. Bolivia 5150, 4400 Salta, Argentina

Abstract

The northern part of the Argentinean South Atlantic passive continental margins (SAPCM) is represented by the Salado Basin, the Sierras Septentrionales (Tandil Hills or Sierras Tandil), the intracratonic Claromeco basin, and the Sierras Australes (Ventana Hills or Sierra de la Ventana). They represent key areas to unravel the thermal and exhumation history at the low-elevation SAPCM. In general, passive continental margins are extraordinary topographic features that result from processes related to continental rifting, breakup, sea-floor spreading, post-breakup, and climate changes during their living time. As geo-archives the lithologies of the SAPCM store the Pre-rift geological evolution since the Neoproterozoic orogeny. The SAPCM's in Brazil, Namibia, and South Africa are partly high-elevated margins (~2,000m a.s.l.), and the SAPCM in Argentine and Uruguay are of low elevation. The specific characteristic of the SAPCM in Argentine is geological evolution caused by the Gondwanides Orogeny. During the Permo-Triassic the area was partly influenced by compressive deformation and diagenetic to low grade metamorphism. Thermochronological data are characterized by apatite (U-Th-Sm)/He ages between 163.0 (9.8) Ma and 107.4 (3.45) Ma. Apatite fission-track ages range from 242.7 (17.1) Ma to 129.2 (9.3) Ma in the Sierras Australes, whereas the zircon (U-Th-Sm)/He ages show values from 343.6 (27.5) Ma to 206.6 (16.5) Ma. Time-Temperature models lead to a differentiated thermal evolution throughout the region. A complex subsidence and exhumation history since the Ordovician is reported by our data and the corresponding models. The activation of the prominent Sauce Grande Wrench leads to exhumation on the western side and, therefore, induced subsidence on the eastern side. The Sierras Septentrionales and the Salado basin might have been influenced by rift related Upper Jurassic magmatism. Cenozoic exhumation rates (0.005 to 0.006 mm/a for #ARG 02 and 0.014 to 0.017 mm/a for #ARG 01) are relatively constant and do not show any significant changes.

Corresponding author: Sebastian Kollenz, Institute of Earth Sciences, University of Heidelberg, Im Neuenheimer Feld 234, 69120 Heidelberg, Germany, E-mail address: Sebastian.Kollenz@geow.uni-heidelberg.de, Telephone: +49-6221-546058

Eidesstattliche Versicherung gemäß § 8 der Promotionsordnung der Naturwissenschaftlich-Mathematischen Gesamtfakultät der Universität Heidelberg

1. Bei der eingereichten Dissertation zu dem Thema

Long-term landscape evolution, cooling and exhumation history of the South American passive continental margin in NE Argentina & SW Uruguay

handelt es sich um meine eigenständig erbrachte Leistung.

2. Ich habe nur die angegebenen Quellen und Hilfsmittel benutzt und mich keiner unzulässigen Hilfe Dritter bedient. Insbesondere habe ich wörtlich oder sinngemäß aus anderen Werken übernommene Inhalte als solche kenntlich gemacht.

3. Die Arbeit oder Teile davon habe ich ~~wie folgt~~/bislang nicht[1)] an einer Hochschule des In- oder Auslands als Bestandteil einer Prüfungs- oder Qualifikationsleistung vorgelegt.

Titel der Arbeit:_____

Hochschule und Jahr:_____

Art der Prüfungs- oder Qualifikationsleistung:_____

4. Die Richtigkeit der vorstehenden Erklärungen bestätige ich.

5. Die Bedeutung der eidesstattlichen Versicherung und die strafrechtlichen Folgen einer unrichtigen oder unvollständigen eidesstattlichen Versicherung sind mir bekannt.

Ich versichere an Eides statt, dass ich nach bestem Wissen die reine Wahrheit erklärt und nichts verschwiegen habe.

Heidelberg, 29.05.2015 _____

Ort und Datum Unterschrift

[1)] Nicht Zutreffendes streichen. Bei Bejahung sind anzugeben: der Titel der andernorts vorgelegten Arbeit, die Hochschule, das Jahr der Vorlage und die Art der Prüfungs- oder Qualifikationsleistung.